Fabrication of a Novel Bilayered Osteochondral Scaffold Using a Bottom up Approach



Narjes Rashidi

Linacre College

Michaelmass Term 2018

A Thesis Submitted for the Degree of Doctor of Philosophy

Department of Materials, University of Oxford

A Thesis Submitted for the Degree of Doctor of Philosophy

Department of Materials, University of Oxford

Fabrication of a Novel Bilayered Osteochondral Scaffold Using a Bottom up Approach

Narjes Rashidi, Linacre College

DPhil. Thesis, Michaelmass Term 2018

Abstract

Osteoarthritis and osteochondral injuries, caused by damage to both the articular cartilage and the underlying subchondral bone are suffered by over 40 million people in Europe alone. Consequently, osteochondral injuries and its complications are a serious burden to the health service and society as a whole. Tissue engineered grafts should create a more sustainable and long-term substitutes to clinical interventions because they combine the patient's own cells with porous biomaterial scaffolds that regenerate cartilage and bone and will restore the function of the joint.

The aim of this research was to capture the natural biological properties and mechanical strength of the joint, by developing bi-layered osteochondral plugs composed of superficial cartilaginous layers (coresponding to articular cartilage) and underlying calcified tissue (corresponding to subchondral bone). A novel biomimetic bottom-up approach inspired by the structure of the natural joint, with a different composition, pore size and substrate stiffness in each region of the construct was employed. The materials used for the superficial layer scaffold (chondrogenic region) were collagen type II and polymerised chondroitin sulphate (PCS); and for the underlying scaffold (osteogenic region) were collagen type I and hydroxyapatite. Monomeric type I and type II collagens were used as the starting materials since they mitigate the issue of collagen antigenicity on donor and recipient species.

Incorporation of chondroitin sulphate (CS) into collagen scaffolds has been limited in previous research due to a limited number of binding sites available on collagen for the CS attachment. In this study, to increase the incorporation and thus take full advantage of CS presence in scaffolds, CS was successfully polymerised to an 11 time higher molecular weight PCS. Subsequently, scaffolds were developed from crosslinked reconstituted fibrilar collagen II combined with CS or PCS. Rheological properties of collagen dispersions, scaffolds' chemical and porous structure, mechanical properties and the scaffolds chondrogenesis potential were examined. PCS significantly increased the complex viscosity, storage and loss modulus of collagen suspensions, while CS reduced them. The greater viscosity of collagen-PCS dispersions, in relation to collagen-CS gives rise to the formation of smaller pores in the scaffolds. PCS significantly increased the Young's modulus of scaffold (1.7 time), mainly due to the increase in relative density of scaffold. The higher specific surface area and compressive modulus, as well as a smaller pore size in collagen-PCS scaffolds gives rise to a 1.2 time increase in both (MSCs) cell attachment and proliferation. Most importantly, gene expression results showed 3 times increase in aggrecan and 14 times increase in collagen II expression in collagen-PCS scaffolds. Furthermore, histological analysis showed that cells produced considerably more GAGs and cartilage ECM on collagen-PCS compared to collagen-CS.

Osteogenic scaffolds were fabricated using two methods: crosslinked collagen I combined with commercially available HA, and *In situ* precipitation of HA nano particles on collagen fibrils following by

the subsequent crosslinking of suspensions. Rheology of suspensions, scaffolds microstructure and mechanical properties were evaluated. The first method resulted in smaller pores size, significantly higher pore interconnectivity, higher compressive modulus and increased cell differentiation (1.7 times increase in Young's modulus and 1.5 times increase in collagen I expression). Lastly, bilayered scaffolds were fabricated based on the optimum outcomes obtained for the composition, micro-architecture and mechanical properties of cartilage and bone scaffolds. It was established that sheep bone marrow mesenchymal stem cells give rise to distinct behavior of chondrogenesis and osteogenesis in the different regions of the bi-layer.

Acknowledgements

I would like to thank my supervisor Prof. Jan Czernuszka for his support, encouragement and advice he has provided throughout my PhD course. Thank you for giving me freedom to explore and direct the course of this research; Thanks for providing me with invaluable guidance throughout this time.

I also would like to thank Prof. Chaozong Liu in the Biomedical Institute at University College London. Thank you for providing me with all I needed to perform my ever first cell experiments. I cannot express my gratitude enough for your kindness and support.

I also wish to thank Dr. David Brand for kindly providing me with the collagen; this work would not have been possible without it!

My special thanks to the past and present members of Biomaterials group for helpful discussions.

To my lovely family, my parents and my sisters, thank you for your unconditional love, support and encouragement. I owe my success to you, without you I would not be able to accomplish my doctorate.

Preface

The research described in this thesis was undertaken by the author in the Department of Materials, University of Oxford, between October 2013 and December 2018, under the supervision of Prof. Jan Czernuszka. It is original in its contents except where reference to the work of others is acknowledged in the text. No parts of this thesis have been submitted or accepted for a degree at this university or elsewhere. Parts of the work in this thesis have been presented at an international conference.

1. Rashidi, N., Czernuszka, J., (2015)"*Reconstituted Fibrillar Collagen II- Chondroitin Sulphate for Cartilage Tissue Engineering"* in Proceedings of the 27 th European Biomaterials Conference, Poland**.**

Table of Contents

Abstract

Acknowledgments

Preface

Chapter 1. Introduction 10

Chapter 2. Literature Review 16

2.1. Introduction 17

2.2. Articular cartilage 17

2.2.1. Structure and composition of articular cartilage 18

2.2.1.1. Chondrocytes 19

2.2.1.2. Extracellular Matrix 21

2.2.2. Cartilage biomechanical properties 25

2.2.2.1. Compression 26

2.3. Bone 27

2.3.1. Composition 27

2.3.2. Mechanical properties 29

2.4. Osteochondral tissue structure 30

2.4.1. Zonal Cartilage 30

2.4.2. Subchondral bone 33

2.5. Osteochondral defects 34

2.5.1. Defect classifications 35

2.5.2. Osteochondral defect repair 36

2.5.3 Tissue engineering (TE) methods 38

2.5.3.1. Scaffolds 39

2.5.3.2. Cells 41

2.6 Osteochondral tissue engineering 43

2.6.1. Scaffold Design Considerations for Osteochondral Tissue Engineering 45

2.6.1.1. Single phase scaffolds 46

2.6.1.2. Biphasic (Bilayered) 47

2.7. Basis and aims of this research 51
Chapter 3. Techniques 53
3.1. Introduction 54
3.2. Rheology 54
3.3. Fourier Transform Infrared Spectroscopy (FTIR) 55
3.4. X-ray photoelectron spectroscopy (XPS) 57
3.5. Dynamic light Scattering (DLS) 57
3.6. X-ray diffraction analysis (XRD) 58
3.7. Scanning electron microscopy (SEM) 59
3.8. Compression test 60
Chapter 4. Polymerisation of Chondroitin Sulphate 61
4.1. Introduction 62
4.2. Chondroitin sulphate chemical structure, stimulatory effects and challenges in cartilage tissue engineering 62
4.3. Polymerisation of chondroitin sulphate 64
4.3.1. Materials and Method 65
4.3.2. Fabrication of scaffolds 66
4.4. Results 66
4.4.1. Fourier Transform Infra-Red Spectroscopy (FTIR) 67
4.4.2. X-ray photoelectron spectroscopy 69
4.4.3. Dynamic light scattering 71
4.4.4. Rheological experiments 72
4.4.4.1. Molecular weight of PCS based on rheology test 72
4.4.4.2. Rheology tests- Dynamic frequency sweep (constant strain, and temp)/ viscoelastic behaviour of CS and PCS 76
4.5. Scaffolds microstructure 80
4.6. Mechanical properties 83
4.7. Discussion 84
4.7.1. FTIR & XPS 84
4.7.2. Rheology 87

4.7.3. Pore size analysis 93
4.7.4. Relation between pore diameter and shear stress 97
4.7.5. Mechanical Properties 99
4.8. Summary 104
Chapter 5. Fabrication and Characterisation of Chondrogenic Scaffolds 105
5.1. Introduction 106
5.2. Fabrication of scaffolds 108
5.2.1. Materials 108
5.2.2. Collagen suspension preparation 109
5.2.3. Fibrillogenesis 109
5.2.4. EDC/NHS crosslinking 110
5.2.5. Casting and freeze drying 110
5.3. Statistical Analysis 113
5.4. Results 114
5.4.1. Collagen Dispersions Rheology 114
5.4.2. Fourier Transform Infrared Spectroscopy (FTIR) 115
5.4.3. Pore size analysis 119
5.4.4. Degradation study; effect of crosslinking on scaffolds dissolution behavior 120
5.4.5. CS and PCS content of the scaffolds and their CS release profile 122
5.4.6. Mechanical properties of collagen scaffolds under compression 125
5.5. Discussion 126
5.5.1. Rheology of collagen dispersions 127
5.5.1.2. Storage (G') and loss (G") moduli 131
5.5.2. FTIR and degradation studies 132
5.5.3. Pore Size analyses 137
5.5.4. Mechanical properties 138
5.6. Summary 141
Chapter 6. Fabrication and Characterisation of Osteogenic and Bi-layered Scaffolds 143
6.1. Introduction 144

6.2. Synthesis of collagen based scaffold for bone regeneration 144
6.2.1. Materials 145
6.2.2. Method- Preparation of crosslinked reconstituted fibrillar collagen type I mixed with hydroxyapatite 145
6.2.3. In- Situ Precipitation of HA nano crystals on collagen fibrils 146
6.2.4. Fabrication of integrated bilayered osteochondral scaffold 147
6.3. Results 149
6.3.1. Rheology 149
6.3.2. FTIR 152
6.3.3. Xray-diffraction 157
6.3.4. Scanning electron microscopy 158
6.3.5. Mechanical properties 161
6.4. Discussion 163
6.4.1. Rheology of collagen type 1 dispersions, XRD and scaffold microstructure 163
6.4.2. FTIR 166
6.4.3. Mechanical properties 168
6.5. Summary 172
Chapter 7. Biological properties of cartilage, bone and bilayered scaffolds 174
7.1. Introduction 175
7.2. Experimental procedures 176
7.2.1. Cell isolation, expansion and characterization 176
7.2.2. In vitro cell seeding 177
7.2.3. Cell viability assessment by Live/Dead assay 178
7.2.4. Cell metabolic activity 178
7.2.5. Optimisation of DNA quantification method for collagen scaffold 179
7.2.6. Cell proliferation based on DNA quantity 180
7.2.7. Cell differentiation analysis (Gene Expression) 181
7.2.8. Histological analysis 182
7.3. Results for chondrogenic scaffolds 184
7.3.1. Live/ Dead assay (cell viability) 184

7.3.2. Cell metabolic activity 186
7.3.3. Optimization of DNA quantification method 188
7.3.4. Cell attachment and proliferation (DNA quantity) 188
7.3.5. Cell differentiation- quantitative analysis of gene expression using qPCR 190
7.3.6. Histological analysis 190
7.4. Results for osteogenic scaffolds and bilayered 192
7.4.1. Live/ Dead assay (cell viability) 192
7.4.2. Cell metabolic activity 193
7.4.3. Cell proliferation (DNA quantity) 195
7.4.4. Cell differentiation- quantitative analysis of gene expression using qPCR 196
7.4.5. Histological analysis 198
7.5. Discussion 199
7.5.1. Cell viability and scaffold biocompatibility 199
7.5.2. Cell metabolic activity 201
7.5.3. Cell attachment and proliferation 203
7.5.4. Cell differentiation 209
7.5.5. Histological analysis 212
7.6. Summary 213
Chapter 8. Thesis Summary and Conclusions 215
Chapter 9. Future works 221
References

Chapter 1. Introduction

Osteochondral (OC) injuries caused by damage to both the articular cartilage and the underlying subchondral bone are a common problem in clinical practice (See Fig 1.1). There are many causes associated with OC defects ranging from natural degradation of cartilage to traumatic injuries. Osteoarthritis which develops due to natural wear of cartilaginous tissue is often the main cause of OC injuries in the aging population[1]. Reports show that as of 2008 over 39 million people in the European Union and 20 million Americans have suffered from osteoarthritis and this figure is expected to double by the year 2020[2].

Although the incidence of knee OC defects and repair is the most common, it can occur in any joints in the body. For instance OC injuries of the talus (a bone in ankle joints) contribute to over 50% of acute ankle fractures and sprains[3-5].

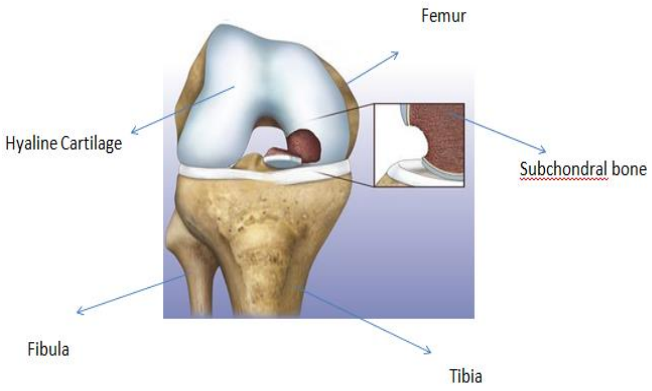


Fig 1.1. Schematic representation of osteochondral defect in knee joint[6]

Clinical treatments of OC defects have only been palliative and not curative and they all suffer from serious limitations. For example, marrow stimulation techniques, arthroscopic repair and autologous osteochondral grafts can postpone the need for total knee arthroplasty (TKA); however, these treatments usually lead to the formation of an inferior fibrocartilage tissue instead of hyaline cartilage, donor site morbidity, pain, hematoma and inflammation[7,8]. Tissue engineered osteochondral grafts, designed to mimic the natural structure of the joint, have emerged as a potential solution. These grafts combine the patient's own cells with porous biomaterial scaffolds of a predefined size and shape to regenerate cartilage and bone, and to thus create substitutes that could restore or enhance the function of the joint[9].

Three fundamental components contribute to the tissue engineering (TE) of an organ including biodegradable scaffolds, tissue forming cells and growth factors[10]. The scaffold as the key basis of tissue engineered constructs, should be made up of materials that closely resemble the structure and materials of the tissue they will replace[9]. OC constructs were initially composed of a single phase structure; more recently it has been proposed that biphasic structures allow for a more accurate mechanical interface[11]. Recent research are focused on the fabrication of integrated graded structures with cartilage-bone interface which mimics the native osteochondral tissue[12-14]. The major challenge in the OC tissue engineering is to obtain a better knowledge of osteochondral interface including its structure, biology and mechanical properties[15]. Interfaces are specific regions which connect two tissues of different biochemical and mechanical characteristics and play a crucial role in transitioning mechanical load between the connected tissues[16].

The aim of this project is to fabricate a bilayered device characterised by its enhanced mechanical strength which mimics the natural joint as closely as possible. Therefore, utilising the approach of biomimetic scaffolds, composites of collagen types I- hydroxyapatite and collagen II-chondroitin sulphate, which are respectively the major constituents of bone and articular cartilage, were used as the materials of the scaffolds. It was hypothesised that the composition, microstructural and mechanical differences will influence the behaviour of cells differently. These layers were produced to mimic the zonal structure and interface of cartilage and bone.

It has been demonstrated that incorporation of (CS) in scaffolds induces the chondrogenic differentiation of mesenchymal stem cells (MSCs) in vitro[17]. Previous research has attempted to exploit the advantage of CS by increasing its amount in the scaffolds[18,19]. However, there are limited binding sites on a biopolymer based scaffolds such as collagen for CS attachment, hence initial CS increase in collagen solution has not led to the increase of CS in the end-product scaffold (See Section 5.4.5). We increased the chain lengths of CS, polymerised it to the higher molecular weight PCS and showed its enhanced characteristics in terms of viscoelastic properties.

It was postulated that the interactions between different constituents of the scaffolds would affect the viscosity of preparations, which in turn would influence the microstructure of the scaffolds. This hypothesis was based on the process of scaffold fabrication. A common method for the fabrication of three-dimensional porous scaffolds is freeze-drying aqueous suspensions. The viscosity of the suspension controls the way water freezes, and affects the microstructure of scaffold as the pores are negative replicas of the ice crystals formed during freezing. It was further assumed that these chemical interactions and the pore structure would affect the mechanical

properties of the scaffolds. Cell behaviour, including attachment, proliferation and differentiation was thought to be modulated by these chemical, microstructural and mechanical factors.

This thesis examines the preparations of composite collagen types I- HA and type II- CS/PCS for osteochondral TE scaffolds. Since a biomimetic approach to TE is taken, a comprehensive review of the bone and cartilage biology, structure, properties and defects, as well as relevant literature in the area of TE is presented in Chapter 2. The main experimental objectives of this research were:

- To polymerise chondroitin sulphate (to a higher molecular weight polymer) in an attempt to increase the amount of CS in chondrogenic scaffolds. CS and PCS chemical structure were analysed using Fourier Transform Infra-red spectroscopy (FTIR) and X-ray Photoelectron spectroscopy (XPS). The rheological properties of CS and PCS preparations were studied using *rheometer.* The microstructure of CS and PCS scaffolds including pore structures, pore sizes and shapes was evaluated using Scanning Electron Microscopy (SEM) and the mechanical properties of scaffolds was assessed by conducting compression test. (Chapter 4)
- To synthesise composite preparations from monomeric collagen extractions incorporating CS/PCS or hydroxyapatite and to fabricate porous three- dimensional chondrogenic (Chapter 5) and osteogenic and bilayered scaffolds (Chapter 6). The different scaffolds were characterised using FTIR to develop an understanding of their properties and behaviours at the molecular level. The rheological properties of preparations were studied using *rheometer* which clarify the behaviour of suspensions at

the molecular level before freeze-drying. The microstructure were evaluated using SEM, compression testing were performed to assess the mechanical properties of fabricated scaffolds to examine their suitability for implantation (Chapter 5&6).

- To determine the biological response to scaffolds, and test whether the scaffolds would provide enough cues for *Mesenchymal Stem Cells* to guide them towards a specific lineage. Cell attachment, proliferation, differentiation and histological analysis were conducted (Chapter 7).

An overall summary and main conclusions of the work in this thesis are presented in Chapter 8.

Chapter 2. Literature Review

2.1. Introduction

The aim of this project is to fabricate a bi-layer device characterised by its enhanced mechanical strength which mimics the natural joint as closely as possible. A full understanding of the natural joint compositions, structures, biomechanical and biochemical properties is essential for the design of an ideal biomimetic scaffold. Therefore, this literature review provides a background on osteochondral tissue structure, OC defects, current clinical treatments and the need for OC tissue engineering as an alternative repair method.

The biology, structure and mechanical properties of cartilage and bone will also be discussed separately in the following chapters.

2.2. Articular cartilage

Joints are comprised of various types of connective tissue including cartilage surfaces, (subchondral) bone, ligaments, and the joint capsule[20].

Cartilage in human body is classified into elastic cartilage, fibro cartilage, and hyaline cartilage. All three types are composed of chondrocytes and extracellular matrix (ECM) macromolecules. Elastic cartilage forms the ear and nose and is characterised by the presence of elastin in the ECM[20]. Fibrocartilage is found at the ends of tendons and ligaments in apposition to bone and has a higher proportion of collagen I in the ECM than hyaline cartilage.[20] Gliding surfaces of synovial joint are covered with the hyaline cartilage, called articular cartilage which has a thickness of 2 to 4 mm depending on the location of the joint and provides a smooth, lubricated surface for articulation of bone ends and facilitates the transmission of mechanical loads with a low frictional coefficient (friction coefficient of 0.0025)[21]. Although it is a few millimeters thick,

articular cartilage has a remarkable stiffness to compression (0.79 MP) and outstanding ability to distribute load, thereby minimising peak stresses on subchondral bone[22].

Hyaline cartilage is an avascular dense connective tissue devoid of lymphatics and nerves possessing high compressive, tensile, and shear strengths (See Section 2.2.2). It provides stable movement with less friction than any prosthetic replacement and can alter its properties in response to differences in loading, so it cannot be fully replaced by any other tissue or device designed to date.[23]

Most importantly, articular cartilage is intrinsically incapable of self-healing and repair [21]. This limited ability to self-repair results in the risk of progressive degeneration in tissues of individuals over 40. Degeneration of articular cartilage and associated changes in subchondral bone lead to joint pain and dysfunction characterised by osteoarthritis[23].

2.2.1. Structure and composition of articular cartilage

Articular cartilage consists of a dense ECM with thinly interspersed highly specialised cells called chondrocytes. The ECM is primarily composed of water, collagen, and proteoglycans, with lower amount of non-collagenous proteins and glycoproteins (See Fig 2.1). These components help preserve water within the ECM, which is crucial to maintain the unique mechanical properties of cartilage[24].

Articular cartilage, as with other connective tissues, does not function directly via its cells but acts through its ECM and its mechanical properties. For instance, in parenchymal organs (e.g. liver) more than 95% of the tissue volume is composed of cells, whereas in connective tissues and particularly in articular cartilage more than 95% of the tissue volume consists of ECM[25]. The

key role of the cells is the synthesis and maintenance of ECM; this involves an appropriate anabolic activity of the chondrocytes which allows a balanced matrix turnover required for the physiological integrity of the cartilage ECM. Moreover, chondrocytes contribute to the matrix catabolic activity by producing matrix degrading molecules[25].

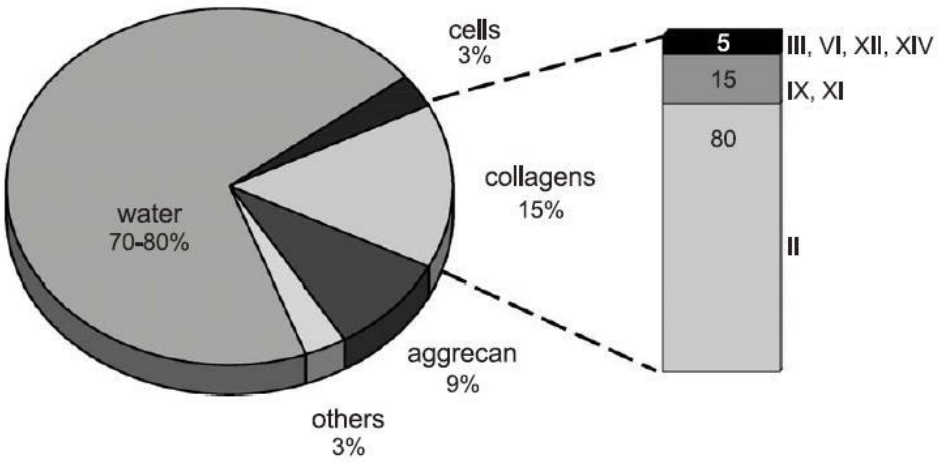


Fig 2.1. Schematic representation of the molecular composition of articular cartilage[25]

2.2.1.1. Chondrocytes

Chondrocytes are the highly specialised cells of articular cartilage which are metabolically active and play a unique role in the development, maintenance, and repair of the ECM. Chondrocytes originate from mesenchymal stem cells and approximately comprise 2% of the total volume of articular cartilage[26](1-10% of dry weight of cartilage[27]). Chondrocytes vary in shape, number and size depending on the cartilage regions they are placed in, but they all contain the cellular organelles necessary for matrix synthesis including endoplasmic reticulum and Golgi membranes[28] (See Table 2.1)

Each chondrocyte creates a specialised microenvironment and is responsible for the turnover of the ECM in its immediate proximity. This microenvironment entraps the chondrocyte within its own matrix and consequently prevents the migration of chondrocytes to adjacent areas of cartilage[28]. Cell communication for direct signal transduction rarely occurs between chondrocytes due to the lack of cell to cell contact. They do, however, respond to a variety of stimuli including growth factors, mechanical loads, piezoelectric forces and hydrostatic pressures[28]. Adult chondrocytes have limited potential for cell replication, a factor that contributes to the limited intrinsic healing capacity of cartilage in response to injury[29].

Amount	1-10% of dry weight of cartilage [16]				
Function	Matrix synthesis; maintaining ECM integrity by replacing the degraded matrix components [30]				
Changes with location	Chondrocytes of different cartilage zones differ in shape, size, orientation relative to the articular surface and metabolic activity[30]	**Superficial zone**	**Middle zone**	**Deep zone**	**Calcified zone**
		Flattened ellipsoid-shaped chondrocytes, Chondrocytes are inactive[31]	Spherical chondrocytes with low density, cells have concentrations of synthetic organelles, endoplasmic reticulum and Golgi membranes[30]	Chondrocytes are typically arranged in columnar orientation, the cells show high synthetic activity in this region, 10 times greater than cells activity in the superficial zone[32]	Chondrocytes are smaller, with almost no reticulum, with very low metabolic activity[32]
Changes with age	With aging the ability of cells to synthesise some type of proteoglycans and also their response to stimuli including growth factors decreases[30]				

Table 2.1. Chondrocytes in articular cartilage, their function and morphology throughout cartilage zones

2.2.1.2. Extracellular Matrix

Collagen- The most abundant structural macromolecule in cartilage ECM is collagen which comprises 60% of cartilage dry weight. Type II collagen constitutes 90% to 95% of the collagen in ECM and forms fibrils and fibers entwined with proteoglycan aggregates. Collagen types I, IV, V, VI, IX, and XI are also present but only in a minimal quantity and their role are to form and stabilise the type II collagen fibril network[33]. Collagen molecules, regardless of their type, are comprised of three α-chains with the amino acid sequence of Glycine-X-Y where X is commonly proline and Y is often hydroxyproline providing stability via hydrogen bonds along the length of the molecule and form a left-handed α-helix[34]. The location of the glycine (Gly) residue (the smallest amino acid) at every third position enables α-chains to twist round each other to represent a super helix [34-36]. The triple helix structure of the polypeptide chains gives rise to the important shear and tensile properties of articular cartilage, which help to stabilise the matrix[33]. (See Fig 2.2)

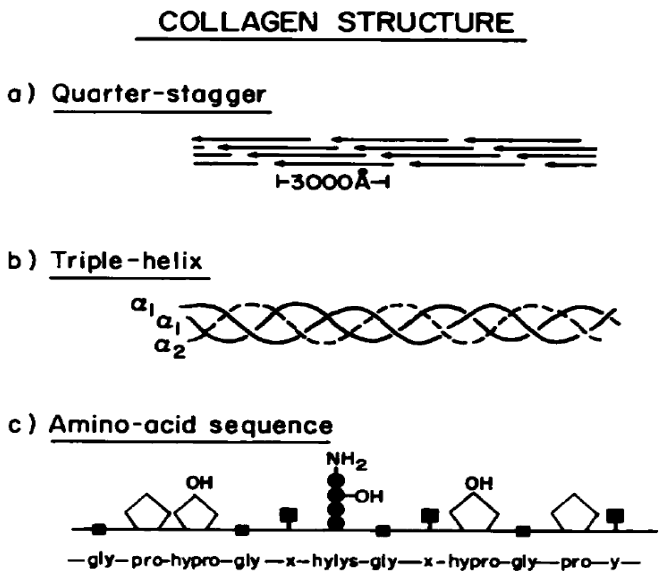


Fig 2.2. Hierarchical structure of articular cartilage collagen[37]

The fibril-forming collagen molecules (as in articular cartilage) consist of an uninterrupted triple helix of approximately 300 nm in length and 1.5 nm in diameter bound to short non-helical telopeptides. These telopeptides do not have a repeating Gly-X-Y structure and triple-helical conformation and they account for 2% of the molecules[35].

<table>
<tr><td>Amount</td><td colspan="5">60% of dry weight of cartilage of that 90-95% is collagen-II [30,38]</td></tr>
<tr><td rowspan="2">Type</td><td>II</td><td>VI</td><td>IX</td><td>X</td><td>XI</td></tr>
<tr><td>a homotrimer composed of a1(II) chains, the most abundant fibrillar protein in articular cartilage, constitutes 80–85% of the total collagen content
has a high hydroxylysine content which facilitates glycosylation [39]</td><td>locates at immediate surroundings of chondrocytes, help them to attach to the matrix[23]</td><td>a heterotrimer, present on the surface of Collagen II fibrils, 3% to 10% of the collagen content [39]</td><td>is not an integral component of the fibril but is found in cartilage matrix near hypertrophic chondrocytes near calcified zone[40]</td><td>resembles Collagen II in structure (uninterrupted helices by noncollagenous domains).
, has an extractable α3(XI) N-propeptide which projects from the fibril [41]</td></tr>
<tr><td>Function</td><td colspan="5">provide tensile strength and stiffness[41]
Type IX: “spacer” between individual fibrils, “glue” to bind the Collagen II lattice, a device for collagen fibrils to interact with proteoglycans[41], increasing network mechanical integrity and providing a restrain for entrapped proteoglycan osmotic swelling pressure[39], controlling fibrillar diameter[40]</td></tr>
<tr><td rowspan="2">Changes with position</td><td colspan="2">Superficial Zone</td><td colspan="2">Middle Zone</td><td>Deep Zone</td></tr>
<tr><td colspan="2">fine and parallel to the joint surface [32]</td><td colspan="2">they are not parallel to the joint surface (obliquely oriented), diameter of fibril increases, their content decrease [32]</td><td>fibrils are the thickest, perpendicular to the surface [32]</td></tr>
<tr><td>Changes with age</td><td colspan="5">Fine fibrils of cartilage change to the thicker and more varied fibril diameters.
Rate of collagen type II and IX synthesis (which regulates the size of fibrils) also decreases with age [39]</td></tr>
</table>

Table 2.2. Collagen in articular cartilage; its types, function and orientation in different cartilage zones

Proteoglycans- They are highly glycosylated protein in articular cartilage which represent the second largest group of macromolecules in the ECM and constitute 10% to 15% of the wet weight. Proteoglycans consist of a protein core with one or more linear covalently attached glycosaminoglycan chains (See Fig 2.3). These chains may be composed of more than 100 monosaccharides; they extend out from the protein core, remaining separated from one another due to the charge repulsion[21]. Articular cartilage contains a variety of proteoglycans that are essential for normal function, including aggrecan, decorin, biglycan and fibromodulin[21]. The largest in size and the most abundant by weight is aggrecan, a proteoglycan that possesses more than 100 chondroitin sulfate and keratin sulfate chains. Aggrecan is characterised by its ability to interact with hyaluronan (HA) to form large proteoglycan aggregates via link proteins. It resides in the interfibrillar space of the cartilage ECM and provides cartilage with its osmotic properties, which are critical to its ability to resist compressive loads[21].

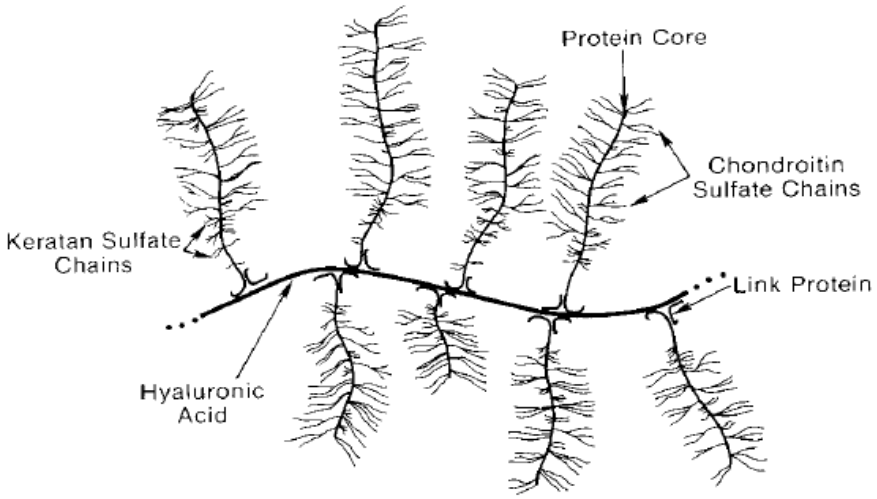


Fig 2.3. Proteoglycan aggregate[38]

Non-collagenous proteins- 10-20% of the dry weight of cartilage is composed of non- collagenous proteins[23].These consist of proteins with a few attached monosaccharides and oligosaccharides [23,32]. Although a number of non-collagenous proteins and glycoproteins are found within articular cartilage, their specific function has not been fully characterised. Some of these molecules (such as fibronectin and CII, a chondrocyte surface protein) likely play a role in the organisation and maintenance of the macromolecular structure of the ECM[21].

Water and tissue fluid- The most abundant component of articular cartilage is water which contributes up to 80% of its wet weight. Approximately 30% of this water is related to the intrafibrillar space within the collagen, although a small percentage contains the intracellular space; the remainder is present in the pore space of the matrix[42,43].

The relative water concentration decreases from about 80% at the superficial zone of cartilage to 65% in the deep zone[23].The flow of water through the cartilage and across the articular surface helps to transport and distribute nutrients to chondrocytes, in addition to providing lubrication. Much of the interfibrillar water appears to exist as a gel and most of it may be moved through the ECM by applying a pressure gradient across the tissue -by compressing the solid matrix[44,45]. Frictional resistance against this flow through the matrix is very high; thus, the permeability of the tissue is very low. It is the combination of the frictional resistance to water flow and the pressurisation of water within the matrix that forms the two basic mechanisms by which articular cartilage develops its ability to withstand significant loads, often multiple times of one's body weight[21].

In addition to water the fluid contains gasses, metabolites and large amount of cations to balance the negatively charged proteoglycans in the ECM[32,38]. The inorganic ions are also dissolved in water including sodium, calcium, chloride and potassium[46-48].

2.2.2. Cartilage biomechanical properties

The mechanical function of articular cartilage is to minimise the contact stresses and friction between two sliding joint; this depends on the optimum load distribution in articular cartilage matrix, which is influenced by the mechanical properties of the matrix. Any changes in the matrix (e.g. injuries) can interfere with load transmission and lead to higher contact stresses, which is more likely to exceed its strength limits[49].

Articular cartilage exhibits biphasic viscoelastic behaviour[21] due to two mechanisms[50,51]:

1. A flow-independent mechanism, which is exhibited in all polymeric materials due to intermolecular friction.

2. A flow-dependent mechanism, which arises if interstitial fluid can flow through the structure.

The mechanical properties of cartilage are determined by the interaction of its major constituents–collagen, proteoglycans and interstitial fluid [52]–by electrostatic interaction and physical entanglement[53]. Cartilage behaves mechanically as a viscoelastic material.

Tensile strength of matrix comes from the collagen network, which hinders expansion of the viscoelastic aggrecan component and, thus, provides compressive stiffness of the tissue. On the other hand, the aggrecan-hyaluronan aggregates are responsible for the elasticity of the tissue as they bind to high amounts of intercellular water due to their extensive fixed charges. Therefore, under compression, the cartilage matrix is compliant, but rapidly regains its elasticity

as water molecules are drawn back into the matrix upon unloading by the strongly hydrophilic aggrecan aggregates[25].

The native cartilage has an equilibrium compressive modulus of 0.79MPa [54,55], a shear modulus of 0.68MPa, and a tensile modulus of 0.3-10.2MPa [54,56].

2.2.2.1. Compression

In compression, biphasic behaviour is the dominant mechanism of deformation[51]. Elastic modulus of articular cartilage matrix can be obtained by dynamic (indentation) or static (confined compression or indentation) methods.

Dynamic methods (either stress-relaxation as a function of time or load-displacement as a function of frequency) using indentation methods which will give us "dynamic elastic modulus IE*I" or "dynamic shear modulus IG*I [50].

Static methods (either stress-relaxation or creep) using confined compression or indentation techniques when either the short-time modulus [57-60] (usually after 1-2 seconds) or equilibrium modulus[60,61] (usually after few hours) is determined. Compressive stiffness is related to the GAGs content of native cartilage[61,62] (chondroitin sulphate and keratan sulphate) and increases as a function of total GAGs, with keratan sulphate having a greater influence on stiffness than chondroitin sulphate[62]. No correlation between collagen and compressive stiffness[52] or a less significant one[62] has been observed. Compressive stiffness decreases with increasing water content and compressive equilibrium modulus decreases with age. Table 3 shows the mechanical properties of human articular cartilage under compression.

Elastic Modulus(MPa)	Shear Modulus (MPa)	Bulk Modulus (MPa)	Poisson's ratio	Method
0.53-0.701	-	-	0.098	Equilibrium creep indentation
0.13-1.91 (average: 0.79)	-	-	-	Equilibrium confined compression
5.06	1.72	31.5	0.47	Short-time confined compression[57]
8.14-10.15	-	-	-	Short-time (2s) creep indentation[58]
11.6	4.1	25	0.42	Short-time (1s) creep indentation[59]

Table 2.3. Mechanical properties of human articular cartilage under compression using different methods

Note that E short-time > E equilibrium (5-11 MPa vs. 0.5–0.7 MPa)

2.3. Bone

2.3.1. Composition

Bone consists of cells and ECM. This ECM is a composite of organic (30%) and inorganic components[63]. The primary organic component is collagen type I[63-65], but it also includes collagen V, VIII, XII, proteoglycans, non-collagenous proteins (osteocalcin, osteopontin) bone sialoprotein, thrombospondin and bone growth factors. The inorganic component is mainly hydroxyapatite, $Ca_{10}(PO_4)_6(OH)_2$ [64].

By weight, bone contains approximately 60% mineral, 10% water and about 30% collagenous matrix[64].

Cells- Four types of cells are present in bone: osteoblasts, osteoclasts, osteocytes and bone lining cells. Bone is constantly remodeled with osteoblasts producing and mineralising matrix, osteocytes maintaining the matrix and osteoclasts resorbing the matrix. Bone lining cells are

inactive cells that are considered to be precursors for osteoblasts[66]. This process of production and resorption of bone matrix by osteoblasts and osteoclasts plays important roles in bone physiology such as bone remodeling [63].

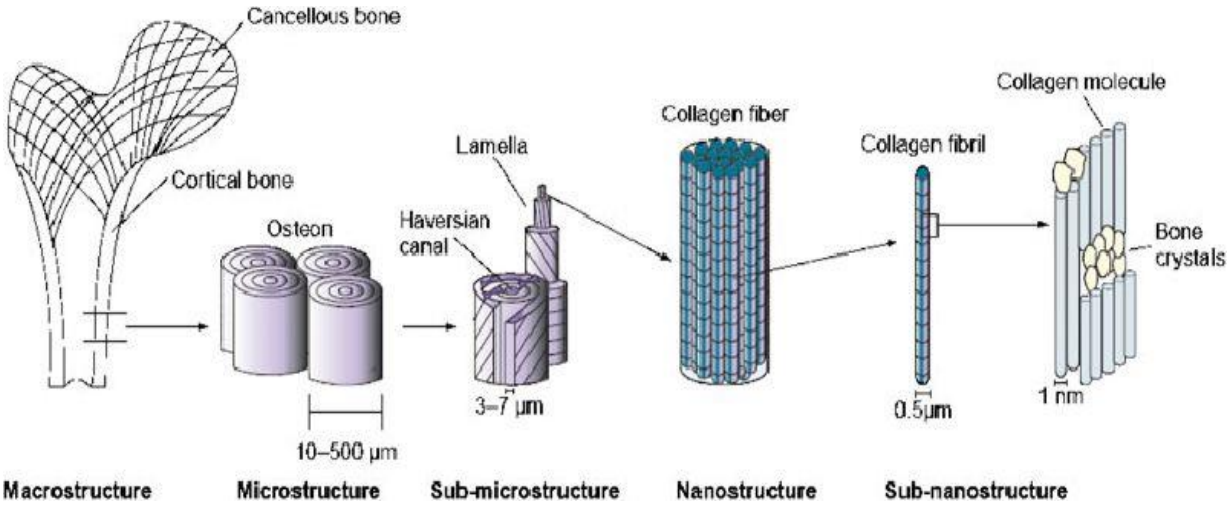


Fig 2.4. Schematic representation of the different levels of hierarchical structure of bone[67]

The macro-scale organisation of osteons, osteoids and haversian canals provides the mechanical anisotropy of long bones. On the other hand, the micro-scale porosity helps with cell migration and vascularisation and the nano-scale characteristics play a role in cell and mineral binding architecture[63].

There are two types of bone: (1) compact or cortical bone and (2) cancellous or trabecular bone[64,68]. They are different by their location, structure, spatial orientation of the mineral and organic elements [69].

cortical bone consists of osteons or Haversian systems (parallel cylindrical units, about 200 µm in diameter and 10.0–20.0 mm long[64]), which have a central canal called osteonic (haversian) canal

containing blood vessels, surrounded by concentric rings (lamellae, 3.00–7.00 μm thick)[64,68] of matrix. The bone cells (osteocytes) are located between the rings of matrix in spaces called lacunae. Small channels (canaliculi) extend outward from the lacunae to the haversian canal to provide microcirculating system through the hard matrix[63,64,70].(See Fig 2.4)

Trabecular bone consists of plates (trabeculae, 100–300 μm thick with spacing of 300–1500 μm between adjacent trabeculae[64]), adjacent to small, irregular cavities that contain red bone marrow [63].

2.3.2. Mechanical properties

As a polymer/ceramic composite of collagen and HA, bone exhibits high toughness and relatively high modulus[68]. A representative stress-strain curve for bone is shown in Fig 2.5. There is an initial linear elastic region, followed by a flat plastic region. Failure occurs at strains up to 3%. Bone is a tough material at low strain rates but as it can be seen from Fig 2.5, at high strain rates its fracture behaviour resembles more to a brittle material. The slope of the stress- strain curve (i.e., the stiffness), increases with increasing in mineral content. High toughness (~ 6.4 MPa $m^{1/2}$ for male human femoral bone[71]) is mostly due to hierarchical structure of bone, which stops cracks after little propagation. The main toughening mechanisms therefore, seem to be micro cracks, which appear in the plastic region of the stress-strain curve, crack deflection, and pullout effects[68].

Factors affecting the mechanical properties of bone can be divided into compositional and organisational factors[65]. Compositional factors include degree of mineralisation and porosity. Bone stiffness and strength increases with increase in mineralisation and decrease with increase in porosity[65]. Decrease in fracture strain happens with increase in the level of mineralisation[68].

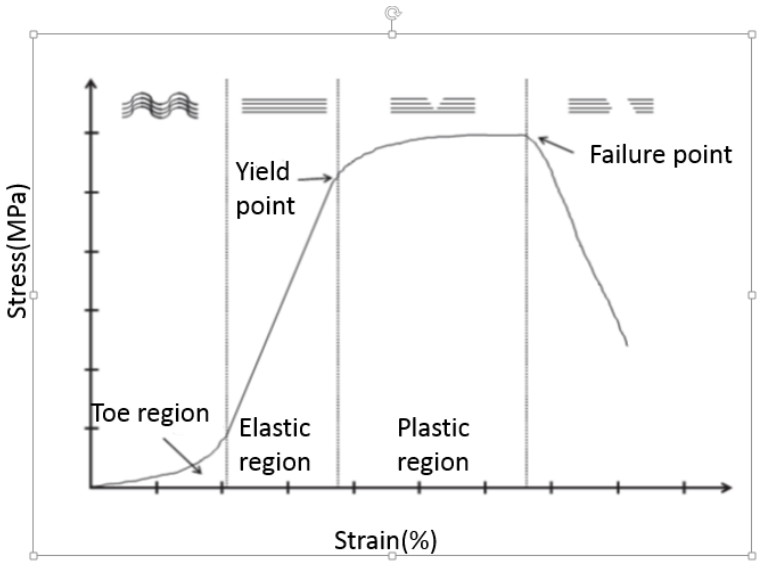


Fig 2.5. Typical stress-strain curve for bone[68]

Organisational factors include the arrangement of the collagen fibrils .The orientation and spacing of trabeculae and the anisotropy of collagen fibres influence the elastic modulus and strength of cancellous bone[65].

The mechanical properties of bone are highly anisotropic and depend on the porosity, mineral content, collagen fibre orientation and cross-linking which means the mechanical properties vary with species, age, disease state, bone type and position within a bone[65].

2.4. Osteochondral tissue structure

2.4.1. Zonal Cartilage

The upper region of osteochondral tissue is the articular cartilage layer. Articular cartilage can be distinguished into four zones according to the distance from the surface- the superficial, middle, deep and calcified zones[38] (See Fig 2.6 and 2.7). Organisation, composition and concentration of

cells and ECM molecules vary throughout the zones. However collagen fibrils constitute a dense and highly interconnected matrix in the whole regions of the tissue. Within the matrix, aggrecans which are highly glycosylated negatively charged molecules are bound to hyaluronic acid chains to form proteoglycan aggregates. These aggregates elevate the osmolarity of the tissue, which prompts an influx of water. The resultant swelling is counteracted by the resistance of the collagen matrix which creates a large internal pressure and confers cartilage its unique mechanical properties[72].

Each cartilage zone is characterised by a specific makeup and organisation of cells and ECM components. Chondrocytes of different zones differ in morphology, size and metabolic activity[73].

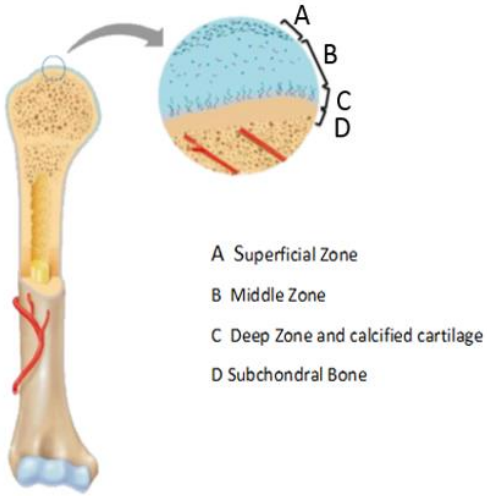


Fig 2.6. Osteochondral tissue structure [74]

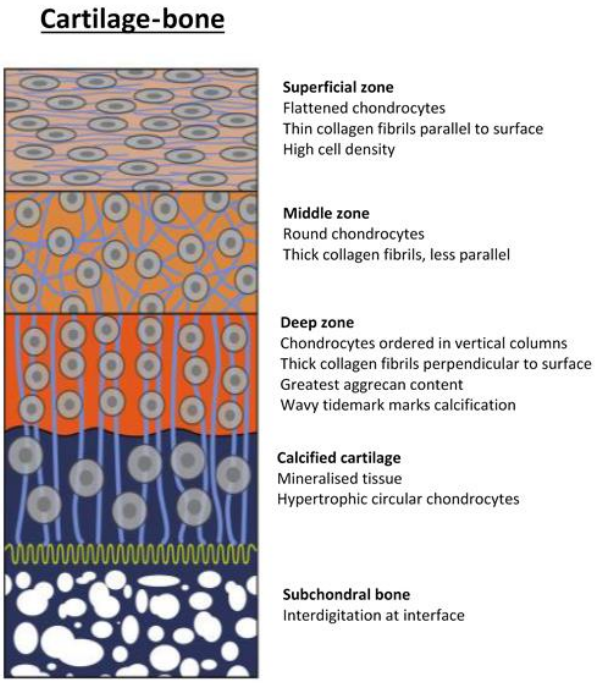


Fig 2.7. Schematic structure of cartilage zones [27]

The superficial/tangential zone forms approximately 10 to 20% of the articular cartilage volume. This zone is in contact with synovial fluid and undertakes the majority of the tensile properties of cartilage. Moreover, it protects deeper layers from shear stress.[21] The superficial zone is comprised of flattened chondrocytes and thin collagen fibrils that are packed tightly and aligned parallel to the articulating surface.[73] This zone is characterised by the highest cell density[73].

The middle/transitional zone constitutes 40 to 60% of the total cartilage thickness, and contains proteoglycans and thicker collagen fibrils. In this layer, the collagen is organised obliquely, and the chondrocytes are spherical and at low density. Functionally, the middle zone is the first line resists compressive forces.[21]

In the deep zone, both chondrocytes and fibres are organised perpendicular to the articular surface, with chondrocytes ordered in vertical columns[72,75]. Collagen fibril has the maximal diameter is in this region, however collagen content is at its lowest[21]. The deep zone represents approximately 30% of articular cartilage volume and contains high proteoglycan content therefore provides the greatest amount of resistance to compressive forces[21].

The tide mark distinguishes the deep zone from the calcified cartilage. The calcified layer plays an integral role in securing the cartilage to the bone underneath, by anchoring the collagen fibrils of the deep zone to the subchondral bone. In this zone, the cell content is at the lowest and chondrocytes are hypertrophic.[21]

The calcified zone represents a unique role as a transition between the compliant cartilage and the rigid subchondral bone. It minimises the stiffness gradient between the cartilage and subchondral bone.

Across the zones, aggrecan concentration highly rises by increasing tissue depth[76].Variation of ECM composition through the regions, along with the arrangement of ECM components has a great impact on the mechanical properties of each part of the tissue. For example, the superficial zone is strong in tension along the alignment of its collagen fibrils, which assists the tissue in resisting shear at the surface[73,75]. Through the depth of the tissue, the deep zone is more than an order of magnitude stiffer in compression compared to the superficial zone[77]. Each zone of tissue possess notably different mechanical properties: the compressive modulus varies an order of magnitude between each zone. The approximate moduli of the superficial zone, deep zone, calcified cartilage, and subchondral bone are respectively 0.079, 2.1, 320MPa and 5.7GPa [77,78].

2.4.2. Subchondral bone

The lower region of osteochondral tissue is the subchondral bone. It is the region under the calcified cartilage comprised of bony lamella and trabeculae. There is surprisingly little information available on the morphology and mechanical properties of the subchondral bone layer of bone which immediately place below the cartilage: [79].

'Subchondral bone plate' or 'subchondral zone' is referred to the bony lamella lying immediately under the calcified zone of the articular cartilage (See Fig 2.8). The line which separates the calcified zone and the subchondral bone plate is termed 'cement line'. The subchondral bone plate varies in thickness depending on the joint. Subchondral bone encompasses the subchondral bone plate and subarticular spongiosa[79] (trabeculae together with additional bony components). Anatomy of the subchondral region is extremely variable which includes differences in tidemark, cement line, the number and type of perforations in the subchondral bone plate, the thickness,

density and composition of subchondral bone plate[80-82]. Trabecular bone structure and its mechanical properties also vary in weight-bearing and non-weight-bearing areas.[79]

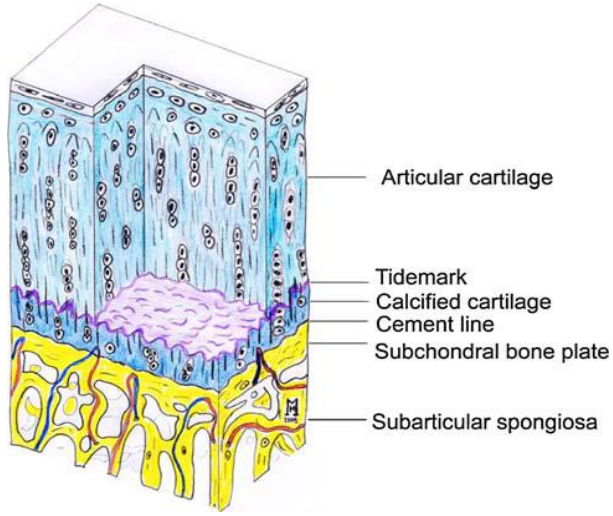


Fig 2.8. Schematic drawing of the different layers of articular cartilage, subchondral bone plate, and subarticular spongiosa[83]

2.5. Osteochondral defects

Different methods are available to classify cartilage defects depending on the size and depth of the defect. Among them, osteochondral defect is the worst and most costly type.[15] Structurally, osteochondral interface is weaker than the transitions within the cartilage zones as there are no collagen fibres extending from calcified cartilage zone to the subchondral bone plate to anchor these two layers. Unlike immature cartilage, adult cartilage is avascular, thin, with increased cell apoptosis. These features cause articular cartilage to be extremely vulnerable to damage with aging.[84]

2.5.1. Defect classifications

Various types of articular cartilage lesions have been defined. Cartilage microftactures is the least damaging type of defects; microfractures cannot be recognised by naked eye and influence on loss of superficial glycosaminoglycans.[85] Cartilage microfractures lead to the thinning of articular cartilage and the thickening of the calcified region.[86]

The next type of cartilage lesion is chondral defect which itself classified into partial thickness and full thickness. The depth of the damage in full thickness chondral defect is larger compared to partial thickness and the lesion progresses through the whole cartilage thickness up to cartilage bone interface. If the subchondral bone is also inflicted by damage, the defect is termed an osteochondral defect.[79]

A number of different systems is used to categorise the types of cartilage region. The most popular one is Outerbridge Classification System illustrated in Fig 2.9. Five grades of cartilage lesions are defined based on this system. Grade 0 lesion is the normal cartilage, Grade I lesion signifies swelling and softening of cartilage. Grade II is partial thickness chondral defect with a diameter less than 1.5 cm[87]. Grade III is a full thickness chondral defect with a diameter greater than 1.5 cm. When the subchondral bone is exposed to injury, the lesion is regarded as Grade IV.[88]

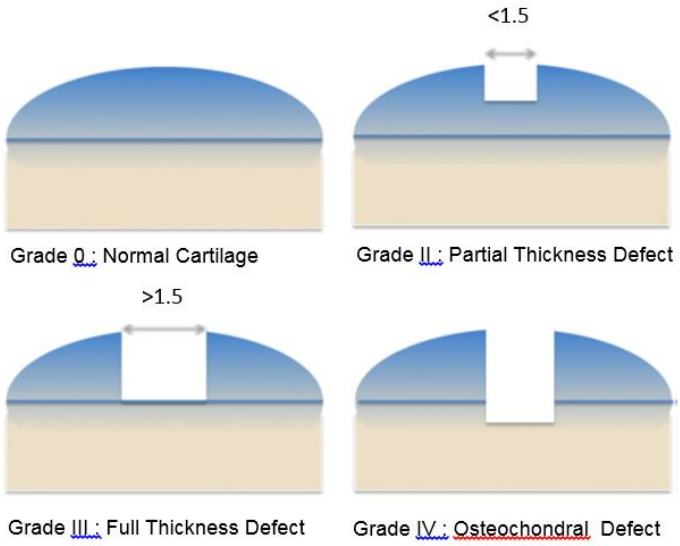


Fig 2.9. Osteochondral defect classification[74]

2.5.2. Osteochondral defect repair

Osteochondral defect repair has been performed by conventional clinical techniques or it can be done by tissue engineering strategies.

Clinical treatment methods can be classified into two groups: palliative methods and reparative methods. Unlike palliative treatments, reparative treatments replace the defect site with biological materials. Nonetheless, the ideal repair method is restorative treatments which assist the native tissue to reconstruct itself [74]. (See Table 2.4)

	Example of surgeries	Advantages	Disadvantages
Palliative	arthroscopic debridement[89]	The least invasive surgical treatment	Not effective for large osteochondral injuries[90]
	abrasion arthroplasty	Minimally invasive	Lead to the formation of fibrocartilage instead of hyaline cartilage, not recommended for lesions on the femur, tibia or patella or for very small lesions [9]
	Chondroplasty	Minimally invasive, recommended for higher grade defects (e.g. Grade III partial thickness)	risk of chondrocyte death due to the exposure of the tissue to high temperature [91]
Reparative	Microfracture (Subchondral drilling)	Microfracture can combine with the other treatment methods	more invasive treatment method [92], formation of fibrocartilage in the defect site[92,93],Postoperative rehabilitation is longer [94]
	Mosaicplasty • Allograft • Autograft	**Allograft:** Uses tissue from other humans (typically cadavers), which may derive from viable or sterilized non-viable sources **Autograft:** Host bone is removed from another site (typically from the pelvis or iliac crest) and used to fill the defect	**Allograft:** shortage of donor organs, disease transmission, immune rejection and the need for lifetime immunosuppressants, and slow remodelling[95] **Autograft:** the lack of tissue in donor site, the risk of donor site morbidity, mismatch of mechanical properties of donor and recipient tissue, potential need for multiple surgeries.[95]
restorative	Autologus Chondrocyte Implantation (ACI) [96]	Truly restorative clinical method [97]	The need for two surgeries, the relatively long recovery time, and the slow tissue maturation time of the implanted chondrocytes [98]

Table 2.4. Clinical treatment methods for osteochondral defects

2.5.3 Tissue engineering (TE) methods

The major goal of tissue engineering is to regenerate tissues including skin, cartilage, bone, nerve and liver. A porous scaffold, or a matrix, which mimics the tissue extracellular matrix is fabricated onto which cells attach, multiply and function. Typically cells are harvested from the patient and dissociated into individual cells by means of enzymes. The cells are then seeded onto the scaffold, or in vitro/ in a cell culture medium. The damaged tissue is removed and the matrix and attached cells are then implanted in the defect site. Over time, the synthetic matrix resorbs and the cells produce their own natural extracellular matrix. [99]

Three key components of tissue engineering are: a scaffold which may be both natural or synthetic, cells and inductive signals such as growth factors or proteins (See Fig 2.10).[8]

Significant interdependencies exist among the elements of this tissue engineering triad, with the challenge of how to optimize each individual element while determining or properly controlling its associated consequences on the other two parameters[100].

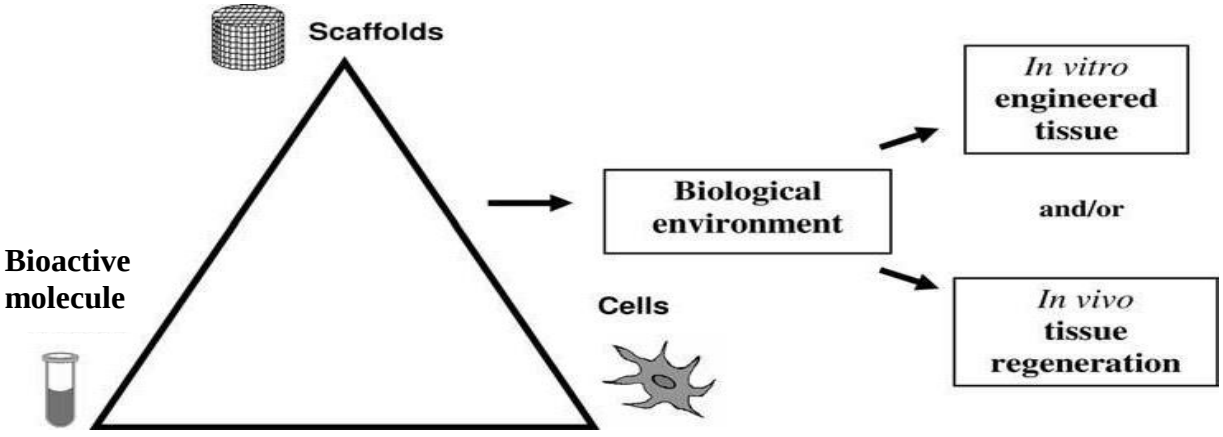


Fig 2.10. Three key elements of tissue engineering [100]

2.5.3.1. Scaffolds

It was proposed that cells might be unable to establish themselves properly within a defect area without any matrix to guide them[25]. The scaffold provides a 3D structure necessary to support cells to proliferate and maintain their differentiated function, and the scaffold architecture defines the ultimate shape of the new bone and cartilage[101-103] .

The role of the biomaterial scaffold in tissue engineering strategies is to operate as an artificial ECM, mimicking and recreating to some extent the structural organisation and functionality of the native ECM so as to guide cell response and promote appropriate tissue growth[100].

A number of scaffold materials have been investigated for tissue engineering of bone and cartilage including hydroxyapatite (HA) and natural polymers such as collagen and chitin[103].

The general roles of a scaffold can be characterized as: form, fixation, function and formation [104]:

- Form refers to the scaffold exterior geometry which fills arbitrarily complex defects.
- Fixation refers to the ability of a scaffold to surgically attach to the native tissue, providing stability and preventing scaffold loosening.
- Function refers to the need for the scaffold to temporarily perform the functions of the native tissue (mechanical, chemical and electrical function).
- Formation refers to the need for the scaffold to enhance tissue formation by providing the proper microenvironment.

Biomaterial used in orthopaedic applications must satisfy several important requirements:

- **Biocompatibility:**
  - Not elicit an unresolved inflammatory response, extreme immunogenicity or cytotoxicity [63,99,101,102,105].

- Be bioactive (either osteoinductive/osteoconductive or chondroinductive/chondroconductive depending on bone or cartilage) [100].

- **Mechanical properties:**
  - Especially important in orthopaedics are the initial mechanical properties of the biomaterials to be implanted [63,102] .
  - Providing appropriate support in the early stages of healing, graded load transfer is needed later in the process of formation of the replacement tissue[106].
  - Interact with their mechanical surroundings to effectively transmit mechanical signals to cells.
  - Mechanical stimuli have also been identified as extrinsic factors that can modify cell behaviour (i.e., differentiation, motility, contractility). The stiffness of ECM can have effects at a transcriptional level, guiding stem cells to specific lineage[107].
- **Controlled degradation:**
  - should degrade in a controlled manner and to facilitate load transfer to develop new bone [63,99,100]
- **Porosity:**
  - Possessing an interconnected pore structure (porosity exceeding 90%) to allow in vitro cell adhesion, and ingrowth [99,102]. Pore interconnectivity directly influences the diffusion of physiological nutrients and gases to cells as well as the removal of metabolic waste and by-products from cells [63,100,102].

- Larger cell distribution needs a high internal surface area to volume ratio. Since an increase in pore size gives rise to a decrease in internal surface area, a compromise must always be made [102].
- Pore size must be within a critical range (usually 100±200 μm): the lower bound is controlled by the size of the cells (~20 μm) while the upper bound is related to the specific surface area through the availability of binding sites[99].

- **Surface properties**:
    - Surface morphology, hydrophilicity, energy and charge affect *in vitro* cell adhesion, migration, phenotype, maintenance and intracellular signaling as well as *in vivo* cell recruitment and healing at the tissue-scaffold interface [102].
- **Sterilisability**:
    - Be easily sterilisable, the method of sterilisation must not interfere with the bioactivity of the material or alter its chemical composition [63,105].

2.5.3.2. Cells

Cells may be obtained from various sources at different stages of differentiation. The factors to take into consideration when selecting the optimal cell type include the proliferative capacity of the cells *ex vivo*, phenotypic stability, and immunogenicity. Fully differentiated autologous cells could serve as a reliable cell source, with minimal concern of immunogenicity, though their lack of proliferative capacity is a potential issue. The legal, political, and ethical questions regarding the use of embryonic stem cells has encouraged researchers to investigate alternative sources of stem cell, including the adult bone marrow, muscle, fat, and brain [101].

- **Mesenchymal stem cells**

Adult bone marrow is a major source of hematopoetic stem cells and non-hematopoetic stem cells, with the former required for the renewal of circulating blood cells. Non-hematopoetic stem cells are also known as mesenchymal stem cells (MSCs) [101], which as multipotent cells capable of differentiating along several lineage pathways [108] giving rise to bone, cartilage, muscle, ligament, tendon, adipose, and stroma [101].

Bone marrow derived stem cells serve as a potential source of autologous cells, suitable for our purpose of creating tissues of interest. However the main challenge with these cells is providing the optimal microenvironment for their growth *ex vivo* needed to create our desired structurally organised tissues[101].

2.3.5.3. Growth factors

Growth factors are proteins synthesised and released by cells which act as local regulators of nearby cells. Most growth factors are released at very low physiological levels [7].

Growth factors including bone morphogenic proteins (BMPs), transforming growth factors beta (TGF-β), insulin-like growth factors (IGF), fibroblastic growth factors (FGF), platelet-derived growth factor (PDGF) and vascular endothelial growth factor (VEGF) have the capability to act on both resident as well as transplanted cells. These growth factors can be attached to a scaffold by either covalent or non-covalent binding. The latter can be achieved by physical entrapment of the growth factor into the scaffold structure, its adsorption on the scaffold surface or through the formation of ionic complexes between the growth factor and the scaffold material [102].

Glycosaminoglycans (GAGs) play an important role in regulating the activity of growth factors, for instance by sequestering them within the matrix, preventing their degradation and presenting them to cell-surface receptors. Chondroitin Sulphate (CS) may also perform a similar function, including modulating the activity of cell-derived signaling factors[107].

2.6. Osteochondral tissue engineering

As mentioned earlier, due to the limitations of current clinical treatment techniques the concept of osteochondral tissue engineering and the simultaneous regeneration of bone and cartilage, has been of great interest recently; particularly as a method for promoting superior cartilage integration[109].

Joint damage that extends to the whole thickness of articular cartilage and penetrates into the subchondral bone has a unique repair response that differs from that of chondral defects[97]. Unlike the chondral repair mechanism, which is controlled by the intrinsic healing capabilities of the tissue's single cell source (the chondrocyte), the osteochondral defect healing processes requires progenitor cells from surrounding bone marrow to contribute to the regeneration of cartilage and the underlying bone tissue[110]. Once subchondral penetration occurs, immediately thereafter a fibrin clot is formed within the defect. It has been proposed that this deposit of fibrin serves as a scaffold which regulates the migration, proliferation and differentiation of the bone marrow mesenchymal progenitor cells[111]. These mesenchymal progenitor cells are then thought to differentiate into chondroblasts in the superficial regions of the defect and initiate the synthesis of matrix structural molecules. This is whilst in the immediate lower layers the mesenchymal progenitor cells promote bone formation (ossification) via endochondral

differentiation. The intermediate zone represents the formation of the chondral–subchondral interface. Osteoblasts derived from the marrow progenitor cells mediate the direct formation of bone via intramembranous ossification which occurs at the final depths of the defect[111].

It has been shown that the nature and structure of the repaired cartilage in osteochondral defects depends primarily on the host and is influenced by the location and size of the defect; the amount and viability of progenitor cells that infiltrate the defect, as well as the characteristics of cytokines and growth factors present during repair[112]. These factors affect the production of a range of repaired tissues in the defect site, varying from fibrocartilage to hyaline-like cartilage[113]. Inferior mechanical properties of the fibrocartilage produced during the healing process will lead to further degeneration of the repaired tissue and the surrounding articular cartilage[114].

The mechanisms underlying the lack of formation of hyaline cartilage is far from clear, although it has been suggested that inadequate progenitor cell recruitment and viability as well as contradicting cytokine signaling may be responsible[112]. In order to facilitate the regeneration of hyaline cartilage via an osteochondral tissue engineering strategy, it may be necessary to utilize the body's natural repair mechanisms. Appropriately directed growth factor signaling and biological cues, could stimulate superior hyaline-like cartilage formation rather than fibrocartilage at the defect site[112].

As described above, the role of biomaterials scaffold in tissue engineering is to act as an artificial ECM, simulating the structural organisation and mechanical function of the native ECM, so as to guide cell response and stimulate tissue formation. A large number of scaffolding materials and fabrication methods have been developed and studied for cartilage and bone tissue engineering individually.[115,116]Nonetheless, the criteria for scaffold design for osteochondral tissue

engineering, including a hybrid of both cartilage and bone, is more complicated compared to the formerly explored single tissue type strategies.

2.6.1. **Scaffold design considerations for osteochondral tissue engineering**

There are several fundamental parameters to be considered for tissue engineering of scaffolds (See Section 2.5.3.1). These are necessary to optimise cell attachment and proliferation as well as subsequent tissue growth. These criteria dictate the choice of biomaterials and fabrication methods used for individual tissue engineering applications. For osteochondral scaffolds, additional design criteria must be taken into consideration to simultaneously allow the best possible growth for the two independent tissues involved[100].

Various analytical and computational modelling techniques have been employed to design the ideal scaffold for osteochondral tissue engineering by optimizing the previously mentioned properties required for scaffolds[117,118] . It was shown by computational simulations that the optimal scaffold for osteochondral applications may need depth-dependent mechanical properties and permeability[118]. It was also proposed that scaffold material properties suitable for *in vitro* culture may not necessarily be appropriate for *in vivo* applications[118], thus implying that the scaffold representing an artificial ECM should mimic the properties of the native ECM of the host tissue for best outcomes. For osteochondral tissue engineering, it is also necessary to develop a structure with a gradient of mechanical and structural properties, so as to imitate the zonal regions of articular cartilage. The feasibility of this will be highly dependent on the emergence of novel fabrication approaches such as the solid free form (SFF) fabrication techniques[100].

To mimic natural osteochondral structures, the design of the calcified cartilage region that represents the transition and interface between the bone and cartilage tissues. Even variations within the subchondral bone layer itself may also be of importance [100].

2.6.1.1. Single phase scaffolds

The earliest generation techniques used for osteochondral tissue engineering were the single-phase scaffolds. They were composed of a single material (Fig 2.11) and designed to fit the shape of the defect area, using materials such as hydroxyapatite or polymers like poly (lactic-co-glycolic acid) and polycaprolactone [119-121]. Scaffolds made from these materials have different ideal degradation rate, strength and porosity to appropriately simulate the properties of the surrounding tissue and facilitate the timely reconstruction of the host tissue. Structurally, a single phased scaffold contains the same materials with the same proportions throughout the scaffold. It could also contain several materials mixed together, including a polymer combination or the addition of a gel phase throughout the pores of the scaffold[122]. Single phase scaffolds support chondrocyte and osteoblast cell attachment and proliferation, however, they lack the inherent physical structure required for the repair or regeneration of osteochondral tissue[123].

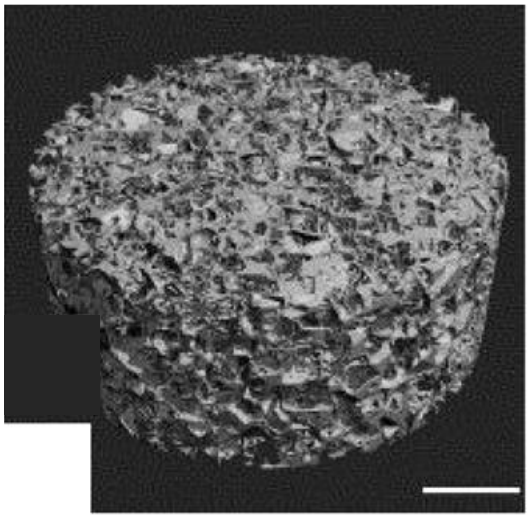


Fig 2.11. Single phase scaffold fabricated through compression molding[9]

2.6.1.2. Biphasic (Bilayered)

In order to mimic the structure of osteochondral tissue the use of bilayered scaffolds has been widely investigated. Bilayered scaffolds can significantly improve the integration between cartilage and bone due to the enhanced scaffold fixation in the subchondral region as well as providing the enhanced repair conditions for cartilage and bone tissue. The highly challenging problem of cartilage and bone layer integration has led to the development of numerous bilayered scaffold designs; however, complete success in tissue regeneration remains to be achieved [100].

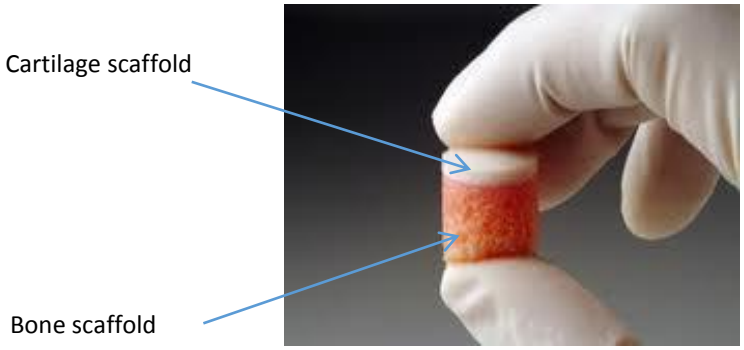


Fig 2.12. Bilayered osteochondral scaffold[124]

Bilayered structures (Fig 2.12) are preferred over single phase for a number of fundamental reasons. Firstly, bilayered scaffolds provide variations in mechanical, structural and chemical characteristics in each layer which subsequently leads to the creation of optimised, tissue-specific biological environments in each respective layer. This means that the bilayered scaffold can be constructed to more closely mimic the native ECM for each tissue type, rather than creating a construct that compensates for the functional requirements of both cartilage and bone in a single structure. Moreover, homogenous and heterogeneous single phase scaffolds, despite some satisfactory results[125,126], fail to inhibit the action of growth factors which induces angiogenesis and up growth of osseous (bony) tissue into the cartilage region. In contrast bilayered scaffolds owing to their characteristic interfacial region avoid this problem, by providing a superior means of segregating loaded bioactive molecules in cartilage and bone layer whilst also allowing for a straightforward cell seeding process for *in vitro* cell culture.[100]

The bilayered scaffolds have been classified into three unique types [100]: type 1- cartilage tissue on bone scaffold; type 2 - assembled bilayered scaffolds; type 3 - integrated bilayered scaffolds. These are further described below.

- **Scaffold type 1—cartilage tissue on bone scaffold**

In type 1 bilayered scaffold, chondrocytes or new cartilage tissue is directly seeded onto a bone scaffold base. It is obtained by forming a cartilage tissue on top of a subchondral construct to create the secondary layer. It has been suggested that this cartilage layer -having its own ECM- immediately integrates with native host cartilage. The underlying bone substrate on the other hand has been incorporated into the bilayered design to provide proper fixation at the defect site, thereby assisting cartilage integration with the host. This method was originally used in a brief (2 weeks) in vitro investigation, as part of which isolated chondrocytes were seeded and cultured on top of an osseous scaffold composed of calcium phosphate crystals infused in a collagen sponge matrix[127]. Although chondrocyte proliferation was observed, structural investigations using scanning electron microscopy (SEM) exhibited very little evidence of cartilage growth. More extensive investigation into this scaffold strategy was performed by other groups, where isolated porcine articular chondrocytes were seeded and cultured on top of three routinely utilised biomaterials.[128] The subchondral scaffolds were made of poly-L-lactide, poly-D, L-lactide, and collagen hydroxyapatite. The outcome of these studies was that the collagen–hydroxyapatite scaffold performed best, particularly in terms of cell viability, implant morphology, and integration between the neocartilage and the scaffold. However these findings were not confirmed in vivo under normal physiological conditions. The first in vivo study using this approach was conducted using b-tricalcium phosphate (b-TCP) as the subchondral base by Guo *et al*. in a sheep model [129]. The findings from this study suggested that hyaline-like cartilage could be detected 24 weeks after the implantation of the bilayered scaffold into a shoulder defect. Despite the short term success of these studies, long-term studies would be required to

justify the effectiveness of this ceramic base scaffold. A more recent investigation by Kandel *et al*. sought to use the type 1 bilayered strategy to form a region or zone of calcified cartilage in vitro to improve the mechanical integrity (i.e. shear properties) of the cartilage layer[130]

- **Scaffold type 2—assembled bilayered scaffold**

Perhaps the most widely explored strategy for bilayered scaffolds involves the use of single individual scaffolds for the bone and the cartilage layers that are subsequently joined together either before or during surgical implantation[123]. This strategy can be as simple as combining together two predefined bone and cartilage scaffolds that have been previously shown to promote satisfactory growth of their individual tissues, using innovative fabrication methods that have been developed to produce two separate and independent scaffolds and combine them simultaneously[123]. The first reported investigation of this scaffold type used fibrin glue gel to suspend isolated chondrocytes in the cartilage layer that was placed on top of an underlying hydroxyapatite scaffold[131].

- **Scaffold type 3—integrated bilayered scaffold**

The use of an integrated structure which enables a complete transition between the bone and cartilage layers without requiring a joining mechanism represents the third category of bilayered scaffolds. Unlike traditional heterogeneous scaffolds, these bilayered structures incorporate various components to form unique composite layers for bone and cartilage[123]. Bilayered scaffolds represent an appropriate strategy for osteochondral tissue engineering. However, more long-term in vivo investigations will be required to accurately determine important parameters that are required to process the optimal scaffolds for successful osteochondral defect regeneration[123].

2.7. Basis and aims of this research

This research is based on the scaffold preparation and characterisation techniques developed at the Biomaterials Group, Department of Materials, University of Oxford. Monomeric collagens were extracted and prepared by the University of Tennessee's Collagen Research Group of the Veterans Affairs Medical Centre Research Service.

A notable approach to engineering a tissue that arose from the literature was to simulate the natural structure, composition and biology of the target tissue (in the case of this study: cartilage and bone). For osteochondral tissue engineering, the separate design and manufacturing of bone and cartilage scaffolds often leads to scaffold loosening, due to the inability of renewed cartilage to fully integrate, on a biological and mechanical level, with the surrounding tissue. A further limitation is that the regenerated tissue tends to have inferior mechanical properties. As such, it was proposed that the fabrication of osteochondral scaffolds – including both cartilage and subchondral bone – may offer a solution for both integration with the host tissue and recruitment of the MSCs residing in the subchondral bone.

From the literature on scaffold material used for bone and cartilage TE, collagen is most frequently used for this purpose in its insoluble, naturally fibrillar form. However, do to this, several issues can arise: the existence of crosslinks can lead to batch variation, and the existence of telopeptides can cause antigenicity. Consequently, the soluble form of collagen 'atelocollagen' was proposed in this research as an alternative material. To the author's knowledge, few studies have produced atelocollagen reconstituted fibrillar types II scaffolds with CS incorporation for cartilage and tropocollogen with hydroxyapatite for bone scaffold, while systematically

characterising both in terms of their properties. Yet, only a limited amount of CS can be attached to collagen due to a restricted number of attachment sites. As a proposed solution, CS was polymerised to produce a higher molecular weight substitute (PCS). The polymerisation of CS is a novel approach, as no previous scaffolds had to date been produced from crosslinked reconstituted fibrillar collagen II combined with PCS for cartilage TE.

Therefore, the development of novel conjugated monomeric types I and II collagen scaffolds (with introduction of HA and PCS respectively) for bone and cartilage TE was identified as the logical next step to address this gap in the literature.

Thus, the principal aims of this research are as follows:

1. The polymeristion of chondroitin sulphate, as well as determining its molecular weight and rheological properties

2. To develop layers of osteochondral scaffolds that correspond to both bone and cartilage, by firstly following the natural structure and composition of the bone and cartilage interface, and secondly by using different types of collagen (types I and II), as well as other major components of these tissue (i.e. hydroxyapatite and PCS)

3. To investigate the properties of the porous, composite scaffolds fabricated from the reconstituted fibrillar form of collagens (in terms of their structures, microstructures, mechanical properties and rheological properties), and to evaluate the stem cell response to these scaffolds

Chapter 3. Techniques

3.1. Introduction

In this chapter, the characterisation techniques used in the current study are described. The experimental procedures include rheology of collagen suspensions (Section 3.2), analysis of functional groups in a compound by Fourier Transform Infra-Red (FTIR) and X-ray photoelectron Spectroscopy (Section 3.3 & 3.4), polymer size measurement using Dynamic Light Scattering (DLS) (Section 3.5), hydroxy-apatite size measurement using X-ray diffraction (XRD) (Section 3.6), analysis of scaffolds microstructure using Scanning Electron Microscopy (SEM) (Section 3.7) and mechanical testing (Section 3.8).

3.2. Rheology

Rheological properties of a suspension describe the flow behaviour of the fluid and varies based on the molecular structure, molecular weight and molecular weight distribution of the fluid. Analysis of the viscoelastic behavior of a suspension helps to understand the formation of ice crystals during freezing of the suspension and helps to control the final scaffold microstructure and hence mechanical and biological properties.

A rheometer measures the rheological properties of a complex fluid as a function of rate or frequency of deformation.

The flow behavior and viscoelastic properties of suspensions, including storage modulus (G'), loss modulus (G"), complex modulus (G*) complex viscosity (η*), and loss tangent (tanδ) were determined by performing dynamic frequency test, using an Anton Paar 301 with plate-plate geometry according to Equations 3.1, 3.2, 3.3 and 3.4:

$$(t) = \gamma_0[G'(\omega)sin(\omega t) + G''(\omega)cos\,(\omega t)] \qquad \text{(Equation 3.1)}$$

Where shear stress (σ) produced by a small amplitude deformation is proportional to the amplitude of the applied strain (γ_0), which is sinusoidally varying in time (t). The regime of small amplitude straining in which stress can be represented by this equation is called the linear viscoelastic region[132].

$$\tan\delta = G''(\omega)/G'(\omega) \qquad \text{(Equation 3.2)}$$

Where tanδ is the loss tangent based on loss (G'') and storage (G') moduli.

$$G^* \equiv G' + iG'' \text{ and therefore, } |G^*| = \sqrt{G'^2 + G''^2} \qquad \text{(Equation 3.3)}$$

Where G* is the complex modulus of a viscoelastic material based on storage (G') and loss (G'') moduli.

$$\eta^* = \eta' + i\eta'' \qquad \text{(Equation 3.4)}$$

Where η^* is the complex viscosity, $\eta' = G''/\omega$ and $\eta'' = G'/\omega$, and therefore,

$$|\eta^*| = \sqrt{\eta'^2 + \eta''^2}$$

The measuring head for the Toolmaster © was 50mm and the gap between the cylinder head and the base was set to 1mm. A few drops of the suspension was pipetted into the gap, the head was lowered and its surrounding was trimmed. Temperature was controlled at 20°C with a Peltier temperature control with accuracy of ±0.1°C. Dynamic frequency sweeps were conducted within LVR, at 1% strain with angular frequency of 0.1 to 100%.

3.3. Fourier Transform Infrared Spectroscopy (FTIR)

FTIR spectroscopy is a useful analytical technique used to probe the functional groups/chemical bonds of a compound, in which the transmission of infrared light through a thin section of specimen is measured as a function of wavelength. Detection of the transmitted IR light specified

the amount of energy absorbed at each wavelength. Each wavelength is characteristic of a specific resonant bond vibration which makes the IR spectra a useful method for determining chemical bonds present in a specimen. The resonant bond vibrations include symmetrical/ antisymmetrical stretching, scissoring, rocking, wagging and twisting.

Infrared absorption at specific wavelength (A) is related to the concentration of the different molecular species(c) in a sample according to Beer-Lambert law:

$$A = \log_{I0} I = \varepsilon bc \qquad \text{(Equation 3.5)}$$

Where ε is the wavelength - dependent absorptivity coefficient, b is the optical path length of light, i.e. thickness of the sample section, and I and I_0 are intensities of sample and reference, respectively[133].

Fourier transform infrared (FTIR) spectroscopic imaging is one of the firmly established experimental techniques for the analysis of secondary structure of polypeptides and proteins. Nevertheless, analysis of FTIR spectroscopic data is complex since absorption peaks of different components often overlap with each other[134]. To address this issue, second derivative spectroscopy was used which improved the separation of overlapping peaks. Here, the registered raw spectrum is numerically differentiated twice. The peak frequency is identical to the original one and the intensity of the second derivative is proportional to the original peak intensity[135]. The second derivative spectra are calculated by using Savizky – Golay algorithm in OriginPro 9.1 software. The samples were analysed in the absorbance mode at 4 cm^{-1} resolution 64 times over the range of 500 – 4,000 cm using an Agilent FTS 3500 Excalibur.

3.4. X-ray photoelectron spectroscopy (XPS)

X-ray photoelectron spectroscopy is a quantitative surface analysis technique that used to determine the chemical composition of a material to a depth of around 10 nm. X-ray photons are fired onto the specimen, which excites and ejects electrons at specific binding energies depending on the spatial configuration of electrons in the atoms (e.g. 1s, 2s, 2p…)[136]. To obtain a spectrum, the energy of this phenomenon (binding energy) and the number of electrons emitted are recorded.

Samples were analysed using a Thermo Scientific K-Alpha XPS instrument equipped with a microfocussed monochromated Al X-ray source. The source was operated at 12 keV and a 400 micron spot size was used. The analyser operates at a constant analyser energy (CAE) 200 eV for survey scans and 50eV for detailed scans.

Charge neutralisation was applied using a combined low energy / ion flood source. The data acquisition and analysis was performed with Thermo Scientifics Avantage software. Peak fitting (Lorentzian / Gaussian (L/G) 30%) was applied following removal of a Smart background. Normalised atomic percentages were determined from peak areas of the elemental main peaks detected on the survey scan following background subtraction and application of Thermo sensitivity factors.

3.5. Dynamic light Scattering (DLS)

Malvern ZetaSizer is a non-invasive technique and provides information about size and particle size distribution (PSD) of particles and molecules dispersed and dissolved in a liquid. The ZetaSizer performs size measurements using a process called Dynamic Light Scattering. DLS also known as

Photon Correlation Spectroscopy (PCS) measures Brownian motion and relates it to the size of the particle. The instrument has a laser light source and the particle is illuminated with the laser. The generated scattered light fluctuates at a speed depending on the particle size. With the velocity of the Brownian motion, derived from the analysis of these fluctuations, and the Stokes-Einstein equation, particle size can be obtained.

$$d\,(H) = kT/\,3\pi\eta D \qquad \text{(Equation 3.6)}$$

Where d (H) is hydrodynamic diameter, D is translational diffusion coefficient (the velocity of the Brownian motion), k is Boltzmann's constant, T is absolute temperature and η is viscosity.

The particle size of chondroitin sulphate (CS) and polymerised chondroitin sulphate (PCS) was measured by a Malvern ZetaSizer Nano ZS (size range: 0.3 nm to 10 µm). To obtain the average diameter, a cuvette was filled with 1 ml of the CS /PCS suspensions in water (1 % w/v) and inserted in the instrument. 5 measurements were performed and the mean particle size was calculated.

3.6. X-ray diffraction analysis (XRD)

X-ray diffraction analysis is used to characterise crystallographic properties of powder materials including crystal phase, size and texture. A monochromatic X-ray beam is applied on a sample at specific angles and the diffracted intensity of the X-rays of specific lattice planes of the crystals is measured[137].

X-ray diffraction (XRD) analysis was carried out using a fully automated Bruker D8 powder diffractometer employing copper ka radiation (l = 0.15406 nm) and an energy dispersive silicon detector. Samples were prepared by spreading onto a low background Silicon single crystal

smeared with grease and then scanned using a step size of 0.02°2θ between the range of 10° - 80°2θ with a data collection time of approximately 30 minutes (for HA powder and XCol1-HA1) and 1hr for XCol1-HA2. Sample rotation was used in all samples. Phase id analysis was carried out using the BRUKER AXS *Diffrac EVA* software package along with the ICDD powder diffraction database.

The crystalline size, t of the commercial and synthesized HA was calculated from the XRD pattern using the Debye-Scherrer equation[138].

$$B = 0.9 \lambda / t \times \cos \theta \qquad \text{(Equation 3.6)}$$

Where B is the Full Width at Half Maximum (FWHM) of the peak (002), λ = 0.15418 nm (Cu Kα radiation source), θ is the peak diffraction angle and t is the crystallite thickness.

3.7. Scanning electron microscopy (SEM)

Scanning electron microscopy was used to examine the microstructure and pore sizes of scaffolds. SEM images a surface by scanning it via a focused electron beam. The electrons in this study were produced from a tungsten filament, which were then accelerated towards the specimen through a controlled magnetic field. Secondary electrons emitted back from the specimen were then collected and processed into an image. Specimens were cut horizontally by sharp medical scalpel, mounted on SEM stubs and coated with gold using a Bio-Rad ES400 sputter coater at 20mA for 45 seconds. A Zeiss EVO SEM was operated at the accelerating voltage of 10 kV and probe current of 100 pA and images of different magnifications were taken in order to distinguish any hierarchical microstructure. The pores were measured by using the image processing software ImageJ.

3.8. Compression test

The compression test has been widely established for evaluating the mechanical strength of porous scaffolds. Compressive modulus is particularly important when the scaffold is implanted into a defect site, as it must withstand the forces generated by surgeon during press-fitting. Besides, the mechanical properties of scaffolds can influence the behaviour of cells in vitro and in vivo.

Stress-strain behavior and compressive modulus of scaffolds were measured using Zwick Mechanical equipped with a 5N cell load operated at the crosshead speed of 5 mm/min. All compression tests were conducted perpendicular to the plane of the scaffold disc in a dry state. Tests were repeated on average 5 times to achieve mean data. The compressive modulus of scaffolds obtained as the slope of the linear region of stress-strain curves.

Chapter4. Polymerisation of Chondroitin Sulphate

4.1. Introduction

Chondroitin sulphate (CS) is one of the major Glycosaminoglycans (GAGs)[139]. GAGs are linear polymers comprising disaccharide residues and are found as the side chains of proteoglycans (PGs) in the extracellular matrix or at the cell surface[140] (See Section 4.2). A number of studies have shown the stimulatory effects of CS on cell proliferation, differentiation, migration and cell morphogenesis and it is widely used in the tissue engineering of cartilage, neurons, skin and also in drug delivery devices[141-144]. However, it is difficult to incorporate sufficient CS into collagen based scaffolds to take full advantage of its benefit (See Section 5.4.5). In this study, chondroitin sulphate has been polymerised (PCS) in an attempt to increase the amount of CS that can be contained in the scaffold. The molecular size of CS and PCS were measured using dynamic light scattering (DLS) system and their viscoelastic properties were determined by rheology experiments. The molecular weight of PCS was obtained using two different methods: Einstain's Equation based on DLS results, Mark Houwink Equation based on rheological results. Fourier transform infra-red (FTIR) spectroscopy together with X-ray photoelectron spectroscopy (XPS) were carried out to obtain information about the chemical structure and elemental composition of CS and PCS. Scaffolds of CS and PCS were then prepared using casting and freeze-drying techniques and they were analysed in terms of their microstructure and mechanical properties.

4.2. Chondroitin sulphate chemical structure, stimulatory effects and challenges in cartilage tissue engineering

Chondroitin sulphate is a key component of cartilage extracellular matrix (ECM). It is considered a member of the Glycosaminoglycans (GAGs) family and is an unbranched sulphated, highly

water soluble anionic polysaccharide. The chain is composed of sulphated, negatively charged, repeating disaccharides, N-acetylglucosamine or N-acetylgalactosamine and glucuronic acid as the second sugar residue [140] (Fig 4.1).

It has been demonstrated that the incorporation of chondroitin sulphate (CS) in scaffolds for cartilage tissue engineering induces the chondrogenic differentiation of mesenchymal stem cells (MSCs)[141]. CS provides a microenvironment which enhances clustering of cells (pre-cartilage condensation of mesenchymal cells), upregulates cartilage specific genes, and provides cell-mediated degradable sites for the cell clusters to grow further and produce ECM[141]. Studies have also demonstrated that CS increases the compressive stiffness of collagen scaffolds[145].

Despite these advantages, there has been a challenge in incorporating CS into biopolymer based scaffolds such as collagen. There are limited binding sites on a collagen molecule for CS attachment (carboxyl group of CS attaches to amine group of collagen), thus the amount of CS attached to collagen cannot exceed a limited amount (See Section 5.4.5). Moreover, CS is water soluble and dissolves in cell culture medium within the early hours of culturing (See Section 5.4.5). We aim to solve this problem by polymerising CS; it is expected that the higher molecular weight CS would be water insoluble and should not be readily washed away during the cell culture process; and additionally, would provide an increase in the number of potential cell attachment sites due to a longer chain length or increased number of side chains. We hypothesize that PCS can further increase viscoelastic properties of scaffolds which lead to an increase in scaffolds stiffness and biostability after implantation (See Section 5.4.1 & 5.4.6).

A number of studies have been carried out on scaffolds composed of a combination of biopolymers with CS[145-149]; but to the best of our knowledge no study has been previously done

on scaffolds made purely of CS. Scaffolds of only CS and PCS were fabricated in this research and their structures and mechanical properties were investigated.

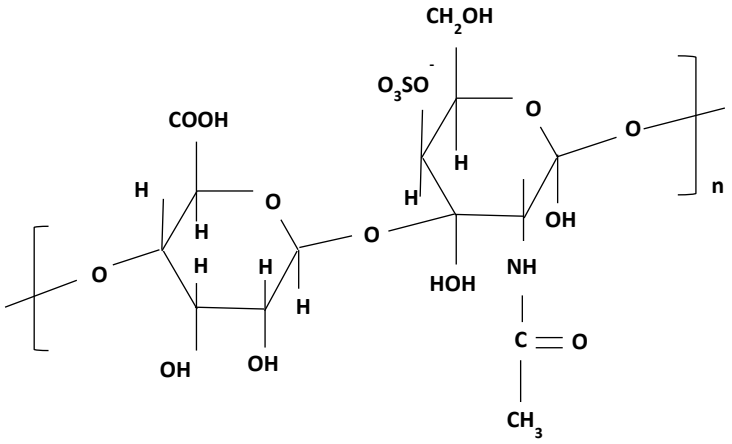


Fig 4.1. Chondroitin sulphate chemical structure

4.3. Polymerisation of chondroitin sulphate

There are a number of studies on the synthesis of oligo- and poly-saccharides by chemical[150-155] and enzymatic methods[156-158]. There is also a patent on producing water insoluble polysaccharides by using a cross-linking agent[159] and also on producing polysaccharides by polycondensation of saccharides in the presence of carboxylic acid catalysts at reduced pressure[160].

From the existing methods for polymerisation of a saccharide, two chemical methods were selected. Solid-state polycondensation which is also called powder to powder polycondensation or anhydrous melt polymerisation is a method used for the polymerisation of natural saccharides. The reaction was found to take place in the presence of a catalyst (P_2O_5) under reduced pressure (or under nitrogen flow) [161]. This method of polymerisation was implemented to CS at the

temperature of 100˚C in a vacuum oven (Heraeus vacutherm) at pressure below 20 kPa. The product was a black mass showing that CS was oxidised. This was decided therefore that the solid-state polycondensation is not an appropriate method for polymerisation of CS.

Polycondensation of natural saccharides[162] was the second method investigated, in which saccharides are heated above their melting points in the presence of acid catalysts to produce branched polysaccharides, such a method has been adopted in this research.

4.3.1. Materials and Method

The chain length polycondensation/ chain crosslinking was conducted by heating CS (Sigma Aldrich, UK) in deionised water in the presence of phosphoric acid (Sigma Aldrich, UK) as a catalyst. In order to obtain the highest amounts of PCS in the form of precipitate, the proportions of acid, water and CS were varied. The baseline reaction temperature was 150˚C following the reaction temperature range offered for the polymerisation of saccharides[163]. After several iterations, the optimum amount of reagents with the least reaction duration (3 hrs) was found to be 5g CS, 150 ml water and 0.1ml phosphoric acid, which produces a relatively higher amount of precipitate by visual inspection. The reaction took place in a Pyrex beaker covered by aluminum foil (to prevent water loss by evaporation) on a hot plate (IKA RCT basic) at 150˚C and results in two separate phases of solution and precipitate. The precipitate was separated from the solution by centrifugation (Thermo Scientific, CL10 centrifuge). The precipitate was then washed with deionised water, frozen at -20 C (Zanussi, DF 50/16) and freeze dried (Christ Alpha 1-5).

4.3.2. Fabrication of scaffolds

Porous scaffolds of CS and PCS were fabricated using a freeze-drying technique. A dispersion was prepared by adding 0.1g of CS or PCS in 10 ml deionised water. CS was observed to be soluble while PCS formed a uniform suspension. The mixture was subsequently poured into cylindrical moulds (height: 9.4 mm, internal diameter: 13.8 mm, thickness: 1.8 mm) made of PTFE (Fig 4.2.) The moulds were then frozen at -20˚C overnight (Zanussi, DF 50/16) and freeze dried (Christ Alpha 1-5) for 24 hours. During freeze drying ice crystals sublime and the porous structure is achieved.



Fig 4.2. PTFE moulds, one end is sealed

4.4. Results

This section describes the outcomes of FTIR and XPS spectroscopy (Section 4.4.1 & 4.4.2). Dynamic light scattering and rheology results are shown in sections 4.4.4 and 4.4.5 respectively and are used to obtain the molecular weight of PCS (Section 4.4.3). Rheological behavior of CS and PCS dispersions, their complex viscosity and moduli in a dynamic frequency sweep test evaluate in section 4.4.3.2.

4.4.1. Fourier Transform Infra-Red Spectroscopy (FTIR)

FTIR spectroscopy has been conducted on CS and PCS to examine any possible peak shifts or new bond formation. (Fig 4.3)

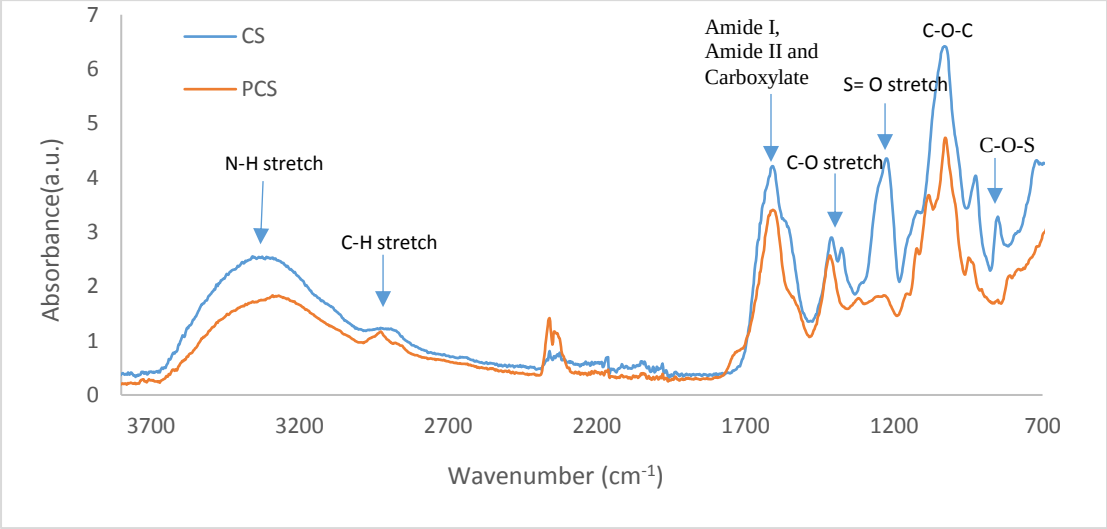


Fig 4.3. FTIR spectra of CS and PCS (n=3), normalised spectra against C-H band

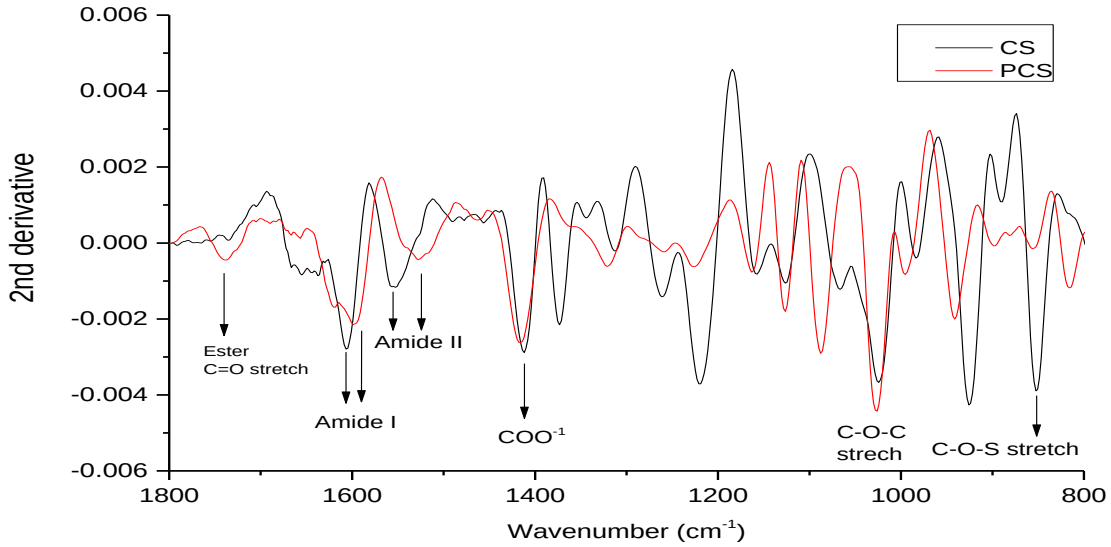


Fig 4.4. Second derivative FTIR bands of CS and PCS, The peak shift to higher wavenumbers and the increase in peak intensity for C=O bond (2.2 times) as well as the increase in peak intensity for C-O-C bond (1.4 times) both indicate the occurrence of polymerisation in PCS

Band Assignment	CS	PCS
Amide A (N-H stretching)	3321	3315
C-H stretching	2912	2922
Amide I (C=O stretching)	1604	1595
Amide II (C-N stretching, N-H bending)	1552	1525
COO^- (Ester bond)	1728	1736
C-O stretching	1406	1411
O-H bending	1370	1309
S=O stretching	1220	1224
C- O-C stretching	1018	1020
C-O-S stretching	850	852

Table 4.1. FTIR band assignment for CS and PCS

The FTIR spectra of CS and PCS depicted in Fig 4.3 were normalised against the C-H stretch band (which was assumed to remain unchanged by polymerisation). The FTIR spectrum of CS exhibits O-H and N–H stretching (amide A) vibrations at 3,321 cm^{-1} in which the O-H stretching vibration is overlapped by N–H stretching; the C–H stretching of methyl or methylene group at 2,925 cm^{-1}; the stretch vibrations of C–O at 1,020 cm^{-1}; the band at 1,602 cm^{-1} corresponding to amide I, amide II and carboxylate which are overlapped (these peaks are decomposed by deconvolution in Origin Pro 9.1 software and depicted in Fig 4.4); the band at 1,406 corresponding to C–O stretch vibration; the peak at 1,220 cm^{-1} corresponding to the stretching vibrations of S=O bond (SO_4^{2-})

(which is used as a characteristic peak of CS[164]). These bands are all present in the FTIR spectrum for PCS with a shift in wavenumbers (Tabulated in table 4.1). Amide A, Amide I and amide II bands were down shifted to 3315, 1595 and 1525 cm^{-1} in PCS which indicates weaker N-H bonds in PCS. Carboxylate band shifted to a higher wavenumber of 1736 cm^{-1} signifying that the C=O bond is stronger/shorter in PCS than CS. S=O, C-O, C-O-C and C-O-S stretching bands did not change significantly. The significant increase in C=O (2.2 times) and C-O-C bands (1.4 times) in PCS IR spectrum supports that polymerisation has taken place.

4.4.2. X-ray photoelectron spectroscopy

The chemical composition of PCS and CS was further characterised by X-ray photoelectron spectroscopy (XPS). Survey scans of sample powders identified peaks correspond to C1s (286 eV), O1s (532 eV) and N1s (400 eV) as the main constituents of CS and PCS (Fig 4.5). The presence of sodium in the spectra could be due to the use of chondroitin 4-sulfate sodium salt as the material tested.

Table 4.2 shows the atomic percentage of PCS and CS. It is revealed that the atomic percentage of carbon significantly increased for PCS, whereas oxygen and sodium percentage slightly decreased. C (1s) peak analysis of PCS and CS (Fig 4.6) showed a higher concentration of COO^- (ester bond) and C-O which supports the polymerisation of CS by the formation of ester bond (side branches) and along the polymer chain (chain length polymerisation). This result is in agreement with the FTIR result and further confirms that the polymerisation has occurred.

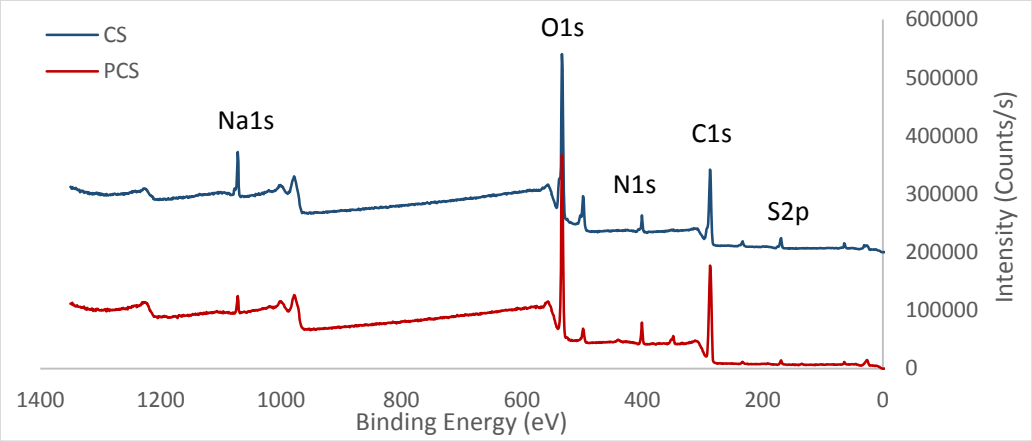


Fig 4.5. Survey scan XPS spectra of CS and PCS (n=3)

Name	Peak center (eV)	CS atomic %	PCS atomic %
O1s	532.7	39.85	34.84
C1s	286.9	46.7	55.64
Na1s	1071.9	4.82	1.66
N1s	400.18	5.7	5.76
S2p	169.32	2.9	2.05

Table 4.2. XPS atomic analysis of CS and PCS (n=3); significant increase in C1s for PC

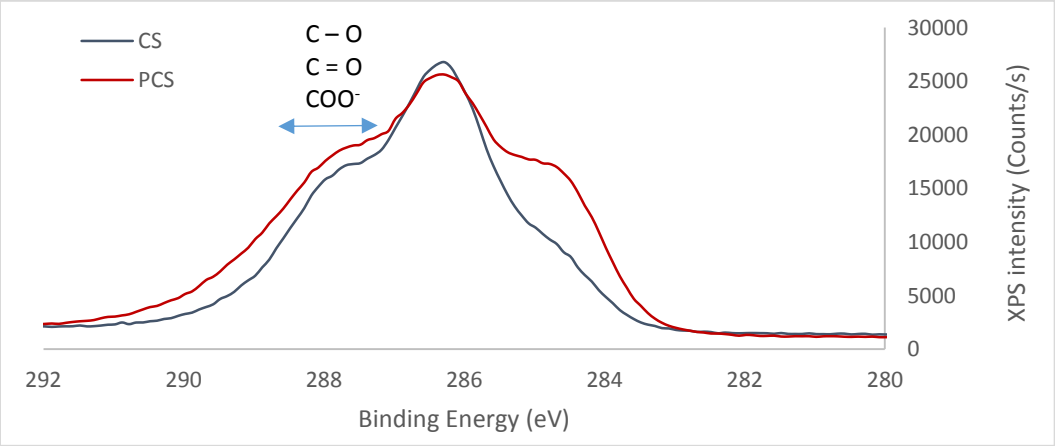


Fig 4.6. The C (1s) XPS regions of PCS and CS; higher concentration of COO^- (ester bond) and C-O supports for PCS supports polymerisation has occured

4.4.3. Dynamic light scattering

Dynamic light scattering (DLS) were performed to measure the average diameter of CS and PCS in deionised water. The average diameter of CS and PCS were found to be 551 and 2871 nm respectively (Table 4.3). The average PCS size significantly increased ($p< 0.001$) by polymerisation (5.2 times). This results together with FTIR and XPS confirmed the occurrence of polymerisation. Furthermore, the hydrodynamic radius obtained by DLS aids to calculate the molecular weight of PCS using the Einstein's viscosity relation[165] (Equation 4.1).

$$\eta = 2.5\ N\ V_e\ /M \qquad \text{(Equation 4.1)}$$

Where η = viscosity of polymer solution, M = polymer molecular weight (g/mol), N = Avogadro's number, and Ve = the volume of an equivalent spherical particle (cm^3).

Viscosity of CS and PCS will be shown in the following section and molecular weight of PCS will be determined and compared by two different methods: Mark Houwink equation, Einstein viscosity relation.

Sample	Average Diameter (nm)	Standard Deviation
CS	551	± 125
PCS	2871	± 494

Table 4.3. Average particle diameter for CS and PCS; significant increase in PCS diameter

4.4.4. Rheological experiments

Rheological properties of suspensions can be helpful to further explain the chemical bonding investigated by FTIR and XPS in previous sections and will aid to illuminate the microstructure and mechanical properties of scaffolds in the following sections. Rheological tests in two different conditions have been performed on CS and PCS solutions. First, to obtain the viscosities of CS and PCS, oscillatory shear test has been conducted to measure the molecular weight of PCS. Second, the viscoelastic properties of solutions, including storage modulus (G'), loss modulus(G"), complex modulus (G*) and complex viscosity (η*) were determined using oscillation frequency sweep over an angular frequency range.

4.4.4.1. Molecular weight of PCS based on rheology test

In this section, the molecular weight of PCS will be obtained based on the viscosity of polymer and using the Mark -Houwink equation. The polymer solutions were prepared by dissolution of CS/PCS in 0.2M NaCl solution. Mark-Houwink constants were found in the literature which were determined using size exclusion chromatography (SEC). 0.2 M NaCl is the solvent used for SEC, thus this solvent was used for the following viscosity measurements.

The dynamic viscosity of CS and PCS solutions in 0.2M NaCl at the constant shear rate of 100/s and temperature of 25 °C was measured by a rheometer (Fig 4.7) using a flat plate (50mm diameter). At low concentrations of a polymer it is usual to assume that the intrinsic viscosity equals the inherent viscosity[166] (Equation 4.2).

$$\eta = \lim_{C \to 0} \frac{\eta_i}{C} = \lim_{C \to 0} \eta_{inh} \qquad \text{(Equation 4.2)}$$

To identify a sufficiently low concentration at which inherent and intrinsic viscosity can be assumed to be equal, the dynamic viscosity of CS at different concentrations was measured (Fig 4.8).

There is a linear relation between viscosity and concentration at concentrations higher than 0.1 (g/ml), yet viscosity remains relatively constant at concentrations lower than 0.05. The concentration of 0.01 (g/ml) was taken to be sufficiently dilute to allow the use of Equation 4.2. Therefore, solutions of CS and PCS with concentration of 0.01 were prepared for rheology.

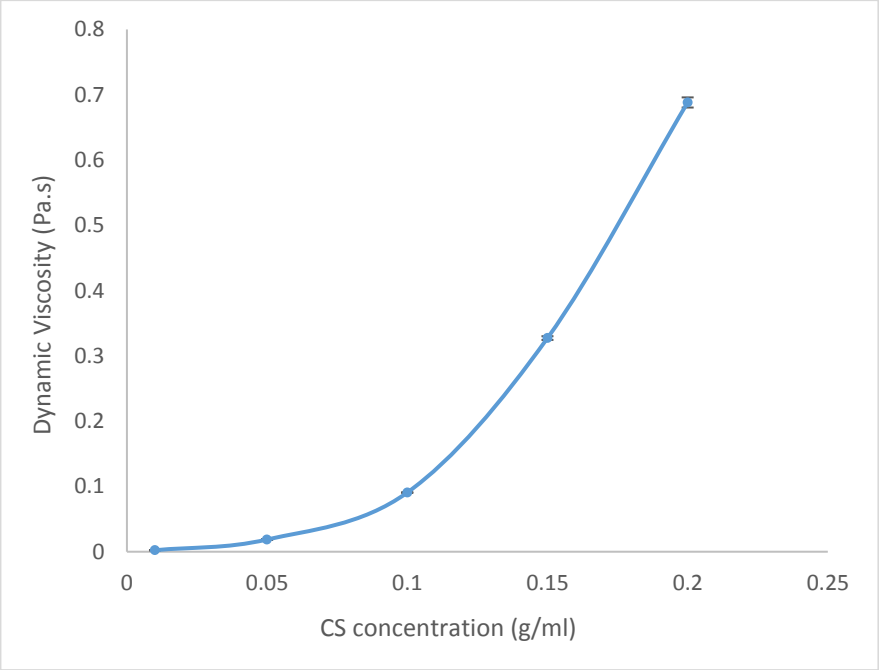
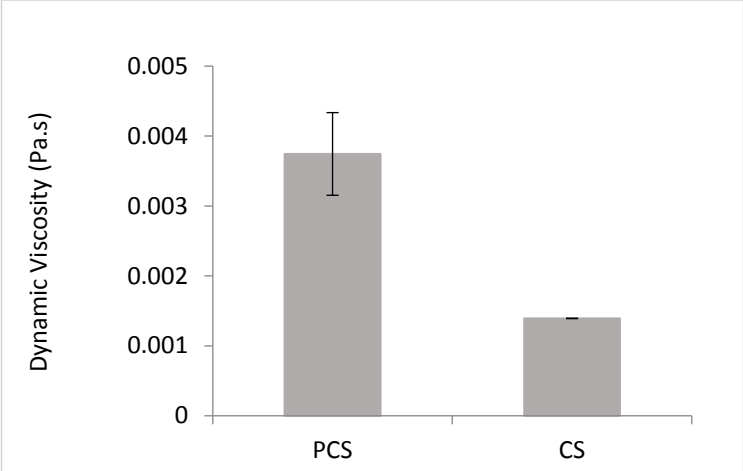


Fig 4.7. Dynamic viscosity of CS at various concentrations (shear rate=100 s^{-1})



4.8. Dynamic viscosity of CS and PCS at solutions concentration of 0.01 (g/ml) and shear rate of 100 s^{-1}

Knowing the dynamic viscosity of CS, PCS and the solvent (measured with rheometer), the relative viscosity of both polymer can be calculated using Equation 4.3.

$$\eta_{relative} = (\eta_{dynamic})_{CS} / (\eta_{dynamic})_{solvent} \quad \text{(Equation 4.3)}$$

The intrinsic viscosity is then calculated using Equation 4.4:

$$\eta_{intrinsic} = \eta_{inherent} = \ln(\eta_{relative})/C \quad \text{(Equation 4.4)}$$

	$\eta_{dynamic}$ (Pa.s)	$\eta_{relative}$	$\eta_{intrinsic}$
PCS	0.003744 (SD: ± 0.0011)	2.948	108.11
CS	0.00134 (SD: ±6.32*10^{-6})	1.096	9.21
NaCl	0.00127 (SD: ± 2.9*10^{-6})		

Table 4.4. Dynamic, relative and intrinsic viscosity of a very dilute solutions (C=0.01 g/ml) of CS and PCS

Mark-Houwink equation relates intrinsic viscosity of a polymer (η) to its molecular weight (M).

$\eta_{intrinsic} = KM^a$ (Equation 4.5)

K and *a* are the Mark-Houwink constants which depend on the polymer−solvent system, temperature and polymer conformation[167]. The M–H exponent is a function of the three-dimensional configuration of a polymer chain in a solvent and ranges from 0 to 2. Values of *a* ranging from 0 to 0.5 implies rigid sphere in an ideal solvent, between 0.5 to 0.8 corresponds to random coil in a good solvent, and from 0.8 to 2 infers rigid or rod like polymers (stiff chain). Equation 4.6 represents the Mark Houwink parameters of chondroitin sulphate in 0.2 M NaCl at 25 °C indicating that the chondroitin sulphate molecules assume a shape intermediate between a random coil and a stiff rod[168].

$[\eta]\ (cm^3/g) = 1.7 \times 10^{-5} M_w^{1.01}$ (Equation 4.6)

The ratio of Mark Houwink equation for PCS and CS is (assuming the same *a* for CS and PCS):

$\eta_{pcs} / \eta_{cs} = (M_{pcs} / M_{cs})^a$ (Equation 4.7)

Thus the molecular weight ratio of PCS to CS is: $M_{pcs} / M_{cs} = \exp(\ln(\eta_{pcs} / \eta_{cs})/a)$, the ratio of CS and PCS intrinsic viscosities can be obtained from table 4.4 to be 11.45. Molecular weight of CS was claimed to be 20kD by the supplier (Sigma Aldrich, UK), in which case the molecular weight of PCS is 230 KDa.

As mentioned above, the molecular weight of PCS can also be obtained using the Einstein viscosity relation, the below equation (Equation 4.8) is derived by dividing the Einstein viscosity equation of PCS to that of CS.

$M_{pcs} / M_{cs} = (\eta_{cs}/\eta_{pcs})(r_{pcs} / r_{cs})^3$ (Equation 4.8)

Using this equation, the molecular weight ratio of PCS versus CS is 11.97. This is almost the same as the ratio obtained by the Mark- Houwink equation, which was 11.45. This strongly suggests that the Mark- Houwink constants of CS and that of PCS can be assumed to be equal and confirms that these two methods for obtaining MW are in agreement.

There are a few other conventional methods for measuring the molecular weight of a polymer including gel permeation chromatography (GPC), matrix-assisted laser desorption/ionization (MALDI) mass spectroscopy. From the all mentioned techniques, rheology measurements were informative to approximate the molecular weight of PCS. Samples of PCS were tried to be tested by GPC and MALDI mass spec, however an appropriate solvent could not be found to carry out the experiments. Likewise, to directly obtain the molecular weight of a polymer by DLS, the polymer should be soluble in the carrier solvent. Various solvents were tried for PCS with no success.

4.4.4.2. Rheology tests- Dynamic frequency sweep (constant strain, and temp)/ Viscoelastic behaviour of CS and PCS

The viscoelastic properties of CS and PCS were examined by oscillatory frequency sweep tests on 1% w/v suspensions of CS and PCS (in deionized water) at 20° C using a parallel-plate system (50mm diameter) to measure the complex viscosity (η^*), storage modulus (G') and loss modulus (G'') as a function of angular frequency (0.1 to 100 s^{-1}). Storage modulus (G') indicates the energy stored and the elasticity of a material whereas loss modulus (G'') shows the dissipated energy as a characteristic of viscous material[169].

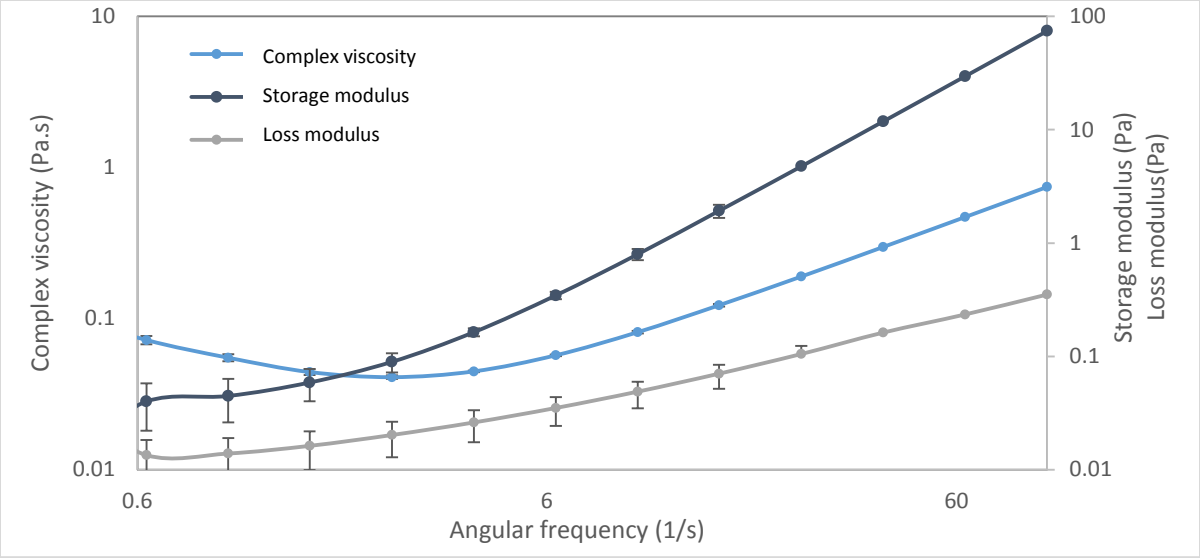


Fig 4.9. Complex viscosity, storage and loss modulus of CS solution

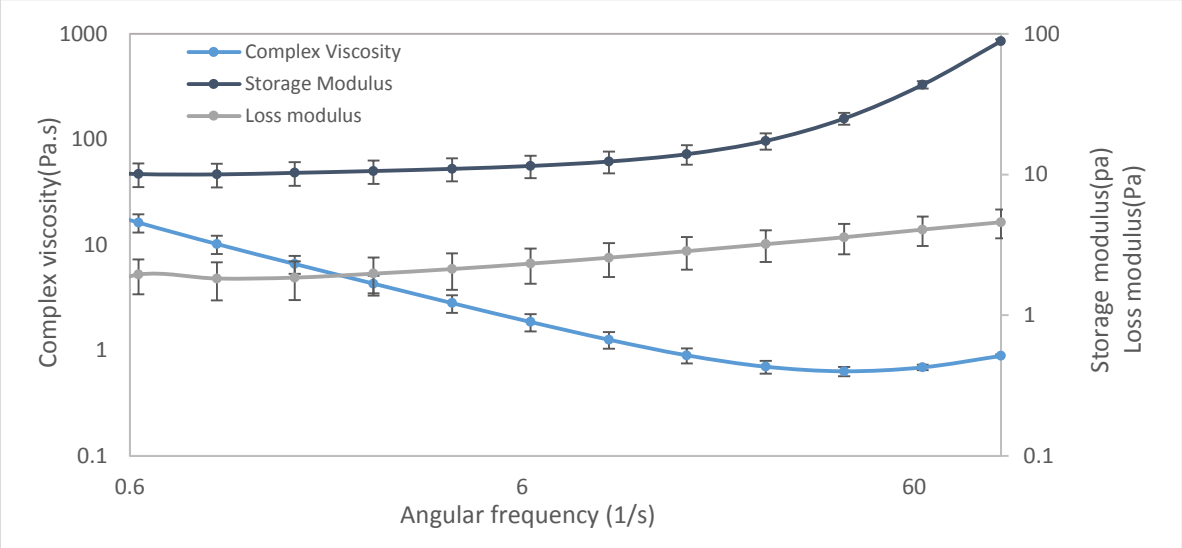


Fig 4.10. Complex viscosity, storage and loss modulus of PCS solution

It can be seen from Fig 4.9 that at low angular frequency (< 2.5 s^{-1}), the complex viscosity of CS decreases by increasing the angular frequency which represents a shear thinning property of CS,

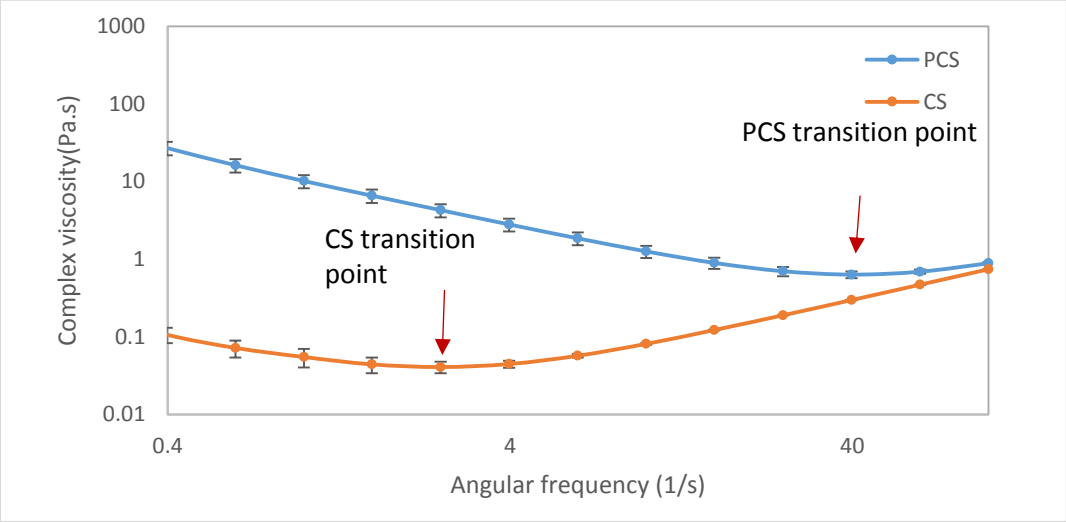
however at higher angular frequency (between 2.5 to 100 s^{-1}) the complex viscosity of CS increases by increasing the angular frequency signifying a shear thickening property.

Fig 4.10 shows that PCS has also a shear thinning property at frequencies less than 40 s^{-1} and shear thickening property at higher frequencies. PCS has a shear thinning property over a more extended range of frequencies than CS. As depicted in Fig 4.11, the transition between shear thinning and shear thickening occurred at lower angular frequency for CS as opposed to PCS.

The storage (G') and loss modulus (G") of CS enhances over the entire range of frequency while the increase in storage modulus is more prominent. The storage modulus of PCS is constant at angular frequency lower than 25 s^{-1} and increases at high angular frequency, but its loss modulus is approximately constant over the whole range of frequency.

CS and PCS solutions both have a higher storage modulus than loss modulus which indicates that their elastic characteristic is dominant. The complex viscosity of PCS is higher than that of CS providing further evidence that PCS has a higher molecular weight and polymerisation has occurred. Furthermore, the storage and loss modulus of PCS are significantly greater than CS. Yet, the increase in loss modulus of PCS versus CS is extremely higher than the increase in its storage modulus. In other words, the viscous component is greatly increased by polymerisation. As shown if Fig 4.11, complex viscosity of PCS is highly greater than that of CS in low angular frequency in which they both have the shear thinning property. At angular frequency higher than 2.5/s, CS represents shear thickening behaviour and its viscosity converge to PCS viscosity at angular frequencies greater than 60/s. PCS viscosity reduced significantly by increasing angular frequency (*covalent bonding* between the polymer chain may be disrupted due to shear). Fig 4.11 illustrates that the magnitude of decrease in viscosity of PCS during thinning is much greater than

the viscosity increase during thickening. In contrast, the magnitude of decrease in viscosity of CS during thinning is considerably less than the rise in viscosity during thickening. Fig 4.12 represents the loss factor for CS and PCS. The decrease in loss factor is not significant for low angular frequency (<4/s), however the loss factor decreased dramatically when angular frequency exceeds 4/s signifying the increase in storage modulus (elastic behaviour prevails viscous).



4.11. Transition between shear thinning and shear thickening properties in CS and PCS

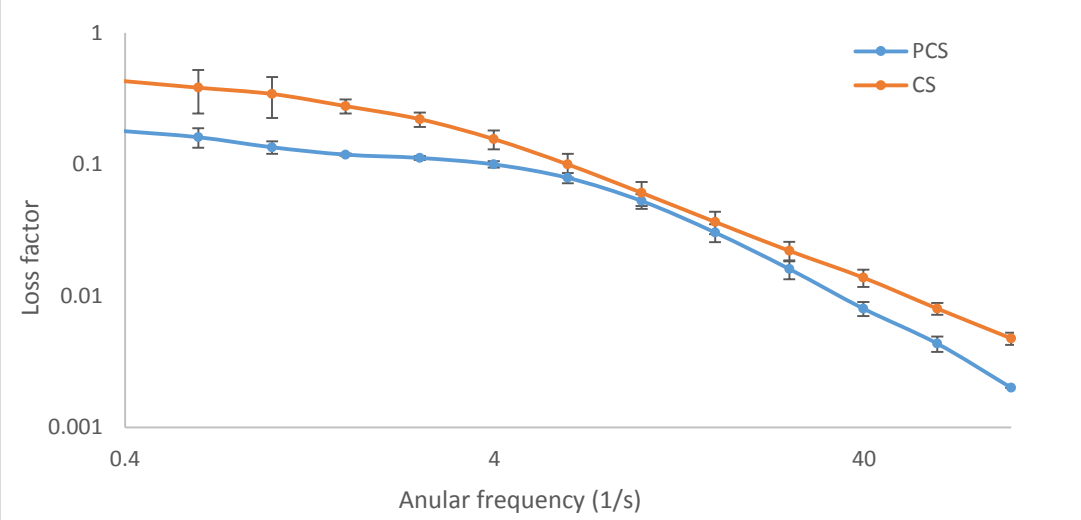


Fig 4.12. Loss factor (tan δ) for CS and PCS

4.5. Scaffolds microstructure

The porous structure of scaffolds originates from the ice crystal morphology during the freezing process of suspensions[170,171]. During freezing, suspensions undergo a heterogeneous nucleation of ice crystals from their exposed ends in the mould. Ice crystal dendrites propel CS/PCS into the interval/space between ice crystals, CS/PCS can also be surrounded by the growing dendrite - the mechanism of ice growth is controlled by ice front velocity, which is a function of the freezing temperature and viscosity of suspension[170,171].

Fig 4.13 shows that the microstructure of CS scaffolds appears different from that of PCS scaffolds, it exhibits a non-porous structure composed of series of stacked plates which have little interconnection (Fig 4.13a). Each cluster of plates/planar pores are oriented in a different direction. Pores in the wall of primary pores are referred to as secondary pores. Secondary pores are arranged orderly in CS scaffolds and there are thick interstitial spaces between them (Fig 4.15a). The average distance between parallel sheets of a pore (d), the average length of pores (l), the average aspect ratio of the primary pores (l/d) and also the average secondary pore size are tabulated in table 4.6. The average size of secondary pores was obtained using image J software.

SEM images of PCS (Fig 4.13b, 4.14b) revealed the formation of a highly porous structure, pores are extremely interconnected and randomly oriented. Pores are not perfectly rounded and are estimated by ellipse defined by cross- sectional area and quotient of circularity. Using major (*b*) and minor (*a*) axes of ellipse, the cross-sectional area (*A*) can be defined as:

$$A = \pi \left(\frac{a}{2}\right) \left(\frac{b}{2}\right) \qquad \text{(Equation 4.9)}$$

From Equation 4.9, circularised pore diameter (d) is defined as:

$$d = 2\sqrt{A/\pi} \qquad \text{(Equation 4.10)}$$

Using Equation 4.9, the quotient of circularity (Q) is expressed as:

$$Q = 4\pi A/L^2$$

Where L is the ellipse circumference (Pore perimeter), which can be adequately described by[18]:

$$L = 2\pi\sqrt{\frac{(\frac{a}{2})^2+(\frac{b}{2})^2}{2}} \qquad \text{(Equation 4.11)}$$

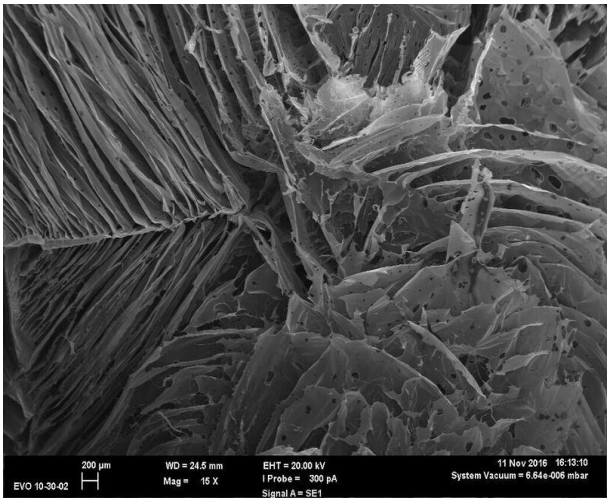


Fig 4.13a. SEM image of CS

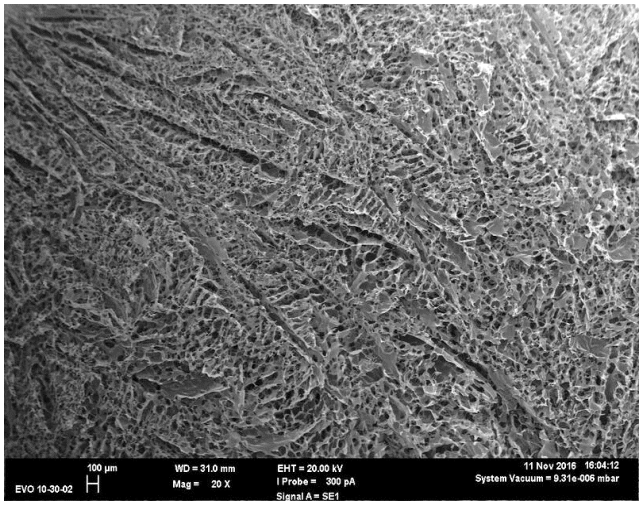


Fig 4.13b. SEM image of PCS

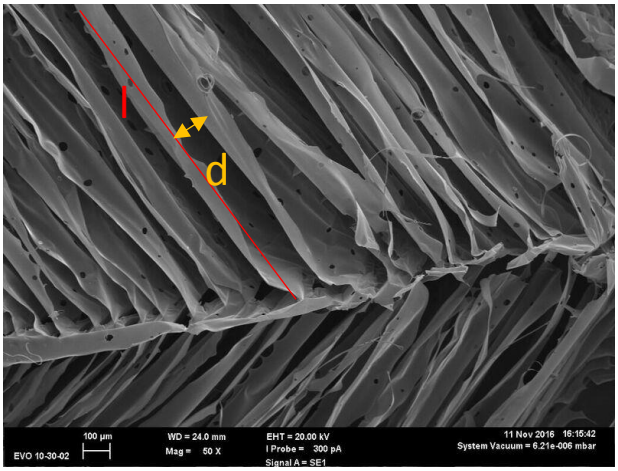


Fig 4.14a.primary and secondary pores in CS scaffold

(l: pore length, d:distance between pores)

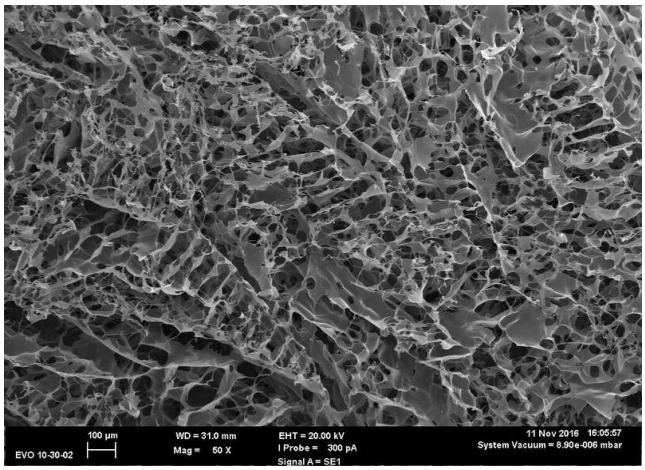
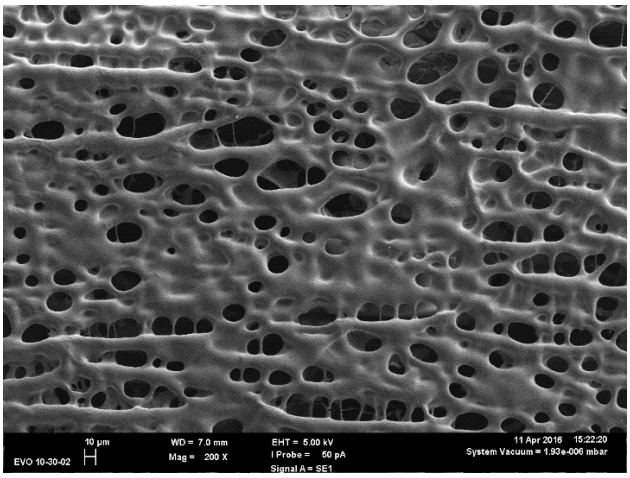
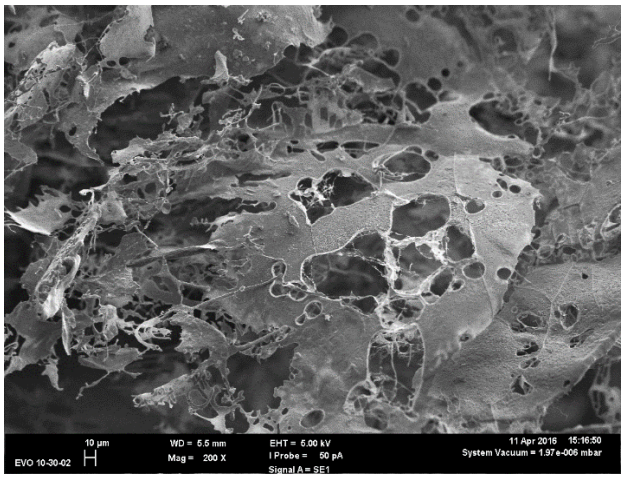


Fig 4.14b.primary and secondary pore in PCS



4.15a. secondary pores on CS pore wall



4.15b. secondry pores on PCS pore wall

The average area of pores was found to be 3800 µm^2 (SD: ±1190) for 321 counts (measured by Image J software) with the average pore circularity quotient of 65%. The majority of pores (92%) have an area less than 5000 µm^2. Average major and minor pore diameters were 76 µm (±25) and 39 µm (±12) respectively. Fig 4.15 represents the presence of secondary pores on the walls of primary pores, ruptures in pore walls are observed in PCS scaffolds.

d(µm)	l (µm)	aspect ratio (l/d)	secondary pore area (µm^2)	Quotient of circularity
150	1950	18	119.6	0.76

Table 4.6. CS scaffolds pore dimensions (average of 100 counts)

4.6. Mechanical properties

To determine the compressive modulus of the scaffolds, compression test was conducted on 5 scaffolds of each polymer. The average strain rate used was 5.3%/min. Fig.4.16 represents the stress-strain curve for CS and PCS in compression. There are three deformation phases, the first stage is linear elastic dominated by pore edge bending, and the second region is stress plateau dominated by pore wall buckling. The final region is densification dominated by pore collapse throughout the scaffold. Compressive (Young's) modulus of the scaffolds were calculated from the slope of initial linear part of the stress- strain curve (Fig 4.17).

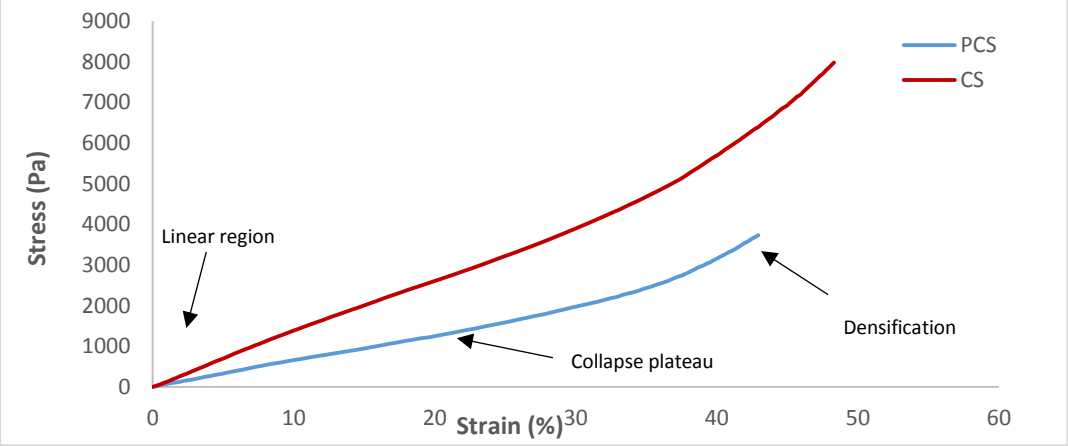


Fig 4.16. Representative stress-strain curves for CS and PCS

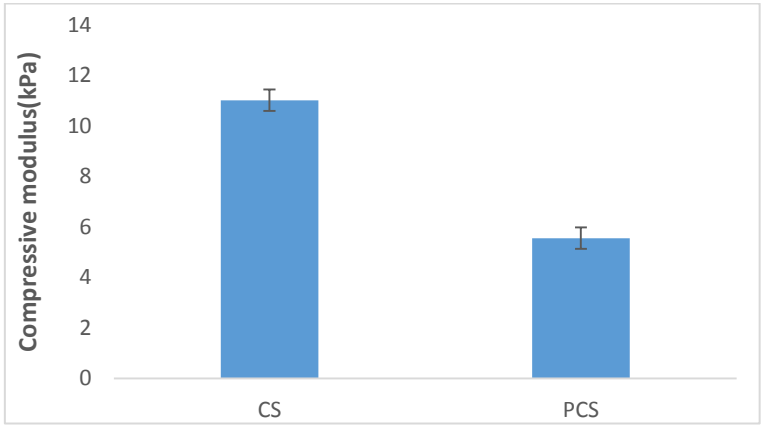


Fig 4.17. Compressive modulus of CS and PCS scaffolds (n=5)

The average Young's modulus of CS scaffolds is 13.5 kPa which doubles the average young's modulus of PCS scaffolds (6.8 kPa).

4.7. Discussion

This section discusses FTIR and XPS outcomes which used to confirm the occurrence of polymerisation by analysis of chemical structure of CS and PCS. Additionally, the mechanism of polymerisation will be explained by the aid of these two techniques (Section 4.5.1). Rheological behavior of CS and PCS is discussed in section 4.5.2. Rheology and DLS also supported the occurrence of polymerisation by showing the increase in the viscosity and size of PCS. The parameters affecting the pore size is explained in section 4.5.3 and the angular frequency/ shear stress of suspensions during freezing are determined based on the pore size of scaffolds and the viscosity of the suspensions. The differences in the compressive moduli of scaffolds, the mechanism of deformation as well as the parameters affecting it will be clarified in section 4.5.4.

4.7.1. FTIR & XPS

The FTIR spectrum of PCS resembles that for CS in terms of the presence of similar peaks. This suggests that the CS backbone structure and its chemical bonds have not changed due to the polymerisation process; that is the structure of CS has not been disrupted by the polymerization. Second derivative spectra of PCS (Fig 4.6) depicted an infrared band associated with the C=O stretch at 1,735 cm^{-1}. The shift in the peak position of C=O band (corresponding to an ester bond) and the increase in its intensity (2.2 times) as well as the increase in the peak intensity of C-O-C band (1.4 times) strongly suggests the occurrence of polymerisation. There are two possible

routes for polymerisation of CS considering the chemical structure of CS (Fig 4.1): 1. Formation of side branches through the carboxylic group, 2: Chain length polymerisation along the polymer chain. FTIR and XPS outcomes will be used to help understand the mechanism of polymerisation.

Polymerisation routes:

1. intramolecularly along the polymer chain (Fig 4.18A)

Polymerisation along the polymer chain would create an ether group (-C-O-C-). The increase in the intensity of ether band by 1.4 times in PCS spectrum indicates the polymerisation along the polymer chain. This route of polymerisation is further confirmed based on XPS results.

Polymerisation along the CS chain is a polycondensation process in which an anomeric hydroxyl group (an anomeric carbon is bonded to two oxygens) is activated by phosphoric acid to produce a carbocation, then chain addition can take place intramolecularly (along the polymer chain) or intermolecularly (via carboxylic group route) [161]. The nature of polymerisation route has also investigated further via rheology. This will be discussed in the next section (4.5.2).

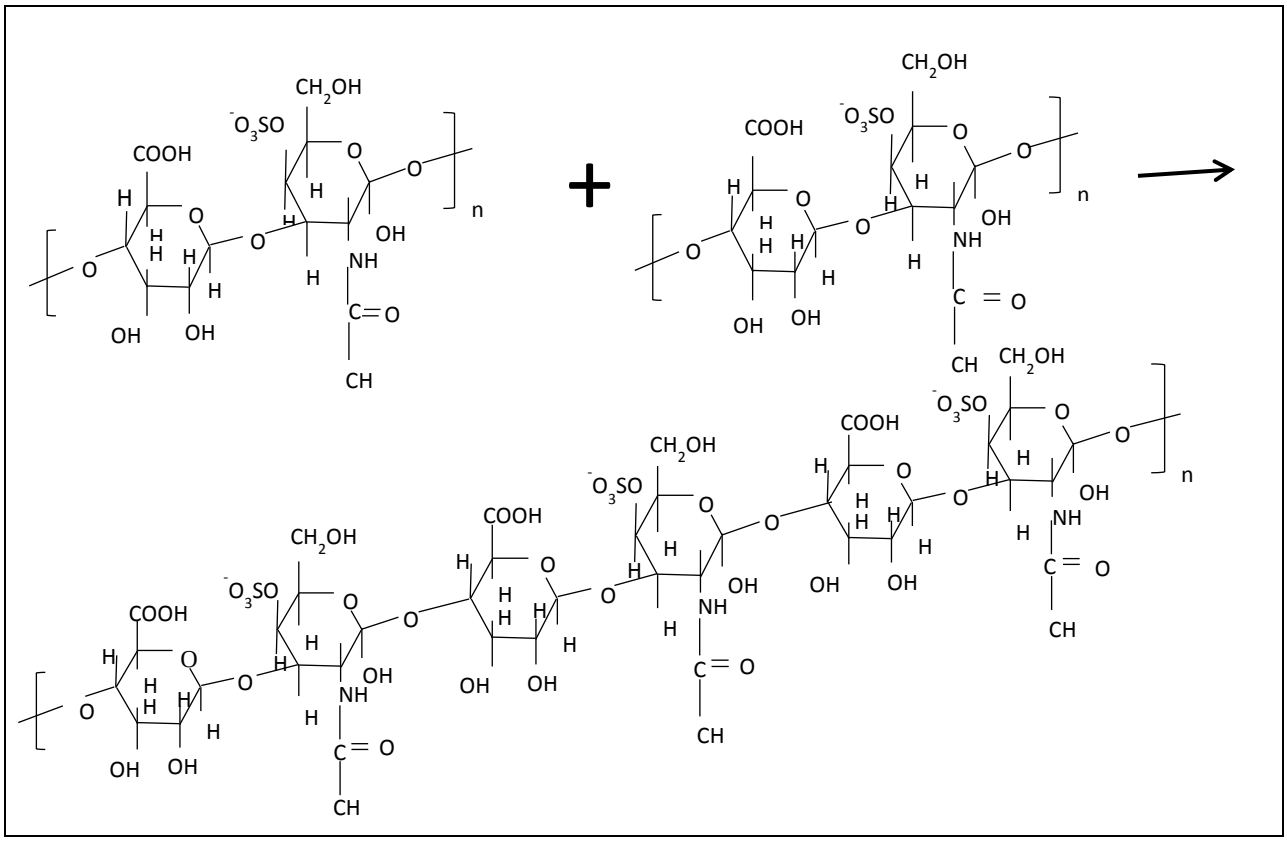


Fig 4.18A. Intramolecular chain growth (chain length polymerisation)

2. intermolecularly via carboxylic group route (Fig 4.18B)

Second derivative spectra of PCS (Fig 4.6) showed an infrared band associated with the C=O stretch at 1,735 cm^{-1}. The significant increase in the peak intensity of ester band suggests that polymerisation has occurred through the carboxylic group to form side branches in PCS. XPS results are also in agreement with the FTIR results. C (1s) peak analysis of PCS and CS (Fig 4.8) also showed a higher concentration of ester and ether bond for PCS which further supports the polymerisation of CS by the formation of side branches or polycondensation.

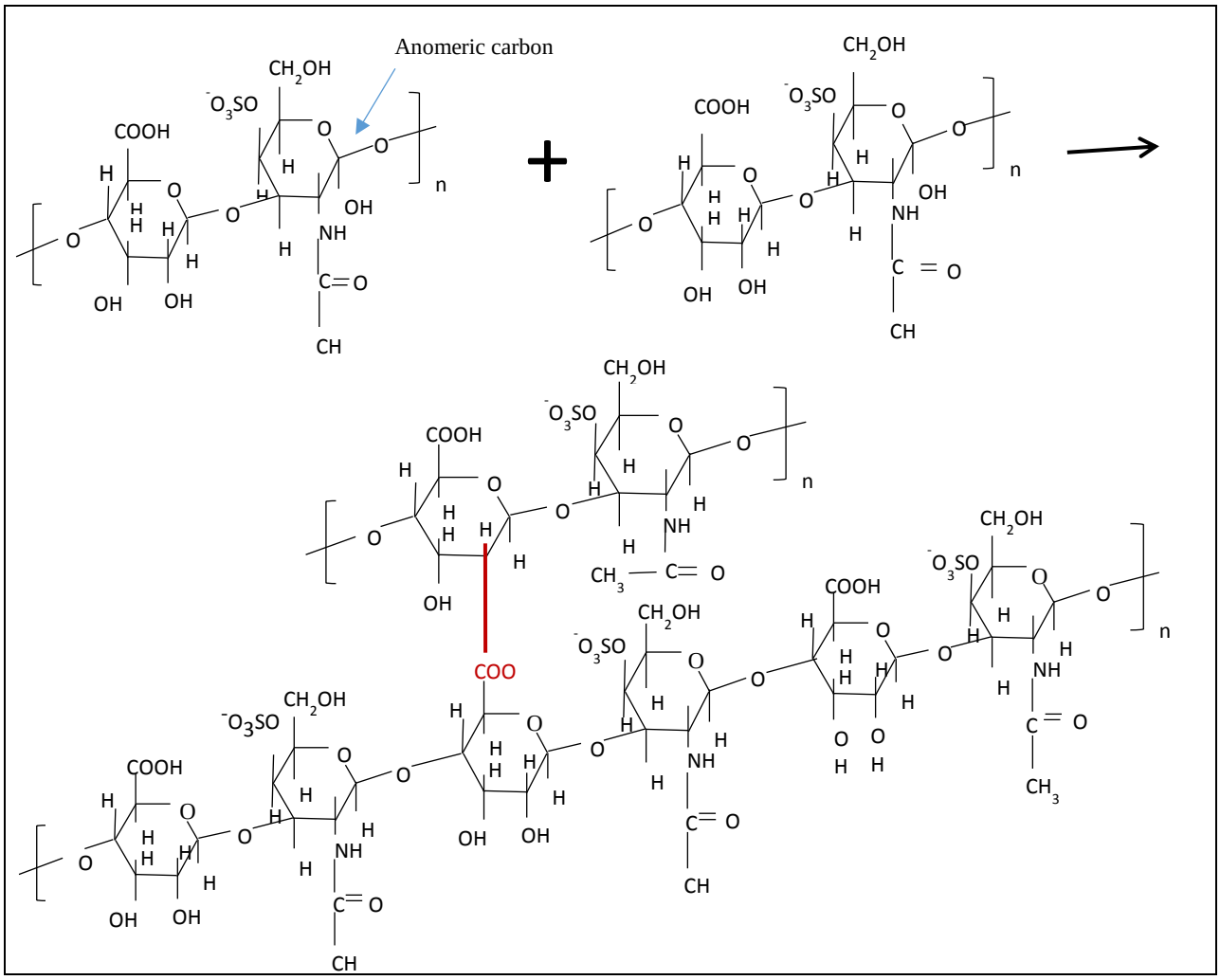


Fig 4.18B. Intermolecular chain growth (formation of side branches), through the carboxylate functional group

4.7.2. Rheology

PCS showed a significantly higher viscosity, complex and loss moduli than CS over the entire range of frequency. They both depicted a shear thinning regime at lower angular frequencies followed by a shear thickening regime at higher frequencies. Yet, PCS has a more extended shear thinning and shorter shear thickening behavior compared to CS (See Fig 4.11).

Here, the parameters give rise to the difference in PCS and CS rheology and the mechanism of the polymers shear thinning and thickening will be discussed.

Polymer-solvent and polymer-polymer interactions influence the rheological properties of a polymer solution. CS is soluble in water, however, PCS is not water soluble. The interaction between polymer and solvent affects the configuration of the polymer in solvent. The polymer size (radius of gyration), its molecular weight and the concentration of polymer solution/suspension influence the interactions between polymer chains in the form of entanglements. We speculate that PCS are highly entwined polymer networks due to the length, configuration (branched polymer) and its molecular weight, so the dynamics of chains will be greatly hindered by entanglements. CS could be less entangled due to the linearity of chains, lower molecular weight and size and higher interaction with solvent. These are the main factors that contribute to the different rheological behavior of CS and PCS.

Polymers with a high molecular weight are likely to be entangled and randomly oriented when they are at rest. Under shear, they begin to disentangle and to align which causes a reduction in viscosity.[172] Shear thinning is thought to arise from chain orientation or alignment of microstructures with the flow direction, thus reducing the local drag (Fig 4.19). As the shear rate is increased further the alignment with the flow follows, which results in further reduction in the shear viscosity. Deformation gives rise to microstructural anisotropy which may reduce intermolecular interactions, particularly the entanglements.[173] Shear thinning can be explained in terms of the forces exerted to a particle in a solution.

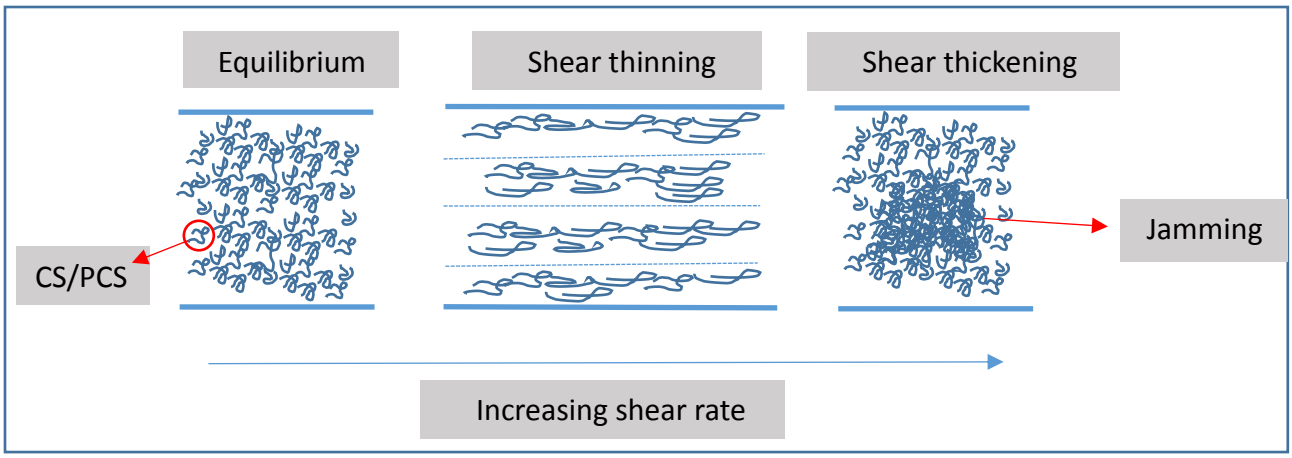


Fig. 4.19 Schematic representation of particles during shear thinning and shear thickening [174], at shear thinning regime polymer molecules orient and align with the flow direction

Specifically, there is an equilibrium of forces between polymers/particles in a solution/suspension and shear can interrupt this equilibrium, hence the arrangements of polymers are forced toward an unfavorable state of lower entropy, weakening intermolecular / interparticulate forces[145]. These forces include: attractive *Van der Waals force*, repulsive forces based on excluded volume repulsion, electrostatic and steric repulsion[175-177]. This shear thinning regime was observed at lower angular frequency for CS than for PCS which showed shear thinning behavior over a broader range. It has been suggested that a linear molecule under shear elongates and form a prolate ellipsoid configuration, whereas a branched molecule flattens and form an oblate ellipsoid[178]. Moreover, it has been observed that the increase in alignment occurs more intensely for a linear molecule rather than a branched molecule[178]. This could explain why PCS had shear thinning behaviour over a broader range of frequency compared to CS.

PCS showed an approximately constant storage modulus over a broad range of frequency. In polymer rheology, the region of constant G' is identified as the plateau modulus and implies that little relaxation occurs in this range of frequencies (relaxing back to an equilibrium orientation

and configuration following the removal of stress). The relaxation is hindered by the entanglements[172]. As the molecular weight of the polymers increases, the range of frequencies over which G' is independent of frequency increases (Fig 4.20), reflecting the larger number of entanglements per chain and the more hindered relaxation process. PCS showed a considerably broader region of constant G' compared to CS (Fig 4.21), this provide a further evidence that PCS has a higher molecular weight or it has longer chain and or more side branches compared to CS (See Section 4.4.4.2) .

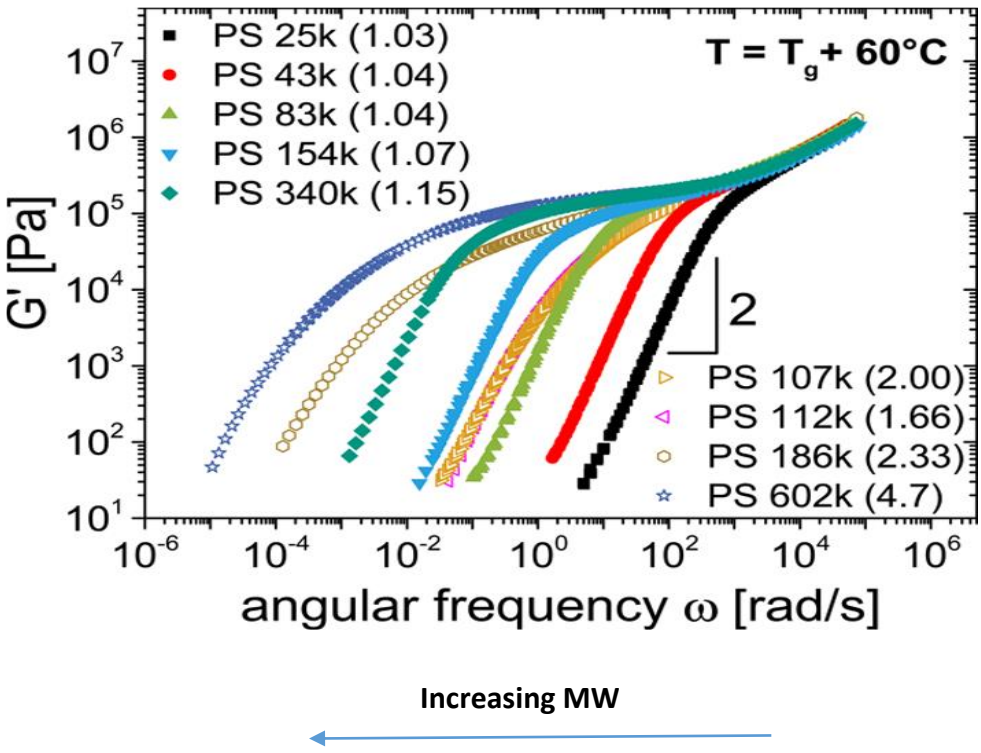


Fig 4.20. Storage modulus of polystyrene melts at 160 C for a range of molecular weights[179]

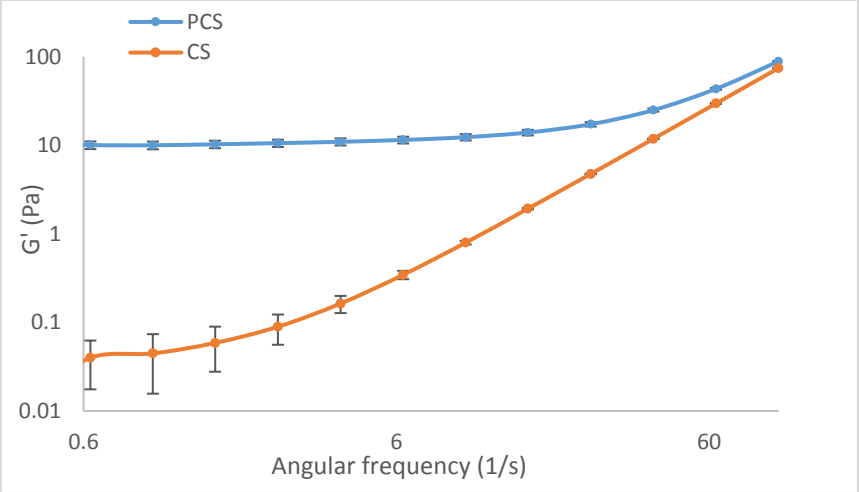


Fig 4.21. Storage modulus of CS and PCS, broader range of constant G' by increasing Molecular weight in PCS

The rheological behaviour of PCS resembles that of gels. The major difference between gels and a concentrated polymer solution is the existence of bonds between the polymer molecules in gels rather than just entanglements (characteristic of concentrated polymer solutions). Gels commonly show more elastic behavior than polymer solutions at the same concentration because chemical bonds are stronger than simple physical entanglements[172]. The number of bonds in gels affects its strength and elasticity; as the number of bonds increases the gel elastic modulus increases. The bonds between the molecules in a gel also restrict the relaxation processes of the system as opposed to polymer solutions. In polymer solutions, molecules can entirely disentangle from one conformation and diffuse into another. However, the presence of bonds in the gel network restrict the molecules movement or their relaxation, resulting in a great increase in the relaxation times of the system. FTIR and XPS showed the existence of bonds between CS molecules to form a PCS molecule (See Fig 4.4 & 4.6), this makes PCS (which has 12 times higher molecular weight and 5 times greater diameter) to more likely behave as a gel. It is

also speculated that there is likely more hydrogen bonds between PCS molecules than CS. Most importantly, the storage modulus G' of PCS is independent of frequency over a broad range. This constant storage modulus indicates that there is little relaxation occurring over these frequencies and PCS is acting like an elastic solid. Second, the loss modulus, G", is approximately six times smaller than the storage modulus. This substantial difference in the magnitude of these two moduli is further evidence that PCS acts like a strong gel and its rheology is dominated by the elastic contribution.

For both CS and PCS in the thinning regime, loss factor (tan δ) is less than 1, showing a higher storage modulus. When polymer solutions shear thicken, a significant decrease in tanδ occurred (Fig 4.12). These rheological transitions associate with changes in particle configurations. In shear thinning, the configuration is isotropic. However, in shear thickening, a slight anisotropy happens due to particle layering induced by shear plate confinement[180].

Shear thickening can then be interpreted as the consequence of dilatancy: the system under flow wants to dilate but instead undergoes a jamming transition because it is confined[181](Fig 4.19). Order-disorder transition in the particle configuration and aggregation of clusters creating a jammed network cause shear thickening. An order-to-disorder transition[182,183], formation of particle clusters induced by lubrication hydrodynamics[184-188], or the confinement and dilation of suspended particles under shear[181,189] have been shown to be the reason of shear thickening.

Shear thickening of a suspension is controlled by the physical parameters of the particle/ polymer including phase volume, particle size (distribution) and particle shape, as well as those of the liquid phase: viscosity and details of deformation including shear or extensional flow, steady or transient, time and rate of deformation[190]. In most of polymer cases, a suspension exhibits shear

thinning behavior at low shear rates. At higher shear rates, the fluid undergoes a transition into a shear thickening regime which typically continues no more than one order of magnitude of shear rate before changing to another shear thinning region[191]. The onset of this transition is commonly characterised by the critical shear rate, or critical shear stress, and can vary significantly between systems. The degree to which the viscosity increases over this shear thickening region can also vary greatly between systems, from the modest increase to an increase of several orders of magnitude[192]. This process is completely reversible, and the material will return to a viscous liquid again after the stress is removed[193]. The shear rate at which these transitions occur and the magnitude of the viscosity increase are determined by a number of factors, including particle concentration, size, shape, size distribution and inter-particle interactions[194].

To summarize, the size of the particles within a suspension and the interaction between polymer molecules has a great effect on its rheological properties. As PCS size is 5 times of CS, this gives rise to their difference in rheological behavior and the onset of shear thickening. The critical shear rate increased in PCS as the particle size increased.

4.7.3. Pore size analysis

The porous structure of scaffolds after freeze drying results from the formation of ice crystals during freezing and their subsequent removal during freeze drying[171]. The freezing process initiates by heterogeneous nucleation of ice crystals from the uncovered end of solutions in the cylindrical mould which is in direct contact with the freezing air. The rate of nucleation, which can be controlled by freezing temperature and the available nucleation sites, determines the

number and size of ice crystals. Lower temperatures mean larger undercooling of the freezing front, resulting in an increased rate of nucleation and hence smaller ice crystals. The freezing-front, then travels through the sample. The velocity of this freezing- front, and the manner in which the liquid carrier, in this case water solidifies, determine the sample pore structure[195]. The viscosity of the solution is a particularly important processing parameter in freeze-casting. It determines, for a given particle size the critical freezing-front velocity at which particle trapping occurs during solidification. Viscosity is thus a structural parameter that determines the scaffold' micro-architecture[196].

CS /PCS suspended in water during freezing, may either be trapped and encapsulated in the ice area or repelled by the moving freezing front into the liquid region[195]. The velocity of crystal growth during solidification defines the freezing-front (the interface between the newly formed solid and the liquid) velocity, which determines whether a particle in the solution will be rejected and pushed ahead, or engulfed and trapped by the approaching liquid–solid interface. The important factor is the balance between two opposing forces that act on each particle: a repulsive Van der Waals, and an attractive force due to viscous drag.

A definable porous structure forms if the polymers are rejected from the ice crystal and trapped between adjacent crystals. The thermodynamic criterion for this particle repulsion is described by Equation 4.12.

$$\Delta\sigma = \sigma_{ps} - (\sigma_{pl} + \sigma_{sl}) > 0 \qquad \text{(Equation 4.12)}$$

Where the interfacial free energy between particles and solidification front σ_{ps} should be larger than the sum of interfacial energies of solid–liquid σ_{pl} and particle–liquid σ_{sl}[197].

A particle in a liquid phase experiences a repulsive force due to molecular van der Waals interactions at the solid–liquid interface.

$$F_\sigma = 2\pi R\Delta\sigma_0 \left(\frac{a0}{d}\right)^n \quad \text{(Equation 4.13)}$$

Where *R* is the particle radius, *a* is mean distance between the molecules in the liquid layer, *n* is a constant between 1 and 4.

In addition to this repulsive force, the particle also experiences an attractive force owed to viscous drag.

$$F_n = \frac{6\pi\eta\upsilon R2}{d} \quad \text{(Equation 4.14)}$$

Where d is liquid film thickness, η is viscosity of suspension and υ is the velocity of the ice front.

From an equilibrium of repulsive and attractive forces, a critical velocity v_{cr} of the freezing front can be calculated at which particle entrapment takes place

$$V_{cr} = \frac{\Delta\sigma 0\ a0}{12\eta\mu r} \quad \text{(Equation 4.15)}$$

Where Δσ=free energy, η=liquid viscosity, r=particle radius, a=mean distance between the molecules in the liquid layer, $\mu = \lambda_p/\lambda_l$ is the thermal conductivity ratio of particle to liquid[198]. At low velocities, there is a net repulsive force (F_σ) on particles, which repels them into the liquid phase; however, as the velocity increases and reaches the critical value (V_{cr}) (Eq 4.15), the attractive force (F_n) becomes dominant and the particles are encapsulated into the growing ice crystals[171,196] . Therefore, at freezing-front velocities below this critical value, the particles are pushed ahead by the solid–liquid interface.

PCS solution has larger particles and higher viscosity than CS solution, thus favours particle

entrapment by increasing the attractive drag force (F_n) on particles according to Eq. 4.13 and Eq. 4.14. Moreover, PCS has a less critical freezing front velocity than CS, which is the reason for different ice morphology and consequently different porous structure after freeze drying.

A number of factors determines the final microstructure of a freeze- dried scaffold: the break of the planar ice- front either by pinning by particles or constitutional undercooling at the tip of ice crystal because of solute rejection and the viscosity of solutions, as well as the interaction between the growing ice front with particles[197]. A definable pore structure is created by the rejection of CS/PCS into the solidifying liquid. The nucleation of ice and its subsequent growth controls/affects the number and size of the pores. The freezing mode which can be homogeneous or directional also affects the overall morphology of the pores.

When ice crystals are formed any soluble molecule/particle initially present in water is separated from the ice crystal, which causes increase in local concentration of solutes leading to a lower freezing point and constitutional undercooling at the head of the ice crystal. This eventually leads to breaking of planar ice front and formation of a columnar interface, also known as Mullins–Serkerka instability[199] . This needs to be controlled in a way that polymer is rejected from the ice-front during freezing and concentrate in regions between the growing ice crystals[171]. Therefore, the solute concentration and the cohesion/viscosity of the suspensions (based on Equations 6.6, 6.7 and 6.8) play parts in the manner in which the ice crystals grow and the final microstructure. CS and PCS scaffolds showed different microstructural features; the pore structure of CS can be explained in the light of its relatively low cohesion during freezing, as the growing ice crystal can more easily reject CS molecule into the liquid, hence it is less likely to get random particle entrapment. Conversely, PCS showed a less defined/random structure, higher viscosity/cohesion

of PCS is expected to provide a greater opposing force to growth of the ice crystals, hindering the ice front velocity. The growth is slowed down leading to the formation of smaller ice crystals and hence smaller pore sizes.

4.7.4. Relation between pore diameter and shear stress

Here, the pore size of scaffolds is related to shear stress during freezing. We assume that the scaffolds pore size is proportional to the ice front velocity.

$D_{PCS} / D_{CS} \approx V_{PCS} / V_{CS}$ (Equation 4.16)

Where D: pore diameter and V: ice front velocity.

According to the Equation 4.15: $V_{PCS} / V_{CS} = (\eta r)_{CS} / (\eta r)_{PCS}$

where V: ice front velocity, η: viscosity of polymer solution, r: polymer radius.

Based on the Equations 4.15 & 4.16 it can be shown that: $D_{PCS} / D_{CS} = (\eta r)_{CS} / (\eta r)_{PCS}$

Where $D_{PCS} / D_{CS} = 0.038$, obtained based on SEM images (See Section 4.5) and $r_{CS} / r_{PCS} = 0.2$ measured by DLS (See Table 4.3). Accordingly, the ratio of CS to PCS viscosity is calculated to be:

$\eta_{CS} / \eta_{PCS} = 0.203$

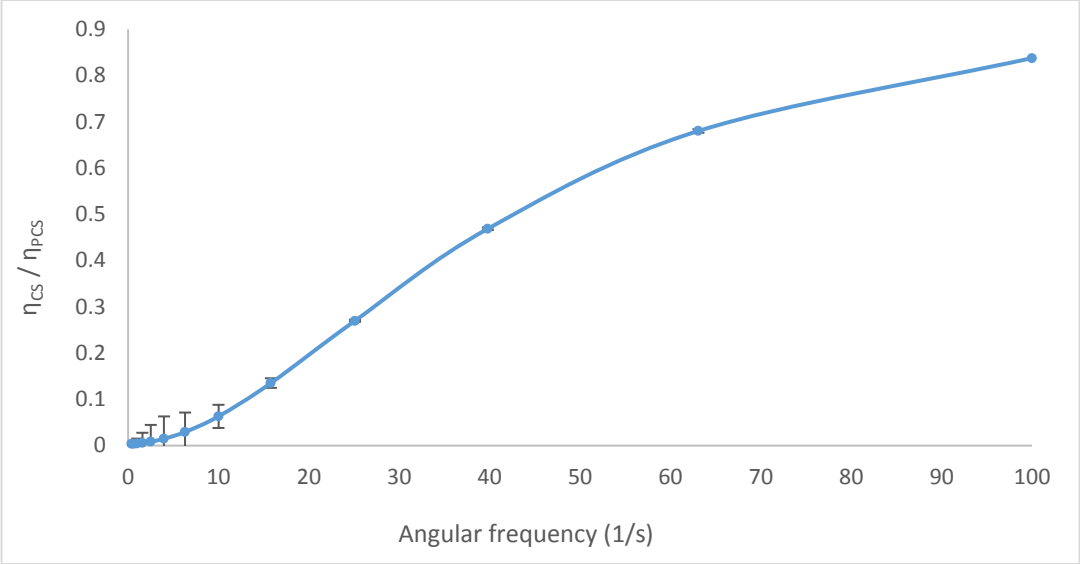
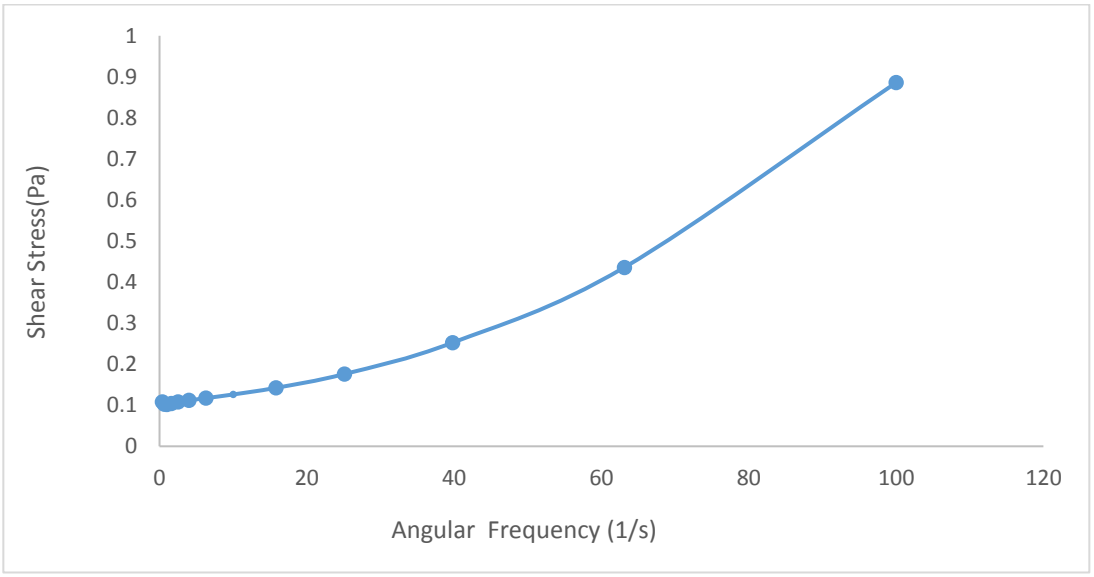


Fig 4.22. The ratio of CS to PCS viscosity

According to Fig 4.22 , the angular frequency at which η_{CS} / η_{PCS} equals to 0.203 was obtained to be 25 s^{-1}. Therefore it could be said that the polymer suspension when freezing is under the angular frequency of 25 s^{-1} and shear stress of 0.18 Pa (Fig 4.23) to create the pore size with the dimensions represented in the section 4.5.



4.23. Correlation between shear stress and angular frequency during freezing of suspensions

4.7.5. Mechanical Properties

The mechanical behaviour of CS/ PCS scaffolds in compression was examined and their respective compressive moduli (E*) measured.

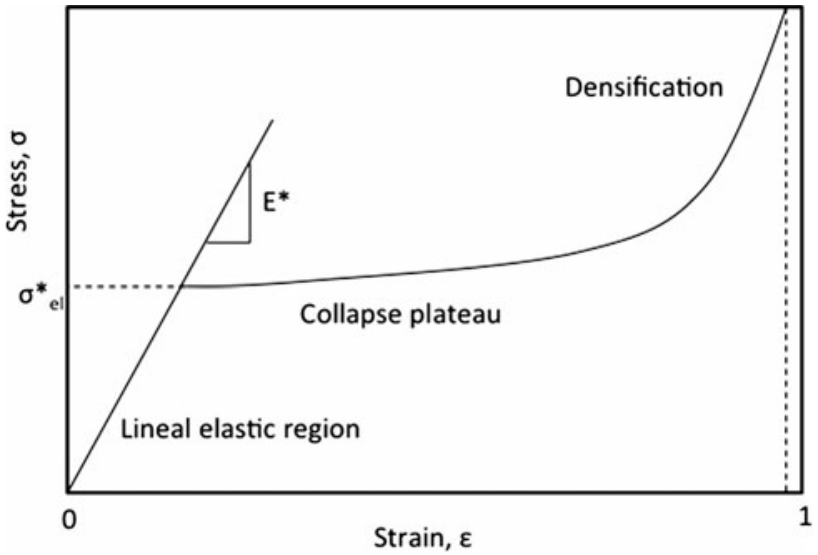


Fig 4.24. Schematic stress-strain curve for elastomeric foam[200]

Fig 4.24 shows the typical behavior of low density foams under compression[200], it can be seen from Fig 4.16 that CS and PCS scaffolds exhibit a similar behavior. Cellular solid mechanics are classified into three distinct regions of the stress-strian curve: a linear elastic regime (controlled by pore-edge bending) occurring at approximately 5% strain, a collapse plateau (controlled by pore wall buckling) and a densification regime (controlled by complete pore collapse) occurring at around 80% strain[200-203]. A similar classification has been made by Gibson and Ashby (1997) for an open-cell elastomeric foam. They postulate collapse plateau is dominated by the pore edge buckling; while CS/PCS scaffolds may undergo pore edge and pore wall buckling due to their

microstructural analysis.

Factors affecting the mechanical properties of these cellular foams include: the relative density (density of scaffold ρ* /density of solid ρ_S), their topology (pores morphology and interconnectivity) and the solid material they are comprised of [203]. As the scaffolds in this study behaves similar to an elastomer, their compression moduli are buckling- dominated (Fig 4.25) and Equation 4.17 is used to determine their compressive modulus.

$$E^* = C_1 . (\rho^*/ \rho_s)^2 E_s \qquad \text{(Equation. 4.17)}$$

Where C_1 is an empirical constant (~1) and E_S is the solid modulus[200,201,204] :

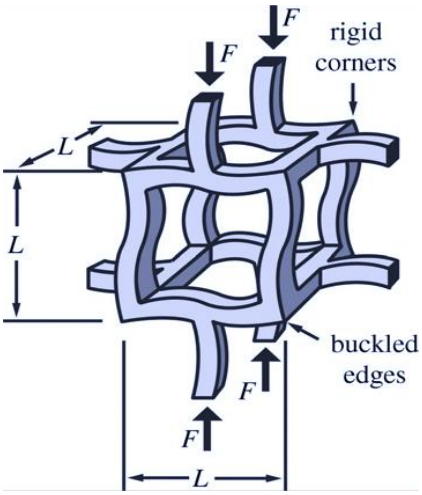


Fig 4.25. Buckling dominated behavior of a pore [203], See Fig 4.14 for comparison of pores

The densities of scaffolds (Table 4.7) were determined using the measurements of scaffold weight and dimensions which were not significantly different (p =0.037). The density of solid PCS can be calculated using the experimental values for CS and PCS molecular weight and volumes

obtained in Sections 4.4.4.1 & 4.4.3 : ρ_{pcs} / ρ_{CS} =2.2 . Therefore, the relative densities were calculated as shown in table 4.7. The relative density of CS is significantly higher than that of PCS which could predict its higher compressive modulus compared to PCS.

Scaffolds	**CS**	**PCS**
Scaffolds 'density, ρ^* (g/cm^3)	0.0144	0.0182
Relative density (ρ^*/ρ_s)	0.00263	0.00152

Table 4.7. Scaffolds density (ρ^*) and relative density (ρ^*/ρ_s); no significant difference at level of 0.05 was observed between the scaffolds density. Density of solid materials (ρ_{CS}=5.5 g/cm3, ρ_{pcs} = 12.1)

Another factor affecting mechanical behaviour is the pore anisotropy.

$E = \frac{F}{\varepsilon.A}$, $A_3 >> A_1 = A_2$ and $\varepsilon_1 = \varepsilon_3 >> \varepsilon_2$ (See Fig 4.26)

Therefore, the compression modulus in the direction of anisotropy is higher than that of in isotropic pore. Thus, increasing anisotropy would increase the compressive modulus when loaded in the direction of anisotropy. That is, in compression testing, if pores are more anisotropic in the transverse direction (Fig 4.26 (2)), the compressive modulus would increase respective to that of its isotropic structure. However, if pores are more anisotropic in the longitudinal direction (Fig 4.26 (3)), the compressive modulus would decrease. The direction of anisotropy is indicative of thermal gradient during freezing of suspensions.

Pores in CS are more anisotropic (aspect ratio = 18) than pores of PCS (aspect ratio = 2). Yet, the direction of anisotropy is oblique and each clusters of planar pores are elongated in a different direction (See Fig 4.14a) which means it has elements of anisotropy in both transverse and longitudinal directions and therefore CS pore anisotropy would have a minor effect on compressive modulus of the scaffold.

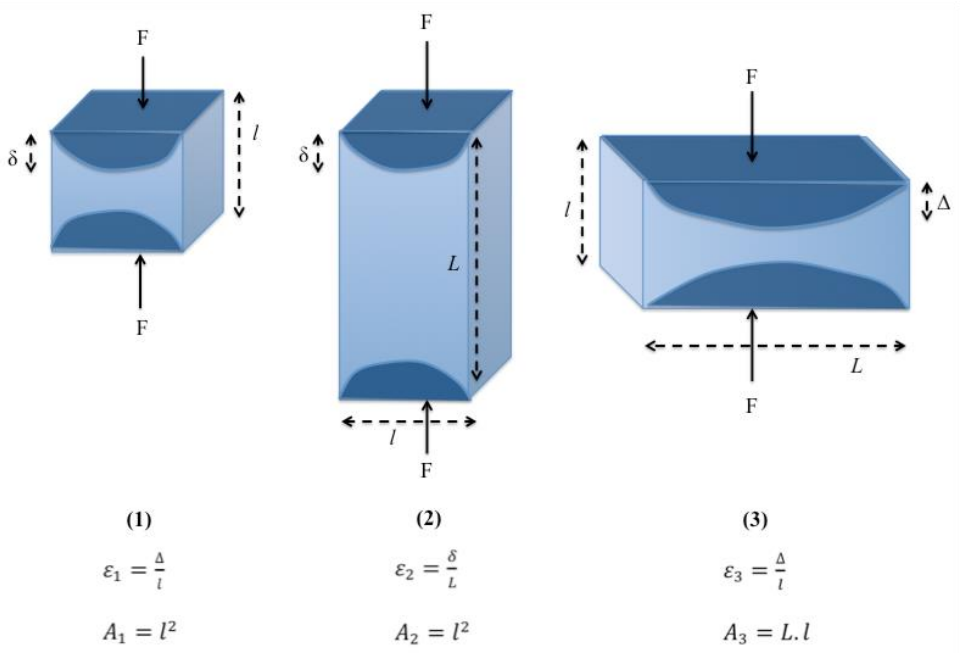


Fig 4.26. Schematic representation of deflection (δ and Δ) by force (F) on a (1) isotropic cell, (2) anisotropic cell in direction of anisotropy and (3) anisotropic cell in opposite direction of anisotropy [205].

The last parameter to be considered is the modulus of the solid pore wall (E_s). The relative density of CS is 1.73 times greater than that of PCS (Table 4.7) which increase its Young's modulus by 3 times (Eq 4.17). However, the experimental data for compression test (Fig 4.17) showed that CS compressive modulus is twice as that for PCS. Therefore, it can be concluded that PCS has likely

a greater solid modulus than CS ($E_{pcs} > E_{CS}$) which contributes to the reduction of CS compressive modulus (from 3 times to 2) versus PCS.

4.8. Summary

A higher molecular weight chondroitin sulphate (PCS) was successfully produced. FTIR and XPS showed the formation of an ester bond between CS molecules as well as the increase in the intensity of ether bond which supports polymerisation along the polymer chain as well as the formation of side branches. Rheology outcomes also provided evidence of the occurrence of polymerisation along CS chain.

Rheology experiments together with Dynamic Light Scattering revealed that the molecular weight and size of PCS are respectively 11.5 and 5.2 times greater than that of CS (again further support for the occurrence of polymerisation).

Rheological analysis of PCS and CS showed that PCS possesses a higher viscosity, storage and loss modulus over a wide range of angular frequency. Both polymers exhibited shear thinning behavior following by a shear thickening behaviour, however the shear thinning regime for PCS occurred over a broader range of frequency than for CS and its shear thickening regime occurred over a shorter range of frequency.

Scaffolds were produced from CS and PCS, the microstructure investigation by SEM revealed different pore morphology: parallel planar pores in CS and randomly oriented circular/ elliptical pore shape in PCS. A model was proposed to link the pore diameter to the viscosity of polymer suspensions and diameter of polymers and accordingly the shear stress during freezing process was obtained to be 25 s^{-1}.

The combination of the higher relative density as well as pore anisotropy led to higher compressive modulus of CS scaffold , while the higher solid wall modulus of PCS is thought to be the reason for counteracting 3-fold increase in compressive modulus to 2 folds.

Chapter 5. Fabrication and Characterisation of Chondrogenic Scaffolds

5.1. Introduction

Current surgical techniques used for the treatment of osteochondral defects include: total joint replacement, osteotomy, marrow stimulation and autologous chondrocyte implantation. The details of these techniques and their limitations were discussed in Section 2.5.2.

Recent research has demonstrated that tissue engineering approaches provide a more promising alternative to surgical interventions[9,32,206-208]. Tissue engineered grafts, designed to mimic the natural structure and composition of cartilage, could be the key for the treatment of cartilage injuries. These grafts combine the patient's own cells with porous biomaterial scaffolds of predefined size and shape to regenerate cartilage, and to thus create substitutes that could restore or enhance the function of the joint[209]. The main aim and focus of many studies in this field has been to increase the interaction of cells with the substrate. The interaction of cell surface receptors with the substrate is enhanced when the scaffold composition mimics the native cartilage extracellular matrix (ECM). The primary components of native cartilage are collagen type II and chondroitin sulphate (CS) (See Section 2.2.1.2). CS is a polymeric polysaccharide consisting of repeating disaccharide units which are negatively charged because of the presence of sulphate and carboxyl groups. CS is non-immunogenic and can influence cellular behavior enhancing cell adhesion, migration, and differentiation. It has been demonstrated that incorporation of CS in scaffolds induces the chondrogenic differentiation of mesenchymal stem cells (MSCs) in vitro[141,210]. A substrate containing CS prompts cell aggregation. This clustering of cells (pre-cartilage condensation of mesenchymal cells) leads to an increase in chondrogenic gene expressions and the synthesis of cartilage specific matrix. It is also found that the CS-mediated microenvironment significantly influenced the early expression

of cartilage specific markers: type II collagen, versican, aggrecan, and SOX9[141]. These findings show the importance of scaffold composition and cytokine-mediated biologicl signals in guiding MSCs toward development of specific tissue.

Previous research has attempted to exploit the advantage of CS by increasing its amount in the scaffolds[145,211]. However, there are limited binding sites on a biopolymer based scaffolds such as collagen for CS to attach to (carboxyl group of CS attaches to amine group of collagen), hence initial CS increase in collagen solution has not led to the CS increase in the end-product scaffold. In Chapter 4, the chain length of CS was increased (PCS) and its properties characterised. Cartilage scaffolds are now fabricated using PCS combined with atelocollagens (monomeric collagen type II). It is predicted that longer chains will provide a higher interaction of CS with the cells (due to the higher amount of CS in a chain). Furthermore, PCS was crosslinked to help preserve its integrity. The majority of collagen scaffolds produced to date have been from insoluble naturally fibrillar collagen (polymeric)[212-214] while atelocollagens have only been used in a few studies[140,145,215,216]. Atelocollagen is telopeptide-free and does not elicit immunogenicity associated with naturally polymeric collagen. It has shown that atelocollagen II scaffolds promote chondrogenic differentiation of human bone marrow mesenchymal stem cells *in vitro*[210].

A secondary objective of the study was to reduce CS/PCS loss due to dissolution in cell culture media which can happen within the early hours of culturing. To address this, chemical crosslinking has been used which covalently links CS to collagen. Previously, chemical crosslinking was applied to polymeric scaffolds by immersion of scaffolds in crosslinking reagents[217-221] (this affects pore size and may disturb scaffold structure). However, monomeric collagen II scaffold is

not stable in crosslinking solution and disintegrates rapidly. To address this problem, I proposed the idea of crosslinking the collagen suspension prior to freeze drying.

Collagen II was used in an attempt to mimic the composition of natural cartilage (See Section 2.2.1.2). Previous work confirmed the advantage of using collagen II for cartilage/chondrogenic scaffolds[215]. This study used these previous promising results that showed the stimulatory effect of collagen II on mesenchymal stem cells differentiation towards chondrogenesis. With this successful background, the focus of this research was to show the advantage of using collagen II-PCS over collagen II-CS. In all experiments collagen II scaffolds was used as a control. While some work has been done by others on using collagen I, the use of collagen II was seen a positive improvement on this[228].

In this chapter, the impact of the incorporation of PCS on the viscoelastic properties of collagen suspension, microstructure and mechanical properties of collagen scaffolds will be discussed. Three types of scaffolds were produced from reconstituted fibrillar collagen type II: (collagen II, collagen II – CS, collagen II- PCS). Rheological properties of collagen dispersions, scaffolds chemical bonding (FTIR), pore structure (SEM) and mechanical properties will be presented.

5.2. Fabrication of scaffolds

5.2.1. Materials

Type II collagen was extracted from fetal bovine articular cartilage using a limited pepsin digest followed by differential salt fractionation[222] (Kindly donated by Dr. David Brand, Argentis Company, US). Chondroitin sodium sulphate extracted from bovine trachea supplied by Sigma

Aldrich (Poole, Dorset, UK). Other consumables and reagents supplied by Sigma Aldrich or Fischer Scientific, unless otherwise stated.

5.2.2. Collagen suspension preparation

1 %(w/v) pure afibrillar collagen type II solutions were produced, by addition of lyophilised collagen monomers to dilute ethanoic acid (pH 3.2). The solutions were then homogenised in a pyrex beaker, using a hand-held blender (Braun 400W). Homogenisation occurred on an ice bath to remove the heat produced by blending which may denature collagen. The solutions were then degassed using centrifugation (Thermoelectric Corporation IEC CL10) at 5000 rpm for 5 minutes.

5.2.3. Fibrillogenesis

Monomeric collagen solutions were induced to form reconstituted fibrillar structure under certain conditions. In order to provide the suitable ionic strength and pH conditions, monomers were moved to a neutral salt solution (Tris Buffer was the buffer of choice). Then, in order to encourage fibrillogenesis, the temperature of the monomeric solutions was raised to 37°C as a representation of physiological temperature[223].

100 ml of Tris-buffered saline (TBS) solution (50mM tris-(hydroxymethyl)-aminomethane, 150mM sodium chloride was added to afibrillar collagen solution and the pH raised to 7.5 by addition of NaoH (5M). The solution was subsequently placed in an incubator at 37°C for 2hrs to allow formation of a fibrillar hydrocolloid gel. To remove TBS, the collagen solution is centrifuged, the pellet was then collected and washed.

5.2.4. EDC/NHS crosslinking

CS/PCS was added to collagen suspensions. Reconstituted fibrillar collagen II-CS/PCS solution was subsequently crosslinked using ethyl-3-(3-dimethylaminopropyl)-carbodiimide (EDC) and N-Hydroxysuccinimide (NHS). The method commonly used to crosslink collagen scaffolds (made from naturally insoluble polymeric collagen) is to submerge freeze dried scaffolds in the crosslinking solution for a few hours followed by freezing and freeze drying of scaffolds. However, reconstituted fibrillar collagen scaffolds (made from monomeric collagen) were not stable in the crosslinking solution and disintegrated, hence this method was not suitable. To address this issue, we came up with the idea of crosslinking the collagen prior to making the scaffold (before casting and freeze drying). Furthermore, by crosslinking the collagen solution rather than collagen scaffolds, two cycles of freezing and freeze drying were reduced to one cycle. To achieve the highest degree of covalent crosslinks, a strong molar concentration of crosslinker agent was used. Collagen solutions (100ml) were mixed with CS and PCS and crosslinked in 400 ml de-ionised water with 60 mM ethyl-3-(3-dimethylaminopropyl)-carbodiimide (EDC) and 30 mM N-Hydroxysuccinimide (NHS). The mixture was crosslinked for 3 hrs. To remove crosslinking reagents, solutions were then centrifuged for 5 minutes. Collagen pellets were collected from the centrifuge tube and transferred to a beaker to wash twice in 400 ml Na2HPO4 (0.1m) for 2 hours and twice in 400 ml deionized water for 1 hour[223].

5.2.5. Casting and freeze drying

Collagen suspensions were syringed into the prepared cylindrical PTFE moulds (sealed at one end) and were then transferred to a -20 °C freezer (Zanussi, DF 50/16) and left to freeze overnight. Two different sizes of casting moulds were made as shown in Fig 4.2. Moulds with

greater dimensions (wall thickness: 1.5mm, diameter: 0.8cm and length: 1.2cm) were used to produce scaffolds for characterisation and moulds with smaller dimensions (diameter: 6mm and length: 4mm) used to fabricate scaffolds for cell work. The frozen samples were moved to a freeze dryer (Christ Alpha 1-5) and freeze dried for 24 hours. During freeze drying process, ice crystals sublime from the samples and porous three-dimensional structure were produced. Fig 5.1 represents the stages of scaffold production; the scaffold formulations are also shown in Table 5.1.

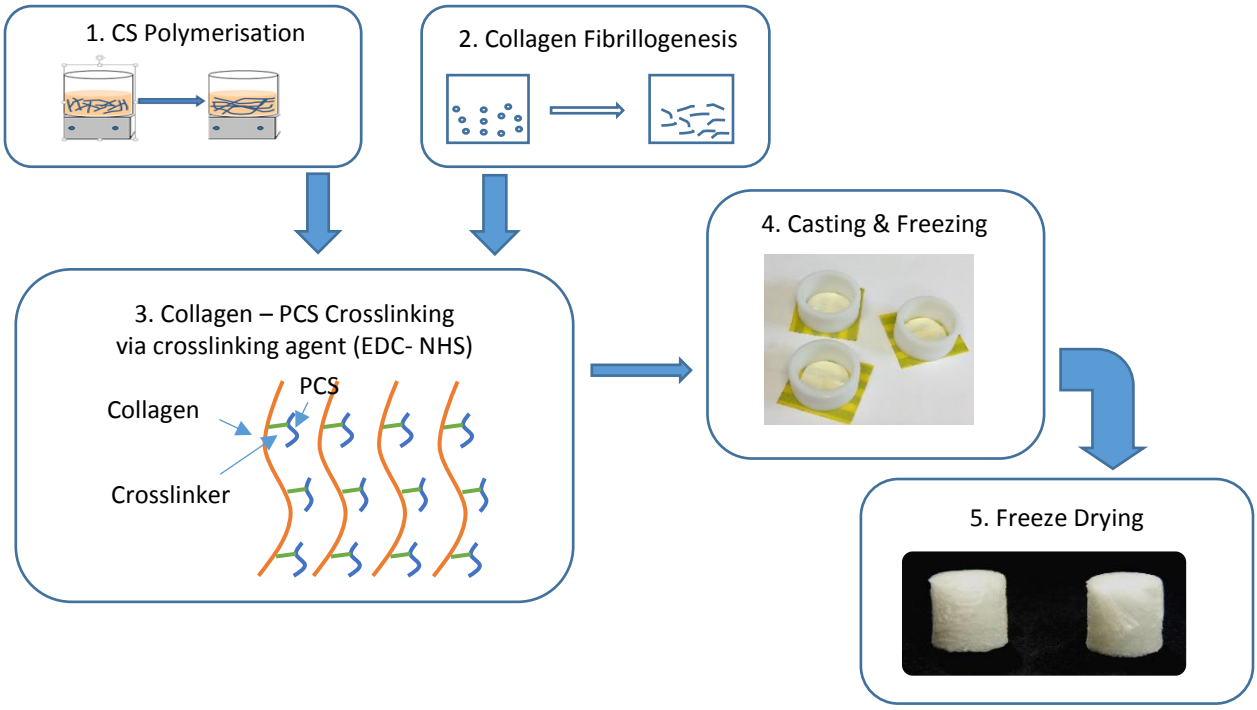


Fig 5.1. Schematic diagram of scaffold fabrication steps

Scaffolds acronym	Collagen Type	Collagen:CS/PCS weight ratio
XColl2- PCS	Crosslinked reconstituted fibrillar collagen Type II	1: 0.4
XColl2- CS	Crosslinked reconstituted fibrillar collagen Type II	1:0.2
XColl2	Crosslinked reconstituted fibrillar collagen Type II	

Table 5.1. Scaffold composition: type of collagen (type II), ultrastructure (reconstituted fibrillar) and the quantity of CS and PCS

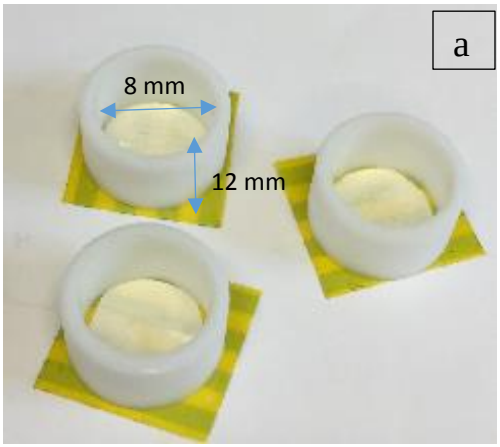


Fig 5.2(a). PTFE mould, sealed at one end used for casting collagen solution for characterization test

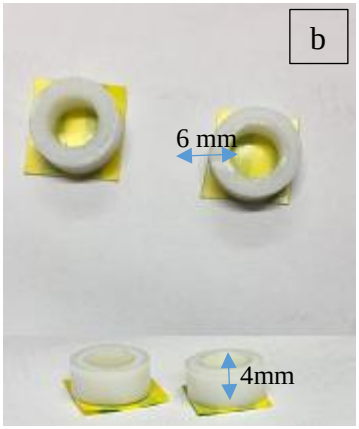


Fig 5.2(b). PTFE mould, used for casting of collagen solution for cell studies

5.3. Scaffolds' CS Content Measurement (Blyscan assay)

CS release from the scaffolds was studied to investigate the effect of crosslinking on CS/PCS attachment to collagen. CS release for Coll2- CS, XColl2- CS and XColl2-PCS scaffolds in basal medium (DMEM-Low Clucose, Sigma-Aldrich) was measured at different time points using Blyscan™ Glycosaminoglycan Assay (Biocolor Ltd, UK) following the manufacturer's protocol.

Briefly, scaffolds were placed in a microcentrifuge tube (Brand, Germany) with the addition of 1 ml of Papain Extraction Reagent. The tubes were then placed in a heating block at 65 °C for 3 hours. Tubes were then centrifuged (Heraeus Biofuge) at 10000rpm for 10 minutes. Supernatant were decanted off to a fresh micro tube for use with Blyscan sGAG Assay protocol. 1 ml of Blyscan dye reagent was added to each tube, the contents were mixed and tubes were then placed in a mechanical shaker for 30 minutes. A sulphated glycosaminoglycan-dye complex is formed and precipitates from the soluble unbound dye. The tubes were subsequently transferred to a micro tube and spun at 12000 rpm for 10 minutes. The unbound dye was removed and dissociation reagent (0.5 ml) was added to the tubes. The contents of tubes were then vortexed for 10 minutes to release the bound dye in solution. This followed by centrifugation at 12000 rpm for 5 minutes. 200 µl of each sample in triplicate is transferred into 96 white micro well plate (Costar, Corning Inc, USA). Absorbance were measured by a plate reader (Tecan, infinite M200 PRO) at 659nm for reagent blanks, standards and test samples. Glycosaminoglycan standard was provided in the kit and 1,2,3,4,5 µg of reference standards was prepared and their absorbance were measured and thus the samples CS content was obtained using the standard curve.

5.4. Statistical Analysis

Analysis of variance (ANOVA) tests were performed in SPSS for each test. All post hoc tests were Bonferroni corrected for multiple comparisons. Significance was accepted at level of 0.05. If spherecity was violated, Greenhouse Geiser correction values for ANOVA are reported. Experimental groups for each test are as follows: for mechanical testing: n=5, rheology experiments, FTIR, metabolic activity and DNA quantification: n=3, for qPCR test n=4.

5.5. Results

5.5.1. Collagen Dispersions Rheology

Rheological behavior of suspensions can help to clarify the influence of the introduction of CS and PCS into the collagen suspension. Rheological properties together with the chemical bonding help to explain the scaffold microstructure and the consequent mechanical and cellular response. The material response to increasing frequency was examined at a constant strain and temperature. Dynamic frequency sweeps were conducted within the Linear Viscoelastic Region (LVR) at 1% strain with angular frequency of 0.1 to 100%. Tamaddon (2014) determined LVR for collagen II suspensions by performing strain sweep (0.1-100%) oscillatory shear test (T=20 °C) [205] and it has been confirmed that the strain level of 1%, which was used for all further examinations is within the LVR. Fig 5.3 demonstrates complex viscosity, storage and loss moduli in terms of angular frequency.

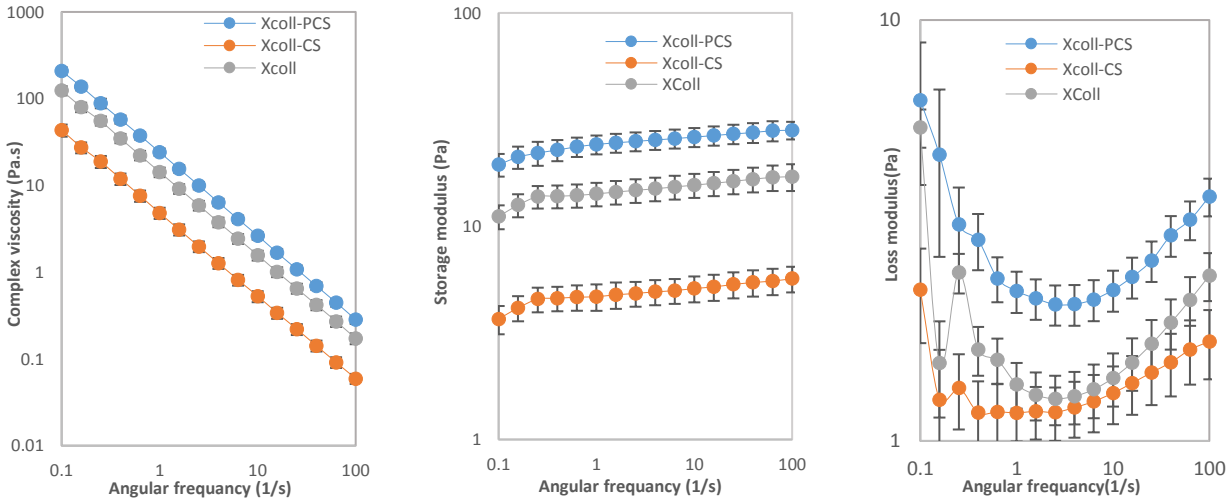


Fig 5.3. Complex viscosity (a), storage (b) and loss modulus(c) of collagen II, collagen II-PCS and collagen II-CS solutions in oscillatory shear test; frequency sweep (angular frequency = 100-0.1 rad/s, strain amplitude γ = 1%, T =20C). Effect of CS and PCS addition in collagen type II preparations.

As shown in Fig 5.3, the viscosity of all the dispersions decreased by increasing angular frequency and exhibits the shear thinning, hence they can be categorised as pseduplastic materials. The storage modulus of all the solutions remained approximately linear over the entire range of angular frequency. The loss modulus was almost linear in frequencies between 0.4 and 16 s^{-1} and increased slightly at higher frequencies (> 25 1/s). All solutions showed a higher storage modulus than loss modulus suggesting that the solutions elastic property dominates their viscous property.

XColl2 – PCS has a significantly higher viscosity ($p< 0.05$) than the pure collagen solution in the whole range of angular frequency, however XColl2 –CS has a lower viscosity compared to pure collagen solution. The average complex viscosity, storage, loss and complex moduli are the highest for XColl2- PCS as compared to the other solutions. It can be seen that the introduction of PCS to collagen increased the viscoelastic properties of suspensions, yet addition of CS to collagen reduced the viscoelastic properties.

5.5.2. Fourier Transform Infrared Spectroscopy (FTIR)

Fig 5.4 shows the averaged (n=3) FTIR spectra of Coll2-CS, XColl2-CS and XColl2-PCS. All spectra have been normalised against the C-H band (absorption at 3300 cm^{-1}) which unexpectedly remain unchanged after chrosslinking. It can be seen that the bands of collagen and CS overlapped and second derivative aids to deconvolute the overlapped peaks. Fig 5.5 represents the second derivative spectra. The FTIR spectra of all samples showed characteristic collagen amide A, I, II and III bands. CH2 side chain vibration peak at 1338 cm^{-1} is also a key characteristic feature of collagen, which was present in all samples. Table 5.2 shows the band assignment of second

derivative spectra. There are no significant changes (<4 cm^{-1}) in the frequency of amide I, II, III in the samples. The only significant peak shift is in amide A band (8 cm^{-1}) that occurred in the crosslinked sample. Crosslinking shifted the amide A band to a lower wavenumber (from 3265 to 3257 cm^{-1}).

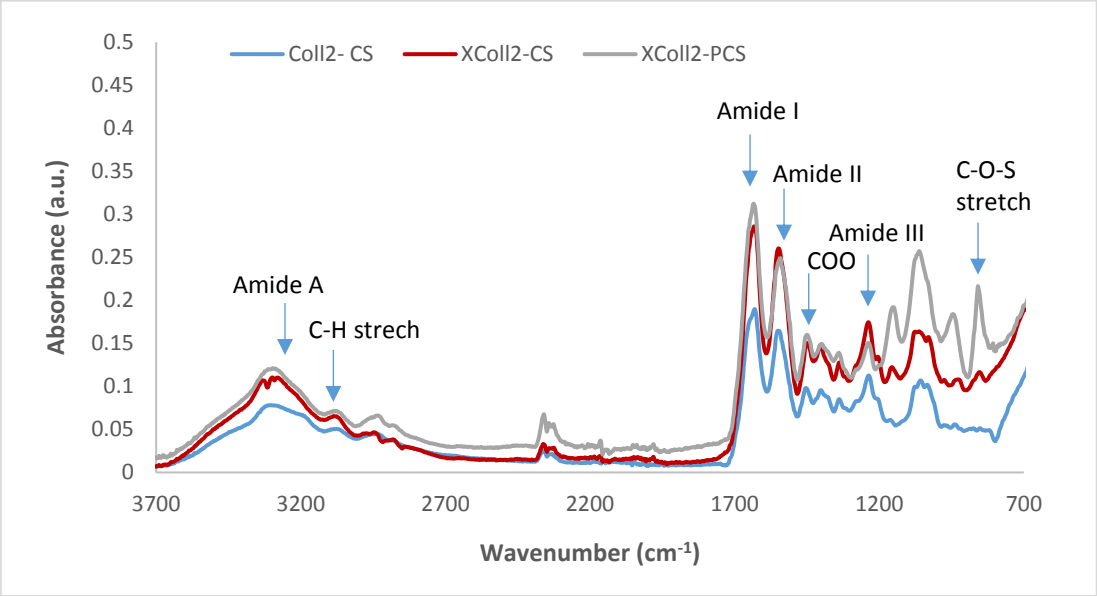


Fig 5.4. FTIR spectra for Coll2-CS, XColl2-CS and XColl2-PCS, spectra were normalized against C-H band (n=3)

Coll2- CS and XColl2- CS showed no significant changes in their peak positions (Fig 5.5) except for C-O-S band. Crosslinking significantly shifted the C- O-S band to a higher wavenumber suggesting the likelihood of a bond between CS and collagen. The only significant variations between the spectra of XColl2- PCS and XColl2-CS are related to the C-O-S asymmetric stretching in CS and PGs/SO^{3-} stretching. These two bands shifted to lower wavenumbers in XColl2- PCS.

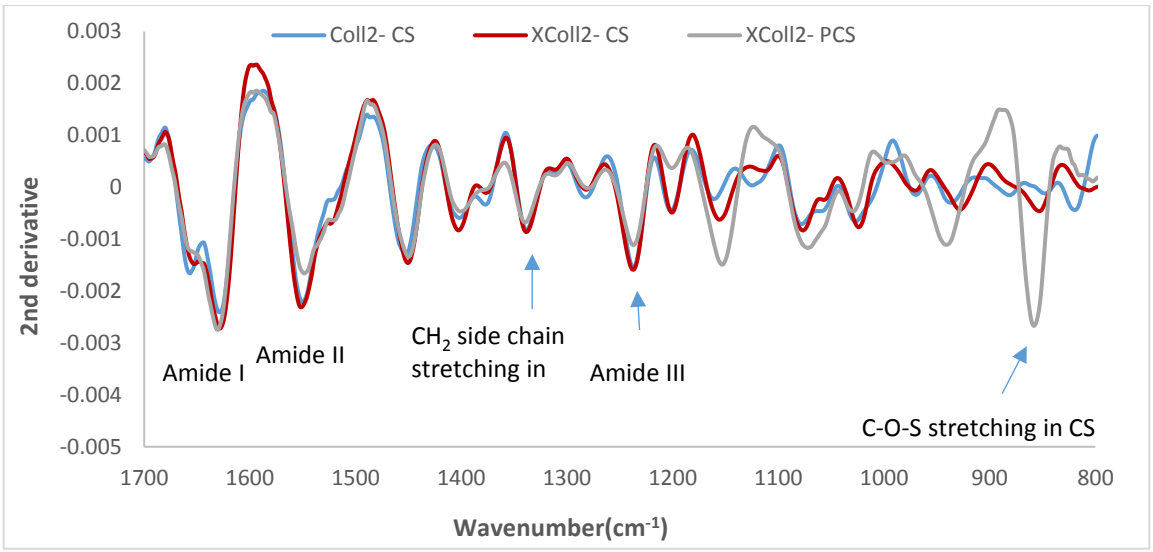


Fig 5.5. 2nd derivative spectra for XColl2-PCS, XColl2-CS and Coll2-CS

Band Assignment	XColl2 - PCS	XColl2 - CS	Coll2 - CS
Amide A	3257	3257	3265
Amide I (C=O stretch)	1630	1630	1626
Amide II (C-N stretch, N-H bend)	1547	1550	1550
Amide III, combined with CH_2 wagging from glycin bachbone and proline side chain	1236	1236	1236
CH_3 asymmetric bending	1448	1450	1448
COO (stretch of amino side chain)	1400	1402	1400
CH_2 (side chain stretching, characteristic of collagen)	1338	1338	1338
C –O –S asymmetric stretching in CS	856	870	845
C–O stretching of carbohydrate residues in collagen and PGs/SO^{3-} stretching	1069	1080	1082

Table 5.2. FTIR band assignment for XColl2-PCS, XColl2-CS and Coll2-CS

5.5.3. Pore size analysis

SEM images (Fig 5.6) showed that all scaffolds possess a highly porous structure, pores are randomly distributed and showed different sizes in XColl2-CS and XColl2-PCS.

The pores don't appear to be circular, and so they can be better quantified as ellipses with a cross-sectional pore areas and a measure of circularity. The pore analysis data is first presented in terms of cross-sectional primary pore areas, A, and the isoperimetric quotient of circularity (Q) is also indicated as $Q= 4\pi A/L^2$ where L is the circumference of the ellipse.

The average pore area of XColl2-CS scaffolds was found to be 4290 μm^2 (measured by Image J software) with the average pore circularity quotient of 78 %. The majority of pores (83 %) have an area less than 5000 μm^2 Average major and minor pore diameters are respectively 81 µm and 43 µm. (Table 5.3)

The average pore area of XColl2-PCS scaffolds was found to be 2237 μm^2 with the average pore circularity quotient of 77 %. The majority of pores (82%) have an area less than 2500 μm^2 Average major and minor pore diameters are respectively 61 µm and 33 µm.

Sample	Average Size (μm^2)	Major pore diameter (µm)	Minor pore diameter (µm)	Quotient of circularity
XColl2-CS	4290 (SD: ± 1200)	81 (SD: ± 24)	43 (SD: ± 13)	0.77
XColl2-PCS	2237 (SD: ± 380)	61 (SD: ± 14)	33 (SD: ± 6.4)	0.78

Table 5.3. Average pore size and circularity in XColl2- CS and XCOll2- PCS

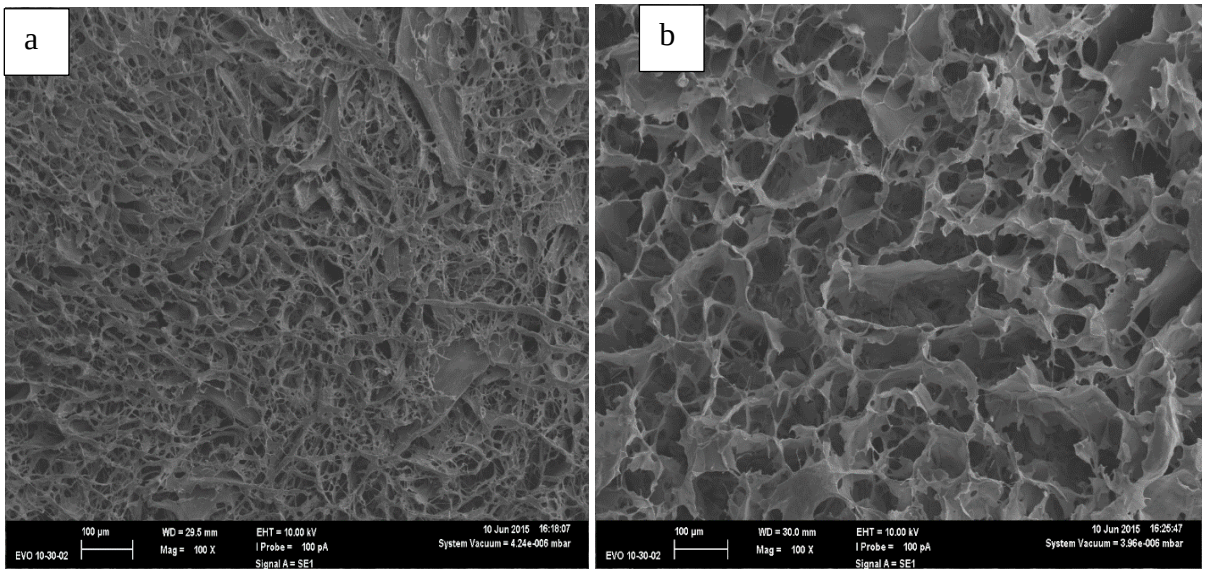


Fig 5.6. SEM images of (a) XColl2 -PCS and (b) XColl2-CS

5.5.4. Degradation study; effect of crosslinking on scaffolds dissolution behavior

To study the effect of crosslinking on the dissolution behavior of scaffolds, uncrosslinked monomeric (Coll2- CS) scaffolds and crosslinked scaffolds (XColl2- CS) were immersed in TBS (Tris Buffer Saline) up to two weeks and four weeks respectively. The mass of the scaffolds was measured at 3 time points. Three samples were used for each type at each time point. 88% of the uncrosslinked scaffolds mass was reduced after two weeks (Fig 5.7). However, crosslinked scaffolds showed approximately no mass reduction (0.5%). The dissolution study was continued for an extra 2 weeks for crosslinked scaffolds. As shown in Fig 5.8, the mass of the crosslinked scaffolds was almost unchanged over 4 weeks.

Uncrosslinked scaffolds were stable in culture medium for only a very short period of time (2 days), hence we were not able to compare their cell behavior with uncrosslinked samples. Crosslinked scaffolds were not disintegrated in TBS over a period of 28 days and they were also stable in cell culture media through the whole period of culturing (Chapter 7).

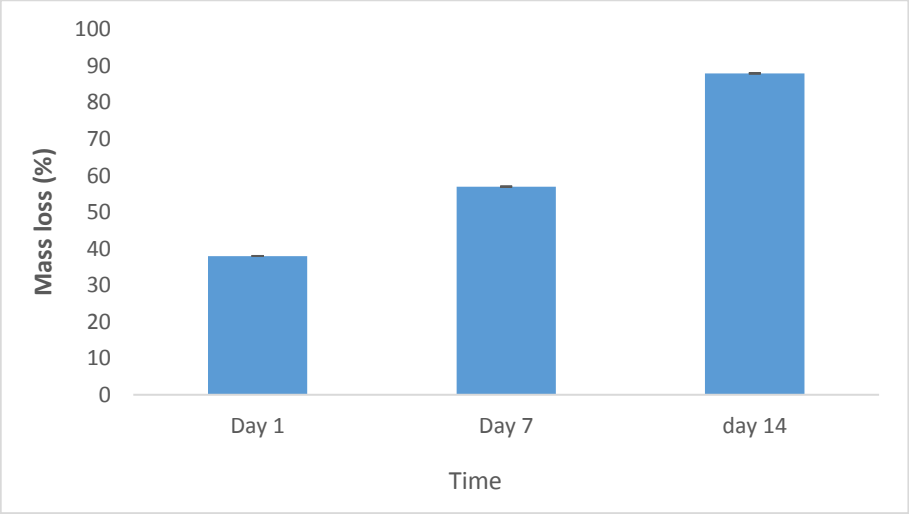


Fig 5.7. Uncrosslinked Coll2- CS degradation behavior in 14 days (n=3)

(Day 1 SD= 0.007, Day7 SD=0.007, Day 14 SD=0.023)

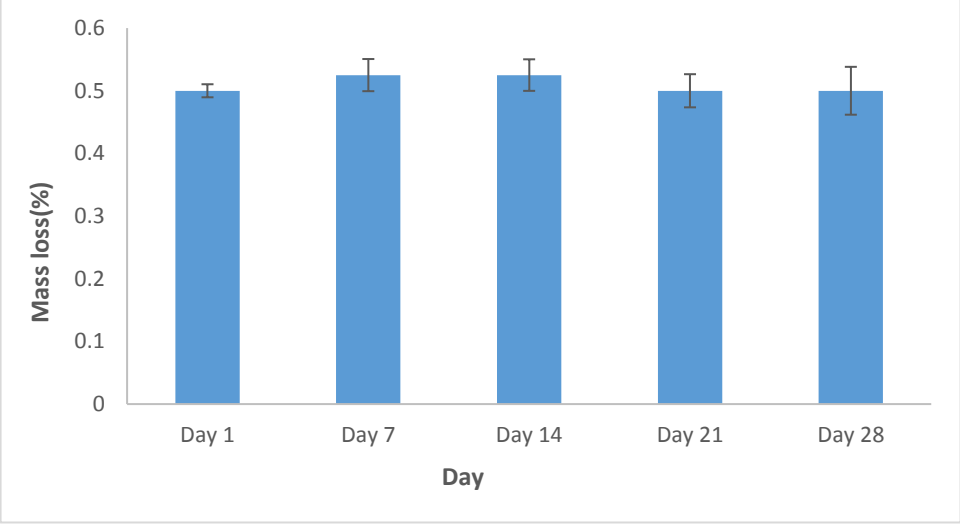


Fig 5.8. Crosslinked Coll2- CS weight loss during 28 days (n=3), approximately 0.5% mass loss at each time point

5.5.5. CS and PCS content of the scaffolds and their CS release profile

Fig 5.9 shows the CS content of XColl2- PCS, XColl2- CS and Coll2- CS scaffolds. The CS content of crosslinked scaffolds (XColl2- CS & XColl2- PCS) are substantially greater (approximately 7 times) than that of the uncrosslinked scaffold (Coll2-CS). The CS release is depicted in Fig 5.10, which reveals that uncrosslinked Coll2 - CS released 80% of its CS content after just 1 hour of immersion in cell culture medium, however XColl2-PCS and XColl2-CS only released 2 % of PCS and 1.2 % of CS respectively. Thus, it can be concluded that crosslinking gave rise to a large reduction in the CS loss. Thus it is expected that the CS/PCS would remain in the scaffolds for a longer period of time which would enable them to play their stimulatory role on stem cells towards the cartilage lineage (Chapter 7).

The CS release study continued for XColl2-CS and XColl2-PCS until 5 days, CS release quantities are insignificant in day 1, day 2 and day 5. CS release quantity after 5 days for XColl2-CS and XColl2-PCS were 0.3 and 0.7% respectively.

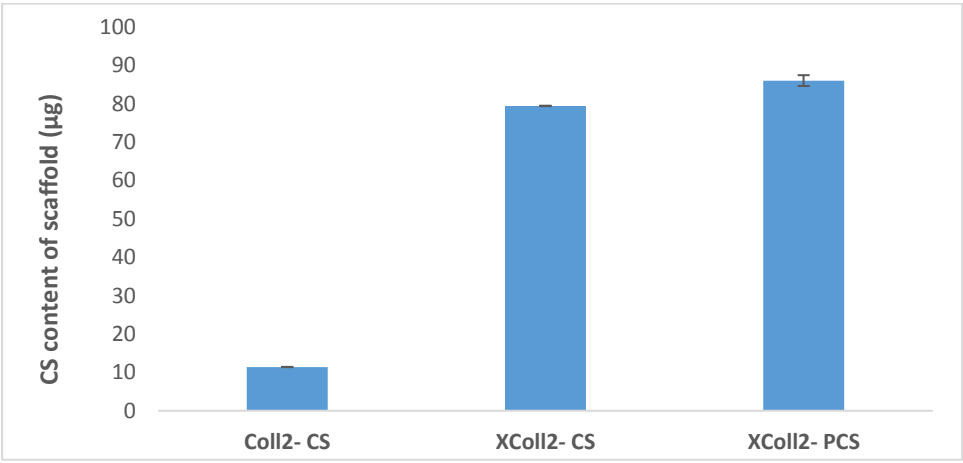


Fig 5.9. Scaffolds' CS content; crosslinking increased the scaffolds' CS content by approximately 7 times

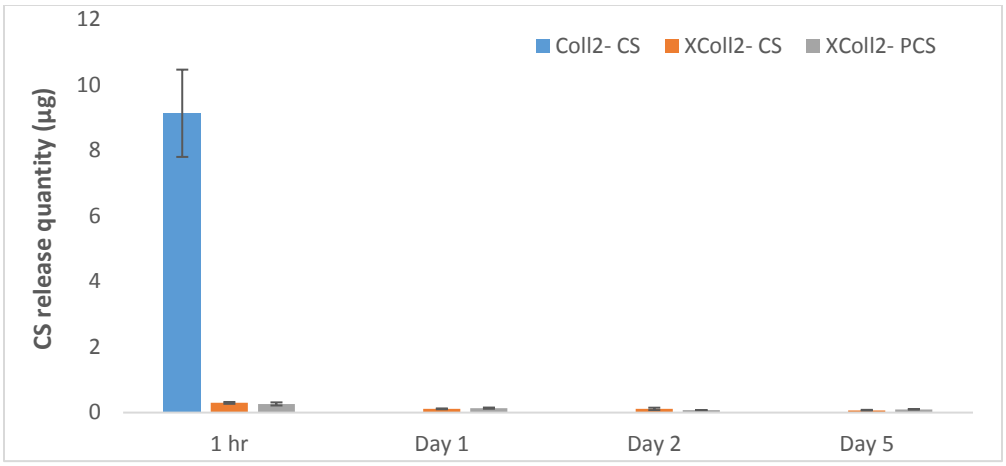
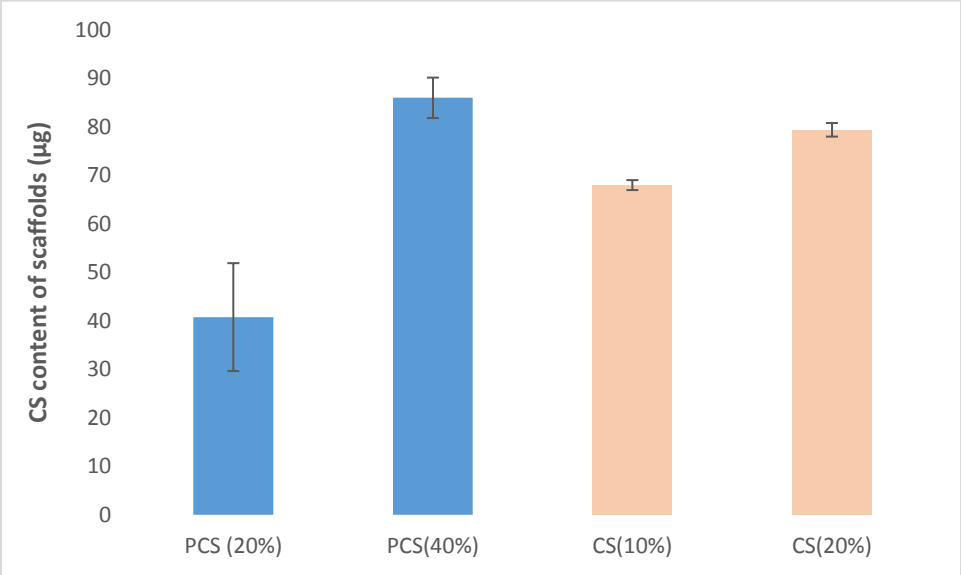


Fig 5.10. CS release profile in culture medium during 5 days

Fig 5.11 illustrates the CS/PCS amount (percentage) which were initially added to the collagen suspension. The quantity of CS in XColl2- CS was approximately two times of the quantity of PCS in XColl2- PCS in spite of adding the same amount (20%) initially. It is possibly due to the fact that part of the carboxylic group of CS is involved in the polymerisation reaction to produce PCS. The linkage between CS/PCS to collagen is between the carboxylic group of CS/PCS and amine group of collagen (See Fig 5.16). FTIR has also confirmed that carboxylic group reduced in PCS compared to CS. The FTIR results for pure CS and PCS together with the measurement of scaffolds' CS content help to understand the amount of CS and PCS that is needed to be added to collagen to have the same PCS attachment to collagen as that of CS; it was found that 2 times higher quantity of PCS was needed. Therefore to compare scaffolds that contain the same number of CS and PCS attached to collagen, XColl- CS (20%) and XColl-PCS (40%) were prepared for biological studies.

The CS content of XColl2- CS (10%) and XColl2- CS (20%) shows that by doubling the initial amount of CS in the collagen suspension, the CS attached to collagen did not increase by 2 times

(Table 5.4). In fact, only a limited amount of CS is linked to collagen. In other words, the amount of CS which can attach to collagen does not exceed 12%. Introduction of PCS to collagen solution slightly increased the PCS amount in the scaffolds. The maximum amount of CS attached to collagen in XColl2-CS is 79.4 µg which increased to 86 µg in XColl2-PCS (Fig 5.11).



5.11. CS content of XColl2- PCS (20% & 40%) and XColl2- CS (10% & 20%)

Scaffolds	CS content (µg)
PCS (20%)	40.77 (Stdev: ±11.12)
PCS (40%)	86 (Stdev: ±4.17)
CS (10%)	68 (Stdev: ±1.03)
CS (20%)	79.4 (Stdev: ±1.4)

Table 5.4. CS content of XColl2-CS and XColl2- PCS scaffolds at different CS/PCS concentration of collagen suspensions

5.5.6. Mechanical properties of collagen scaffolds under compression

Compression testing was carried out on cylindrical samples (0.8 cm diameter, 1.2 cm height) and 5 samples were tested for each scaffold type. Fig 5.12 and 5.13 depict representative stress-strain curves for XColl2- PCS, XColl2- CS and XColl2 respectively. They all show the three characteristic regions of deformation under compression of a cellular foam, except the initial linear region is hard to distinguish in XColl2 scaffolds. The compressive (Young's) modulus is calculated from the slope of the initial linear regime of the stress-strain curve. Fig 5.14 represents the average compressive modulus of samples. The value for XColl2- PCS is significantly higher than that for XColl2- CS and XColl2.

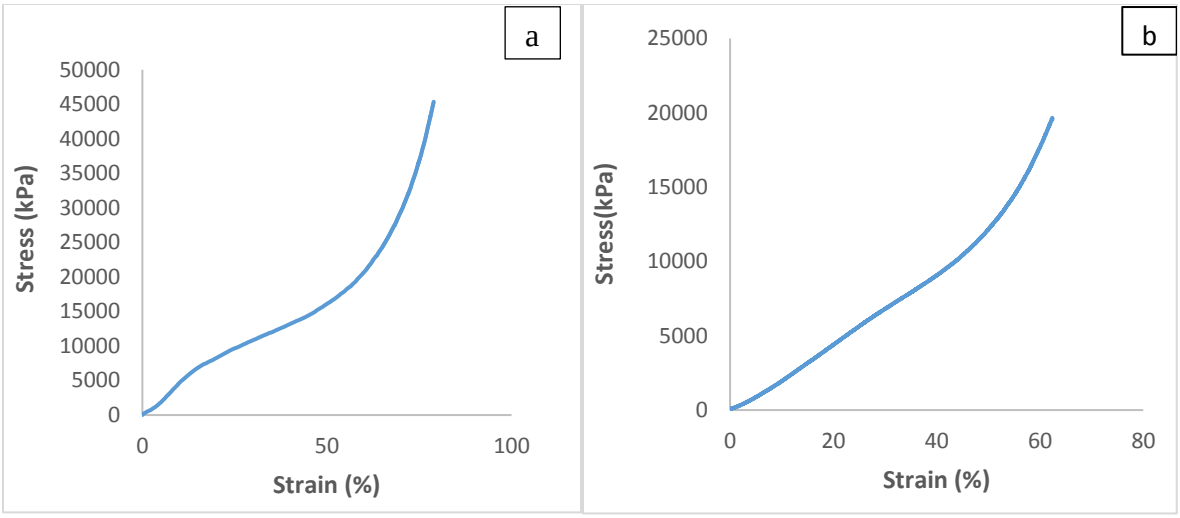


Fig 5.12. Representative stress- strain curves for (a) XColl2 - PCS and (b) XColl2- CS at strain rate of 3.2%/min

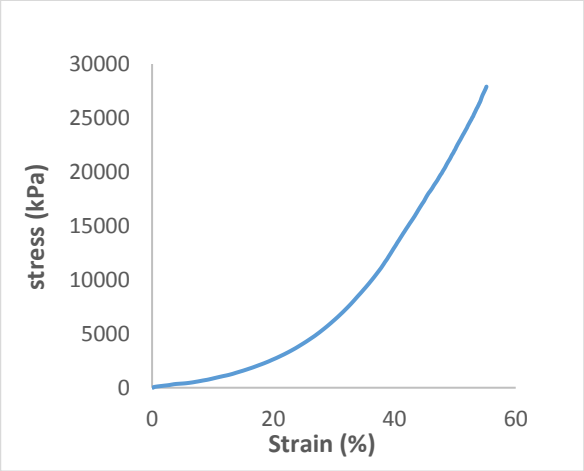


Fig 5.13. Representative stress- strain curve for XColl2 (Strain rate of 3.2%/min)

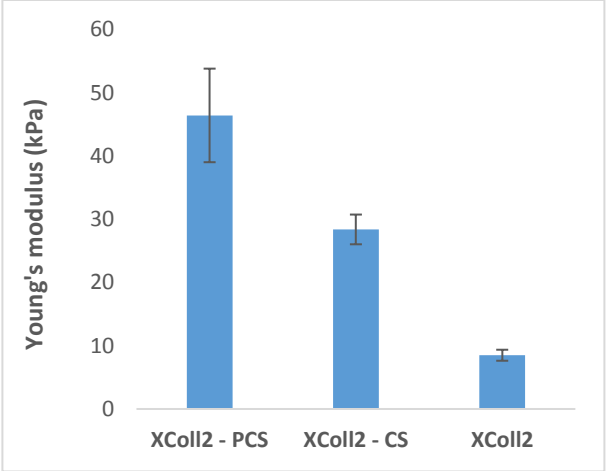


Fig 5.14. Young's modulus of XColl2- PCS, XColl2- CS and XColl2

The compression modulus of XColl2- PCS is signifcantly higher than the other two types (p< .001). It shows that the introduction of PCS to collagen scaffolds significantly increased the compressive modulus. The compressive modulus of XColl- CS scaffold is also significantly greater than XColl2 which indicates that CS improved the compressive modulus of scaffolds which is of true agreement with other work[150]. The increase in Young's modulus by crosslinking is by a factor of 100, this is much greater than the other work which only used uncrosslinked samples[224].

5.6. Discussion

This section discusses the rheological behaviour of collagen suspensions under shear (Section 5.5.1.). FTIR and degradation outcomes are discussed in section 5.5.2 to analyse both the occurrence of crosslinking between collagen and CS/PCS and the effect of crosslinking on the scaffold's stability. The pore structure and mechanical properties of the scaffolds are lastly discussed in section 5.5.3 and 5.5.4.

5.6.1. Rheology of collagen dispersions

All collagen suspensions showed shear thinning behaviour. PCS significantly increased the complex viscosity, storage and loss modulus of collagen suspensions, while CS reduced them. As stated in Section 4.5.2, to understand the behaviour of suspension under shear, the molecular structure, state of the preparation, and defects in the system need to be assessed. The molecular structure of CS and the state of the polymer suspension were discussed in section 4.5.2. As CS is a polysaccharide and collagen is a protein, the collagen structure and its suspension state is discussed separately here.

Collagen monomers in suspension are rod-like and have a triple helical configuration; they are neither flexible nor completely rigid but, rather, show partial flexibility[225-227].There are furthermore hinge-like flexible regions showing considerable freedom on the collagen molecule, where the triple-helical structure is interrupted. Moreover, the gradual bending of the helical structure gives rise to molecule's partial flexibility[228,229]. Fig 5.15 illustrates Kuhn chain and "worm-like" chain models.

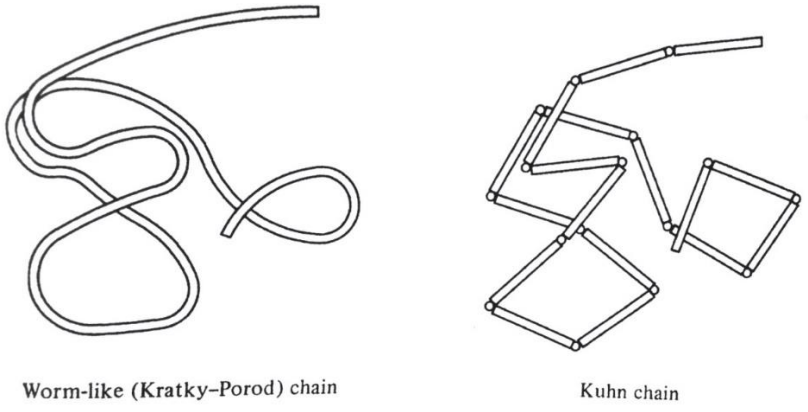


Fig. 5.15. Schematic illustration of worm-like polymer chains with continuous flexibility and Kuhn chains with rigid and flexible domains[132].

The typical chain length (L) and the diameter (d) of a collagen monomer are 300nm and 1.4nm respectively. The collagen has the persistent length λ_p of 170nm, which denotes its partial resistance to bending[132,228,229].Since the chain length is larger than the persistent length, the monomer is not completely rigid and exhibits semi-flexibility. The state of the mixture is also of significance, particularly in relation to its concentration (i.e. diluted, semi-diluted, isotropic concentrated or nematic). This is because it greatly impacts upon the behaviour of (and interaction between) the molecules/particles in the solution. For suspensions of rod-like molecules with a high aspect ratio (L/d), such as collagen molecules (L/d= 300/1.4 = 214), diluteness only occurres when the concentration/volume fraction of molecules (Φ_0) is low enough that a single rod can rotate freely without hindrance from the neighbouring rods. The following equations was used to calculate the transition boundaries[132]:

$$\Phi_0 = 24(d/L)^2 \sim 0.05\% \quad \text{(Equation 5.1)}$$

$$\Phi_0' = \pi d/4L \sim 0.6 - 1\% \quad \text{(Equation 5.2)}$$

$$\Phi_1 = 3.3\,(d/L) \sim 1.5\text{-}2.5\ \% \quad \text{(Equation 5.3)}$$

ϕ_0, ϕ'_0 and ϕ_1 denote the transition from: dilute to semi-dilute, semi-dilute to concentrated, and concentrated to nematic. The above equations are for rigid rods. Hence, an upper limit can be calculated if L is substituted for the persistent length λ_p.

The volume fraction of collagen monomers is calculated based on $\phi_A = C/\rho = c.\ V_{mon}\, N_{Av}/\, M_{mon}$, where c: polymer concentration, V_{mon}: monomer volume, N_{Av}: Avogadro's constant, M_{mon}: monomer molar mass. Given that the collagen molecular weight is 300kDa, and its initial

concentration is 0.01g/ml, the value for the volume fraction is calculated to be around 0.92%. It can therefore be concluded that the state of pure collagen solutions is semi-dilute.

The basic forces, defects in monomers, and polydispersity can influence the rheological properties of solutions as well as the molecular structure. The reason for this shear thinning behaviour is that there is a force equilibrium between collagen/particles in suspension. In this respect, shear is likely to disturb the equilibrium, so that the arrangements of molecules are pushed towards an unfavourable state of lower entropy, which serves to weaken the intermolecular/interparticulate forces. These basic forces have notable effects. Based on *excluded volume repulsion*, if two molecules (or two parts of one molecule) are pushed together so that their electron clouds collide, a repulsive force is experienced[132]. Through this process, it is possible that the shear sends the collagen molecule to a conformation which is unfavourable in terms of excluded volume[230]. It may also align the molecules/fibrils and bring them into close proximity, hence producing a repulsive force.

Due to *electrostatic forces*, the same repulsive force can be generated between the molecules, where the shear-induced breaking of water-bridge bonds between them can lead to the production of like-charged groups[230]. These groups may repel one another when they are forced together during shear, weakening the intermolecular bonds[231]. Moreover, both the electrostatic interaction and *covalent bonding* between collagen and CS/PCS may be disrupted due to shear. The dipole-dipole interaction between the molecules can further lead to an attractive *Van der Waals force*[132] that, again, can be affected during shear.

The combined effect of the repulsive forces, and interruption of attractive forces, can lead to the

less cohesion between molecules, fibrils, and particles and, therefore, reduce viscosity by increasing the shear. The network is in a semi-diluted state where some entanglements exist. Moreover, as the collagens are chemically crosslinked, there are covalent bonding and crosslinking between the molecules. This poses difficulties when they need to rearrange themselves and, as a result, the network may break under shear. From this we can conclude that, when bonding and cross-linking exists, extensive molecular rearrangement is not possible and, instead, network failure occurs. This in turn leads to viscosity reduction (i.e. shear thinning).

All the samples showed reduced viscosity with increased angular frequency. In particular, XColl2-PCS showed the highest complex viscosity, in agreement with the statements above. That is, the presence of PCS (which is either attached covalently and electrostatically, or locked in the network mechanically) gives rise to a higher flow resistance, thus leading to higher viscosity. Interestingly, XColl2- CS suspension showed the least complex viscosity. We may assume that CS has reduced the available interaction sites for collagen to collagen binding during the crosslinking process, so that the formation of larger networks is inhibited. This reduces the viscosity in comparison to crosslinked reconstituted fibrillar collagen (XColl2). Furthermore, the addition of CS to the reconstituted fibrillar collagen prevents the crosslinking of collagen to collagen, due to CS competing (with collagen) to covalently attach to other collagen. In this way, CS acts as an inhibitor to the growth of collagen networks.

The size and molecular weight of a fibrillar collagen is extensively higher than that of a CS molecule because the molecular weight of a collagen monomer is 15 times higher than that of CS. As such, a pure crosslinked fibrillar network of collagen has a higher size/molecular weight

than collagen-CS. This gives rise to the noted viscosity drop in XColl2-CS solution compared to XColl2.

Previous work by Tamadon (2014) showed that the presence of CS in monomeric collagen suspensions increases the viscosity compared to a pure monomeric collagen suspension[205]. It was previously seen that, due to the extended flexible nature of CS, an effective network of entanglements may be produced and, when combined with possible electrostatic/hydrogen bonding with collagen, may contribute to an increased complex viscosity[205]. Notably, in the current study, the reverse effect of CS on the viscosity of crosslinked fibrillar collagen solutions was observed. Indeed, CS showed the inverse impact on the viscosity of monomeric collagen solutions, as opposed to the viscosity of crosslinked fibrillar collagen suspensions. In this study the CS/PCS was added to collagen suspensions after fibrillogenesis while in the previous work, CS was added before. Therefore, the presence or absence of CS in fibrillogenesis would give rise to the opposite effect of CS on the collagen suspension viscosity.

A monomeric collagen solution is a uniform distribution of relatively low weight molecules with a narrow distribution, whereas fibrillogenesis produces a system of large macromolecules containing crosslinks that contains a large distribution in molecular weight. As we have here observed, crosslinking further produced larger molecules, or networks between molecules, thus acting as an effective hindrance to flow.

5.5.1.2. Storage (G') and loss (G") moduli

The technique of dynamic oscillation is capable of resolving the structural properties of a suspension into its elastic (G') and viscous (G'') components[232]. Thus any variation in G' or G"

must reflect some changes in the intermolecular interactions[233].

All of the reconstituted fibrillar suspensions remained in plateau region over the measured angular frequencies; the weak dependency of G' on frequency is typical for biopolymer gels[234]. Such behaviour is thought to arise from the rigidity of chains due to the presence of CS/PCS and strong interactions between collagen molecules due to fibrillogenesis and crosslinking.

5.6.2. FTIR and degradation studies

All samples revealed the presence of Amide A, I, II and III bands. This confirmed that the primary structure of collagen was maintained during the scaffolds fabrication. Furthermore, no major peak shifts in Amide A, I, II and III bands were observed after crosslinking.

The FTIR spectra of all polypeptides and proteins generate bands whose positions are particularly sensitive to conformational changes in the polypeptide backbone and, hence, may serve as markers for the integrity of the secondary structure[235-238]. For most of the proteins, the marker is the Amide I band, whose frequency is found to be independent of the underlying amino acid sequence. However, for a triple-helical polypeptide, such as collagen, such independence is not observed, as both the amino acid composition and protein secondary conformation contribute to this band[239]. Therefore, while this band was not selected as a determinant of the secondary structure of the preparations, the observed band frequencies do however serve as indicators of bond strength. This is because higher wavenumbers correspond to stronger bonds, and lower wavenumbers to weaker bonds.

Amide I bands, arising from C=O (carbonyl) vibrational stretching along the polypeptide

backbone, are observed between 1600 and 1700 cm^{-1} (along with minor C-N stretching vibrations and N-H bending[238]). In contrast, amide II bands are seen to be more complex, as they mainly arise from an out of phase combination of N–H in-plane bending (60%) combining with the C–N stretching vibrations (40%) of the peptide bonds[238]. Finally, amide III bands primarily result from C–N stretching and N–H deformation vibrations[238], while the peaks between 1331-1339 cm^{-1} are due to the presence of a dissociated carboxyl group (COO^-) from the proline side chain.

Collagen type-II possesses a secondary helical structure that is stabilised by the hydrogen bonds arising between carboxyl and hydroxyl groups of the three αII strands. This forms a supercoiled triple helical conformation, as shown by the amide A (N-H stretching of the core polypeptide and also basic amino acid side chains, e.g. lysine and arginine) band[238]. Its frequency determines the extent of supercoiling, as this leads to an angular distortion (or 'lengthening') of the hydrogen bonds. No changes were observed in the amide A band of XColl2-PCS and XColl2-CS, however amide A band shifted to a lower frequency after crosslinking. The 8cm^{-1} downshift in the frequencies of crosslinked samples may indicate the formation of a longer/weaker hydrogen bond and so a less compact triple helical structure.

As shown in Fig. 5.5, the amide I region of collagen showed two distinct peaks in the spectra of the second derivative. In general, the peaks in the amide I region are associated with three carbonyl groups of Gly-X-Y, where Gly and Y are almost always in contact with the solvent. Accordingly, X (proline), which is considered to be responsible for the formation of a 1660 cm^{-1}

band, is susceptible to conformational changes due to internal H-bond[240]. Using the second derivative method, it was possible to detect two of the three amide groups (at 1628 and 1657 cm^{-1}) that remained constant throughout the preparation. The band at 1628 cm^{-1} has been associated with the hydroxyproline carbonyl group. Based on the observations above it can be concluded that the addition of CS/PCS and fibrillogenesis did not have any effect on the carbonyl groups of proline and hydroxyproline. This points to the preservation of the internal H-bonds during the interaction with CS or other triple helices during fibrillogenesis, and the preservation of triple helix conformation.

It is further shown that the addition of proteoglycans and glycosaminoglycans may hinder lateral fibril growth, either by sterically hindering the approach of additional collagen molecules or through anionic repulsion (when the indicated glycans are attached to collagen[241]). Moreover, it was found that there are at least three binding sites on each collagen molecule that are able to interact with CS-4 and that the number of sites remain constant[242]. However, due to the increasing ionic strength, the binding affinity decreases. This is because some of the bonds between collagen and CS in the acidic environment are weakened or abolished during fibrillogenesis[242,243]. Hence, to avoid the adverse effect of CS/PCS on collagen fibrillogenesis, it was decided to add CS/PCS to the collagen suspension after collagen fibrilogenesis.

Fig. 4.5 shows the molecular structure of collagen and CS, as well as potential sites for their interaction. Since CS is an anionic polymer, it is expected to interact with the cationic regions of collagen. However, the chemical binding of CS to collagen is still not fully understood, and is yet to be investigated. That said, it is generally accepted that the interaction between collagen and

CS is of an electrostatic nature[244-247] under physiological conditions, or when outside of the isoelectric point of collagen and CS. The corresponding groups could be sulfate or a carboxyl group of CS and positively charged collagen side-chains such as arginine and lysine (they are both cationic in the acidic and physiological environment[246]). It was also revealed that this interaction was not only electrostatic, but could also comprise other types, such as hydrogen bonding[246]. For instance, in neutral pH close to the isoelectric point of collagen, the net charge of collagen is very small; as such, the interaction mechanism is expected to be mainly dictated by hydrogen bonding. As these interactions are weak (and CS can be easily washed away through multiple steps of washing), CS was immobilised on collagen via EDC-NHS crosslinking. EDC crosslinking of collagen and CS results in the formation of covalent attachment between collagen and CS (Fig 5.16).

FTIR spectra (Fig 5.4) shows higher absorption intensities for crosslinked samples compared to the uncrosslinked sample. These increases in intensity are more pronounced at the amide's characteristic peaks (C-N band), indicating covalent bonding between the collagen and CS.

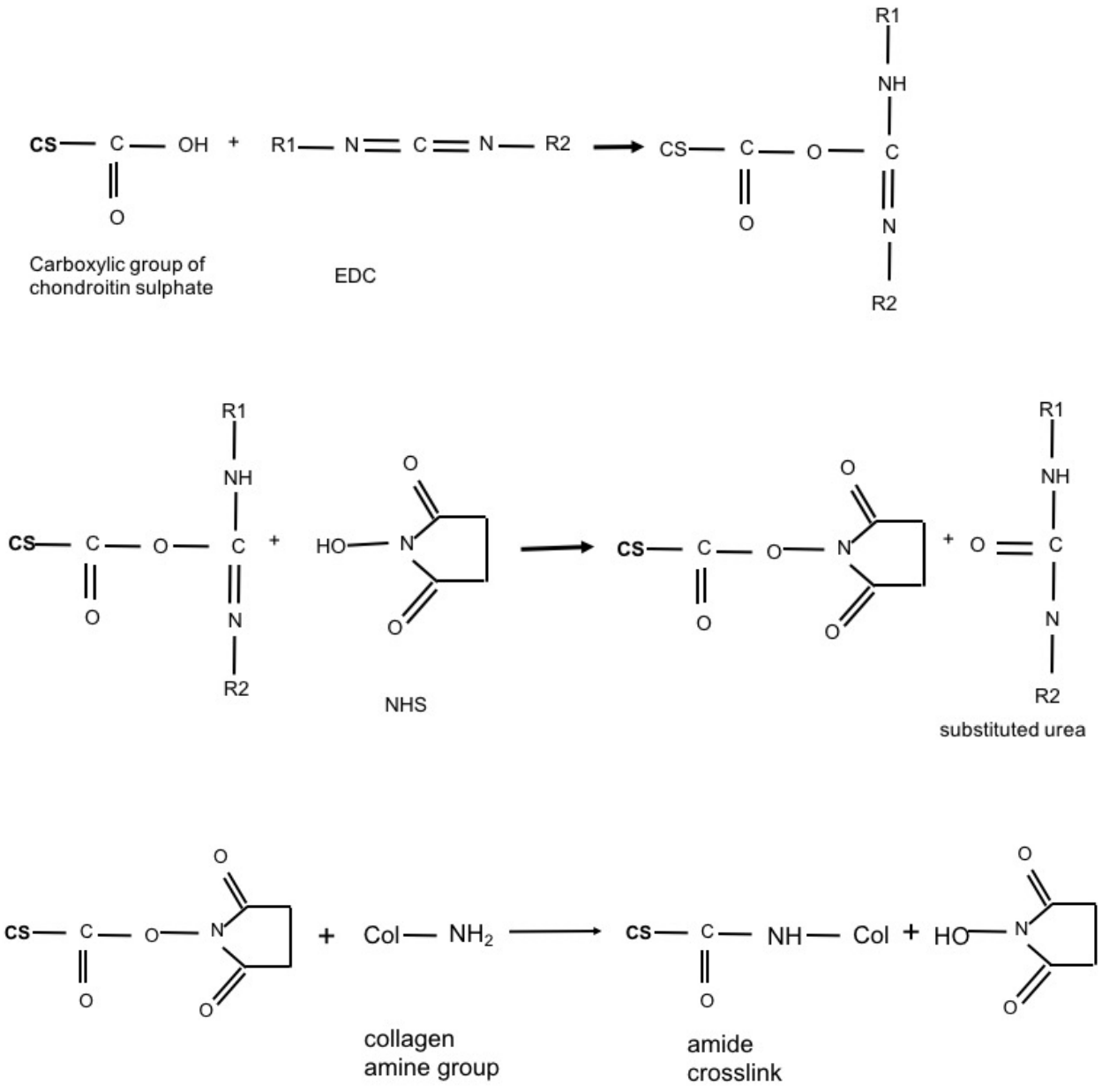


Fig 5.16. Mechanism of covalent attachment of chondroitin sulfate (CS) to collagen (Col) using 1-ethyl-3(3-dimethyl aminopropyl)carbodiimide (EDC) and N-hydroxysuccinimide (NHS)[248].

R_1 = —CH_2 —CH_3; R_2 = — (CH_2 _ NH^+—$(CH_3)_2$ Cl^-

The degradation test results, alongside the FTIR and rheology, firstly confirm the formation of crosslinking between collagen and CS/PCS. The CS release profile, as well as mechanical testing,

further support the formation of bonding between CS/PCS and collagen.

The CS release profile also indicates the introduction of a strong bond between the collagen and CS (See Section 5.5.5). In this respect, the degradation results suggest that crosslinking significantly improved the stability of scaffolds, both in the TBS and culture medium. It can thus be said that, without crosslinking, scaffolds could not be used for cell culture analysis as they collapsed in cell culture medium.

Immobilisation of the CS/PCS on collagen fibrils by covalent attachments leads to the preservation of CS/PCS in the scaffold structure. This is because they cannot be washed away during the washing steps following fibrillogenesis or crosslinking, or in the culture medium during the cell experiments. Hence, CS/PCS should be able to assume their stimulatory role on cell behavior, as will be discussed in Chapter 7.

5.6.3. Pore size analyses

The porous structure of the scaffolds stems from the ice crystal morphology during the freezing process. The nucleation of ice crystals, ice front velocity, and the opposing force acting against growing ice crystal dendrites were all discussed previously (See Section 4.5.3). It was established that, during freezing, suspensions undergo a heterogeneous nucleation of ice crystals from their exposed ends in the mould. As shown by SEM images, a microstructure of interconnected pores was achieved, demonstrating that constitutional undercooling is essential for the formation of the pore structure.

During the growth of ice crystal dendrites, collagen CS/PCS is either pushed into the interstitial space between ice crystals or becomes enclosed in the growing dendrite; this depends on the ice

front velocity, which is a function of the freezing temperature and the suspension's viscosity. Thus, variations in the scaffolds' pore size could be explained by the differences in viscosity/cohesion during freezing. The greater cohesion of XColl2-PCS, in relation to XColl2-CS, retards ice front growth by providing an opposing force. This consequently leads to the formation of smaller pores.

Assuming that the scaffold pore dimensions is proportional to the ice front velocity (which is accordingly proportional to the inverse of solution viscosity and the polymer size (See Section 4.5.4), then the experimental data for viscosity and pore size obtained by rheology and SEM imaging are in agreement with Eq 4.8 :

$$D_{XColl2\text{-}PCS} / D_{XColl2\text{-}CS} = (\eta r)_{XColl2\text{-}CS} / (\eta r)_{XColl2\text{-}PCS}$$

The average complex viscosity of XColl2-PCS is approximately 4 times the average complex viscosity of XColl2-CS (Table 5.2) and it is assumed that $r_{Xcoll2\text{-}pcs} = r_{XColl2\text{-}CS}$. This leads to the formation of pores in XColl2-PCS that are 3.2 times smaller (Table 5.4).

5.6.4. Mechanical properties

The mechanical behavior of collagen scaffolds under compression were evaluated and their compressive modulus (E^*) were obtained. XColl2- PCS showed a significantly higher compressive modulus compared to other compositions. That is to say that PCS had a greater impact on the compressive modulus of collagen scaffolds than CS. The typical behaviour of low-density foams under compression, and the factors affecting their compressive modulus, were discussed earlier (See Section 4.5.5). These are here reviewed alongside the characterisation of their mechanical properties.

The scaffolds under compression exhibited behaviour typical of low-density foams. The three distinctive regions, which are characteristic of low-density elastomeric foam under compression, were present in the stress-strain curve of the samples. The initial linear elastic region was hard to distinguish for XColl2, the reason likely being that the pore edge bending and pore wall buckling occurred at the same time.

Factors affecting the mechanical properties of the scaffolds include: the relative density (i.e. density of scaffold ρ* to the density of solid ρ_s), pore morphology and interconnectivity, and the solid material they are comprised of. The compressive modulus of scaffolds was determined using Eq 4.18 (See Section 4.5.5):

$$E^* = C_1 . (\rho^*/ \rho_s)^2 E_s$$

By substituting E_s for its equivalent from the rule of mixture, it is determined that:

$$E^*_{XColl2\text{-}CS} = C_1 . (\rho^*/ \rho_s)^2 (\nu_{col} . E_{col} + \nu_{cs} . E_{cs}) \quad \text{(Equation 5.4)}$$

$$E^*_{XColl2\text{-}PCS} = C_1 . (\rho^*/ \rho_s)^2 (\nu_{col} . E_{col} + \nu_{PCS} . E_{PCS}) \quad \text{(Equation 5.5)}$$

Having measured the scaffolds weight and dimensions, their densities were calculated. The relative densities of the scaffolds were determined (as presented in Table 5.5) using the density of the scaffolds and the density of solid material (ρ_{col} =1.3 g/cm^3, ρ_{CS} =5.5 g/cm^3, ρ_{PCS} =12.1 g/cm^3).

It can thus be seen from Table 5.5 that the relative density of XColl2-PCS is significantly higher than the relative density of XColl2-CS and XColl2. Therefore, according to Eq 5.4 and Eq 5.5, it can be concluded that the higher relative density gives rise to the higher modulus of XColl2-PCS.

Samples	Relative density (ρ^*/ρ_s)	E^* (kPa)
XColl2-PCS	0.017	46.43
XColl2-CS	0.0129	28.4
XColl2	0.013	8.5

Table 5.5. Relative density and compressive modulus of scaffolds

The relative density of XColl2-CS and XColl2 are not significantly different, while the Young's modulus of XColl2- CS is significantly greater than XColl2. The Young's modulus of solid CS (E_{CS}) would then be responsible for such an increase in Young's modulus (given the scaffolds same relative density).

Another factor affecting mechanical behaviour is the pore anisotropy. The compression modulus in the direction of anisotropy is higher than that of in isotropic pore (See Section 4.) Pores in XColl2-CS and XColl2-PCS have the same morphology/quotient of circularity and the same anisotropy (both have the aspect ratio of 2). Therefore anisotropy is not a determining factor on higher compressive modulus of the XColl2-PCS.

The modulus of the solid pore wall (E_s) is the last parameter to be considered. The relative density of XColl2-PC is 1.32 times greater than that of XColl2-CS which increase its Young's modulus by 1.7 times (Eq. 5.4 & 5.5). However, the compressive modulus of XColl2-PCS is 1.63 times as that for XColl2-CS. Therefore, it can be concluded that XColl2-PCS has approximately the same pore wall solid modulus as XColl2-CS.

5.7. Summary

Collagen fibrils were crosslinked in the suspension by EDC-NHS chemical crosslinker. Collagen scaffolds were fabricated with three different compositions. The effect of the addition of PCS on collagen solution viscosity, scaffold microstructure and mechanical properties were evaluated.

The state of collagen suspensions, their shear thinning behaviour under oscillatory measurements were discussed. It was shown that monomeric collagen suspensions were in a semi-dilute state. The shear thinning of suspensions were explained based on the excluded volume repulsion, Van der Waals, electrostatic and covalent interactions between molecules. It was shown that PCS significantly increased the complex viscosity, storage and loss modulus of collagen suspensions, while CS reduced them.

FTIR confirmed that the primary structure of collagen was maintained during the scaffolds fabrication. No substantial changes were observed in the Amide A band (N-H bond) of the samples, indicating that the collagen triple helix structure was not affected by crosslinking and CS/PCS addition. However, the $8cm^{-1}$ downshift in the frequencies of crosslinked samples may indicate the formation of a weaker hydrogen bond and so a slightly less compact triple helical structure.

CS release profile showed that crosslinking hugely decreased CS release in medium. Furthermore, dissolution study confirmed that crosslinking substantially increased the stability of scaffolds in TBS.

The pore sizes were explained by ice growth rate and viscosity of suspensions. The pores were anisotropic and described by major and minor axes of ellipse. The greater viscosity of XColl2-PCS,

in relation to XColl2-CS, retards ice front growth by providing an opposing force and gives rise to the formation of smaller pores.

PCS significantly increased the Young's modulus of the scaffold, mainly due to the increase in relative density of the scaffold. CS also increased the Young's modulus, yet not to the level of PCS. The increase in solid wall modulus of XColl2-CS is thought to be the main reason for the increase in its compressive modulus in relation to XColl2.

Chapter 6. Fabrication and Characterisation of Osteogenic and Bi-layered Scaffolds

6.1. Introduction

In this chapter, two types of bone scaffolds are fabricated using different techniques. Collagen type I and hydroxyapatite (HA) are the main constituents of natural bone. Hence, the scaffolds were produced from collagen I and HA to mimic the composition of native bone. Monomeric type I collagen was used and collagen suspension went through the fibrillogenesis and crosslinking process to achieve crosslinked fibrillar collagen. Scaffolds were produced from: 1. Crosslinked collagen I combined with commercially available HA, 2. Insitu precipitation of HA nano particles on collagen fibrils followed by the subsequent solution crosslinking. Collagen suspensions rheology, scaffolds' microstructure and mechanical properties were evaluated. Bilayered scaffold were then fabricated based on the optimum outcomes obtained for the composition, micro structure and mechanical properties of cartilage and bone scaffolds. Furthermore, the cell results presented in the next chapter was effectively a determining parameter for the choice of the composition of bilayered scaffolds. Microstructure and mechanical properties of bilayered scaffolds are also discussed herein.

6.2. Synthesis of collagen based scaffold for bone regeneration

Bone scaffolds were produced using two different methods:

1. Crosslinked reconstituted fibrillar collagen type I mixed with hydroxyapatite (HA)
2. In Situ deposition/precipitation of hydroxyapatite nano crystals onto the collagen fibrils which followed by chemical crosslinking of collagen -HA suspension.

6.2.1. Materials

All the consumables and reagents supplied by Sigma Aldrich or Fischer Scientific, otherwise stated. Hydroxyapatite (nano powder, <200nm) supplied by Sigma Aldrich (Poole, Dorset, UK). Type I pepsin-digested tropocollagen monomers extracted from foetal calf skin were in lyophilised form provided by Dr. David Brand, Argentis Company, Tennessee, US.

6.2.2. Method- Preparation of crosslinked reconstituted fibrillar collagen type I mixed with hydroxyapatite

1 %(w/v) pure afibrillar collagen type I solution was prepared according to the instruction detailed in Section 5.2.2. Monomeric collagen solutions were then induced to form reconstituted fibrillar structure (See Section 5.2.3). Reconstituted fibrilar collagen I was subsequently crosslinked using EDC-NHS (See Section 5.2.4). Hydroxyapatite were then added to the crosslinked collagen solution with the mass ratio of 70 % HA to 30% collagen. The solution was then mixed on a vortex (IKA MS2 Minishaker), casted and freeze dried (See Section 5.2.5). Fig 6.1 represents the scaffold fabrication steps.

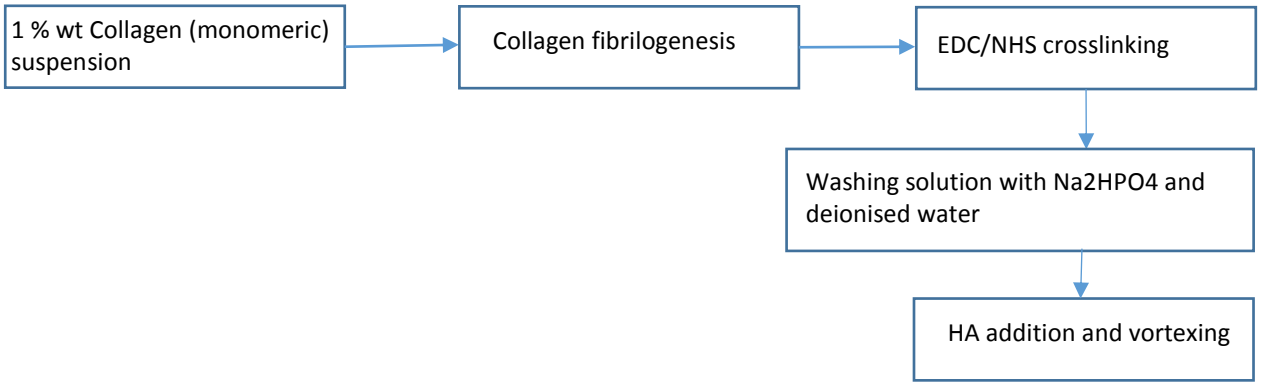


Fig 6.1. Schematic diagram of bone scaffold production, crosslinked collagen I mixed with HA.

6.2.3. In- Situ precipitation of HA nano crystals on collagen fibrils

In this method, monomeric collagen type I was polymerised to form a network within which the in situ precipitation of nano-scaled hydroxyapatite crystals performed. This is a *bottom up* approach towards the fabrication of bone scaffolds and the scaffolds microstructure produced by this approach resembles the native bone structure. To date, no three-dimensional bone scaffold produced by this method has been commercialised. The problem stems from the fact that nano crystals of hydroxyapatite precipitate on collagen fibrils at basic pH (8-9), while collagen is soluble on acidic pH (3.2).

Afibrillar collagen solution was prepared (as described in section 5.2.2) and $Na_2 HPO_4$ (0.3 M) was added with gentle stirring to collagen solution to achieve the final phosphate concentration of 20 mM. NaOH (2M) was added to the stirring solution to reach the pH of 7.2. Reaction took place in an ice bath to maintain the temperature below 10 °C and the solution was stirred during the reaction period. To produce the composite, $(NH_4)_2 HPO_4$ aqueous solution was added to the neutral collagen solution (that was) followed by dropwise addition of $Ca (NO_3)_2$ solution into the vigorously agitated collagen solution. During the reaction, the pH was kept between 8 and 9 using ammonium hydroxide. The amount of diammonium phosphate and calcium nitrate added was calculated to provide the weight ratio of 70 to 30% of HA to collagen. Reaction at low temperature provides uniform dispersion of HA in collagen solution without the aggregation of collagen fibrils at the first few hours. The solution was stirred for 2 hours and then transferred to an incubator for 16 hours. The composite gel of collagen and HA was then crosslinked using the protocol described in previous chapter (Section 5.2.4). Fig 6.2 represents the scaffold fabrication stages; the scaffolds formulation is also shown in table 6.1.

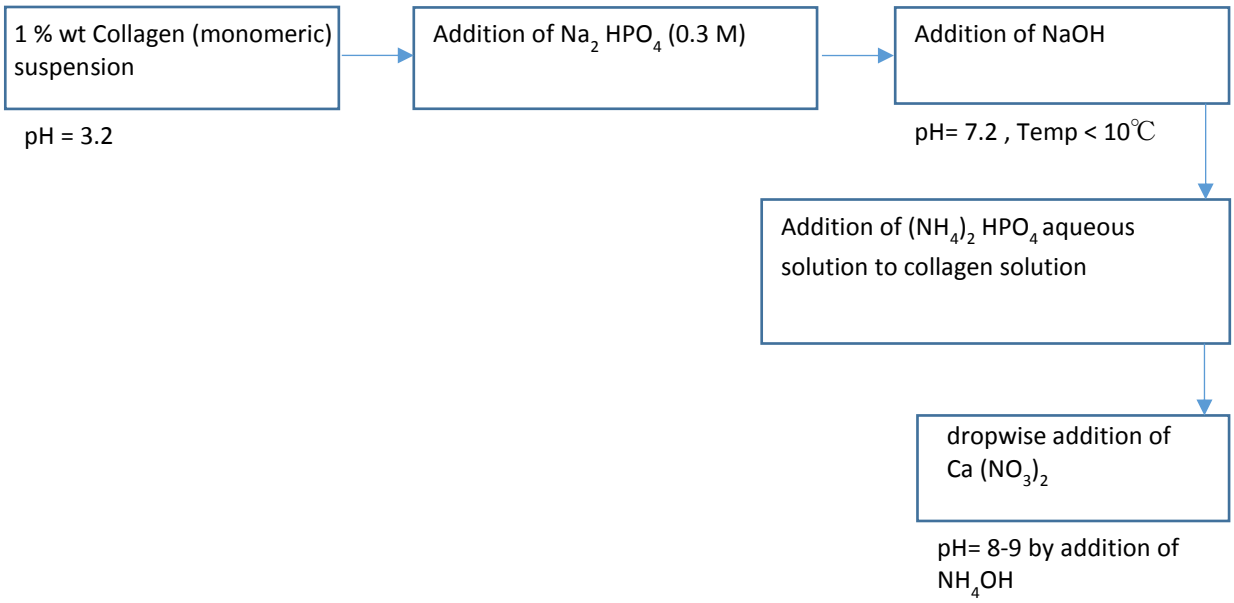


Fig 6.2. Schematic diagram of bone scaffold production, In situ precipitation of HA nano particles on collagen fibrils.

6.2.4. Fabrication of integrated bilayered osteochondral scaffold

Bilayered scaffolds were achieved with an integrated seamless transition between the two layers by the repeated steps of layer addition followed by freeze-drying technique. The thickness of each layer was the same. The aim was to acquire a smooth transition between layers to prevent delamination which could occur because of the elastic mismatch between layers.

The superficial layer scaffold (suitable for cartilage regeneration) is collagen type II and PCS, and the bottom layer (suitable for bone regeneration) is made up of collagen type I and hydroxyapatite. (Fig 6.3)

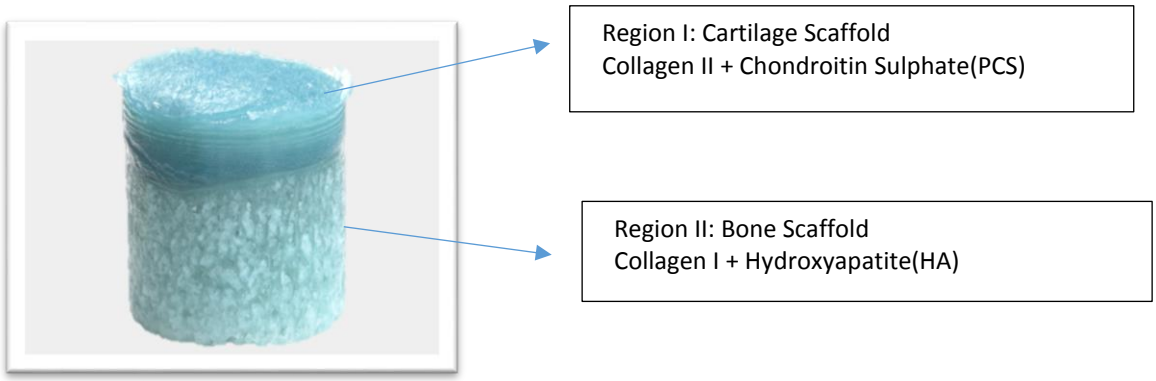


Fig 6.3. Schematic representation of bilayered scaffold

Scaffolds acronym	**Collagen Type**	**Collagen: HA1/HA2 weight ratio**
XColl1- HA1	Crosslinked reconstituted fibrilar collagen Type I	70:30 %
XColl1- HA2	Monomeric collagen Type I (fibrilar crosslinked after nucleation of HA nano particles on collagen)	70:30%
XColl1	Crosslinked reconstituted fibrilar collagen Type I	

Table 6.1. Scaffold composition: type of collagen (type I), ultrastructure and the quantity of HA

6.3. Results

6.3.1. Rheology

Oscillatory frequency sweep tests were performed on 1% w/v suspensions of XCol1, XCol1- HA1 and XCol1-HA2 (in deionized water) at 20° C using a cone plate system (25mm diameter).

The viscoelastic properties of solutions, including storage modulus (G'), loss modulus (G"), and complex viscosity (η*) were determined.

As Fig 6.4 shows, the viscosity of XCol1 and XCol1-HA1 decreased by increasing angular frequency which exhibits the shear thinning property of the solutions. However, XCol1-HA2 showed shear thinning behaviour at frequency lower than 10 s^{-1} and shear thickening at frequency greater than 10 s^{-1}.

The storage and loss modulus of XCol1 and XCol1-HA1 suspensions remained approximately linear by increasing the angular frequency (Fig 6.5 and Fig 6.6). The loss modulus of XCol1- HA2 is linear while its storage modulus raised when angular frequency exceeds 10 s^{-1}.

All suspensions possess higher storage modulus than loss modulus suggesting that the suspensions elastic property dominates their viscous property.

XCol1 – HA1 have higher viscosity (5 times) than XCol1 suspension in the whole angular frequency range. At lower angular frequency (<10 s^{-1}), XCol1 suspension is more viscous than XCol1-HA2 while this reverse at higher angular frequencies when XCol2-HA2 shear thickens. The viscosity of XCol1-HA1 is also higher than XCol1- HA2 at frequencies lower than 40 but at higher frequencies XCol1-HA2 suspension is more viscous.

The average complex viscosity, storage, loss and complex modulus are the highest for XCol1- HA1 compared to the other suspensions and XCol1- HA2 has the least average viscosity. (Table 6.2)

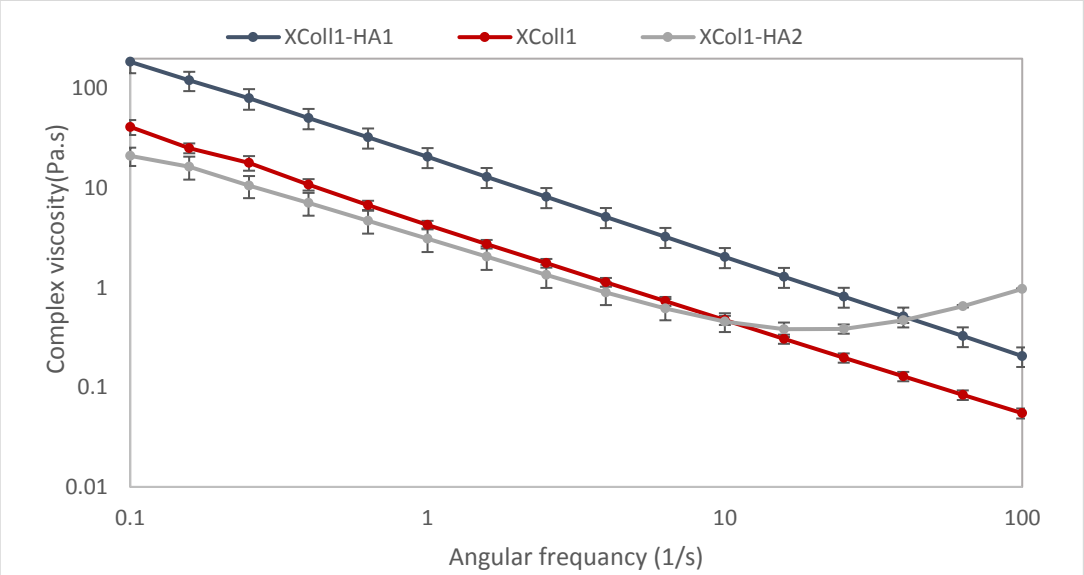


Fig 6.4. Complex viscosity of XCol1, XCol1-HA1, XCol1-HA2. XCol1 and XCol1-HA1 show shear thinning behavior over entire frequency range. XCol1-HA2 shows shear thinning behaviour at frequency lower than 10 s^{-1} and shear thickening at frequency greater than 10 s^{-1}.

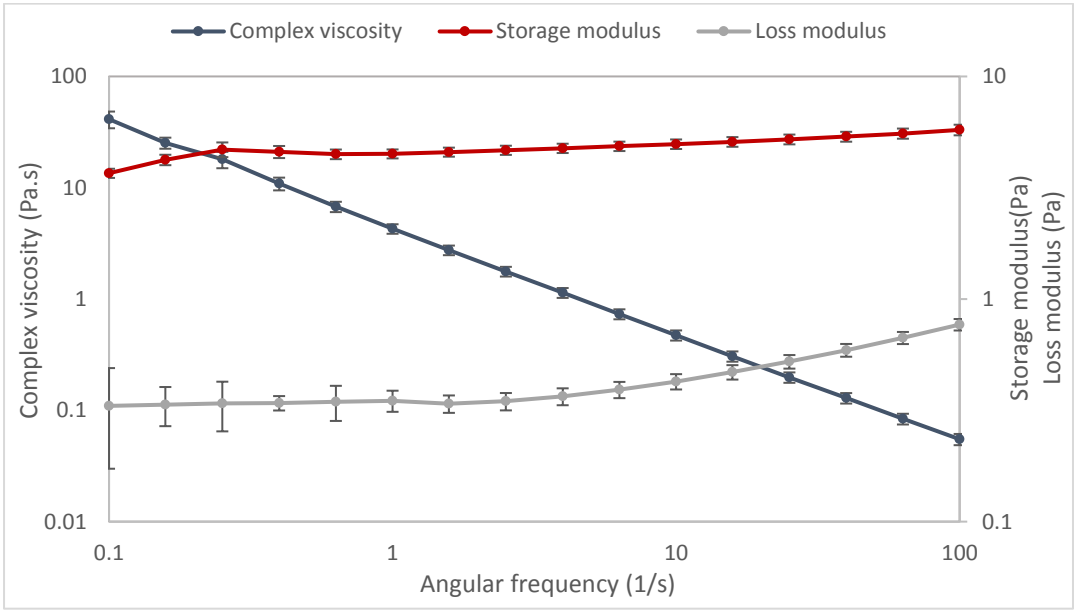


Fig 6.5. Complex viscosity, storage and loss modulus of XCol1 solution

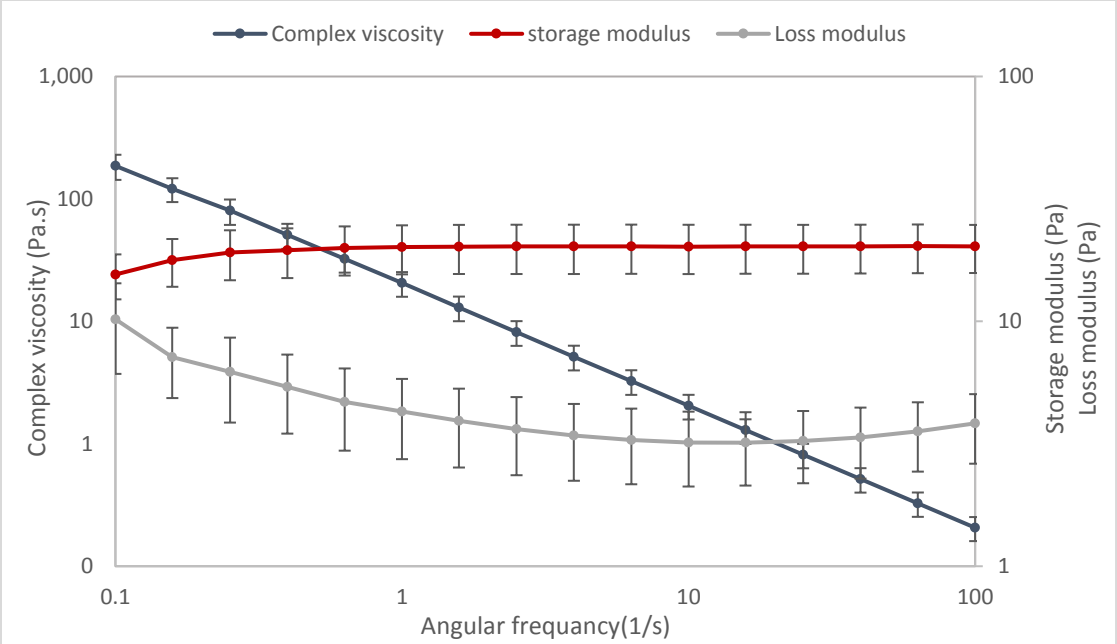


Fig 6.6. Complex viscosity, storage and loss modulus of XCol1- HA1 solution

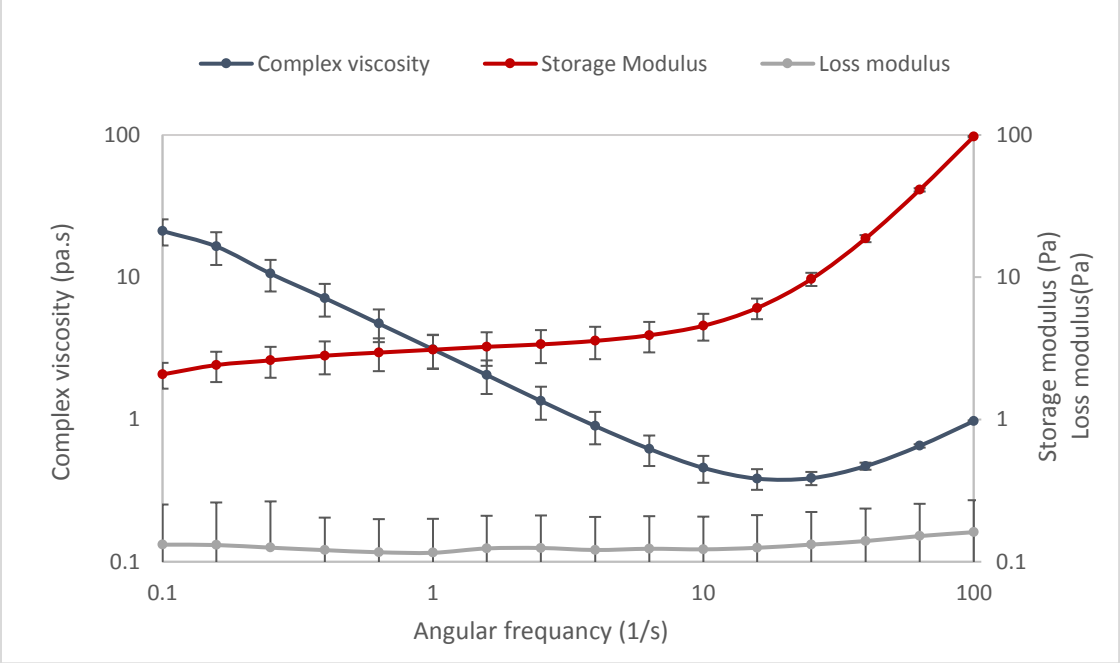


Fig 6.7. Complex viscosity, storage and loss modulus of XCol1- HA2 solution

Samples	Complex Viscosity (Pa.s)	Storage Modulus (Pa)	Loss Modulus (Pa)	Complex Modulus (Pa)
XCol1	7.17	4.8	0.46	4.83
XCol1 – HA1	32.9	19.64	4.53	20.16
XCol1 – HA2	4.46	12.97	0.13	12.97

Table 6.2. Average complex viscosity, storage and Loss modulus of collagen suspensions

6.3.2. FTIR

To study the effect of fibrillogenesis and crosslinking on collagen I, FTIR has been conducted on tropocollagen, afibrillar collagen, reconstituted fibrillar collagen and crosslinked fibrillar collagen. Fig 6.8 shows the averaged (n = 3) FTIR spectra of collagen I samples and Fig 6.9 shows the second derivative of the spectra. Band correlations for the second derivate spectra are shown in Table 6.3. The FTIR spectra of all samples showed characteristic collagen amide A, I, II and III bands. CH2 side chain vibration peak at 1338 cm^{-1} is a key characteristic feature of collagen, which was present in all samples. The afibrillar, fibrillar and crosslinked collagen spectra perfectly match those for the trpocollogen spectrum, with no significant changes (**<**4 cm^{-1}) in the frequency of amide I, II, III. The only significant shift is in amide A bands (10 cm^{-1}) occurred in crosslinked samples.

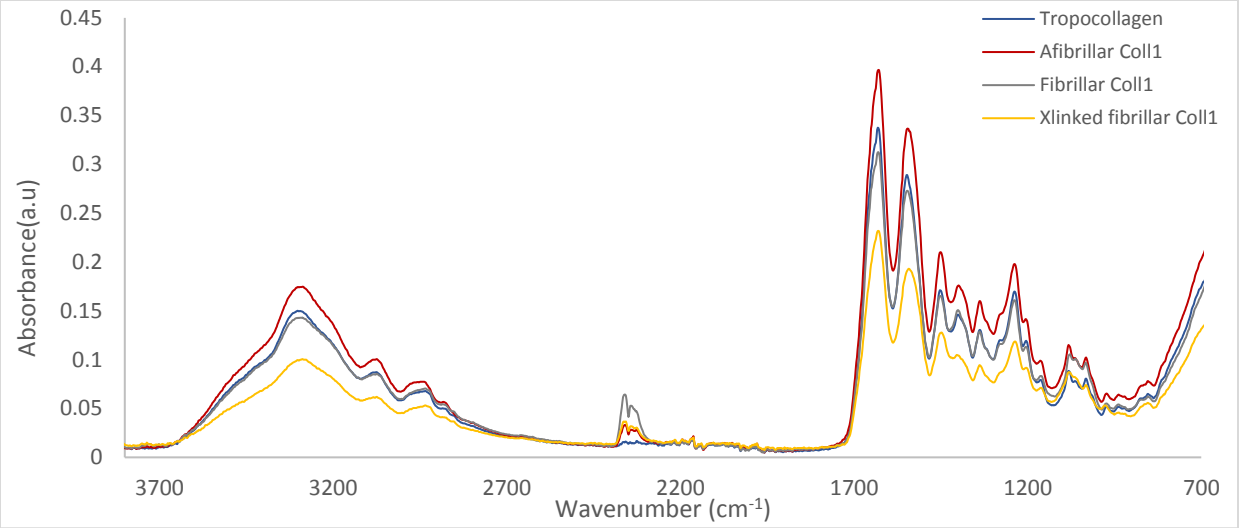


Fig 6.8. FTIR spectra for tropocollagen I, afibrillar collagen I, reconstituted fibrillar collagen I, crosslinked fibrillar collagen I (n=3)

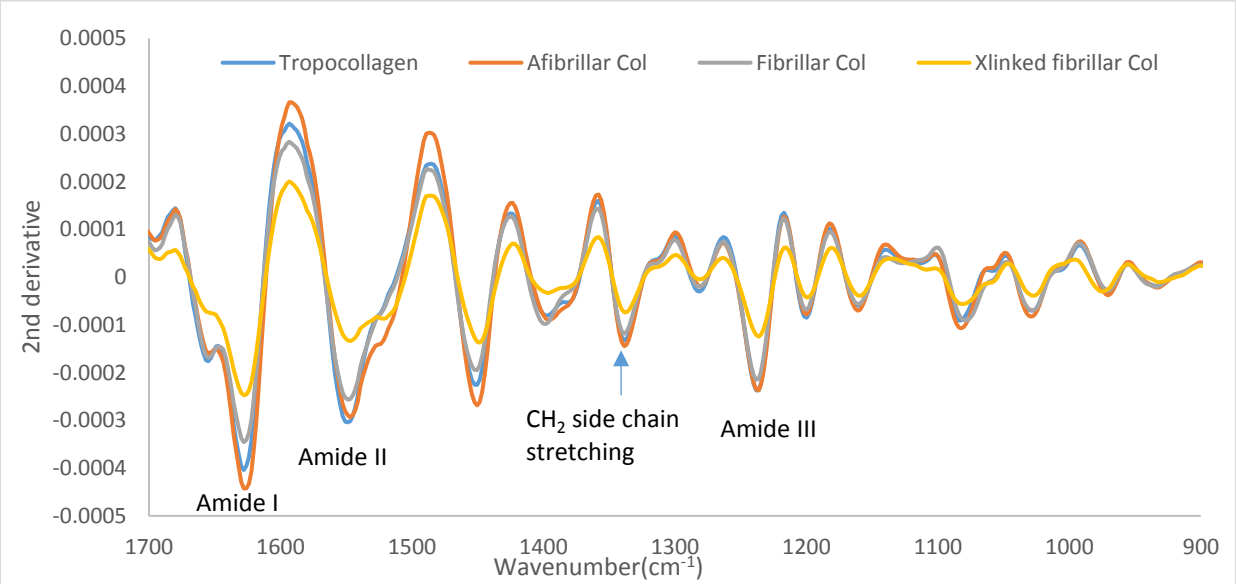
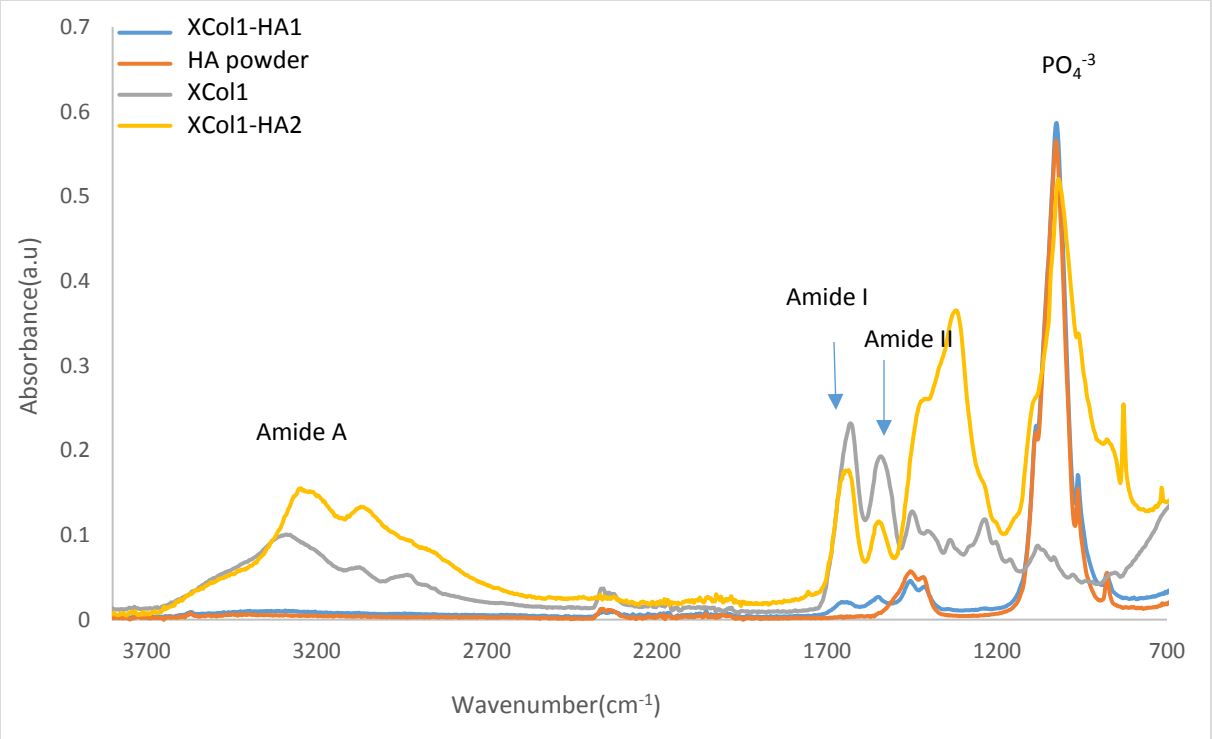


Fig 6.9. Second derivative spectra (900- 1700 cm^{-1}) of tropocollagen I, afibrillar collagen I, reconstituted fibrillar collagen I, crosslinked fibrillar collagen I.

Band Assignment	Tropocollagen I	Afibrillar Col1	Fibrilar Col1	Xlinked fibrillar Col1
Amide A (N-H stretch)	3294	3292	3292	3284
Amide I (C=O stretch coupled with H-bonding)	1628, 1655 shoulder	1626, 1653 shoulder	1628, 1653 shoulder	1628,1653 shoulder
Amide II (C-N stretch coupled with N-H bending)	1547,1522 shoulder	1547,1522 shoulder	1548,1522 shoulder	1547,1520 shoulder
Amide III (C-N stretch & N-H in-plane deformation)	1236	1236	1238	1236
Crboxyl group with wagging of proline (CH2 Streching)	1338	1336	1338	1337

Table 6.3. Second derivative band assignment for type I collagen samples, crosslinking shifted the amide A band to lower wavenumber (from 3294 to 3284 cm^{-1}). Amide I, II, III and CH_2 stretching shifts are not significant, the maximum shift occurred in peak position is 2 cm^{-1}.

Fig 6.10 shows the averaged (n = 3) FTIR spectra of collagen I composite samples and Fig 6.11 shows the second derivative of the spectra. Band correlations for the second derivate spectra are shown in Table 6.4. Amide A of all samples displayed a shoulder at higher wavenumber (3408-3425 cm^{-1}). Addition of HA to crosslinked fibrillar collagen I significantly shifted the amide A band to a lower wavenumber.



6.10. FTIR spectra of type I collagen composite scaffolds (n=3)

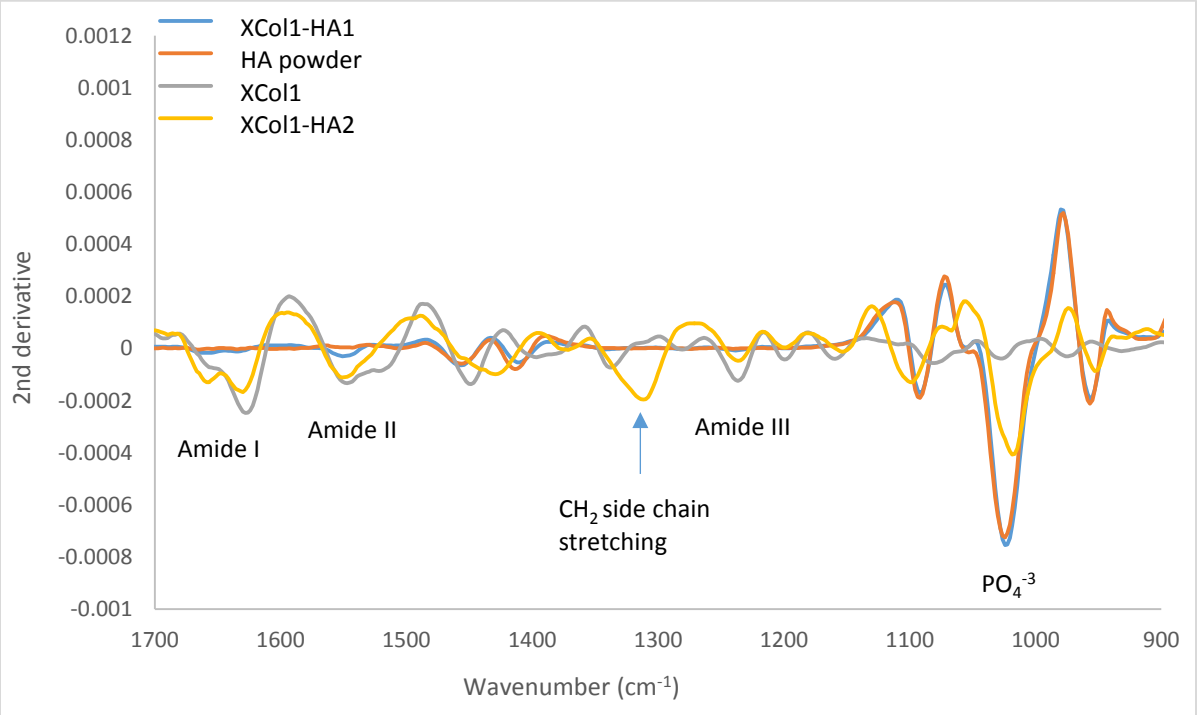


Fig 6.11. Second derivative spectra (900- 1700 cm^{-1}) of XCol1, XCol1-HA1, XCol1-HA2, HA powder

Band	XCol1	XCol1-HA1	XCol1-HA2	HA
Amide A (N-H stretch)	3284	3275	3230	
Amide I (C=O stretch coupled with H-bonding)	1628,1650 shoulder	1629, 1652 shoulder	1629,1658 shoulder	
Amide II (C-N stretch coupled with N-H bending)	1547,1520 shoulder	1547	1548,1528 shoulder	
Amide III (C-N stretch & N-H in-plane deformation)	1236	1234	1236	
Crboxyl group with wagging of proline (CH2 Streching)	1337	1340	1371	
PO^{-3}_4 (P-O stretching)		1022, 956	1016, 951	1024,956

Table 6.4. Peak wavenumbers (cm^{-1}) of collagen I and composite of collagen I and HA

Amide I, II, II bands did not shift significantly, the only variation is the disappearance of a shoulder at amide II band in XCol1- HA1. CH2 peak did not shift significantly in XCol1-HA1 as compared to pure collagen (XColl1), while it experienced a significant upward shift in XCol1- HA2 (from 1337 cm^{-1} to 1371 cm^{-1}). Peaks of PO_4^{-3} appeared in both XCol1- HA1 and XCol1-HA2, the PO_4^{-3} peak appeared in XCol1- HA1 with a minor downshift in one of the peak wavenumber. PO_4^{-3} bands slightly downshifted in XCol1- HA2 (8 and 5 cm^{-1} shifts in wavenumbers respectively).

6.3.3. Xray-diffraction

Fig 6.12 shows the X-ray diffraction spectrum of commercial (HA) and XCol1-HA1 and XCol1-HA2. Commercial HA and XCol1-HA1 showed sharper peaks compared to XCol1-HA2 which nano crystal of HA were synthesized on collagen fibrils. The spectra were compared to the JCPDS hydroxyapatite reference spectrum 09-0432 to assign lattice planes to the peaks observed. Furthermore, the presence of additional peaks corresponding to other phases of calcium phosphates at specific diffraction angles was searched in order to determine the purity of synthesised HA. The HA crystallite size measurements were carried out using HA (-4, 2, -2) at ~46.6 2θ and is shown in Table 6.5.

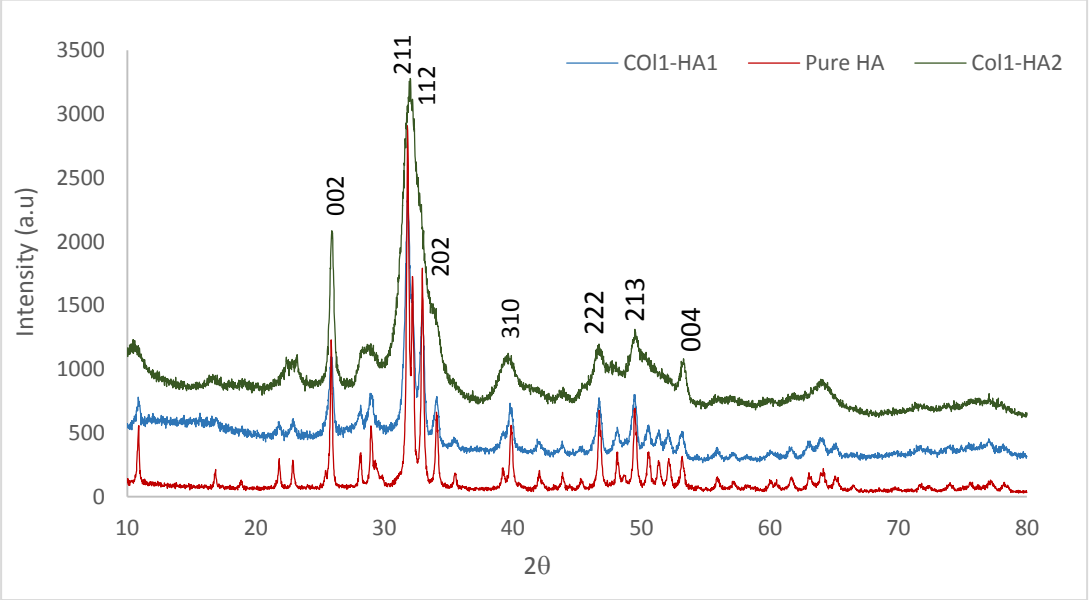


Fig 6.12. Xrd spectra of Hydroxyapatite, XCol1-HA1 and XCol1-HA2

Sample	HA powder	XCol1-HA1	XCol1-HA2
HA size (nm)	52	22	20

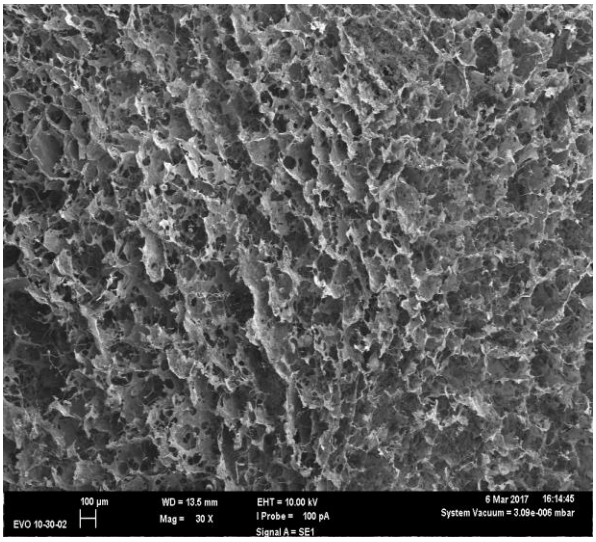
Table 6.5. Hydroxyapatite particle size in HA powder (Sigma Aldrich), XCol1-HA1 and XCol1-HA2

6.3.4. Scanning electron microscopy

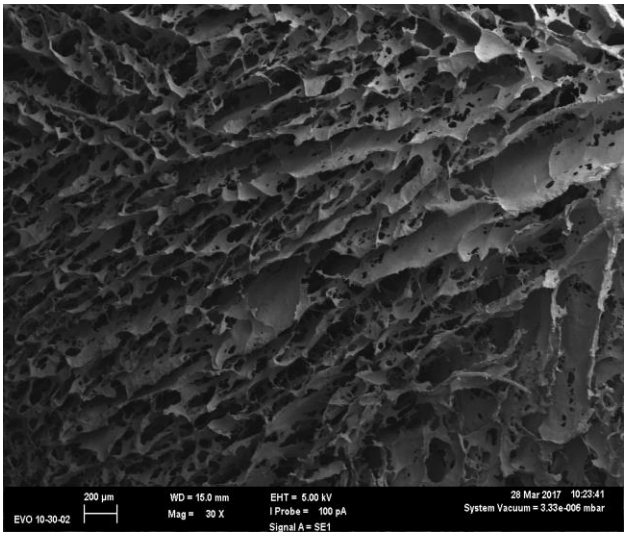
Fig 6.13 and 6.14 represent the SEM images of XCol1-HA1 and XCol1-HA2 scaffolds. The microstructure of XCol1-HA1 appears different from that of XCol1-HA2. It can be seen that pores are more circular, highly interconnected and randomly oriented in XCol1-HA1 while pores in XCol1-HA2 are elongated and formed between parallel plates with a relatively large variation in their size, and each cluster of plates are oriented in different directions. XCol1-HA2 showed more interconnectivity (secondary pores) between pores in relation to XCol1-HA1(Fig 6.15 & 6.16), however it possess smaller primary pore size, secondary pores were observed and clusters of HA were detectable on pore walls of XCol1-HA1. Fig 6.17 represents an SEM image of a bilayered scaffold composed of cartilage (top layer) and bone (lower layer) scaffold. An integrated interface (soft transition) between layers has been achieved as shown by Fig 6.17. Moreover, differences between cartilage and bone pore morphology and size was observed. Pores are more circular and larger in cartilage scaffold compared to bone scaffold. Table 6.6 represent pore characteristics for the scaffolds.

Sample	Average Pore Area (μm^2)	Major and minor pore diameter (µm)	Quotient of circularity
XCol1-HA1	5500 (SD: ± 1130)	72 (SD: ±22) – 40 (SD: ±12)	0.56
XCol1-HA2	7200 (SD: ±690)	98 (SD: ± 20) – 39 (SD: ±9)	0.4

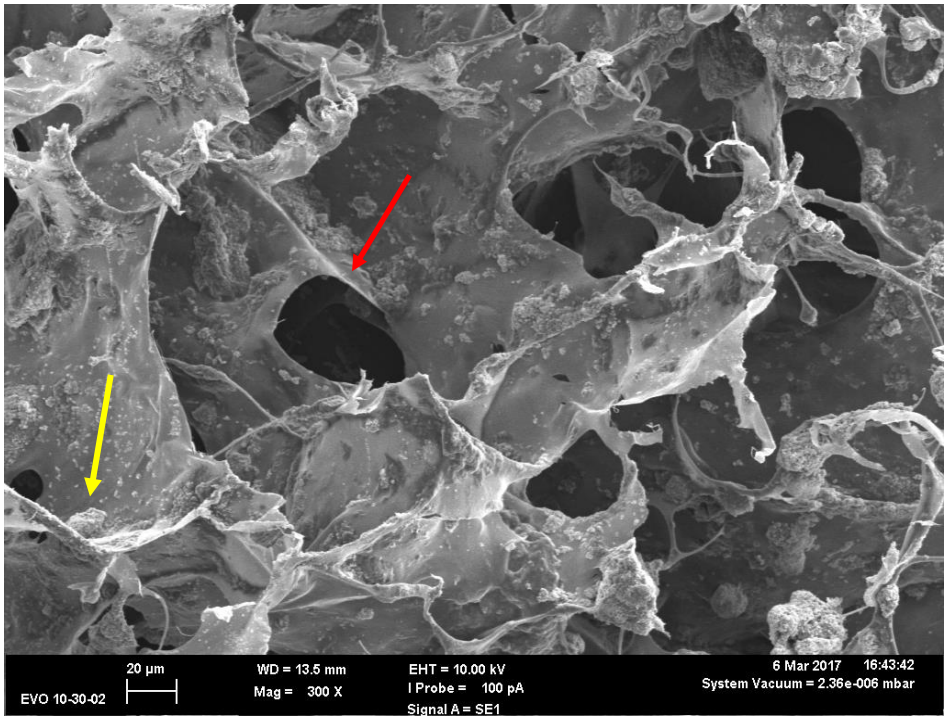
Table 6.6. Average pore area, major and minor pore diameter and pore circularity for XCol1-HA1 and XCol1-HA2



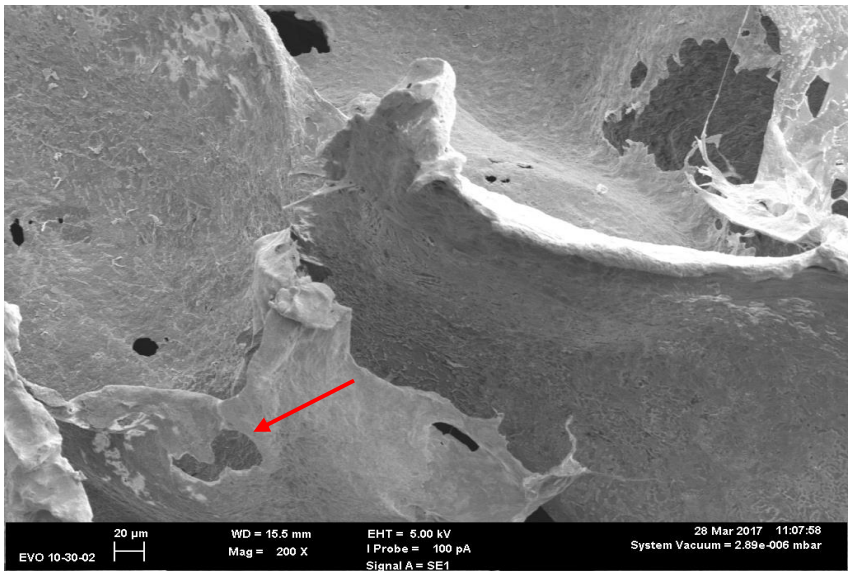
6.13. SEM micrograph of XCol1-HA1 (low magnification)



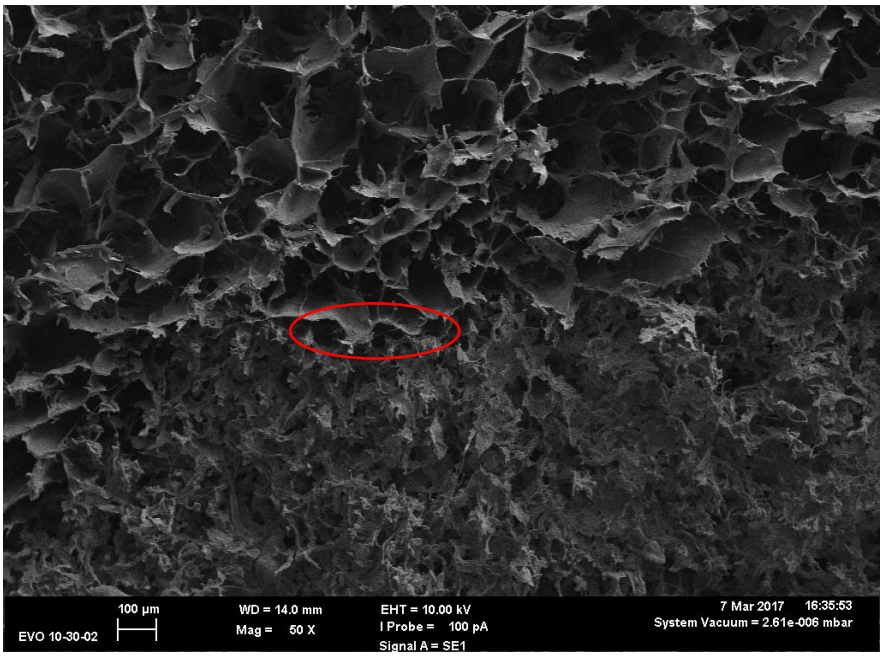
6.14. SEM micrograph of XCol1-HA2 (low magnification)



6.15. SEM image of secondary pores of XCol1- HA1 and HA on pore walls at high magnification with red row indicating a secondary pore and yellow arrow indication HA deposit



6.16. SEM image of secondary pores and pore wall of XCol1- HA2 at high magnification with red row indicating a secondary pore

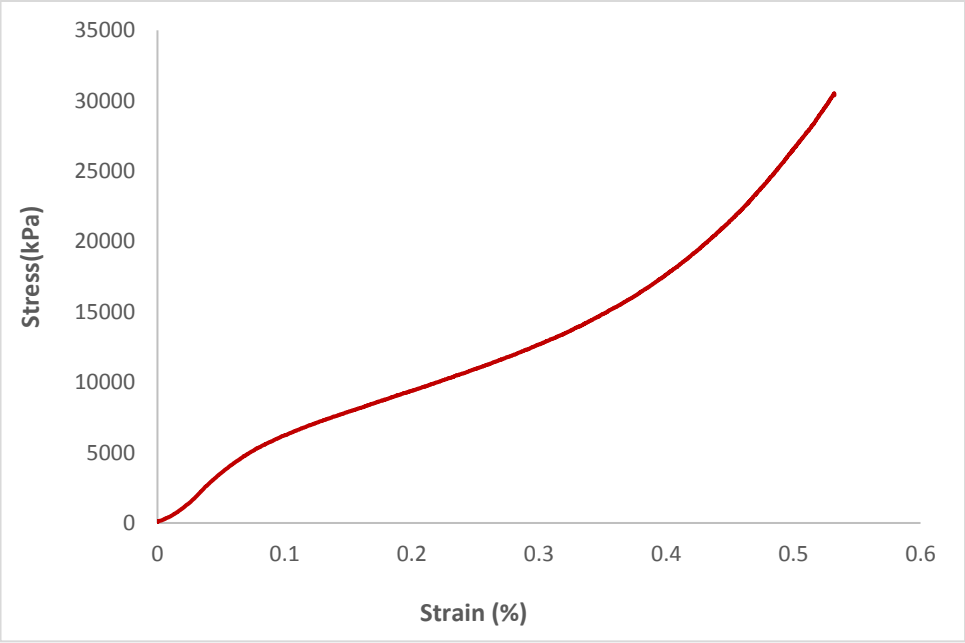


6.17. SEM micrograph of bilayered scaffold; the top layer is XColl2- PCS and the bottom layer XCol1-HA1. Integrated interface formed between the layers indicated by red circle.

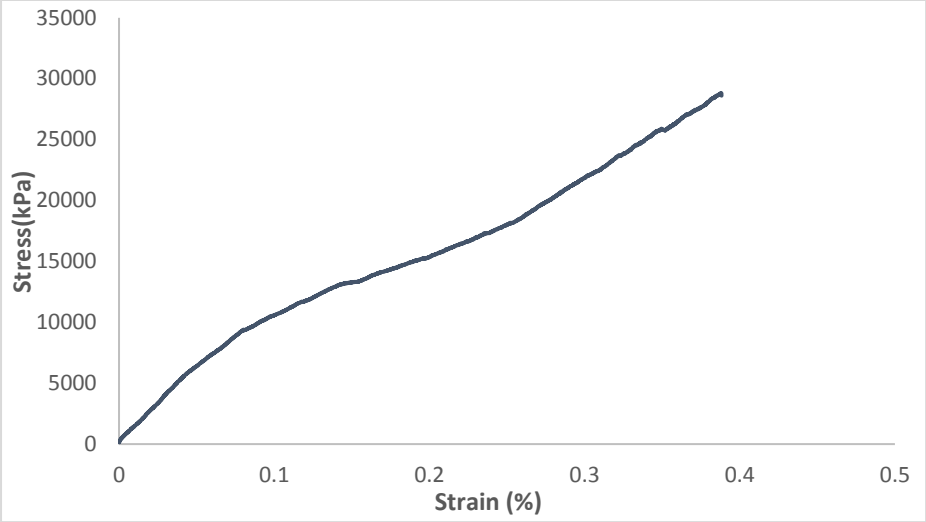
6.3.5. Mechanical properties

The mechanical behavior of bone scaffolds in dry state under compression is studied herein. Fig 6.18 & 6.19 represents the stress-strain curves of XCol1 –HA1, XCol1-HA2 composites under compression. The test was conducted on 5 samples. Compressive modulus (E*) of cellular solids can be obtained by linear regression of the initial elastic region of the stress- strain curve. The average samples' dimension and their Young's modulus are shown in Table 6.7.

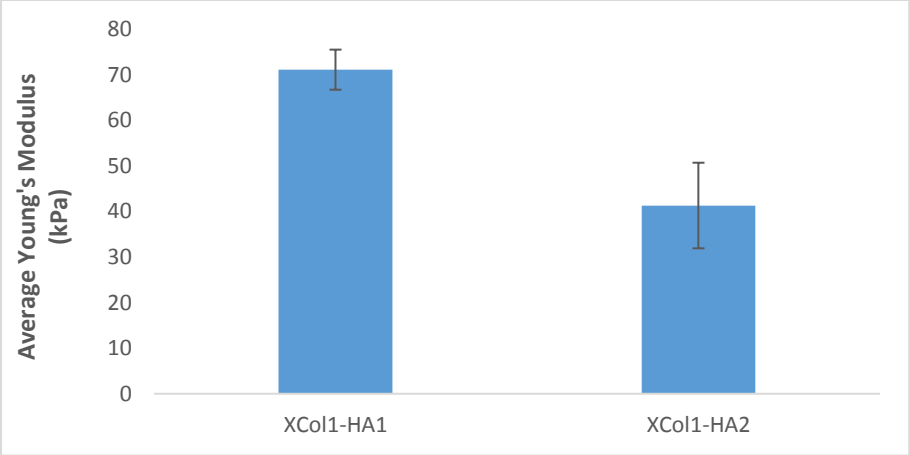
As shown in Table 6.7, the average Young's modulus of XCol1-HA1 is significantly higher that of XCol1-HA2 and bilayered (p<0.05). The strain- stress curve of XCol1-HA1 displays a toe region in strain less than 0.02 (Fig. 6.18) while this region does not appear in XCol1-HA2 scaffolds (Fig 6.19).



6.18. Representative stress- strain curves for XCol1- HA1



6.19. Representative stress- strain curves for XCol1- HA2



6.20. Average Young's modulus of Col1- HA composites

Sample name	Ave height (mm)		Ave diameter (mm)		Ave Young's Modulus (Kpa)	
XCol1- HA1	8.74	SD: ±0.12	12.82	SD:±0.19	71.11	SD: ±4.4
XCol1- HA2	8.86	SD: ±0.38	13.35	SD:±0.17	41.32	SD: ±9.4
Bilayered	9.4	SD:± 0.1	12.1	SD:± 0.14	37.42	SD: ±6.2

Table 6.7. Average samples' dimension and their compressive modulus

6.4. Discussion

6.4.1. Rheology of collagen type 1 dispersions, XRD and scaffold microstructure

XCol1 and XCol1-HA1 showed reduced viscosity with increased angular frequency, while XCol1-HA2 demonstrated reduced viscosity at a low angular frequency and increased viscosity at a high angular viscosity. XCol1-HA1 showed a higher complex viscosity than XCol1 throughout the entire frequency range.

The higher viscosity of XCol1-HA1 versus XCol1 is because the presence of HA, which is covalently/electrostatically attached (or locked into the network mechanically), leads to a higher viscosity. The drop in the viscosity of XCol1-HA1 with increased viscosity (1-100 1/s) could be attributed to the unbounding of HA from the network, resulting in the agglomerates breaking down. This, in turn, gives rise to a less effective resistance to flow. The reasons for the shear thinning property of XCol1 are the same as those presented earlier for XColl2 (See Section 5.5.1).

XCol1-HA2 showed the lowest complex viscosity at a low angular frequency. It is likely that the synthesis and deposition of HA nano particles on the collagen molecules have either reduced the available interaction sites for collagen-collagen binding during fibrillogenesis or physically prevented extensive fibril formation, resulting in the inhibition of fibril growth. Hence, while it presented the lowest complex viscosity, at a higher frequency, it demonstrated a shear thickening property. At a frequency higher than 10 s^{-1}, its complex viscosity exceeds that of XCol1, whereas at a frequency higher than 40 s^{-1}, its complex viscosity exceeds both XCol1 and XCol1-HA1. It is therefore suggested that, due to inhibitory effect of HA in fibril formation, XCol1-HA2 possesses the smallest collagen networks.

It is noteworthy that the rheological behaviour of the aqueous nanoparticle suspensions of HA, like other ceramic slurries, is mainly controlled by: the content of solid particles, particle size and shape, and particle agglomeration[249]. At a very low shear, the ceramic nanoparticles agglomerate into a 3D-network that permeates throughout the suspension. This network is responsible for the elastic properties of the suspension[250]. As the shear rate increases, the network breaks down into smaller agglomerates whose sizes continue to decrease. The agglomerated dispersion is broken up into primary aggregates (i.e. nanoparticle aggregates) that align themselves in the shear field. This further reduces the viscosity[251].

HA suspensions typically demonstrate pronounced shear thinning behaviour[250,252], however some ceramic suspensions also present dilatant behaviour (i.e. increased viscosity at high shear rates[253]). Since the agglomeration and break-up kinetics are not instantaneous, the rheological properties are highly time-dependent, resulting in thixotropic behaviour[250,254,255].

These agglomeration phenomena are governed by force balances involving Brownian, hydrodynamic, and inter-particle (attractive or repulsive) forces. Van der Waals attraction between primary flocs is the major force responsible for flocculation. Its effect can be partially reduced by electrostatic repulsive forces arising from the ionic atmosphere surrounding the charged solid particles (electric double layer). However, usually this kind of stabilisation is not sufficient to avoid agglomeration. Often, a steric stabilisation is necessary due to the addition of a proper amount of effective dispersant (a polymer), which is adsorbed by the particle surfaces. Such dispersants create repulsive forces between primary flocs of the dispersed systems that prevail over van der Waals attractive interactions. The effects of strong interparticle attractive

forces are more considerable for colloidal suspensions that are characterised by small elementary particles.

The smaller HA particle size in XCol1-HA2 dispersion compared to that of XCol1-HA1 (as well as its smaller collagen networks and differences in both collagen-HA and HA-HA interactions) gives rise to a discrepancy in their rheological behaviours. Due to the synthesis method of XCol1-HA2, which allows for the precipitation of HA nanoparticles on collagen molecules, collagen and HA have intermolecular interactions in XCol1-HA2. This, in turn, influenced the rheology of suspensions. SEM images therefore confirmed that, while HA particles showed agglomeration in XCol1-HA1, no obvious agglomeration were observed in XCol1-HA2 (Fig 6.15 & 6.16).

SEM images further revealed different microstructural features in the scaffolds of XCol1-HA1 compared to XCol1-HA2. These originate from the difference in the viscosity of the respective solutions, as discussed earlier (See Section 4.5.3). The higher complex viscosity of the XCol1-HA1 solution (in relation to XCo1-HA2) gives rise to the formation of smaller and more circular pores in XCol1-HA1's scaffold.

The particle phase now includes both collagen and HA, which can affect the critical velocity of the ice front. XRD outcomes showed that HA1 has a larger diameter than HA2. According to the Eq. 4.12 ($V_{cr} = \frac{\Delta\sigma 0\ a0}{12\eta\mu r}$), XCol1-HA2 has a higher critical ice front velocity compared to XCol2-HA1. This is due to XCol1-HA2's smaller particle radius (and solution viscosity) leading to the formation of larger ice crystals and, as a consequent, a lager pore size.

6.4.2. FTIR

The FTIR spectrum of all collagen I samples displayed the Amide A, I, II, III bands. This suggests that the primary structure of collagen was preserved during fibrillogenesis, crosslinking and freeze drying.

The secondary helical structure of collagen is stabilised by the hydrogen bonds between carboxyl and hydroxyl groups of the three strands (2 [αI] and 1[αII] in the case of type-I). These hydrogen bonds create a supercoiled triple helical conformation as represented by the amide A band[238] (specifically, the N-H stretching of the core polypeptide and also the basic amino acid side chains, *e.g.* lysine and arginine), the frequency of which represents the extent of the supercoiling. Amide A occurs with a frequency of around 3325-3330 cm^{-1} in collagen, about 25 cm^{-1} higher than in other polypeptides[239]. The tropocollagen used for making preparations in this research exhibited the amide A band at a lower frequency than this (~30 cm^{-1}). This indicates a decrease in the extent of supercoiling within the helices (i.e. a less tightly coiled or 'packed' triple helix).

Fibrilogenesis did not shift the amide A band, which means the helical structure of the collagen was not affected by fibrillogenesis. The shift of this band to lower frequencies, with the addition of HA (~9 cm^{-1}), implies a decrease in the degree of supercoiling within the helices. In the case of the mineralisation of the collagen, the formation of a new bond between the collagen amine group and PO_4^{-3} of HA might possibly lead to a less tightly coiled triple helix, a weaker N-H bond and a shift to lower frequencies.

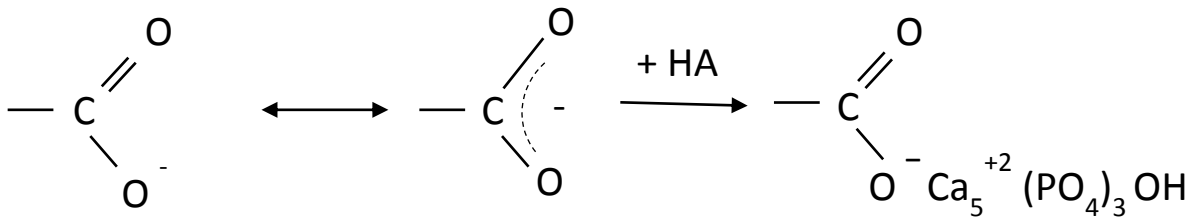
In the case of XCol1-HA2, which was produced by the in situ precipitation of the hydroxyapatite nano particles on the collagen fibrils, the downshift in amide A wavenumber (54 cm^{-1}) and the decrease in supercoiling between helices are more pronounced. It is possibly due to the fact that

HA was synthesised on the collagen monomers from its precursors (as described in Section 2.6) at the monomeric/intermolecular level, it can interact more with the amine groups of the collagen molecule due to its increased contact. This is in contrast to the commercially available HA that dissolved in crosslinked fibrillar collagen and interact with collagen at the intramolecular level. XCol1-HA2's interaction at the monomeric level has further led to the formation of additional bonding with the amine group and the formation of a less compact helical conformation than is observed in the pure collagen and XCol1- HA1 solutions.

Amide I bands, arising from C=O (carbonyl) vibrational stretching along the polypeptide backbone, are observed between 1600 and 1700 cm^{-1}, along with minor C-N stretching vibrations and N-H bending[238]. In contrast, amide II bands are more complex, arising mainly from an out of phase combination of N–H in-plane bending (60%) combined with the C–N stretching vibrations (40%) of the peptide bonds[238]. Finally, amide III bands mainly result from C–N stretching and N–H deformation vibrations[238]; the observed peaks between 1331-1339 cm^{-1} are due to the presence of a dissociated carboxyl group (COO^-) originating from the proline side chain.

In composite scaffolds, the interaction and bond formation between collagen and HA was established by the changes in the position and magnitude of the specific peak frequencies. The carboxyl and amino groups are responsible for approximately 20% of the amino acid residue on a collagen molecule. This makes them ideal targets for calcium and phosphate ions originating from HA[256]. Hence, the carboxyl peak was seen to shift to higher wavenumbers in the scaffolds when HA was added. This observation can be explained by an electrostatic interaction between Ca^{+2} ions and carboxylate groups (C=O and C-O), as well as by the stabilisation of the carboxylate

mezomeric form[238,257,258] (as represented in the Fig. 6.21). The carboxylate groups are predominantly in a mezomeric form, where the two CO bonds are quasi double. When HA is added, the carboxylate groups are stabilised and turn into a single and a double bond. This transformation strengthens the double bond (C=O) and weakens the single bond (C-O), thus shifting the C=O band to higher wavenumbers as observed in the corresponding spectra[258].



Carboxylate anion Mezomeric form Stabilised carboxylate ion

6.21. Interaction and formation of bond between collagen and hydroxyapatite[258]

6.4.3. Mechanical properties

The mechanical behaviour of collagen composite scaffolds in compression was evaluated and the results were presented in the form of a compressive modulus (E*). The mechanism of deformation as well as the parameters affecting it were previously explained (See Section 4.5.5). Collagen type I scaffolds similar to type II exhibited behaviours typical of low-density foams. Likewise, their stress-strain curve (Fig 6.18 & Fig 6.19) is characterised by three distinct regions: a linear elastic regime (controlled by pore-edge bending), a collapse plateau (controlled by pore wall buckling) and a densification regime (controlled by complete pore collapse). It is worth

mentioning that the deformation mechanism of most foams, whether open-cell or closed-cell is bending dominated [203]. If the solid is brittle then its deformation is fracture-dominated and can be depicted by Fig 6.22. Hence, the behaviour of XColl-HA1 and bilayered might be partly controlled by this mechanism due to the presence of HA.

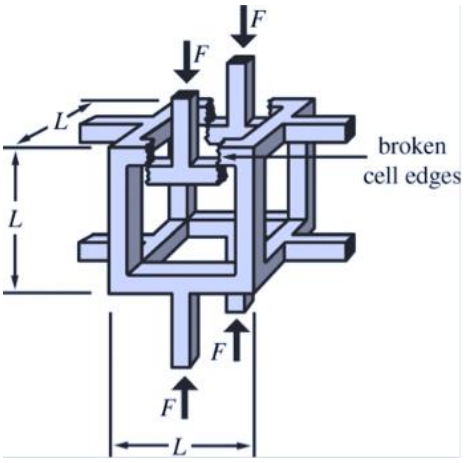


Fig 6.22. Fracture-dominated behavior of a pore[203]

As described earlier, the mechanical properties of these cellular solids are a function of the relative density (density of scaffold ρ* /density of solid ρ_S), pore topology (connectivity and shape of the pores) and the solid material from which they are made[203]. It is also presented earlier that if the solid behaves similar to an elastomer (like collagen/collagen-CS) its compression modulus is buckling-dominated and is described by Equation 4.18 (See Section 4.5.5).

$$E^* = C_1 . (\rho^*/ \rho_s)^2 E_s$$

Where C_1 is an empirical constant (~1) and E_S is the solid modulus. Substituting E_S by its equivalent from rule of mixture, we will have:

$$E^*_{XColl1\text{-}HA} = C_1.\ (\rho^*/\ \rho_s)^2\ (\nu_{col}.\ E_{col} + \nu_{HA}.\ E_{HA}) \qquad \text{(Equation 6.1)}$$

The relative density of scaffolds were determined using the measurements of scaffold weight and dimensions, and density of solid material (ρ_{Col}=1.3 g/cm3, ρ_{CS}=5.5 g/cm3, ρ_{HA}=3.16 g/cm3)[204,259,260].The relative density of XCol1-HA1 (Table 6.8) is significantly higher than XCol1-HA2 (ρ<0.05). Therefore, higher relative density is more likely the most influential parameter which gives rise to the higher compressive modulus of XCol1-HA1 rather than XCol1-HA2.

Scaffolds	**XCol1-HA1**	**XCol1-HA2**
Relative density ($\rho^*/\ \rho_s$)	0.021	0.014

Table 6.8. Relative density of XCol1-HA1 and XCol1- HA2. A paired t-test indicates significant difference (ρ<0.05)

As explained in Section 4.5.5, pore anisotropy is another factor affecting mechanical behaviour. The compression modulus in the direction of anisotropy is higher than that of in isotropic pore (See Fig 4.30). It was shown that, if pores are more anisotropic in the transverse direction (Fig 4.30 (2)), the compressive modulus would increase respective to that of its isotropic structure. However, if pores are more anisotropic in the longitudinal direction (Fig 4.30 (3)), the compressive modulus would decrease.

Pores in XCol1-HA2 are more anisotropic (aspect ratio = 2.2) than pores in XCol2-HA1 (aspect ratio = 1.7). Yet, the direction of anisotropy is oblique which means it has elements of anisotropy in both transverse and longitudinal directions leading to inconsiderable effect on compressive modulus of scaffold.

The compressive modulus of bilayered scaffold can be described based on the simple Reuss model (Eq 6.2) which describes the elastic modulus of two phase laminated composite structures.

$$\frac{1}{\text{Ebi}} = \frac{Vc}{Ec} + \frac{Vb}{Eb} \qquad \text{(Equation 6.2)}$$

$$E_{bi} = \frac{Vc\ Ec + Vb\ Eb}{Ec\ Eb} \qquad \text{(Equation 6.3)}$$

Where V denotes volume fraction and E signifies modulus of each layer.

Therefore, the parameters affecting the compressive modulus of the bilayered osteochondral plug of this study are the compressive modulus of bone and cartilage layer (which itself influenced by the parameters mentioned above) and the volume fraction of each layer (bone and cartilage layers have the same volume fraction in this study). According to Eq 6.2, the stiffness of bilayered cannot surpass the stiffness of the stiffest constituent (here, bone).

6.5. Summary

Bone scaffolds were fabricated using two methods: 1. crosslinked collagen I combined with commercially available HA, 2. In situ precipitation of HA nano particles on collagen fibrils following by the subsequent suspension crosslinking. Collagen suspension rheology, scaffold microstructure and mechanical properties were evaluated.

The shear thinning behaviour of XCol1-HA1 under oscillatory measurements were discussed. Likewise, the shear thinning behavior of XCol1-HA2 at a low frequency and its shear thickening regime at higher frequency were examined. It was shown that HA particle size had an impact on the viscosity of collagen solution and the critical ice front velocity.

FTIR confirmed that the primary structure of collagen was maintained during the scaffolds fabrication. No substantial changes were observed in the amide A band (N-H bond) of the samples, indicating that the collagen triple helix structure was not affected by fibrillogenesis. However crosslinking and specifically HA addition gave rise to a downshift in amide A wavenumber suggesting a less compact/looser helical structure of the composite samples.

The pore sizes were explained by ice growth rate and viscosity of suspensions. The pores were anisotropic and described by major and minor axes of ellipse. The greater viscosity of XColl1-HA1, in relation to XColl1-HA2, retards the ice front growth by providing an opposing force and gives rise to the formation of smaller pores (average pore area of XColl-HA2 was nearly 3 times smaller). However, XColl1-HA1 showed substantially greater pore interconnectivity.

XCol1-HA1 showed higher compressive modulus (71.1 kPa) in relation to XColl1-HA2 (41.3 kPa). The higher relative density of XCol1-HA1 was shown to be the responsible factor.

Bilayered scaffold were fabricated based on the optimum outcomes obtained for the composition, micro structure and mechanical properties of cartilage and bone scaffolds. Furthermore, the cell response was effectively a determining parameter for the choice of composition of bilayered scaffolds (See Chapter 7). Ultimately, crosslinked collagen II plus PCS were selected for the materials of cartilage region and crosslinked collagen I plus HA1 were chosen for bone region. The scaffold was shown to have a relatively smooth transition between the adherent layers. Microstructure and mechanical properties of bilayered scaffolds were discussed.

Chapter7. Biological properties of cartilage, bone and bilayered scaffolds

7.1. Introduction

In vitro cell culture is commonly used in the evaluation of scaffold interactions with cells. It is proposed that the scaffold composition combined with its physical properties would direct the differentiation of stem cells towards a specific lineage in the presence of certain chemical stimuli. To investigate this, the ability of sheep bone marrow mesenchymal stem cells (BMMSCs) to adhere, proliferate, and differentiate were studied on collagen II- CS/PCS, collagen I- HA and bilayered scaffolds. It was shown that the incorporation of PCS has increased cell attachment, proliferation and differentiation in collagen type II scaffolds. Similarly, the addition of HA1 in collagen type I scaffolds showed an increase in cell attachment, proliferation and differentiation.

The cell culture work was performed in collaboration with Prof Chaozong Liu and his group at the Royal National Orthopaedic Hospital, University College London. The scaffolds were prepared as described previously (Section 5.2). BMMSCs were isolated, expanded and characterised (Section 7.2.1). Scaffolds were sterilised and seeded with the cells (Section 7.2.2). The procedures for examination of cells viability and metabolic activity on scaffolds (Sections 7.2.3 & 7.2.4), an optimised protocol for DNA quantification of seeded collagen scaffolds (Section 7.2.5), cell proliferation (Section 7.2.6) and differentiation (Section 7.2.7) are presented. The protocols for histological analysis is explained in Section 7.2.8. Results are presented in Section 7.3 and discussed in Section 7.4.

7.2. Experimental procedures

7.2.1. Cell isolation, expansion and characterisation

Bone marrow mesenchymal stem cells were harvested from the iliac crest of female adult sheep. 5ml of bone marrow was collected in a centrifuge tube with 250ul of heparin. The bone marrow aspirate was transferred to a T225 cell culture flask (Corning, Thermo Fisher Scientific UK) together with Dulbecco's Modified Eagle's Medium (DMEM-Low Clucose, Sigma-Aldrich) supplemented with 10 % Foetal Calf Serum(FCS) (Firs Link Ltd, UK) and 1% Penicillin and Streptomycin (Pen Strep) (Gibco by Life Technologies) and were incubated at 37°C and 5% CO2. After three days, the cells were washed with phosphate buffered saline and fresh culture medium was added to the flask. Once cells reached to 80-100% of their confluency, they were detached with trypsin-EDTA (10%), and were stored at liquid nitrogen.

Sheep bone marrow mesenchymal stem cells were characterized in terms of the ability to selectively differentiate into chondrogenic or osteogenic lineages in response to environmental stimuli. A tri-lineage differentiation experiment was performed in order to confirm the multipotency of BMMSCs.

Osteogenic differentiation: Confluent flasks with sheep BMMSCs at passage 3 were employed. 0.5 million cells were seeded into two wells of a 6 well plate (Corning Inc, Corning, USA). The cells were cultured with 1 ml basal medium for 24 hours until the culture became fully confluent. Then 1 ml of Stem Pro osteogenic medium (Gibco, Life Technologies, USA) was added to one of the wells and incubated at 37°C and 5% CO2 for 21 days. Basal media was added to the other well to act as a control. The cell culture medium was changed every three days. Mineralisation was assessed using Alizarin Red stain to identify calcium deposits in the matrix.

Adipogenic differentiation: The BMMSCs were prepared using the same method described for osteogenic differentiation. However, following the addition of basal media, 1000 µl of adipogenic medium consisting of DMEM supplemented with 10% FCS, 1% PenStrep, 0.5mM isobutyl-1-methylxantine, 1 µm dexamethasone, and 10µg/ml insulin was added. Basal media was added to another well to act as a control. The cells were incubated at 37°C and 5% CO2 for 21 days with a medium change of every three days. Oil Red O staining was employed to identify the lipids in adipocytes.

Chondrogenic differentiation: For chondrogenic differentiation, 0.5 million cells were suspended in 5ml of basal media in 2 universal tubes and centrifuged in a Heraeus Megafuse centrifuge (Thermofisher Scientific, USA) at 2000rpm for 5mins to form a pellet. The universal tubes were placed into an incubator for 24 hours to form spheroids. Chondrogenic differentiation medium (Gibco, Life Technologies, USA) was prepared according to manufacturer's instructions. The basal medium was removed and replaced with 1000µl of chondrogenic medium and incubated at 37°C and 5% CO_2 for 21 days. The cell culture medium was changed every three days. Alcian Blue staining was employed to identify proteoglycans.

7.2.2. In vitro cell seeding

Scaffolds were sterilised by gamma irradiation at 25 kGy using a Gammacell 1000 (Best Teratronics Ltd., Hertfordshire, UK). Scaffolds with the average size of (height: 5.93 mm, diameter: 4.6 mm) and average weight of 1.8 mg were placed in a non-treated 24-well plate (Thermo scientific, Denmark) and seeded with 2 X 10^5 sheep BMMSCs at passage 2 suspended in 50 µl DMEM, scaffolds were incubated for 30 min at 37°C and 5% carbon dioxide to allow cell

attachment. Then 500 µl chondrogenic medium was added into each well. Scaffolds were cultured for the period of 21 days and medium was changed every 3-4 days during 3 weeks of cultivation. Osteogenic scaffolds were seeded by 10^5 BMMSCs and cultured with osteogenic medium (500 µl in each well). In case of bilayered scaffolds, each layer was seeded by 10^5 BMMSCs and 800 µl co-culture medium (prepared by the mixture of the same volume of chondrogenic and osteogenic scaffolds) was added into each well.

7.2.3. Cell viability assessment by Live/Dead assay

The viability of sheep BMMSCs on scaffolds was examined by Live/Dead® Cell Viability assay (Molecular Probes™, Invitrogen, UK) in day 1 and day 21 of culturing. Scaffolds were rinsed twice with PBS and incubated with 4 mM Calcein AM and 4 mM ethidium homodimer-1 in PBS for 20 min. Live and dead cells stained green and red respectively. Cells were imaged using an ApoTome 2 microscope (Zeiss, Germany).

7.2.4. Cell metabolic activity

Metabolic activity of cells was investigated using Presto Blue assay (Thermo Fisher scientific, USA) at 5 time points (day 0, day 1, day7, day 14 and day21). 10% diluted Presto Blue in DMEM was used for measuring metabolic activity of cells. Cell seeded scaffolds were transferred to a new well plate, washed with PBS and added with 600µl of Presto Blue. Absorbance/Fluorescence with excitation at 530-560 nm and emission at 590 was read with a fluorometer (Tecan, Infinite M200 PRO). Three cell seeded scaffolds were analysed at each time point and one acellular construct was used as a control.

7.2.5. Optimisation of DNA quantification method (cell proliferation) for collagen scaffold

In order to find the best protocol for lysis of cells seeded on collagen scaffolds, three different protocols which typically use for cell lysis were assessed aiming to achieve the highest quantity of DNA. These protocols include: 1. digestion of collagen matrix with papain enzyme following by the usage of a cell lysis buffer, 2. freeze- thaw cycles following by the usage of cell lysis buffer and 3. Only the usage of cell lysis buffer.

For each method, 10^5 BMMSCs were seeded onto 3 constructs of XColl2- CS for the period of three days.

1. **Papain digestion – cell lysis protocol**

Papain extraction reagent was prepared according to manufacturer's instruction (Biocolor Ltd, UK). Media were removed from the well plate and scaffolds were washed with PBS few times. Samples were placed in eppendorf tube (BRAND, Germany) and 1 ml of Papain extraction reagent was added to each tube. The tubes then placed in a water bath or a heating block at 65 °C, a digestion time of 3 hours at 65°C is sufficient to break up soft tissue of 20 to 50 mg. Tubes were then centrifuged at 10000rpm for 10 minutes. Supernatant were decanted off to a fresh Eppendorf for cell lysis treatment. 125 µl CelLytic buffer (Sigma Aldrich, UK) were added to each sample, cells were incubated for 15 min on a shaker. The lysed cells centrifuged for 15 min at 12000-20000 rpm to pellet the cellular debris. Then the supernatant was transferred to a chilled tube. DNA Quantification Kit (Sigma Aldrich) was used for quantifying DNA. Hoechst solution was prepared according to the Kit protocol. 50 µl of each sample in triplicate were transferred to a white 96 well plate and then 200 µl of Hoechst assay was added to each well. The emission was

recorded by using a Tecan fluorometer. A standard curve was plotted according to the manufacturer's protocol to correlate the fluorescence to DNA quantities.

2. Freeze-thaw cycles- cell lysis

Media were removed from the well plate and samples were washed with PBS a few times. 600µl microbiology grade water was added to each sample. Then the plate was placed in -80 °C freezer for 30 min, plate then incubated for 30 min at 37 °C. Three cycles of freeze- thaw were conducted. Freeze-thaw process causes the cell membrane to burst and release DNA. The water containing DNA was transferred to an eppendorf tube and went through cell lysis process using CelLytic M as described above.

3. cell lysis protocol

In this method, only 125 µl of CelLytic M plus 1ml of microbiology graded water were added to scaffolds after scaffolds were washed with PBS and placed in an eppendorf tube. The aforementioned steps for cell lysis treatment were conducted.

7.2.6. Cell proliferation based on DNA quantity

Quantifying cell proliferation is an important procedure in both biomedical sciences and cell biology[261,262]. A variety of assays are available to examine cell proliferation based on different chemistries[263] . In this respect, a number of cell counting techniques are commonly used to great effect. These include using nucleic acid binding dyes (such as Hoechst, CyQuant and PicoGreen) and thymidine incorporation for the radioactive labelling of DNA. While various metabolic assays

(such as MTT, MTS, WST-1 and AlamarBlue/PrestoBlue) are used in most research on cell proliferation, it has been revealed that the metabolic activity assay is a significantly less accurate method for determining the actual number of cells[264].

The limitation of metabolic assays is due to the changes in cellular metabolic activity throughout the lifecycle of cells. It has further established that metabolic assays are an inappropriate tool to assess cell proliferation in scaffold and matrix applications, or at high cell densities in two-dimensional (2D) cultures[263]. Because metabolic activity varies greatly with cell density, it does not correlate in a linear fashion with cell numbers. Furthermore, stem cells at various points of differentiation have different metabolic activity. Therefore, in this study, cell proliferation was assessed by using DNA quantification technique.

DNA quantification test was performed using papain digestion followed by cell lysis (lytic buffer) method. These tests were conducted at five time intervals of day 0 (4 hours after cell seeding), day 1, day7, day 14 and day21. Three cell seeded scaffolds were analysed at each time point and one acellular construct was used as a control.

7.2.7. Cell differentiation analysis (Gene Expression)

After 21 days of culturing, total RNA was isolated from the scaffolds using *TRIzol*™ reagent (Life technologies, USA). The isolated RNA quality was then verified by a NanoDrop (Spectrophotometer, labtech). cDNA was synthesized from RNA by reverse transcription using Master Mix reagent (Agillant, USA) and a thermal cycler (Bio-Rad, T100) machine. Gene expression was analyzed by Real-time quantitative polymerase chain reaction (qPCR) using a BioRad CFX96 machine. Primers sequences were derived from papers [265,266] and purchased from

Sigma Aldrich. Primers sequences are as following: b2-microglobulin housekeeping gene (forward: 5 –CCAGAAGATGGAAAGCCAAA–3, reverse: reverse: 5 –AGCGTGGGACAGAAGGTAG–3), COLII (forward: 5 –cctcaagaaggctctgctca–3, reverse: 5 –atgtcaatgatggggagacg–3), AGGRECAN (forward:5 –taggtggcgaggaagacatc–3, reverse: 5 –aaacgtgaaaggctcctcag–3), Primers were validated, and their efficiencies were found to be between 0.96 and 1.07.Expression was quantified using the Brilliant III SYBR Green QPCR Master Mix (Agilent, California, USA) kit in accordance with the manufacturer's instructions. The $2^{-\Delta Ct}$ method was then used to calculate the relative expression of each target gene. Briefly, mean Ct value of target genes in each sample was normalised to the averaged housekeeping gene Ct value to give a ΔCt value.

7.2.8. Histological analysis

Histological examination was conducted to distinguish different components of a section of scaffold using specific stains. For this purpose, samples (at day 1 and day 21) were fixed in 4% (w/v) PFA and stored in PBS. To embed the samples in wax, they were dehydrated through a graded alcohol series, embedded in paraffin wax and sectioned at a thickness of 10 µm with a microtom (Thermo Scientific, Shandon Finesse 325). Sections of chondrogenic scaffolds were stained with Alcian Blue, H&E and Safranin-O, using standard protocols, to visualise sulfated glycosaminoglycans, cells and cartilage respectively. Sections of osteogenic scaffolds were stained with Alazarin Red. The following protocols used for staining.

Alcian blue is one of the most widely used dyes for glycosaminoglycans staining. It is mainly positively charged and therefore, is thought to work by forming electrostatic bonds with negative sites on the polysaccharide staining them blue.

Sections were first deparaffinized by clearing in xylene (2 times, each 3 min), hydrated in ethanol 100%, 90%, 70% ,50% and deionized water each for 2 min. slides were then incubated in 3% acetic acid for 3 min, stained in Alcian Blue solution for 30-45 min and washed in running tap and deionised water for 2 min. slides were dehydrated in 70%, 95%, and 100% EtOH, for 2 min and clear in xylene (2 times, each 3 min). Finally, they were mounted with resinous mounting medium (Permount, Fisher Scientific SP15-500) and dried before observation with a Zeiss ApoTome 2 microscope.

Hematoxylin and Eosin (H&E) is the most commonly used technique for nuclei and cytoplasm staining, where basophilic structures (nucleic proteins) are shown blue, black, and purple or grey by haematoxylin and acidophilic structures (cytoplasmic proteins) are pink and red by Eosin.

The sections were deparaffinised and rehydrated as stated above. They were then washed with deionised water, stained with Haematoxylin for 1 min, washed with running water, deionised water, acid alcohol (1% HCL in 95% IMS), and another round of running and deionised water, and stained with 0.5% Eosin Y (Sigma Aldrich) in 2mM acetic acid for 30 sec.

The sections were washed and dehydrated and mounted with Permount and dried before microscopy.

Safranin-O is the basic histological staining for the general assessment of cartilage matrix. Safranin O is a cationic dye that stain proteoglycans as well as glycosaminoglycans. Safranin O staining is proportional to proteoglycan content and the result is orange to red.

The sections were deparaffinised using xyline (3 times, 4min each) and then hydrated in ethanol 96% (2times), 70% and tap water for 1 min each. Sections were then placed in 1% acetic acid solution for 5-10 sec. Sections were then transferred into 0.1% Safronin O solution for 5 min,

dehydrated with ethanol 100% (3 times, 5 min each) and xylene (5 min). They were finally mounted with resinous mounting media (Permount).

Alazarin Red (pH 4.3) is used to stain calcium-rich deposits by cells for hydroxyapatite screening, where calcium forms an Alizarin Red S-calcium complex in a chelation process, coloured red/orange and the end product is birefringent.

The sections were deparaffinised with two rounds of histoclear each for 10 min, and rehydrated in 100% and 90% IMS for 2 min. The sections were then transferred to Alizarin Red solution for 2 min. They were washed with acetone, acetone-xylene 1:1 solution and xylene, and mounted with DPX and coverslip and dried in an Incubator set at 42°C before microscopy.

7.3. Results for chondrogenic scaffolds

7.3.1. Live/ Dead assay (cell viability)

The cell viability has been examined by Live/Dead assay at day 1 and day 21, where viable cells are shown as bright green regions and dead cells as red regions (Fig 7.1). The staining showed that cells remained viable in scaffolds during the period of 21 days. Staining at day 1 showed the presence of more viable cells on XColl2- PCS suggesting greater cell attachment on this scaffold compared to the other two. Yet, XColl2 showed least viable cells on day1. Staining at day 1 also denotes that cells are randomly distributed and are isolated from one another. L/D staining at day 21 shows abundant green area suggesting more live cells versus dead cells. Furthermore, green regions at day 21 are considerably greater than that of day1 and thus indicates cell growth during 21 days culturing. Cell colonies can also be seen at day 21 which could associate with pre-cartilage condensation.

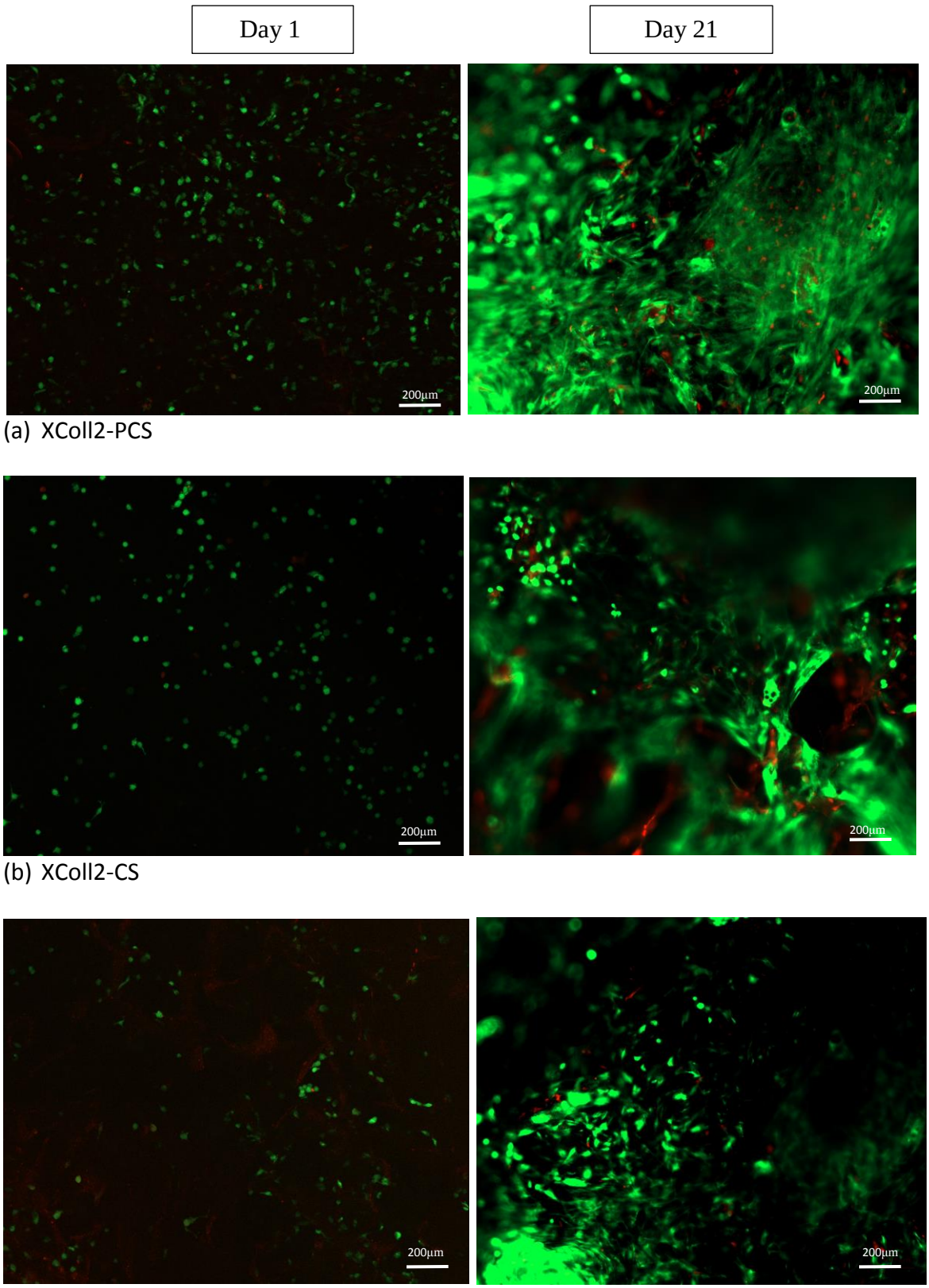


Fig 7.1. Live/Dead cytotoxicity assay showing cell viability on all scaffolds at day 1 and 21. Green colour indicates live cells and red color indicates dead cells.

7.3.2. Cell metabolic activity

Sheep BMMSCs were cultured on scaffolds for 21 days and the metabolic activity of cells were obtained at day 1, day7, day 14 and day 21. Metabolic activity of cells indicates proliferation/ apoptosis of cells. However, in this study cell proliferation was determined based on DNA quantity (Section 7.3.4) which is a more accurate method.

Fig 7.2 demonstrates that all compositions allowed for the cell attachment at day 0 and viability throughout 21 days. Furthermore, cells showed significantly different metabolic activity for each composition (p=.003). Metabolic activity of cells in all three scaffold types significantly increased from day 0 to day 7, (p<.001). Metabolic activity continued to increase from day 7 to day 14 for XColl2-PCS and XColl2-CS (p<0.001) while the metabolic activity did not significantly change for XColl2. There was no significant change in metabolic activity of all the compositions from day 14 to day 21 (p=0.92). XColl2-PCS exhibited significant increase in metabolic activity (p<.001) between day 21 (termination of culturing) and day 0 (day of seeding) while XColl2-CS and XColl2 did not show significant increases (p>0.05). Metabolic activity of cells on XColl2 are higher than XColl2- CS and XColl2- PCS at day 0, day 1, day 7 (p <0.05). Metabolic activity of cells on XColl2-CS and XColl2- PCS are not significantly different at day 0, day 1, day 7. However metabolic activity at day 14 and day 21 are significantly greater for XColl2- PCS. The greatest increase in cell metabolic activity happened at day 7 (the greatest climb took place between day1 and day7).

Fig 7.3 shows metabolic activity of cells which are normalised against metabolic activity at day 0. XCol2-PCS and XCol2-CS shows no significant difference in normalised metabolic activity from day 0 to day 21 ($p > 0.05$). Furthermore, their metabolic activity is higher than XCol2 at every time points except for day1.

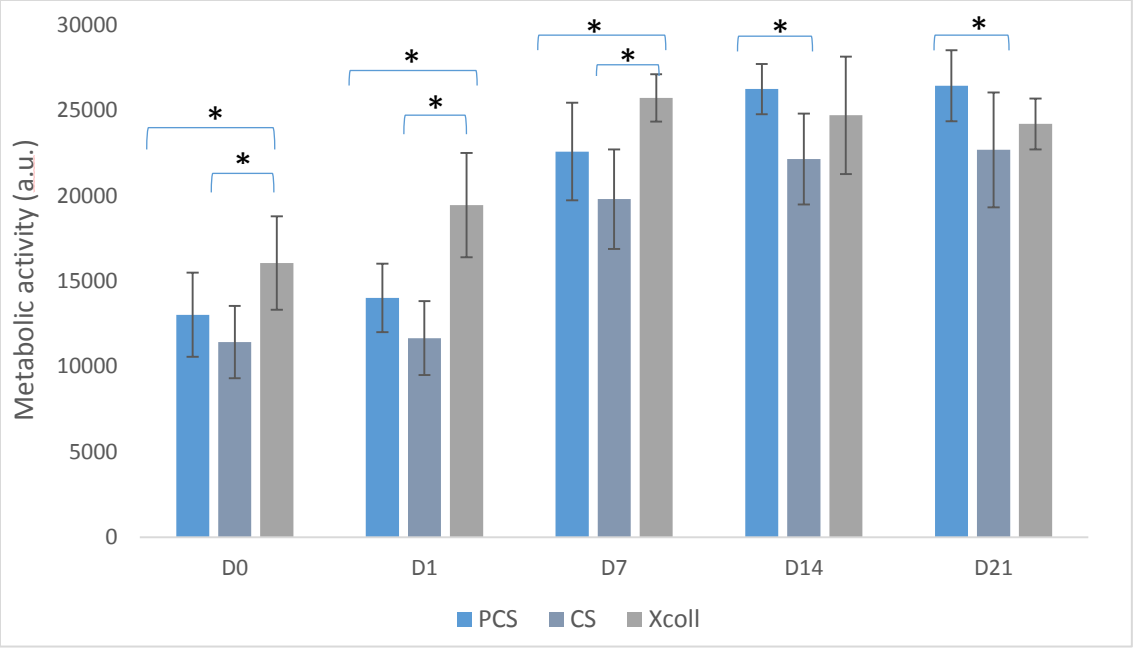


Fig 7.2. Metabolic activity of cells on the scaffolds at D0, D1, D7, D14 and D21, obtained by Presto Blue assay. The significant difference is denoted by * (Anova, Pairwise comparison)

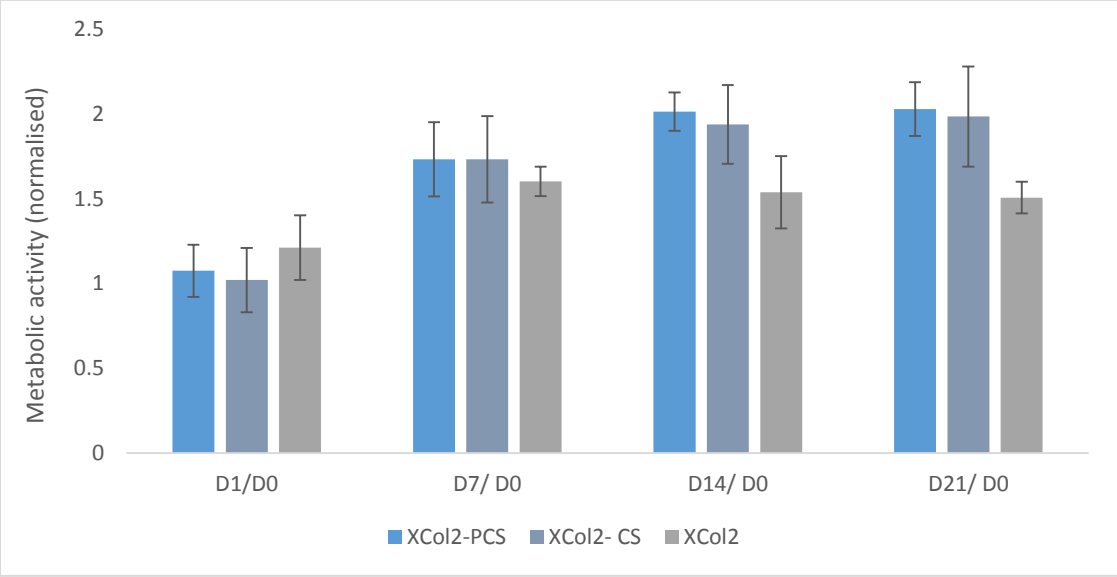


Fig 7.3. Cells' metabolic activity on chondrogenic scaffolds, normalised against day 0, no significant difference between metabolic activity of CS and PCS containing scaffolds

7.3.3. Optimisation of DNA quantification method

The DNA quantity which was obtained by the combination of papain digestion assay and cell lysis treatment was significantly (p<0.001) higher than the other methods (approximately two times greater) as shown in Fig 7.4. The amount of DNA acquired by freeze-thaw cycles following by cell lysis treatment and only cell lysis treatment was not significantly different (p=0.072).

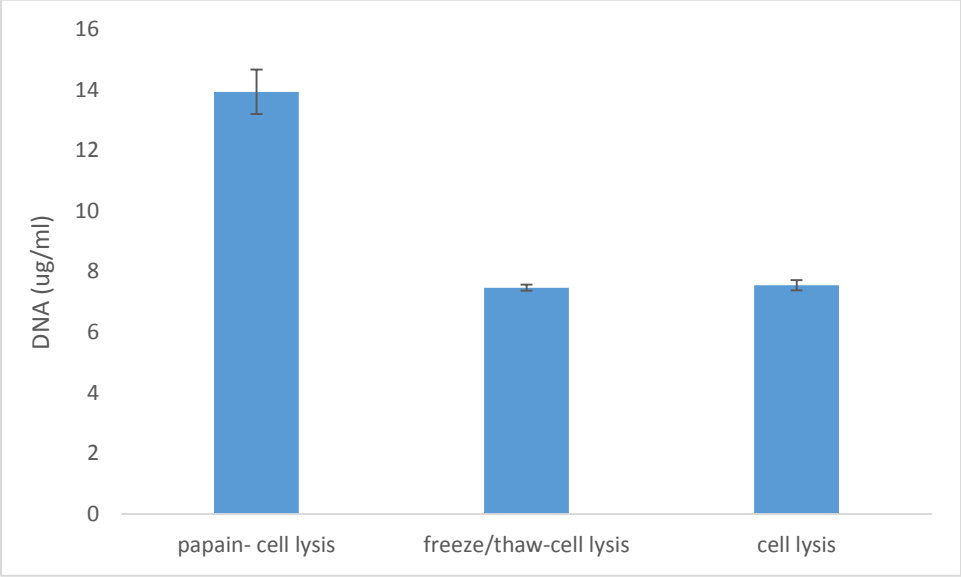


Fig 7.4. Comparison of DNA quantity obtained by papain digestion -cell lysis, freeze/thaw-cell lysis and only cell lysis protocol.

7.3.4. Cell attachment and proliferation (DNA quantity)

Figure 7.5 shows the DNA quantity of samples at day 1 and day 21 obtained by papain digestion combined with cell lysis protocol. The DNA quantity of XColl2- PCS and XColl2- CS at day 1 are not significantly different (p>0.05). However, the DNA content of these two groups are significantly higher than XColl2 (p<0.05) which suggests greater cell attachment on CS/PCS containing scaffolds.

A 2x3 way ANOVA found a significant main effect of composition, F (2, 20) = 19.63, p<0.001, and a significant main effect of day, F (1, 10) =35.42, p<0.001. There was a significant interaction effect (day x composition), F (2, 20) = 6.1, p< 0.05.

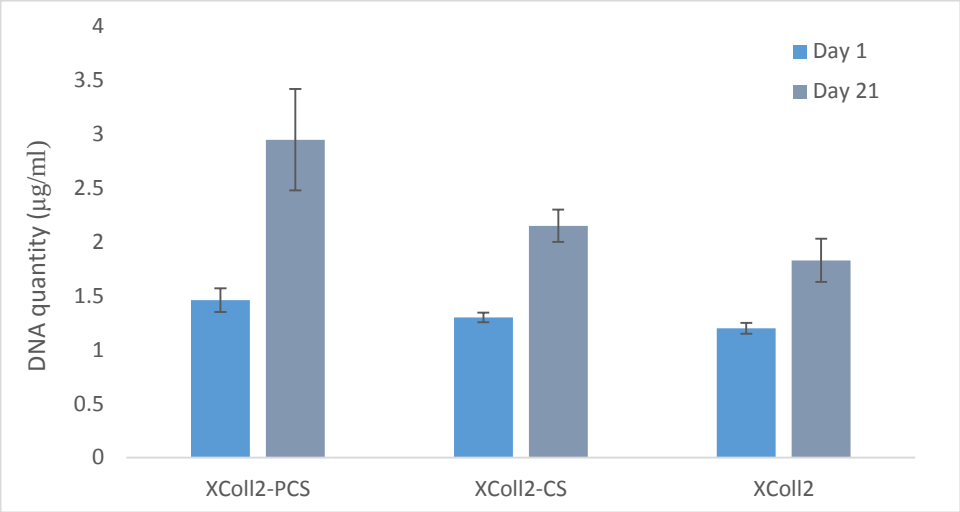


Fig 7.5. DNA quantity for XCOll2- PCS, XColl2- CS and XColl2 at D1 and D21

The DNA quantity has significantly increased at day 21 versus day1 for all three groups. Cell proliferation (calculated based on the ratio of DNA quantity at day 21 to day 1) of XColl2- PCS samples are significantly higher than the other two groups and XColl2 showed the lowest cell proliferation (Table 7.1).

Samples	XColl2-PCS	XColl2- CS	XColl2
Proliferation rate	2.02 ± 0.3	1.7 ± 0.16	1.52± 0.15

Table 7.1. Proliferation rate for XCOll2- PCS, XColl2- CS and XColl2 obtained based on DNA quantity at D21 versus D1

7.3.5. Cell differentiation- quantitative analysis of gene expression using qPCR

The chondrogenic differentiation of MSCs seeded on the scaffolds was determined via gene expression of two cartilage-specific markers, aggrecan and collagen type II after 21 days culturing. As shown in Fig 7.6, XColl2- PCS significantly increased the expressions of Coll2 (10 times) and aggrecan (3.2 times) as compared to XColl2- CS.

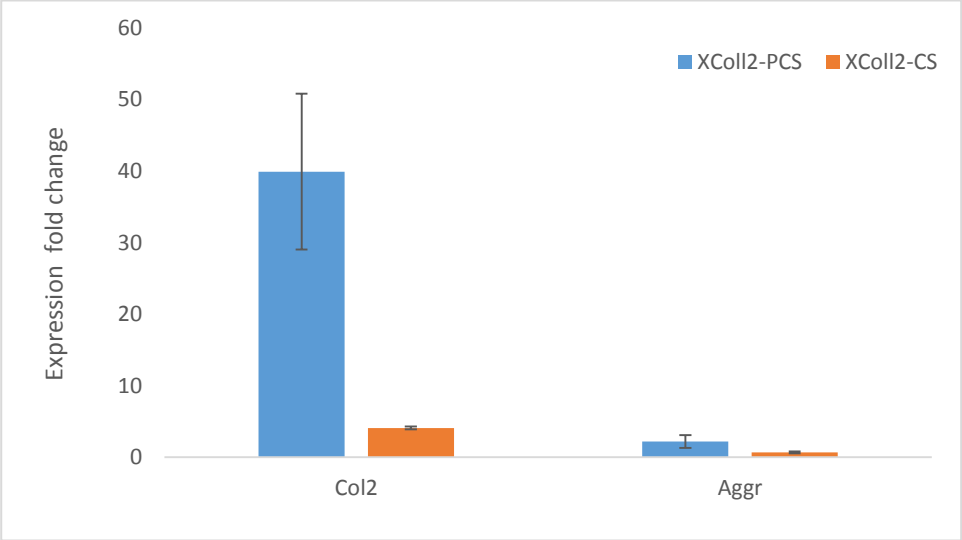


Fig 7.6 Collagen II and Aggrecan expression fold for XColl2-PCS, XColl2- CS (obtained based on $2^{-\Delta\Delta Ct}$), XColl2 used as the control

7.3.6. Histological analysis

Cell spatial distribution was shown by H&E staining of cell nuclei (dark purple/brown). Staining indicates that cells have infiltrated throughout the scaffolds. Higher number of cells can be seen in XColl2- PCS scaffolds (Fig 7.7). Alcian blue staining (Fig 7.8) detected high amount of well distributed glycosaminoglycan (GAGs) on XColl2- PCS. Moreover, the amount of GAGs produced

on XColl2-CS and XColl2 scaffolds were considerably lower than that produced on XColl2- PCS after 21 days.

Safronin-O staining (Fig 7.9) represents the formation of abundant cartilage ECM on the three scaffolds type. It is evident that XColl2-PCS synthesised significantly higher amount of cartilage ECM as opposed to XColl2-CS and XColl2. Furthermore, XColl2-CS showed higher amount of staining than XColl2.

It can be concluded that PCS increased the formation of cartilage ECM to a greater extent than CS. These results show that the composition of scaffolds impact mainly on the synthesis of ECM.

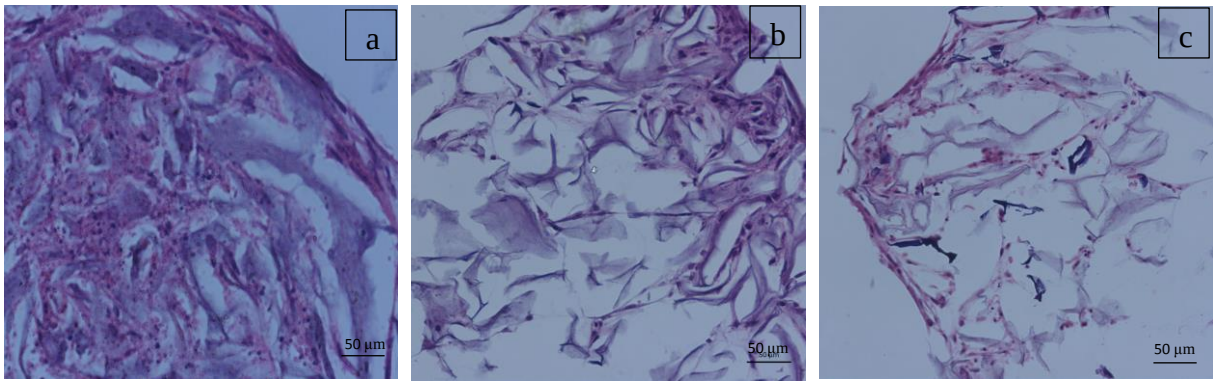


Fig 7.7. H&E staining, Day 21; (a) XColl2-PCS, (b) XColl2-CS and (c) XColl2. Dark purple dots indicate cells nuclei

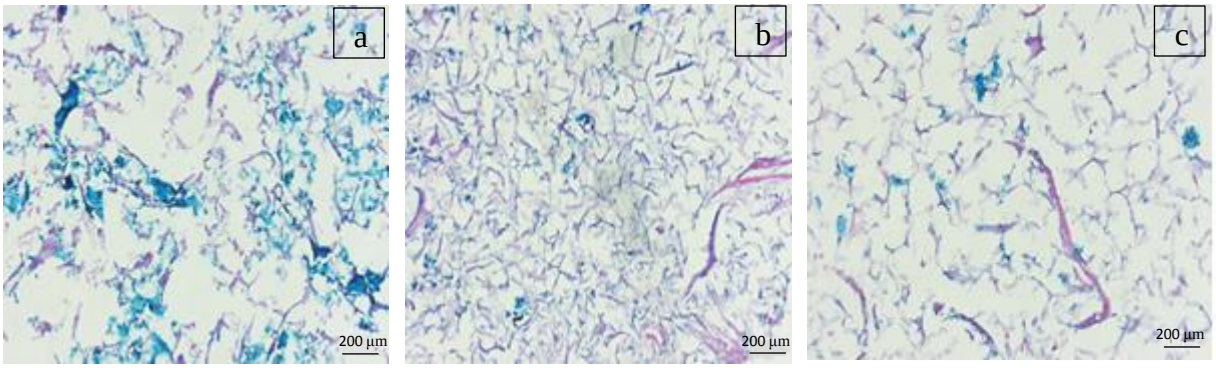


Fig 7.8. Alcian Blue staining, Day 21; (a) XColl2-PCS, (b) XColl2-CS and (c) XColl2

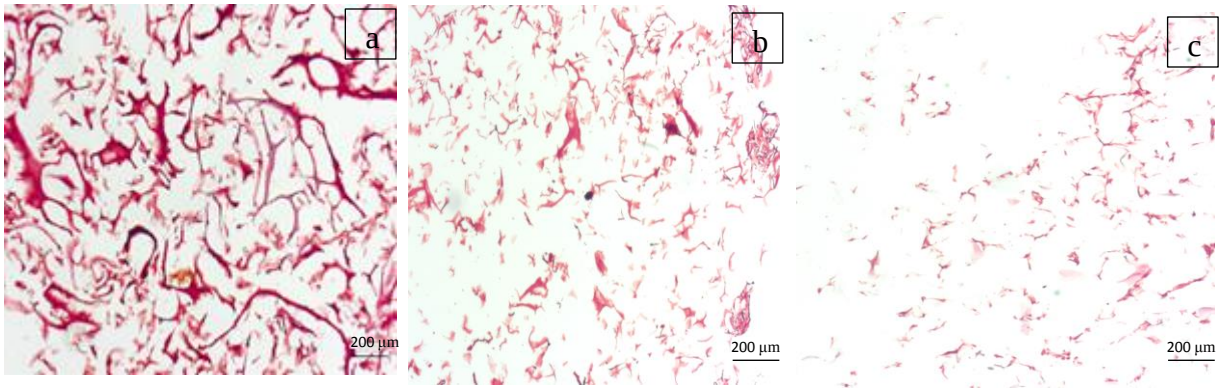
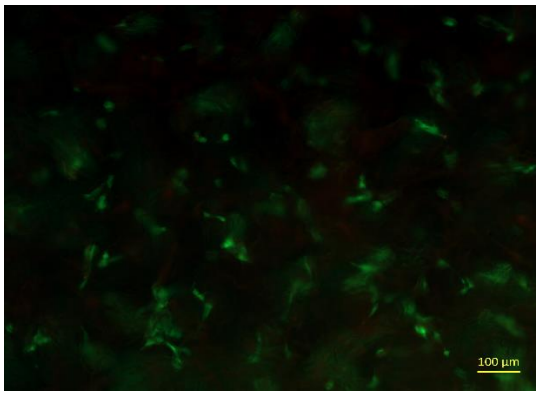


Fig 7.9. Safronin- O staining, Day 21; (a) XColl2-PCS, (b) XColl2-CS and (c) XColl2

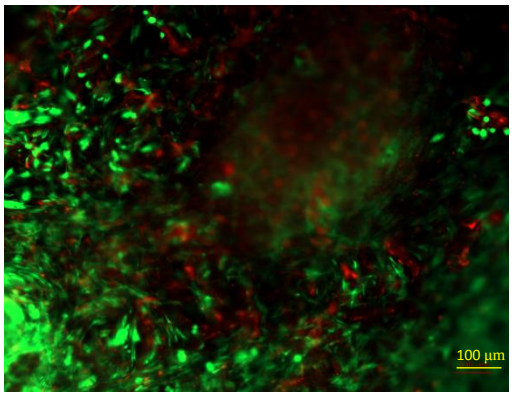
7.4. Results for osteogenic scaffolds and bilayered

7.4.1. Live/ Dead assay (cell viability)

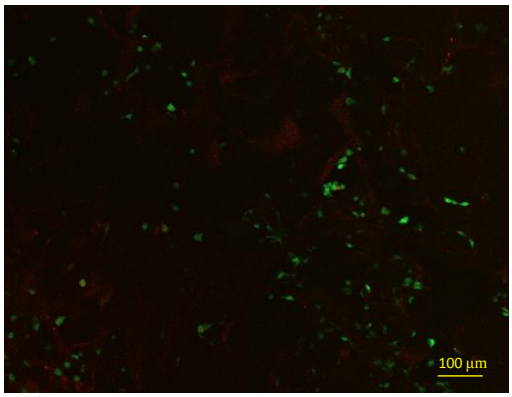
The cell viability has been assessed by Live/Dead assay, where viable cells are shown as bright green regions and dead cells as red regions (Fig 7.10). The staining showed that cells remained viable in scaffolds over 21 days. However, more cells stained red in day 21, indicating the number of dead cells increased. Besides, it can be seen that the number of green dots increased and thus suggesting both apoptosis and cell growth happened after 21 days.



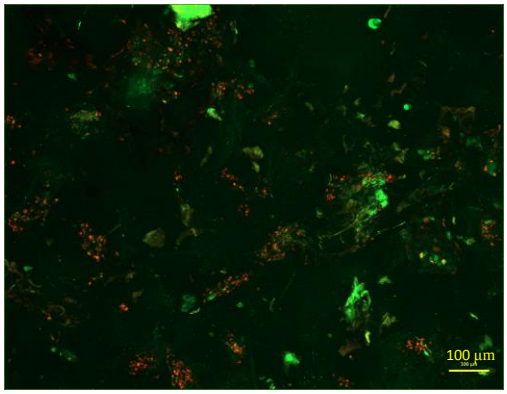
XCol1-HA1, D1



XCol1-HA1, D21



XCol1-HA2, D1



XCol1-HA1, D21

Fig 7.10. Live/Dead cytotoxicity assay showing cell viability on XCol1-HA1 and XCol1-HA2 at day 1 and 21. Green colour indicates live cells and red colour indicates dead cells.

7.4.2. Cell metabolic activity

Fig 7.11 and 7.12 show the metabolic activity of cells at day 1, day7, day 14 and day 21 on osteogenic and bilayered scaffolds respectively. All compositions allowed for the cell attachment at day 0 and viability throughout 21 days. Furthermore, cells showed significantly different metabolic activity for each composition (p=.003).

Metabolic activity of cells in all the three scaffolds significantly decreased from day 0 to day 7, (p<.001). It then increased from day 7 to day 21 for XCol1-HA1 and bilayered (p<0.001) while it did not significantly change for XCol1-HA2.

The metabolic activity of cells on XCol1-HA1 are significantly higher than XCol1-HA2 at every time points except for day 7 (p <0.05). The greatest increase in the cell metabolic activity happened at day 14 (greatest rise between D14 and D7).

The metabolic activity of cells on bilayered scaffold is not significantly different at day1, day 14 and day 21.

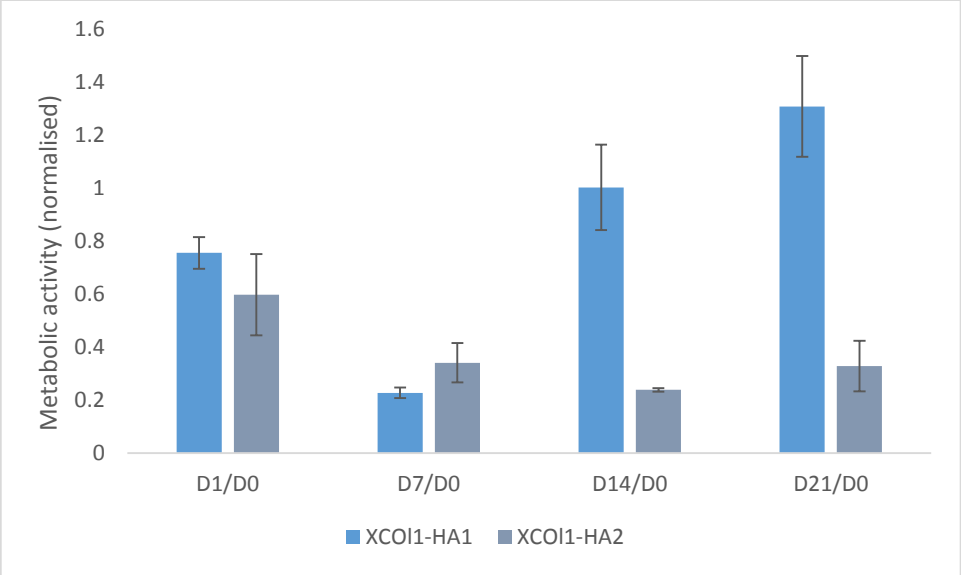


Fig 7.11. Metabolic activity of cell on the XCol1-HA1 and XCol1-HA2 scaffolds at D1, D7, D14 and D21 (normalised against day 0), obtained by Presto Blue assay.

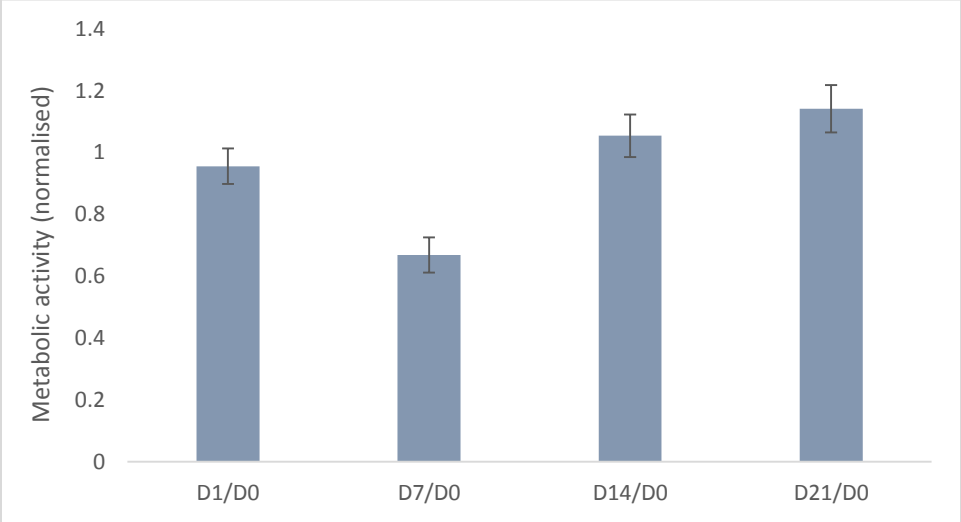


Fig 7.12. Cell metabolic activity on bilayered scaffolds (normalised against day 0)

7.4.3. Cell proliferation (DNA quantity)

Figure 7.13 shows the DNA quantity of XCol1-HA1 and bilayered scaffolds at day 0, day 1, day 7, day 14 and day 21 obtained by papain digestion combined with cell lysis assay (See Section 7.3.3). XCol1-HA2 showed the lowest cell viability and metabolic activity so it was not considered for the DNA quantification test.

A 2x5 way ANOVA found a significant main effect of composition, F (1, 40) = 892, p<0.001, and a significant main effect of day, F (4, 40) =17.8, p<0.001.

There was a significant interaction effect (day x composition), F (4, 40) = 19.05, p< 0.001.

The DNA quantity has significantly increased at day 21 versus day1 for bilayered scaffolds. Cell proliferation (calculated based on the ratio of DNA quantity at day 21 versus day 1) of bilayered samples are higher than XCol1-HA1 (Table 7.2).

For XCol1-HA1, a univariate analysis of ANOVA found a significant main effect of day, F (4, 40) = 3.35, p<0.05. Bonferroni Post Hoc tests found that the DNA quantity for XCol1-HA are not significantly different between the time points, except for day 0 and day 7 (P<0.05).

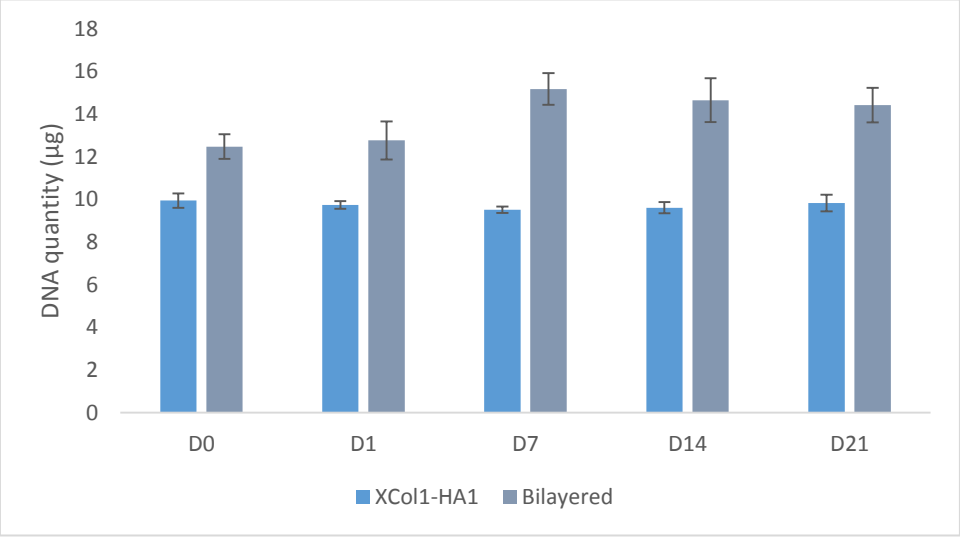


Fig 7.13. DNA quantities XCol1-HA1 and bilayered scaffolds at D0, D1, D7, D14, D21

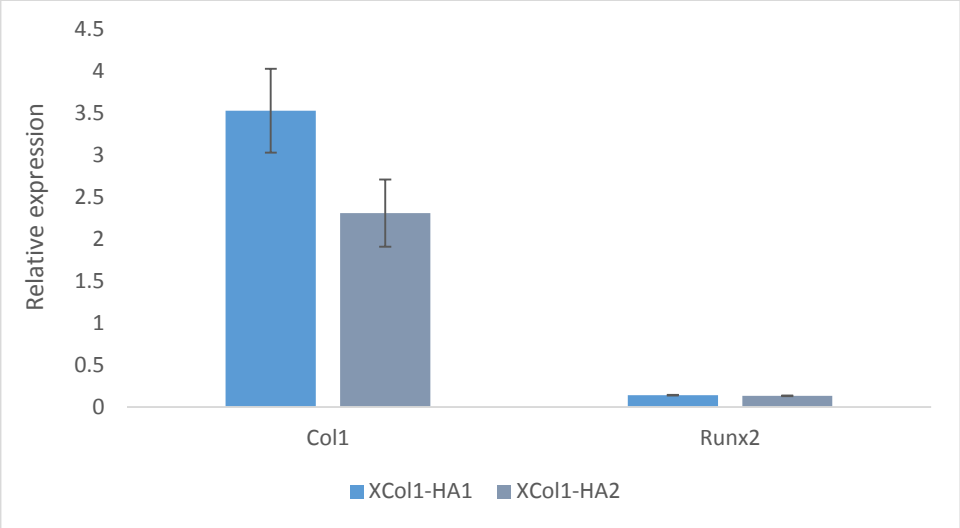
Similarly, a univariate analysis of ANOVA found a significant main effect of day for DNA content of bilayered samples, $F(4, 40) = 20.3$, $p < 0.001$. The DNA quantity was not significantly different at day 0 and day 1, then it significantly increased at day 7 ($P<0.05$) and maintained unchanged at day 14 and day 21.

Samples	XCol1- HA1	Bilayered
Proliferation rate	1.04 ± 0.2	1.4 ± 0.4

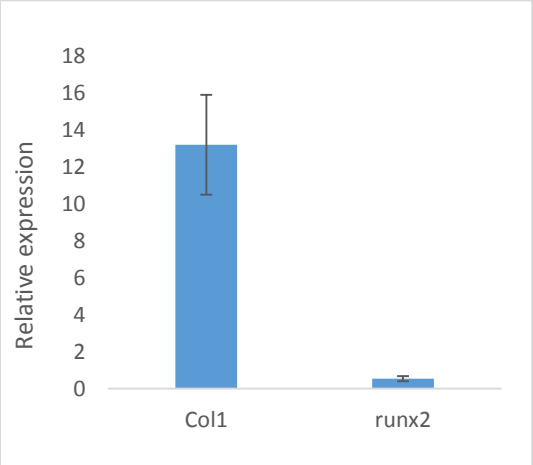
Table 7.2. Proliferation rate for XCol1-HA1 and bilayered scaffolds

7.4.4. Cell differentiation- quantitative analysis of gene expression using qPCR

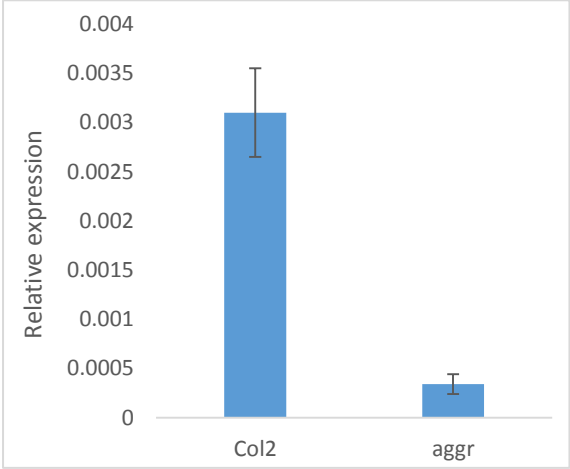
The osteogenic differentiation of BMMSCs seeded on XCol1-HA1 and XCol1-HA2 scaffolds was investigated via gene expression of two bone-specific markers, runx2 and collagen type I after 21 days culturing. As shown in Fig 7.14, the expressions of collagen I is significantly higher in XColl1-HA1 than that of XColl1- HA2 ($p<0.05$). However, runx2 expression is not significantly different between XColl1- HA1 and XColl1- HA2 scaffolds.



7.14. Collagen 1 and runx2 expression fold change for XCol1-HA1 and XCol1-HA2



7.15 (a). Expression of bone osteogenic markers for bilayered scaffolds (bone layer)



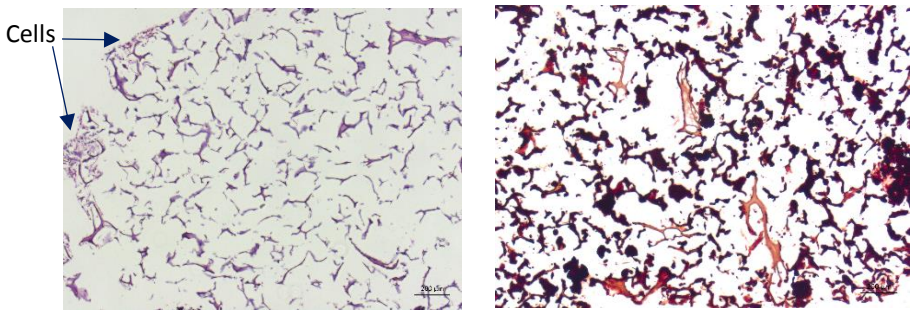
7.15 (b). Expression of cartilage chondrogenic markers for bilayered scaffolds (cartilage layer)

In the case of bilayered scaffolds, as shown in Fig 7.15, each layer gave rise to the expression of specific markers for cartilage and bone. The expression of Col1 is significantly higher than that of runx2 ($p < 0.05$) in osteogenic layer. The expression of Col2 is also significantly higher than that of aggrecan in chondrogenic layer ($p < 0.05$).

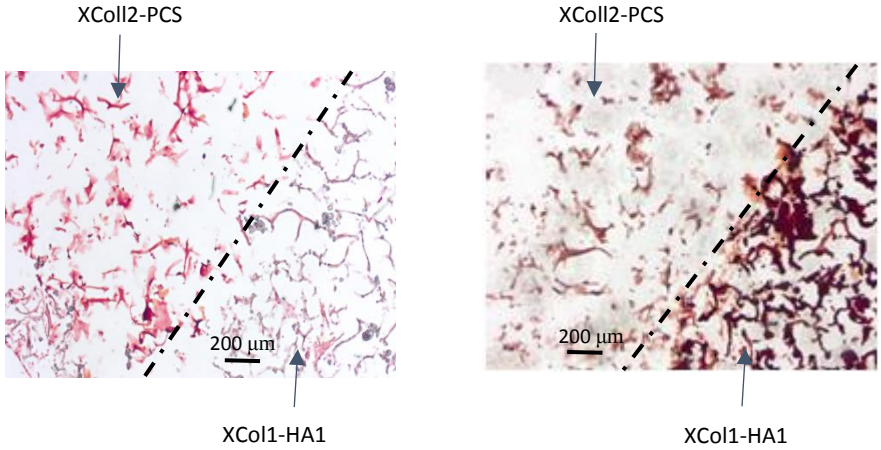
7.4.5. Histological analysis

In XCol1-HA1 scaffold (Fig 7.16a), the cells were primarily observed on the edge of scaffold. It can also be seen (Fig. 7.16b) that most of surface is covered with calcium-rich deposits which are either the HA added to scaffold during fabrication or they are produced by cells.

Fig 7.16b shows the chondrogenic layer positive staining with Safronin-O suggesting cartilage matrix production, interestingly the osteogenic layer was not stained positive for cartilage ECM. The osteogenic region of bilayered scaffold, stained positive with Alazarin Red indicating calcium-rich deposits while its chondrogenic region was not stained positive.



7.16 (a). H&E and Alizarin Red staining of XCol1-HA1 at day 21



7.16 (b). Safronin-O and Alizarin Red staining of bilayered scaffold at day 21

7.5. Discussion

This section discusses the results of cell culture experiments on different scaffold types. Metabolic activity, cell proliferation and differentiation are evaluated with respect to the different scaffold compositions and the days in culture. Histological observations are delineated and the scaffolds' matrix productions are examined accordingly. Additionally, the biological results are discussed alongside the scaffold characterisation results. This helps to assess the performance and advantages of our novel cartilage scaffolds (XColl2- PCS) in relation to other scaffold compositions.

7.5.1. Cell viability and scaffold biocompatibility

As represented by the Live/Dead assay (Fig 7.1 & 7.10), all of the scaffolds allowed cell attachments over the 3 weeks, suggesting their biocompatibility.

All normal tissue-derived cells (except haematopoietic) are anchorage-dependent cells and must be attached to a substrate for viability and proliferation[267]. The extent and strength of cell adhesion significantly influence subsequent cell proliferation and differentiation. Anchorage-dependent cells do not divide (or even undergo apoptosis) without a previous extension on the substrate[268].

Several sequences were identified within the triple helical regions of collagen type I and II, as cell adhesion sites [269]. The adhesion interaction between collagen and integrin was seen to be mediated through specific Arg–Gly–Asp (RGD) sequences in collagen[270,271]. Furthermore, in type I collagen, the α1 (I) chain of the triple helix was found to be more active for cell binding than the α2 (I) chain. It further contained the most active peptide, corresponding to residue between 568

and 835. In type II collagen, a comparable region on the α1 (II) chain was found to be the only active site for cell adhesion[272] .

It is necessary to point out that HA has been reported to be both biocompatible and cytotoxic. The potential toxicity or biocompatibility of HA particles depends on their concentration, size and particular cell type [273]. For example, HA nanoparticles inhibit osteosarcoma (MG63) cell growth and cause apoptosis. The fact that no apoptosis was observed in normal osteoblasts suggests the selective effect of HA nanoparticles on the two different cell types[274].It was also found that concentrations of HA nanoparticles, ranging from 100 to 500 μg/mL, reduce the growth and viability of MG-63 cells[274]. In the present study, the HA concentration was 6400 μg/mL (HA concentration in culture medium) which allowed cell (MSCs) viability, growth and differentiation. XCol1-HA1 scaffolds supported cell viability, most probably by providing a source of calcium and phosphate ions used by cells to create bones[275]. Thus, both XColl1- HA1 and XColl1- HA2 scaffolds, as well as bi-layered scaffolds, are biocompatible. It was also established that collagen-GAG scaffolds are a natural polymer and bioactive which allows cells to maintain high metabolic rates[276].

The size and shape of the cell spreading area is a further decisive factor for the migration, proliferation and differentiation of anchorage-dependent cells. In this respect, a small spreading area, and rounded cells without spreading and focal adhesion, lead to apoptosis[277]. Cell viability and proliferation on the scaffolds, throughout the 21 days of culturing, confirmed that the cells developed adhesion and spread across the scaffolds (See Fig 7.2& 7.5& 7.11& 7.13).

7.5.2. Cell metabolic activity

Three sets of Presto Blue experiments were carried out with different start dates and with cells from three different sheep. The metabolic activity of PCS/CS containing scaffolds increased from day 0 to day 14 and stabilised to day 21. However, the metabolic activity of XColl2 scaffold increased from day 0 to day 7 and decreased slightly on day 14 and stabilised to day 21. The metabolic activity of cells on pure collagen II scaffold was higher than PCS/CS containing scaffolds at early culturing (up to day 7), while the metabolic activity of cells on PCS- containing scaffolds was higher than the other scaffold types at day 14 and at day 21 (Fig 7.2).

The metabolic activity of cells in HA containing scaffolds significantly decreased from day 1 to day 7, it then increased from day 7 to day 21 for XCol1-HA1 and the bilayered scaffolds while it did not significantly change for XCol1-HA2 (Fig 7.11 & Fig 7.12).

The reason for the reduction in metabolic activity of cells (XColl2 in day 14, bone scaffolds and bilayered at day 7) or becoming steady (from day 14 to day 21 for and from day 7 to day 21 for XCol1-HA2) should not just be attributed to the cell necrosis over time. There may be sub-populations of cells at different stages/points in the lineage within these cultures that respond differently to the conditions they are subjected to. Therefore, some may continue to proliferate while others would stop proliferating and start to differentiate (with reduced metabolic activity)[278].

In case of chondrogenic scaffolds (collagen II), cell overcrowding was also likely to happen at day 14 due to the proliferation which offered cells with smaller spaces for further proliferation at day 21 and thus unchanged or reduced metabolic activity. Moreover, the overall contraction of

scaffolds has been shown to cause cell overcrowding and thus their reduced metabolic activity[279].

For osteogenic scaffolds, the metabolic activity of cells on XCol1-HA1 are significantly higher than XCol1-HA2 except for day 7. It could be due to the effect of HA size on the cells metabolic activity. It has been shown that larger size HA promotes cell growth and subsequent metabolic activity[280]. XCol1-HA1 has a larger size HA compared to XCol1-HA2 which would stimulates cell metabolic activity specifically at day 14 and 21. The difference between the metabolic activity of cells on bone and bilayered scaffolds could arise from two factors: firstly the number of cells seeded on the bilayered scaffolds at day 0 was twice that of bone scaffolds; secondly the bone scaffolds (XCol1-HA1 & XCol1-HA2) scaffolds were cultured in osteogenic medium; while the bilayered scaffolds were cultured in co culture media (namely with both osteogenic and chondrogenic components). Thus the media were different, the chondrogenic medium was known to contain TGF beta. The presence of TGF beta could have an effect on proliferation and consequently metabolic activity as well as cell differentiation.

A key point that should be noted is that cell metabolic activity does not necessarily indicate number of cells; a miscorrelation between metabolic activity and cell number has been shown, especially in BMMSCs[264], where the cell proliferation was over-estimated by metabolic activity assay, particularly pronounced over time and at high cell densities. This was the reason that the results were not presented in terms of cell number.

DNA quantification results also support that higher metabolic activity of cells does not signify higher number of cells. Although metabolic activity of cells on XColl2 at day 1 was higher than CS/PCS- containing scaffolds, its DNA quantity was less compared to the other two. DNA

quantification method serves a more accurate approximation of cell numbers as opposed to metabolic assay as will be described in the following section.

It can be deduced that scaffolds composition (presence of CS and PCS) and scaffolds microstructure affected the metabolic activity of cells.

7.5.3. Cell attachment and proliferation

The most reliable strategy for quantifying cell proliferation in high cell density (100,000 cells/ and 3D cultures) is to measure total DNA. It was thus decided, in this study, to evaluate cell proliferation using a DNA quantification method. Although highly accurate, the amount of DNA measured can only however provide an estimation of the actual cell numbers. This is because the amount of DNA in any cell within a given culture is determined by the cell cycle stage it is in, and is thus not constant[263]. In this respect, the results of DNA quantification at day 1 were taken as an indication of initial cell attachment to the scaffolds.

In this study, the DNA quantification protocol was examined and it was found that the combination of papain digestion assay and cell lysis treatment yields significantly higher DNA quantity. Papain digestion assay disintegrate collagen matrix and allow the entrapped cells in collagen scaffolds to release in the water (cells infiltrate in scaffolds when seeded and encapsulated by collagen fibers). Results showed that in the other two protocols a considerable number of cells were not lysed possibly due to the infiltration and entrapment in collagen matrix.

In a number of studies, papain digestion assay was solely employed for lysis of cells on scaffolds but papain is a protease which digests the matrix and is not destructive to cells, thus does not

provide an effective method for lysis of cells. In this research, by the combination of matrix digestion and the subsequent usage of a cell lytic buffer, a higher DNA quantity was yielded.
DNA quantification results showed significantly higher cell attachment on CS/PCS containing scaffolds. This signified that CS and PCS promoted cell attachment. Furthermore, XColl2- PCS scaffolds provided the highest cell proliferation, while XColl2 showed the lowest. This suggests that PCS has a significantly greater stimulatory effect on cell proliferation than CS. The increased proliferation rate of XColl2- CS (compared with XColl2) also confirms that CS facilitates cell proliferation.

Cell attachment is governed by the density of available ligands, with ligand density in turn being influenced by the composition of the scaffold[281]. As explained below, besides scaffold composition, other factors may influence cell attachment. These include: the scaffold's microstructure (pore size), mechanical properties (stiffness), surface roughness and specific surface area.

The adhesion of cells to their substrate and their subsequent proliferation are partly mediated by their interaction with some components of ECM[282]. In other words, molecular interactions regulate the attachment of cells to ECM's specific components. Proteoglycans are one of the ECM components that play a role in these regulatory interactions, possibly acting as ligands for adhesion[283-287]. These events are mediated through charge interactions via glycosaminoglycans (GAGs) chains or, alternatively, through protein- protein interactions via specific domains[288]. Proteoglycans also promote cell proliferation by acting as growth factor receptors[289].
As integrins and proteoglycans have been shown to act as the major ECM adhesion receptors

that cooperate in signalling events, they effectively regulate the signalling outcomes. Proteoglycans, in particular, are the essential cellular mechanisms that sense, integrate and respond to physical and chemical environmental information. By either directly connecting with the local adhesion sites or by controlling global cellular processes (through growth factor receptor signalling pathways), they lead to the integration of both external and internal signals[290]. Accordingly, it can be concluded that, as XCol1-PCS possesses a higher amount of GAGs compared to XCol2-CS and XCol2, it provides higher cell attachment and proliferation.

It has been shown that the binding interaction of cell surface receptors to specific adhesion ligands can depend on the mechanical characteristics (matrix stiffness) of the surface[291]. Focal adhesions can form and grow only if they experience pulling forces through their cytoskeleton. In this respect, growth on soft substrates leads to smaller focal adhesions[292]. Thus the higher stiffness of XCol1-PCS could contribute to the higher cell attachment.

Another factor affecting cellular adhesion is the scaffold specific surface area (i.e. surface to volume ratio)[293] that provides the cells integrin with sites for ligand binding[294,295]. Enabling sites to allow for highly specific interactions between materials and surrounding cells has been achieved by introducing peptide ligands or ECM molecules to the biomaterials surface in order to bind cell surface receptors[296,297]. Therefore, a high surface to volume ratio is believed to enhance cellular response[293].

It has been shown that an open-cell tetrakaidecahedron sufficiently describes/models the random microstructure of a cellular solid[295]. In this case, the specific surface area (SA/V) can be described in terms of the pore diameter (d) and the relative density (ρ^*/ρ_s) by Equation 7.1:

$$SA/V = \frac{c}{d} \ (\rho^*/\rho_s)^{0.5} \qquad \text{(Equation 7.1)}$$

Considering the relationship (d=2.78l) between diameter (d) and edge length of the tetrakaidecahedron (l), c is calculated to be 10.14.

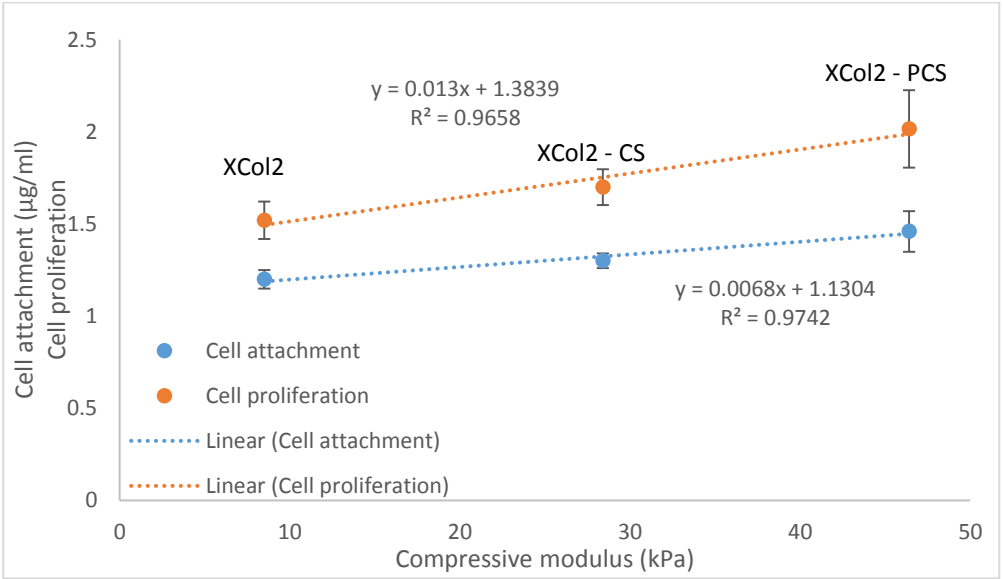
The larger pore size and lower relative density thus provide a smaller surface area for cell ligand binding[298]; however, after the initial attachment, larger pore sizes are preferred to allow cell ingrowth and better proliferation[207,298,299]. The results are presented in Table 7.3.

Sample	Metabolic activity at D1	DNA quantity at D1 (µg/ml)	Proliferation rate	Specific surface area(1/µm)	Compressive modulus (KPa)	Mean Pore area(µm^2)
XColl2-PCS	14000 ±2003	73.3 ± 2.9	2.02 ± 0.3	0.48	46.4 ± 7.4	2237± 382
XColl2-CS	12000 ± 2100	65 ± 1.02	1.7 ± 0.16	0.41	28.4 ± 2.3	4290 ± 1213
XColl2	19000 ± 3060	60.2± 1.2	1.52 ± 0.15	0.41	8.5 ± 0.8	

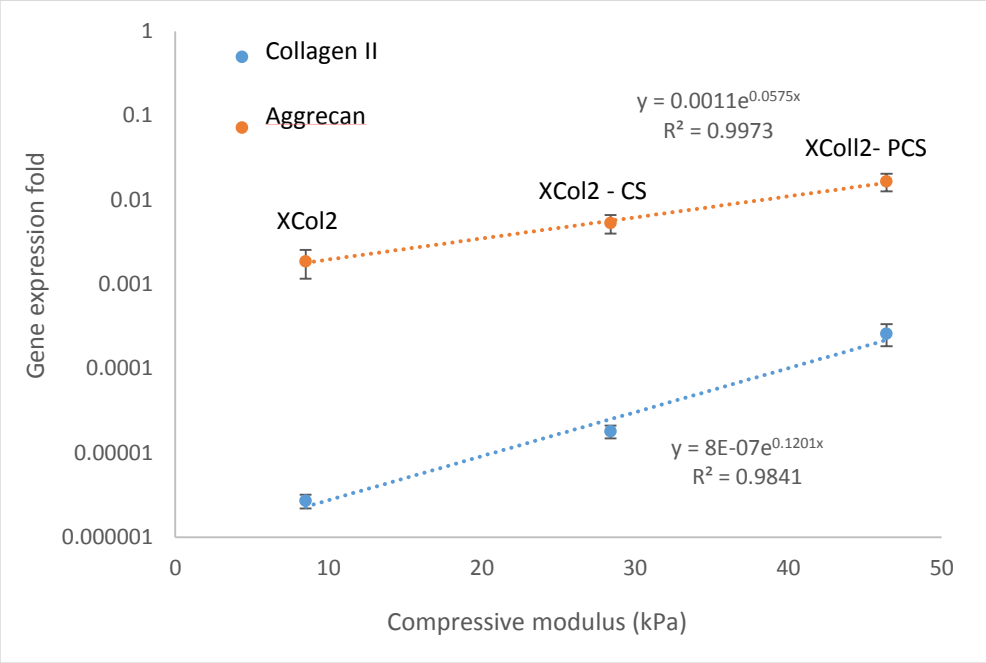
Table 7.3. Chondrogenic scaffolds properties and cell attachment and proliferation and metabolic activity at day1

As seen from the Table 7.3, XColl2-PCS has a higher specific surface area and compressive modulus, as well as a smaller pore size, than those of XColl2-CS and XColl2. This gives rise to its higher cell attachment and proliferation. In cartilage scaffolds, smaller pore size is preferred as it helps cell pre-condensation, leading stem cells towards chondrogenesis. XColl2-CS and XColl2 have the same specific surface area, while XColl2-CS compressive modulus is significantly higher than XColl2. Thus, we can say that its higher cell attachment and proliferation (likely) stems from either its greater compressive modulus or its composition. Fig 7.17 and Fig 7.18 show the cell

attachment, proliferation and differentiation versus compressive modulus. The best curve fit for cell attachment (y= 0.0068x+1.13, R^2 =0.97) and proliferation (y=0.01x+1.38, R^2 =0.96) data are linear, while differentiation is fitted best with exponential regression. It can be seen that with the increase in compressive modulus of scaffolds, cell attachment and proliferation increased by approximately the same ratio of 1.2. But, the cell differentiation increased by a greater rate compared to cell attachment and proliferation (approximately 3 times increase in aggrecan expression and 10 times increase in collagen II expression). Therefore, the increase in compressive modulus, which in turn is a function of composition (See Section 5.5.4), had a higher impact on cell differentiation rather than cell attachment and proliferation. The factors that affect cell differentiation are detailed in next the section.



7.17. Cell attachment and proliferation against scaffolds' compressive modulus. Cell attachment and proliferation increased by roughly a same rate by increasing compressive modulus/increasing CS content



7.18. Collagen II and Aggrecan expression fold versus scaffolds' compressive modulus

In the case of osteogenic scaffolds, XCol1-HA2 showed less metabolic activity at day 1 compared to XCol1-HA1, likely because of its lower cell attachment. Moreover, the metabolic activity of cells on XCol1-HA2 at day 21 was significantly lower than that of day 1, suggesting the likelihood of cell death over time (Fig 7.11). In osteogenesis, bone formation occurs by secreting collagen (type I) from the cells; this is followed by its calcification as nHA/Ca^{2+} ions [256] is released. As a result, it is possible that the diffusion of nutrients to the inner parts of the construct could be prevented, resulting in cell necrosis at the centre of the scaffold.

The higher specific surface area and compressive modulus of XCol1-HA1, compared to XCol1-HA2, justifies the enhanced cell response on XCol1-HA1 (i.e. increased cell metabolic activity and differentiation). Furthermore, the smaller pore size of XCol1-HA1 facilitates cell binding to the scaffold (Table 7.4).

Sample	DNA quantity at D1 (µg/ml)	Proliferation rate	Specific surface area(1/µm)	Compressive modulus (kPa)	Mean pore area (µm^2)
XCol1-HA1	9.74	1.04 ± 0.2	0.021	71.11 ± 4.4	5500 ± 1130
XCol1-HA2		-	0.014	41.32 ± 9.4	1531 ± 690
Bilayered	12.76	1.4 ± 0.4		37.42 ± 6.2	

Table 7.4. Osteogenic and bilayered scaffolds properties and cell attachment and proliferation

The bi-layered scaffolds had a higher cell quantity at day 1 than XCol1-HA1. However, given that they had twice the cell numbers as the XCol1-HA1 and XCol1-HA2 initially seeded on the scaffolds (at day 0), the bi-layered scaffolds were expected to present a higher DNA quantity at day 1. What's more, the bi-layered scaffolds showed a higher proliferation rate as compared to XCol1-HA1, which reflects the total proliferation on osteogenic and chondrogenic layers.

7.5.4. Cell differentiation

The qPCR experiments showed that XColl2-PCS significantly increased the expressions of collagen II (10 times) and aggrecan (3.2 times) compared to XColl2-CS (Fig 7.6). It can therefore be concluded that PCS and CS both induced the chondrogenic expression of stem cells while PCS showed a much higher stimulatory impact. The expression of collagen type-II and aggrecans indicate that cells are moving towards chondrogenic differentiation.

In the case of the bone scaffolds, the expression of collagen I and runx2 implies the osteogenic differentiation of the cells. We observed that HA1 significantly increased the expression of collagen 1, with respect to HA2, suggesting a higher influential effect on osteogenesis.

The signals from the microenvironment regulate the stem cells fate. In other words, the ECM to which the cells adhere, including its composition and physical properties (microstructure, topography and elasticity), can direct cell differentiation towards a specific lineage[300].

Scaffold composition – The scaffold composition is one of the most important stimuli of cell differentiation[301,302]. Collagen (e.g. type I and II), as well as the presence of CS, PCS and HA, are responsible for both specific gene expression and matrix molecule production.

Pore shape – Cells can be encouraged towards a specific lineage by artificially controlling their shape. It has been suggested that cell morphology relates to specific gene expression at different levels[297]. That is, BMMSCs with a more rounded cell shape correlated with a higher expression of chondrogenic markers[303,304]. Consequently, scaffolds with a more circular pore shape could potentially be more suitable for chondrogenic differentiation. In type-II scaffolds, used for cartilage regeneration, XColl2-PCS showed approximately the same pore circularity as XColl2-CS (Table 5.4). In this respect, the increased level of expression of chondrogenic markers in XColl2-PCS may have not be influenced by the pore morphology.

Scaffold stiffness – Scaffold stiffness is another factor affecting the fate of stem cells[300,304-311]. The cells response to the mechanical properties of their matrix involve a feedback loop, where cells exert contractile forces on the matrix and produce strain on the substrate; this strain can be detected by other cells which respond by adjusting their cytoskeleton and overall state [302,312,313]. In collagen type-II scaffolds, the higher stiffness in XCol2-PCS likely contributed to the increased expression of collagen type-II and aggrecan, which are markers of chondrogenic differentiation.

Likewise, in this study, cells on stiffer type-I scaffolds (XCol1-HA1, 71kPa) (Fig. 7.2) expressed increased osteogenic markers. The bulk stiffness of these scaffolds is slightly below the range specified for a substrate for bone regeneration [302,310,313](~100 kPa), though the high porosity of the scaffolds means that the bulk modulus of elasticity would be lower than the local stiffness felt in the cells (approx. by 100 times)[305,314]. Due to the pore sizes of the scaffolds (61-150 μm), it is expected that a high proportion of cells actually bridge the pores[305]. Consequently, they sense a combination of the local and bulk stiffness of the scaffold, which may be in the stiffness range preferred by the cells for osteogenesis.

Pore size – It has been shown that the cartilage formation, by mesenchymal stem cells[315] or chondroprogenitor cells, requires an initial stage of "condensation" where the intercellular space is reduced through cell aggregation and generation of cell-to-cell contacts. This is subsequently followed by chondrogenic differentiation.

Scaffold pore size may also play a role in directing the differentiation of stem cells. It was shown that chondrocytes seeded on smaller pore size scaffolds are more closely packed and therefore the cell-cell interaction likely affects the gene expression[301]. This may be extended to stem cells where condensation is a pre-requisite of chondrogenesis, meaning that higher type-II expression is expected in smaller pore size scaffolds. Hence, the smaller pore size in XColl2-PCS could contribute to its enhanced chondrogenic behavior. It should lastly be noted that pore size is only one of the many interdependent factors affecting cellular behaviour. It is therefore important to identify the effects of each factor, alongside those of the others.

7.5.5. Histological analysis

The qualitative analysis of histology images showed that XColl2-PCS produced considerably more GAGs and ECM compared with XColl2-CS and XColl2 (Fig 7.9 & 7.10). The secretion of cartilage ECM and GAGs further implies that cells are moving towards chondrogenic differentiation. It also can be seen that XColl2-CS synthesised more GAGs and cartilage ECM in relation to XColl2. This shows that the scaffolds' compositions (specifically those of CS and PCS) have an influential effect on cartilage ECM production.

It was particularly seen by XColl2-PCS (Fig 7.8) that the cells grew on the surface and periphery of the constructs, as well as infiltrating the pores of the scaffold. In this respect, cell migration and ingrowth may depend on scaffold pore size and stiffness [148,316]. As a stiff substrate is known to prompt a migratory response from cells[317], the higher compression modulus of XCol2-PCS is likely to be the most influential factor in its enhanced cell penetration.

Lastly, it was observed that, in osteogenic scaffolds, cell ingrowth occurred mainly on the periphery of the scaffolds (Fig 7.17). Alazarin red staining suggests the presence of calcium compounds on the whole section of the scaffold, but this could be due to either the formation of a new bone matrix (secretion of Ca^{+2}) or the presence of hydroxyapatite in the scaffold's composition.

7.6. Summary

In summary, the microenvironment of cells, which includes the substrate properties on which they are seeded, has been shown to influence cell behaviour in terms of their attachment, metabolic activity and differentiation.

Cell attachment and proliferation, in particular, were affected by the combination of composition, microstructure and specific surface area in chondrogenic (type II) and osteogenic scaffolds (type I) scaffolds. In type-II scaffolds, XColl2-PCS showed higher cell attachment and proliferation (1.2 fold increase), due to its higher specific surface area and compressive modulus, as well as their smaller pore size. In case of osteogenic scaffolds (type I), the higher specific surface area and compressive modulus of XCol1-HA1 (in relation to XCol1-HA2) led to increased cell attachment and proliferation. Over time, calcium containing compounds that form on the osteogenic scaffolds may hinder nutrient delivery to cells in the inner parts of scaffolds, causing acellular necrosis and thus reduced metabolic activity.

Cellular differentiation and the production of ECM markers were affected by scaffold elasticity and composition, where stiffer type II scaffolds promoted the expression of collagen type II (14 times) and aggrecan (3 times). It further promoted the secretion of the cartilage matrix. Additionally, stiffer type I scaffolds enhanced the expression of collagen type I (1.55 time), as well as bone matrix formation.

Collagen type, and the existence of CS, PCS and HA, affected the type of ECM marker produced by the cells. It was shown that the presence of PCS stimulated cell differentiation towards

chondrogenesis significantly more than CS. In the case of osteogenic scaffolds, pre-synthesised hydroxyapatite (HA1) increased the expression of osteogenic markers versus *In situ* precipitated hydroxyapatite nano particles (HA2). Lastly, it was established that sheep bone marrow mesenchymal stem cells gave rise to separate behavior, regarding chondrogenesis and osteogenesis, in different regions of the bi-layer.

Chapter 8. Thesis Summary and Conclusions

Tissue engineered grafts have been shown to be an optimal approach to the repair of osteochondral injuries. Yet, important advances in graft's composition, structure and mechanical properties are required that stimulates the progenitor cells towards chondrogenesis and/or osteogenesis. This thesis proposed to capture the natural biological properties and mechanical strength of the joint, by developing bi-layered, controlled matrix composition and mechanical strength osteochondral plugs while also achieving a seamlessly integrated interface. Based on this biomimetic approach, the main constituents of natural cartilage (collagen type II and chondroitin sulphate) and bone (collagen type I and HA) were used as scaffolds' components. Most importantly, the novelty of the work was polymerisation of CS to the higher molecular weight PCS and its subsequent grafting to collagen.

The experimental work has been divided into four chapters. In Chapter 4, chondroitin sulphate has been polymerised (PCS) in an attempt to increase the amount of CS that a chondrogenic scaffold can be retained. Fourier transform infra-red (FTIR) spectroscopy together with X-ray photoelectron spectroscopy (XPS) suggested the formation of a new ester bond between CS molecules which confirmed the occurrence of polymerisation. The molecular weight of PCS was obtained using two different methods: Einstain's Equation based on the DLS results, Mark Houwink Equation based on the rheological results. These revealed that the molecular weight and size of PCS are respectively 11.5 and 5.2 times greater than that of CS. Rheological analysis of PCS and CS showed that PCS possesses a higher viscosity, storage and loss modulus over a wide range of angular frequency (further support for the occurrence of polymerisation). Scaffolds of CS and PCS were then prepared and characterised in terms of their microstructure and mechanical properties. Different pore morphology was observed: parallel planar pores in CS and

randomly oriented circular pores in PCS. It was shown that CS Young's modulus is 2 times as that of PCS. The combination of the higher relative density as well as pore anisotropy led to the higher compressive modulus of CS scaffold.

In Chapter 5, three types of chondrogenic/cartilage scaffolds were produced from reconstituted fibrillar collagen type II: (collagen II, collagen II – CS, collagen II- PCS). The problem of the monomeric collagen crosslinking was addressed by crosslinking of the fibrils in the suspension by EDC-NHS chemical reagent. The effect of the addition of PCS on collagen solution viscosity, scaffold microstructure and mechanical properties were evaluated.

The state of collagen II suspensions, their shear thinning behaviour under oscillatory measurements were discussed. It was shown that monomeric collagen suspensions were in a semi-dilute state. The shear thinning of suspensions were explained based on the excluded volume repulsion, Van der Waals, electrostatic and covalent interactions between molecules. It was shown that PCS significantly increased the complex viscosity, storage and loss modulus of collagen suspensions, while CS reduced them. FTIR confirmed that the primary structure of collagen was maintained during the scaffolds fabrication. No substantial changes were observed in the Amide A band (N-H bond) of the samples, indicating that the collagen triple helix structure was not affected by crosslinking and CS/PCS addition. CS release profile showed that crosslinking hugely decreased CS release in medium. Furthermore, dissolution study confirmed that crosslinking substantially increased the stability of scaffolds in TBS. The pore sizes were explained by ice growth rate and viscosity of suspensions. The pores were anisotropic and described by major and minor axes of ellipse. The greater viscosity of XColl2-PCS, in relation to XColl2-CS, retards ice front growth by providing an opposing force and gives rise to the formation of smaller

pores. PCS significantly increased the Young's modulus of the scaffold, mainly due to the increase in the relative density of the scaffold. CS also increased the Young's modulus, yet not to the level that PCS did. The increase in the solid wall modulus of XColl2-CS is thought to be the main reason for the increase in its compressive modulus in relation to XColl2.

In Chapter 6, bone scaffolds were fabricated using two methods: crosslinked collagen I combined with commercially available HA, and *In situ* precipitation of HA nano particles on collagen fibrils following by the subsequent crosslinking of the suspension. XCol1-HA1 showed a shear thinning behaviour under oscillatory measurements. However, XCol1-HA2 showed a shear thinning behavior at low frequencies and a shear thickening regime at higher frequencies. It was shown that HA particle size had an influence on the viscosity of collagen solution and the critical ice front velocity. FTIR confirmed that crosslinking and specifically HA addition shifted the amide A band to a lower wavenumber and thus causing a less compact helical structure of collagen in the composite samples. The greater viscosity of XCol1-HA1, in relation to XCol1-HA2, gave rise to the formation of smaller pores (average pore area of XCol1-HA2 was nearly 3 times smaller). However, XColl1-HA1 showed substantially greater pore interconnectivity. XCol1-HA1 showed higher compressive modulus (71.1 Kpa) in respect to XColl1-HA2 (41.3 Kpa) and the higher relative density of XCol1-HA1 was shown to be the responsible factor for such an increase. Lastly, bilayered scaffold were fabricated based on the optimum outcomes obtained for the composition, micro-architecture and mechanical properties of cartilage and bone scaffolds. Crosslinked collagen II plus PCS were selected for the materials of the cartilage region and crosslinked collagen I plus HA1 were chosen for the bone region. The scaffolds were shown to

have a relatively smooth transition between the adherent layers. Microstructure and mechanical properties of bilayered scaffolds were discussed.

In Chapter 7, the biological responses of scaffolds to sheep bone marrow mesenchymal stem cells were investigated. The results suggested that all of the scaffolds were biocompatible. It was noted that the cell attachment and proliferation was affected by the combination of composition, microstructure and specific surface area in chondrogenic (type II) and osteogenic scaffolds (type I). In type-II scaffolds, XColl2-PCS showed higher cell attachment and proliferation due to its higher specific surface area and compressive modulus and smaller pore size. In type I scaffolds, higher specific surface area and compressive modulus of XCol1-HA1 respective to XCol1-HA2 led to the increased cell attachment and proliferation. Over time, calcium containing compounds formed on osteogenic scaffolds may hinder nutrient delivery to cells in the inner parts of scaffolds and may have caused acellular necrosis and thus reduced metabolic activity.

Cellular differentiation and production of ECM markers, was affected by scaffold elasticity and composition, where stiffer type II scaffolds promoted the expression of collagen type II and aggrecan as well as the secretion of cartilage matrix. Likewise, stiffer type I scaffolds enhanced the expression of collagen type I and runx2 and bone matrix formation. Collagen type and existence of CS, PCS and HA affected the type of ECM marker production by cells. It was shown that the presence of PCS stimulated cell differentiation towards chondrogenesis much greater than CS did. In case of osteogenic scaffolds, pre synthesized hydroxyapatite (HA1) increased the expression of osteogenic markers versus *In situ* precipitated hydroxyapatite nano particles (HA2).

Lastly, it was established that sheep bone marrow mesenchymal stem cells give rise to a separate behavior of chondrogenesis and osteogenesis in the different regions of the bi-layer.

Chapter 9. Future works

It was established that sheep bone marrow mesenchymal stem cells give rise to separate behavior of chondrogenesis and osteogenesis in the different regions of the bi-layer, giving rise to the separate formation of bone and cartilage. These novel and significant findings can be further developed towards the design and manufacturing of an osteochondral device even closer to that of the natural system (Fig. 9.1 shows a schematic illustration of the proposed design).This includes:

1. Manufacture of multi layered (graded) scaffold, with microstructural characterization to ensure the spatial control and interface integrity.

2. Fatigue tests to ensure mechanical integrity of the interface

3. Culture with hMSCs to examine differentiation pathways throughout the scaffold.

4. Perform a large animal model on these devices.

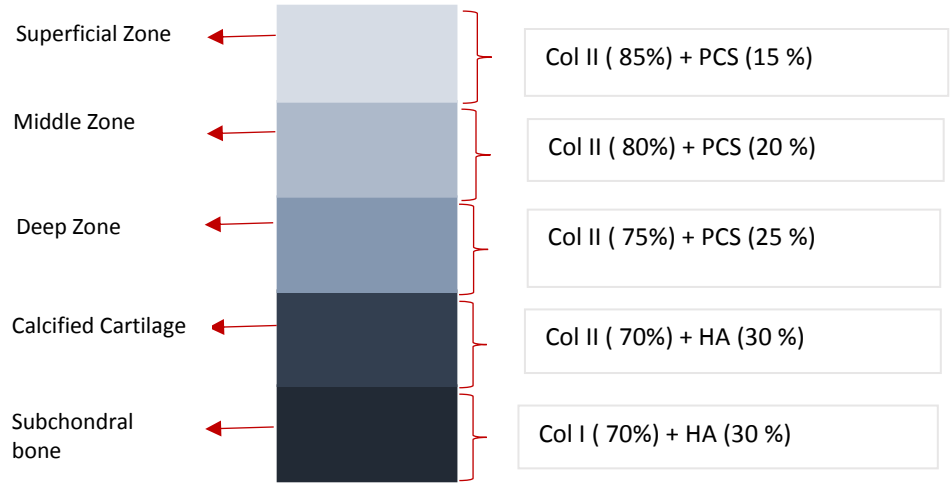


Fig 9.1. Proposed scaffold for osteochondral TE. As going down through the layers, collagen II content is reduced, CS proportion increased from superficial zone to the deep zone. Concurrently, collagen type I replaces by collagen type II, while hydroxyapatite replaces the CS.

References

1. Buckwalter JA, Mankin HJ. Articular cartilage: Degeneration and osteoarthritis, repair, regeneration, and transplantation. *Instr Course Lect*. 1998;47:487-504.

2. Csaki C, Schneider P, Shakibaei M. Mesenchymal stem cells as a potential pool for cartilage tissue engineering. *Annals of Anatomy-Anatomischer Anzeiger*. 2008;190(5):395-412.

3. Alexander AH, Lichtman DM. Surgical treatment of transchondral talar-dome fractures (osteochondritis dissecans) long-term follow-up*†‡. *The Journal of Bone & Joint Surgery*. 1980;62(4):646-652.

4. Berndt AL, Harty M. Transchondral fractures (osteochondritis dissecans) of the talus. *The Journal of Bone & Joint Surgery*. 1959;41(7):1363-1363.

5. Draper SD, Fallat LM. Autogenous bone grafting for the treatment of talar dome lesions. *The Journal of foot and ankle surgery*. 2000;39(1):15-23.

6. eOrthopod. Osteochondritis dissecans of the knee. https://www.orthogate.org/patient-education/knee/osteochondritis-dissecans-of-the-knee. Updated 2006.

7. Porter JR, Ruckh TT, Popat KC. Bone tissue engineering: A review in bone biomimetics and drug delivery strategies. *Biotechnol Prog*. 2009;25(6):1539-1560.

8. Lynn A, Brooks R, Bonfield W, Rushton N. Repair of defects in articular joints. *JOURNAL OF BONE AND JOINT SURGERY-BRITISH VOLUME-*. 2004;86:1093-1099.

9. Nukavarapu SP, Dorcemus DL. Osteochondral tissue engineering: Current strategies and challenges. *Biotechnol Adv*. 2013;31(5):706-721.

10. Vacanti JP, Langer R. Tissue engineering: The design and fabrication of living replacement devices for surgical reconstruction and transplantation. *The Lancet*. 1999;354:S32-S34.

11. Keeney M, Pandit A. The osteochondral junction and its repair via bi-phasic tissue engineering scaffolds. *Tissue Engineering Part B: Reviews*. 2009;15(1):55-73.

12. Mohan N, Dormer NH, Caldwell KL, Key VH, Berkland CJ, Detamore MS. Continuous gradients of material composition and growth factors for effective regeneration of the osteochondral interface. *Tissue Engineering Part A*. 2011;17(21-22):2845-2855.

13. Tang G, Zhang H, Zhao Y, Zhang Y, Li X, Yuan X. Preparation of PLGA scaffolds with graded pores by using a gelatin-microsphere template as porogen. *Journal of Biomaterials Science, Polymer Edition*. 2012;23(17):2241-2257.

14. Nukavarapu SP, Laurencin CT, Amini AR, Dorcemus DL. *Gradient Porous Scaffolds*. 2017.

15. Nukavarapu SP, Laurencin CT, Amini AR, Dorcemus DL. *Gradient Porous Scaffolds*. 2013.

16. Yang PJ, Temenoff JS. Engineering orthopedic tissue interfaces. *Tissue Engineering Part B: Reviews*. 2009;15(2):127-141.

17. Varghese S, Hwang NS, Canver AC, Theprungsirikul P, Lin DW, Elisseeff J. Chondroitin sulfate based niches for chondrogenic differentiation of mesenchymal stem cells. *Matrix Biology*. 2008;27(1):12-21.

18. Chen Q, Bruyneel A, Clarke K, Carr C, Czernuszka J. Collagen-based scaffolds for potential application of heart valve tissue engineering. *Journal of Tissue Science & Engineering*. 2013;2013.

19. Maryam Tamaddon. Characterisation of collagen type I/ type II composite scaffolds for osteochondral tissue engineering. University of Oxford; 2014.

20. Stockwell RA. *Biology of cartilage cells.* Vol 7. CUP Archive; 1979.

21. Fox AJS, Bedi A, Rodeo SA. The basic science of articular cartilage: Structure, composition, and function. *Sports Health: A Multidisciplinary Approach*. 2009;1(6):461-468.

22. Buckwalter JA. Mechanical injuries of articular cartilage. *Iowa Orthop J*. 1992;12:50.

23. Buckwalter JA, Mankin HJ. Articular cartilage: Tissue design and chondrocyte-matrix interactions. *Instr Course Lect*. 1998;47:477-486.

24. Buckwalter JA, Mankin HJ. Articular cartilage: Degeneration and osteoarthritis, repair, regeneration, and transplantation. *Instr Course Lect*. 1998;47:487-504.

25. Aigner T, Stöve J. Collagens—major component of the physiological cartilage matrix, major target of cartilage degeneration, major tool in cartilage repair. *Adv Drug Deliv Rev*. 2003;55(12):1569-1593.

26. Alford JW, Cole BJ. Cartilage restoration, part 1: Basic science, historical perspective, patient evaluation, and treatment options. *Am J Sports Med*. 2005;33(2):295-306.

27. Yang PJ, Temenoff JS. Engineering orthopedic tissue interfaces. *Tissue Engineering Part B: Reviews*. 2009;15(2):127-141.

28. Buckwalter JA, Mankin HJ, Grodzinsky AJ. Articular cartilage and osteoarthritis. *INSTRUCTIONAL COURSE LECTURES-AMERICAN ACADEMY OF ORTHOPAEDIC SURGEONS*. 2005;54:465.

29. Mankin HJ. Current concepts review. The response of articular cartilage to mechanical injury. *J Bone Joint Surg Am*. 1982;64(3):460-466.

30. Buckwalter J, Mankin H. Instructional course lectures, the american academy of orthopaedic surgeons-articular cartilage. part I: Tissue design and chondrocyte-matrix interactions*†. *The Journal of Bone & Joint Surgery*. 1997;79(4):600-611.

31. Buckwalter JA, Mankin HJ, Grodzinsky AJ. Articular cartilage and osteoarthritis. *INSTRUCTIONAL COURSE LECTURES-AMERICAN ACADEMY OF ORTHOPAEDIC SURGEONS*. 2005;54:465.

32. Temenoff JS, Mikos AG. Review: Tissue engineering for regeneration of articular cartilage. *Biomaterials*. 2000;21(5):431-440.

33. Freeman MAR. *Adult articular cartilage.* Pitman Medical; 1979.

34. Cremer MA, Rosloniec EF, Kang AH. The cartilage collagens: A review of their structure, organization, and role in the pathogenesis of experimental arthritis in animals and in human rheumatic disease. *Journal of molecular medicine*. 1998;76(3-4):275-288.

35. Kadler K, Holmes D, Trotter J, Chapman J. Collagen fibril formation. *Biochem J*. 1996;316:1-11.

36. Myllyharju J, Kivirikko KI. Collagens and collagen-related diseases. *Ann Med*. 2001;33(1):7-21.

37. Lane JM, Weiss C. Review of articular cartilage collagen research. *Arthritis & Rheumatism*. 1975;18(6):553-562.

38. Newman AP. Articular cartilage repair. *Am J Sports Med*. 1998;26(2):309-324.

39. Eyre D. Collagen of articular cartilage. *Arthritis research*. 2002;4(1):30-35.

40. Morrison EH, Ferguson MW, Bayliss MT, Archer CW. The development of articular cartilage: I. the spatial and temporal patterns of collagen types. *J Anat*. 1996;189 (Pt 1)(Pt 1):9-22.

41. Cremer MA, Rosloniec EF, Kang AH. The cartilage collagens: A review of their structure, organization, and role in the pathogenesis of experimental arthritis in animals and in human rheumatic disease. *Journal of molecular medicine*. 1998;76(3-4):275-288.

42. Maroudas A, Wachtel E, Grushko G, Katz E, Weinberg P. The effect of osmotic and mechanical pressures on water partitioning in articular cartilage. *Biochimica et Biophysica Acta (BBA)-General Subjects*. 1991;1073(2):285-294.

43. Torzilli PA. Water content and equilibrium water partition in immature cartilage. *Journal of orthopaedic research*. 1988;6(5):766-769.

44. Mow V, Kuei S, Lai W, Armstrong C. Biphasic creep and stress relaxation of articular cartilage in compression: Theory and experiments. *J Biomech Eng*. 1980;102(1):73-84.

45. Mow VC, Ratcliffe A, Robin Poole A. Cartilage and diarthrodial joints as paradigms for hierarchical materials and structures. *Biomaterials*. 1992;13(2):67-97.

46. Lai W, Hou J, Mow V. A triphasic theory for the swelling and deformation behaviors of articular cartilage. *J Biomech Eng*. 1991;113(3):245-258.

47. Linn FC, Sokoloff L. Movement and composition of interstitial fluid of cartilage. *Arthritis & Rheumatism*. 1965;8(4):481-494.

48. Maroudas A. Physicochemical properties of articular cartilage. *Adult articular cartilage*. 1979;2:215-290.

49. Martin JA, Buckwalter JA. Articular cartilage aging and degeneration. *Sports Medicine and Arthroscopy Review*. 1996;4(3):263-275.

50. Stolz M, Raiteri R, Daniels A, VanLandingham MR, Baschong W, Aebi U. Dynamic elastic modulus of porcine articular cartilage determined at two different levels of tissue organization by indentation-type atomic force microscopy. *Biophys J*. 2004;86(5):3269-3283.

51. Mow VC, Holmes MH, Michael Lai W. Fluid transport and mechanical properties of articular cartilage: A review. *J Biomech*. 1984;17(5):377-394.

52. Mansour JM. Biomechanics of cartilage. *Kinesiology: the mechanics and pathomechanics of human movement*. 2003:66-79.

53. Roth V, Mow V. The intrinsic tensile behavior of the matrix of bovine articular cartilage and its variation with age. *The Journal of Bone & Joint Surgery*. 1980;62(7):1102-1117.

54. Lu L, Valenzuela RG, Yaszemski MJ. Articular cartilage tissue engineering. *e-biomed: the journal of regenerative medicine*. 2000;1(7):99-114.

55. Armstrong C, Mow V. Variations in the intrinsic mechanical properties of human articular cartilage with age, degeneration, and water content. *J Bone Joint Surg Am*. 1982;64(1):88-94.

56. Akizuki S, Mow VC, Müller F, Pita JC, Howell DS, Manicourt DH. Tensile properties of human knee joint cartilage: I. influence of ionic conditions, weight bearing, and fibrillation on the tensile modulus. *Journal of Orthopaedic Research*. 1986;4(4):379-392.

57. Hori RY, Mockros L. Indentation tests of human articular cartilage. *J Biomech*. 1976;9(4):259-268.

58. Kempson G, Freeman M, Swanson S. The determination of a creep modulus for articular cartilage from indentation tests on the human femoral head. *J Biomech*. 1971;4(4):239-250.

59. Hayes W, Mockros L. Viscoelastic properties of human articular cartilage. *J Appl Physiol*. 1971;31(4):562-568.

60. McCutchen CW. The frictional properties of animal joints. *Wear*. 1962;5(1):1-17.

61. Athanasiou K, Rosenwasser M, Buckwalter J, Malinin T, Mow V. Interspecies comparisons of in situ intrinsic mechanical properties of distal femoral cartilage. *Journal of Orthopaedic Research*. 1991;9(3):330-340.

62. Kempson G, Muir H, Pollard C, Tuke M. The tensile properties of the cartilage of human femoral condyles related to the content of collagen and glycosaminoglycans. *Biochimica et Biophysica Acta (BBA)-General Subjects*. 1973;297(2):456-472.

63. Porter JR, Ruckh TT, Popat KC. Bone tissue engineering: A review in bone biomimetics and drug delivery strategies. *Biotechnol Prog*. 2009;25(6):1539-1560.

64. Athanasiou K, Zhu C, Lanctot D, Agrawal C, Wang X. Fundamentals of biomechanics in tissue engineering of bone. *Tissue Eng*. 2000;6(4):361-381.

65. Lawson AC, Czernuszka JT. Collagen--calcium phosphate composites. *Proc Inst Mech Eng H*. 1998;212(6):413-425.

66. Karageorgiou V, Kaplan D. Porosity of 3D biomaterial scaffolds and osteogenesis. *Biomaterials*. 2005;26(27):5474-5491.

67. Sato M, Webster TJ. Nanobiotechnology: Implications for the future of nanotechnology in orthopedic applications. *Expert review of medical devices*. 2004;1(1):105-114.

68. Suchanek W, Yoshimura M. Processing and properties of hydroxyapatite-based biomaterials for use as hard tissue replacement implants. *J Mater Res*. 1998;13(01):94-117.

69. Yaszemski MJ, Payne RG, Hayes WC, Langer R, Mikos AG. Evolution of bone transplantation: Molecular, cellular and tissue strategies to engineer human bone. *Biomaterials*. 1996;17(2):175-185.

70. Sikavitsas VI, Temenoff JS, Mikos AG. Biomaterials and bone mechanotransduction. *Biomaterials*. 2001;22(19):2581-2593.

71. Zioupos P, Currey J. Changes in the stiffness, strength, and toughness of human cortical bone with age. *Bone*. 1998;22(1):57-66.

72. Ulrich-Vinther M, Maloney MD, Schwarz EM, Rosier R, O'Keefe RJ. Articular cartilage biology. *J Am Acad Orthop Surg*. 2003;11(6):421-430.

73. Poole AR, Kojima T, Yasuda T, Mwale F, Kobayashi M, Laverty S. Composition and structure of articular cartilage: A template for tissue repair. *Clin Orthop*. 2001;391:S26-S33.

74. Nukavarapu SP, Dorcemus DL. Osteochondral tissue engineering: Current strategies and challenges. *Biotechnol Adv*. 2013;31(5):706-721.

75. Hunziker E, Quinn T, Häuselmann H. Quantitative structural organization of normal adult human articular cartilage. *Osteoarthritis and Cartilage*. 2002;10(7):564-572.

76. Burr DB. Anatomy and physiology of the mineralized tissues: Role in the pathogenesis of osteoarthrosis. *Osteoarthritis and cartilage*. 2004;12:20-30.

77. Schinagl RM, Gurskis D, Chen AC, Sah RL. Depth-dependent confined compression modulus of full-thickness bovine articular cartilage. *Journal of Orthopaedic Research*. 1997;15(4):499-506.

78. Mente P, Lewis J. Elastic modulus of calcified cartilage is an order of magnitude less than that of subchondral bone. *Journal of orthopaedic research*. 1994;12(5):637-647.

79. Madry H, van Dijk CN, Mueller-Gerbl M. The basic science of the subchondral bone. *Knee Surgery, Sports Traumatology, Arthroscopy*. 2010;18(4):419-433.

80. Armstrong SJ, Read RA, Price R. Topographical variation within the articular cartilage and subchondral bone of the normal ovine knee joint: A histological approach. *Osteoarthritis and Cartilage*. 1995;3(1):25-33.

81. Bullough PG, Yawitz PS, Tafra L, Boskey AL. Topographical variations in the morphology and biochemistry of adult canine tibial plateau articular cartilage. *Journal of orthopaedic research*. 1985;3(1):1-16.

82. Müller-Gerbl M, Dalstra M, Ding M, Linsenmeier U, Putz R, Hvid I. Distribution of strength and mineralization in the subchondral bone plate of human tibial heads. *J Biomech*. 1998;31:123.

83. Imhof H, Breitenseher M, Kainberger F, Rand T, Trattnig S. Importance of subchondral bone to articular cartilage in health and disease. *Topics in magnetic resonance imaging*. 1999;10(3):180-192.

84. Athanasiou K, Zhu C, Wang X, Agrawal C. Effects of aging and dietary restriction on the structural integrity of rat articular cartilage. *Ann Biomed Eng*. 2000;28(2):143-149.

85. Radin EL, Martin RB, Burr DB, Caterson B, Boyd RD, Goodwin C. Effects of mechanical loading on the tissues of the rabbit knee. *Journal of Orthopaedic Research*. 1984;2(3):221-234.

86. Athanasiou KA, Darling EM, Hu JC. Articular cartilage tissue engineering. *Synthesis Lectures on Tissue Engineering*. 2009;1(1):1-182.

87. Widuchowski W, Widuchowski J, Trzaska T. Articular cartilage defects: Study of 25,124 knee arthroscopies. *The Knee*. 2007;14(3):177-182.

88. Wheeless C. Wheeless' textbook of orthopaedics. . 1996.

89. Upmeier H, Brüggenjürgen B, Weiler A, Flamme C, Laprell H, Willich S. Follow-up costs up to 5 years after conventional treatments in patients with cartilage lesions of the knee. *Knee Surgery, Sports Traumatology, Arthroscopy*. 2007;15(3):249-257.

90. Moseley JB, O'Malley K, Petersen NJ, et al. A controlled trial of arthroscopic surgery for osteoarthritis of the knee. *N Engl J Med*. 2002;347(2):81-88.

91. Caffey S, McPherson E, Moore B, Hedman T, Vangsness CT,Jr. Effects of radiofrequency energy on human articular cartilage: An analysis of 5 systems. *Am J Sports Med*. 2005;33(7):1035-1039. doi: 0363546504271965 [pii].

92. Steadman JR, Rodkey WG, Rodrigo JJ. Microfracture: Surgical technique and rehabilitation to treat chondral defects. *Clin Orthop*. 2001;391:S362-S369.

93. Blevins FT, Steadman JR, Rodrigo JJ, Silliman J. Treatment of articular cartilage defects in athletes: An analysis of functional outcome and lesion appearance. *Orthopedics*. 1998;21(7):761-7; discussion 767-8.

94. Spahn G, Kahl E, Mückley T, Hofmann GO, Klinger HM. Arthroscopic knee chondroplasty using a bipolar radiofrequency-based device compared to mechanical shaver: Results of a prospective, randomized, controlled study. *Knee Surgery, Sports Traumatology, Arthroscopy*. 2008;16(6):565-573.

95. Haene R, Qamirani E, Story RA, Pinsker E, Daniels TR. Intermediate outcomes of fresh talar osteochondral allografts for treatment of large osteochondral lesions of the talus. *The Journal of Bone & Joint Surgery*. 2012;94(12):1105-1110.

96. Brittberg M, Lindahl A, Nilsson A, Ohlsson C, Isaksson O, Peterson L. Treatment of deep cartilage defects in the knee with autologous chondrocyte transplantation. *N Engl J Med*. 1994;331(14):889-895.

97. Redman S, Oldfield S, Archer C. Current strategies for articular cartilage repair. *Eur Cell Mater*. 2005;9(1):23-32.

98. McNickle AG, Provencher MT, Cole BJ. Overview of existing cartilage repair technology. *Sports Med Arthrosc*. 2008;16(4):196-201. doi: 10.1097/JSA.0b013e31818cdb82 [doi].

99. Freyman T, Yannas I, Gibson L. Cellular materials as porous scaffolds for tissue engineering. *Progress in Materials Science*. 2001;46(3):273-282.

100. O'Shea TM, Miao X. Bilayered scaffolds for osteochondral tissue engineering. *Tissue Engineering Part B: Reviews*. 2008;14(4):447-464.

101. Sharma B, Elisseeff JH. Engineering structurally organized cartilage and bone tissues. *Ann Biomed Eng*. 2004;32(1):148-159.

102. Puppi D, Chiellini F, Piras A, Chiellini E. Polymeric materials for bone and cartilage repair. *Progress in Polymer Science*. 2010;35(4):403-440.

103. Hutmacher DW. Scaffolds in tissue engineering bone and cartilage. *Biomaterials*. 2000;21(24):2529-2543.

104. Hollister SJ. Hierarchical bioactive materials for tissue reconstruction: Integrated design and manufacturing challenges. *JOM*. 2011;63(4):56-65.

105. Temenoff JS, Mikos AG. Injectable biodegradable materials for orthopedic tissue engineering. *Biomaterials*. 2000;21(23):2405-2412.

106. Yaszemski MJ, Payne RG, Hayes WC, Langer R, Mikos AG. < I> in vitro degradation of a poly (propylene fumarate)-based composite material. *Biomaterials*. 1996;17(22):2127-2130.

107. Place ES, Evans ND, Stevens MM. Complexity in biomaterials for tissue engineering. *Nature materials*. 2009;8(6):457-470.

108. Livingston T, Gordon S, Archambault M, et al. Mesenchymal stem cells combined with biphasic calcium phosphate ceramics promote bone regeneration. *J Mater Sci Mater Med*. 2003;14(3):211-218.

109. Martin I, Miot S, Barbero A, Jakob M, Wendt D. Osteochondral tissue engineering. *J Biomech*. 2007;40(4):750-765.

110. O'DRISCOLL SW. Current concepts review-the healing and regeneration of articular cartilage*. *The Journal of Bone & Joint Surgery*. 1998;80(12):1795-1812.

111. Shapiro F, Koide S, Glimcher M. Cell origin and differentiation in the repair of full-thickness defects of articular cartilage. *The Journal of Bone & Joint Surgery*. 1993;75(4):532-553.

112. Caplan AI, Elyaderani M, Mochizuki Y, Wakitani S, Goldberg VM. Overview: Principles of cartilage repair and regeneration. *Clin Orthop*. 1997;342:254.

113. Chu CR. Chondral and osteochondral injuries: Mechanisms of injury and repair responses. *Operative Techniques in Orthopaedics*. 2001;11(2):70-75.

114. Duda GN, Maldonado ZM, Klein P, Heller MO, Burns J, Bail H. On the influence of mechanical conditions in osteochondral defect healing. *J Biomech*. 2005;38(4):843-851.

115. Lee S, Shin H. Matrices and scaffolds for delivery of bioactive molecules in bone and cartilage tissue engineering. *Adv Drug Deliv Rev*. 2007;59(4):339-359.

116. Rezwan K, Chen Q, Blaker J, Boccaccini AR. Biodegradable and bioactive porous polymer/inorganic composite scaffolds for bone tissue engineering. *Biomaterials*. 2006;27(18):3413-3431.

117. Byrne DP, Lacroix D, Planell JA, Kelly DJ, Prendergast PJ. Simulation of tissue differentiation in a scaffold as a function of porosity, young's modulus and dissolution rate: Application of mechanobiological models in tissue engineering. *Biomaterials*. 2007;28(36):5544-5554.

118. Kelly DJ, Prendergast PJ. Prediction of the optimal mechanical properties for a scaffold used in osteochondral defect repair. *Tissue Eng*. 2006;12(9):2509-2519.

119. Chu CR, Coutts RD, Yoshioka M, Harwood FL, Monosov AZ, Amiel D. Articular cartilage repair using allogeneic perichondrocyteseeded biodegradable porous polylactic acid (PLA): A tissue-engineering study. *J Biomed Mater Res*. 1995;29(9):1147-1154.

120. Im G, Lee JH. Repair of osteochondral defects with adipose stem cells and a dual growth factor-releasing scaffold in rabbits. *Journal of Biomedical Materials Research Part B: Applied Biomaterials*. 2010;92(2):552-560.

121. Jeong CG, Zhang H, Hollister SJ. Three-dimensional polycaprolactone scaffold-conjugated bone morphogenetic protein-2 promotes cartilage regeneration from primary chondrocytes in vitro and in vivo without accelerated endochondral ossification. *Journal of Biomedical Materials Research Part A*. 2012;100(8):2088-2096.

122. Khanarian NT, Haney NM, Burga RA, Lu HH. A functional agarose-hydroxyapatite scaffold for osteochondral interface regeneration. *Biomaterials*. 2012;33(21):5247-5258.

123. O'Shea TM, Miao X. Bilayered scaffolds for osteochondral tissue engineering. *Tissue Engineering Part B: Reviews*. 2008;14(4):447-464.

124. Marcus. A. Osteochondral transplants. http://www.normanmarcusmd.com/research/osteochondral-transplants. Updated 2018.

125. Athanasiou K, Korvick D, Schenck Jr R. Biodegradable implants for the treatment of osteochondral defects in a goat model. *Tissue Eng*. 1997;3(4):363-373.

126. Niederauer GG, A Slivka M, Leatherbury NC, et al. Evaluation of multiphase implants for repair of focal osteochondral defects in goats. *Biomaterials*. 2000;21(24):2561-2574.

127. Yaylaoglu MB, Yildiz C, Korkusuz F, Hasirci V. A novel osteochondral implant. *Biomaterials*. 1999;20(16):1513-1520.

128. Wang X, Grogan SP, Rieser F, et al. Tissue engineering of biphasic cartilage constructs using various biodegradable scaffolds: An in vitro study. *Biomaterials*. 2004;25(17):3681-3688.

129. Guo X, Wang C, Duan C, et al. Repair of osteochondral defects with autologous chondrocytes seeded onto bioceramic scaffold in sheep. *Tissue Eng*. 2004;10(11-12):1830-1840.

130. Allan K, Pilliar R, Wang J, Grynpas M, Kandel R. Formation of biphasic constructs containing cartilage with a calcified zone interface. *Tissue Eng*. 2007;13(1):167-177.

131. van Susante JL, Buma P, Homminga GN, van den Berg, Wim B, Veth RP. Chondrocyte-seeded hydroxyapatite for repair of large articular cartilage defects. A pilot study in the goat. *Biomaterials*. 1998;19(24):2367-2374.

132. Larson R. *The structure and rheology of complex fluids* . New York: Oxford University Press; 1999.

133. Saarakkala S, Rieppo L, Rieppo J, Jurvelin J. Fourier transform infrared (FTIR) microspectroscopy of immature, mature and degenerated articular cartilage. *Microscopy*. 2010;1:403-414.

134. Rieppo L, Saarakkala S, Närhi T, Helminen H, Jurvelin J, Rieppo J. Application of second derivative spectroscopy for increasing molecular specificity of fourier transform infrared spectroscopic imaging of articular cartilage. *Osteoarthritis and cartilage*. 2012;20(5):451-459.

135. Susi H, Byler DM. Protein structure by fourier transform infrared spectroscopy: Second derivative spectra. *Biochem Biophys Res Commun*. 1983;115(1):391-397.

136. Castle J. Practical surface analysis by auger and x-ray photoelectron spectroscopy. D. briggs and MP seah (editors). john wiley and sons ltd, chichester, 1983, 533 pp.,£ 44.50. *Surf Interface Anal*. 1984;6(6):302-302.

137. Nuffield E.W. *X-ray diffraction methods.* Wiley, New York & London; 1966.

138. Suryanarayana C GNM. *X-rayn diffraction: A practical approach.* Plenum Press, New York& London; 1998.

139. Buckwalter JA, Hunziker EB. Healing of bones, cartilages, tendons, and ligaments: A new era. *The Lancet*. 1996;348:S18.

140. Douglas T, Heinemann S, Mietrach C, et al. Interactions of collagen types I and II with chondroitin sulfates AC and their effect on osteoblast adhesion. *Biomacromolecules*. 2007;8(4):1085-1092.

141. Varghese S, Hwang NS, Canver AC, Theprungsirikul P, Lin DW, Elisseeff J. Chondroitin sulfate based niches for chondrogenic differentiation of mesenchymal stem cells. *Matrix Biology*. 2008;27(1):12-21.

142. Huang K, Hsu W, Chiu W, Wang J. Functional improvement and neurogenesis after collagen-GAG matrix implantation into surgical brain trauma. *Biomaterials*. 2012;33(7):2067-2075.

143. Wang W, Zhang M, Lu W, et al. Cross-linked collagen–chondroitin sulfate–hyaluronic acid imitating extracellular matrix as scaffold for dermal tissue engineering. *Tissue Engineering Part C: Methods*. 2009;16(2):269-279.

144. Cavalcanti OA, da SILVA CC, Pineda EAG, Hechenleitner AAW. Synthesis and characterization of phosphated crosslinked chondroitin sulfate: Potential ingredient for specific drug delivery. *acta farmacéutica bonaerense*. 2005;24(2):234.

145. Tamaddon M, Walton R, Brand D, Czernuszka J. Characterisation of freeze-dried type II collagen and chondroitin sulfate scaffolds. *J Mater Sci Mater Med*. 2013;24(5):1153-1165.

146. Chang K, Hung L, Chu I, Ko C, Lee Y. The application of type II collagen and chondroitin sulfate grafted PCL porous scaffold in cartilage tissue engineering. *Journal of Biomedical Materials Research Part A: An Official Journal of The Society for Biomaterials, The Japanese Society for Biomaterials, and The Australian Society for Biomaterials and the Korean Society for Biomaterials*. 2010;92(2):712-723.

147. Chen Y, Lee H, Chan H, Sung L, Chen H, Hu Y. Composite chondroitin-6-sulfate/dermatan sulfate/chitosan scaffolds for cartilage tissue engineering. *Biomaterials*. 2007;28(14):2294-2305.

148. Ko C, Huang J, Huang C, Chu I. Type II collagen-chondroitin sulfate-hyaluronan scaffold cross-linked by genipin for cartilage tissue engineering. *Journal of bioscience and bioengineering*. 2009;107(2):177-182.

149. van Susante JL, Pieper J, Buma P, et al. Linkage of chondroitin-sulfate to type I collagen scaffolds stimulates the bioactivity of seeded chondrocytes in vitro. *Biomaterials*. 2001;22(17):2359-2369.

150. Goldstein I, Hullar T. Chemical synthesis of polysaccharides. *Advances in Carbohydrate Chemistry*. 1967;21:431-512.

151. Hirano S, Kashimura N, Kosaka N, Onodera K. Polysaccharide synthesis from mono-and oligo-saccharides by the action of phosphorus pentoxide in dimethyl sulphoxide. *Polymer*. 1972;13(5):190-194.

152. Mora PT, Wood JW, Maury P, Young BG. Synthetic polysaccharides. II. fractionation of Polyglucose1. *J Am Chem Soc*. 1958;80(3):693-699.

153. Satoh T, Imai T, Ishihara H, et al. Synthesis of hyperbranched polysaccharide by thermally induced cationic polymerization of 1, 6-anhydro-β-D-mannopyranose. *Macromolecules*. 2003;36(17):6364-6370.

154. Seeberger PH. Solid phase oligosaccharide synthesis. *J Carbohydr Chem*. 2002;21(7-9):613-643.

155. Uryu T. Artificial polysaccharides and their biological activities. *Progress in polymer science*. 1993;18(4):717-761.

156. Faijes M, Planas A. In vitro synthesis of artificial polysaccharides by glycosidases and glycosynthases. *Carbohydr Res*. 2007;342(12):1581-1594.

157. Kobayashi S, Uyama H, Kimura S. Enzymatic polymerization. *Chem Rev*. 2001;101(12):3793-3818.

158. Kobayashi S, Ohmae M. Enzymatic polymerization to polysaccharides. In: *Enzyme-catalyzed synthesis of polymers.* Springer; 2006:159-210.

159. Yang J, Tsai S, Chen J, Yang C, Hsieh Y. *Method for producing water-insoluble polysaccharides*. 2005.

160. Rennhard H. *Polysaccharides and their preparation*. 1973.

161. Kanazawa A, Okumura S, Suzuki M. Powder-to-powder polycondensation of natural saccharides. facile preparation of highly branched polysaccharides. *Organic & biomolecular chemistry*. 2005;3(9):1746-1750.

162. Nishimura S. *Nishimura, S. 2000, WO 00/09565*. .

163. Kanazawa A, Namiki S, Suzuki M. Thermal polycondensation of sugar fluoride to form highly branched polysaccharide. *Journal of Polymer Science Part A: Polymer Chemistry*. 2007;45(17):3851-3860.

164. Amrutkar JR, Gattani SG. Chitosan–chondroitin sulfate based matrix tablets for colon specific delivery of indomethacin. *Aaps Pharmscitech*. 2009;10(2):670-677.

165. Armstrong J, Wenby R, Meiselman H, Fisher T. The hydrodynamic radii of macromolecules and their effect on red blood cell aggregation. *Biophys J*. 2004;87(6):4259-4270.

166. Pamies R, Cifre JGH, Martínez, María del Carmen López, de la Torre, José García. Determination of intrinsic viscosities of macromolecules and nanoparticles. comparison of single-point and dilution procedures. *Colloid Polym Sci*. 2008;286(11):1223-1231.

167. Flory PJ. *Principles of polymer chemistry.* Cornell University Press; 1953.

168. Wasteson Å. Properties of fractionated chondroitin sulphate from ox nasal septa. *Biochem J*. 1971;122(4):477-485.

169. Kurniawan NA, Wong LH, Rajagopalan R. Early stiffening and softening of collagen: Interplay of deformation mechanisms in biopolymer networks. *Biomacromolecules*. 2012;13(3):691-698.

170. Schoof H, Apel J, Heschel I, Rau G. Control of pore structure and size in freeze-dried collagen sponges. *Journal of Biomedical Materials Research Part A*. 2001;58(4):352-357.

171. Schoof H, Bruns L, Fischer A, Heschel I, Rau G. Dendritic ice morphology in unidirectionally solidified collagen suspensions. *J Cryst Growth*. 2000;209(1):122-129.

172. Harrison G, Franks G, Tirtaatmadja V, Boger D. Suspensions and polymers-common links in rheology. *Korea-Australia Rheology Journal*. 1999;11(3):197-218.

173. Hyun K, Kim SH, Ahn KH, Lee SJ. Large amplitude oscillatory shear as a way to classify the complex fluids. *J Non Newtonian Fluid Mech*. 2002;107(1):51-65.

174. Srivastava A, Majumdar A, Butola B. Improving the impact resistance of textile structures by using shear thickening fluids: A review. *Critical Reviews in Solid State and Materials Sciences*. 2012;37(2):115-129.

175. Nicholson J. *The chemistry of polymers.* Royal Society of Chemistry; 2017.

176. Vasilev M, Kotetskii V, Pukhova Z, Volf L, Istranov L. Collagen precipitation from solutions. *Fibre Chemistry*. 1973;4(5):486-488.

177. Larson R. The structure and rheology of complex fluids. 1999. *New York: Oxford*. 1999;688.

178. Daivis PJ, Evans DJ, Morriss GP. Computer simulation study of the comparative rheology of branched and linear alkanes. *J Chem Phys*. 1992;97(1):616-627.

179. Cziep MA., Abbasi M, Heck M, Arens L, and Wilhelm M. Effect of molecular weight, polydispersity, and monomer of linear homopolymer melts on the intrinsic mechanical nonlinearity ${}^3Q_0(\omega)$ in MAOS. *Macromolecules*. 2016;49(9):3566.

180. Cheng X, McCoy JH, Israelachvili JN, Cohen I. Imaging the microscopic structure of shear thinning and thickening colloidal suspensions. *Science*. 2011;333(6047):1276-1279. doi: 10.1126/science.1207032 [doi].

181. Fall A, Huang N, Bertrand F, Ovarlez G, Bonn D. Shear thickening of cornstarch suspensions as a reentrant jamming transition. *Phys Rev Lett*. 2008;100(1):018301.

182. Hoffman RL. Explanations for the cause of shear thickening in concentrated colloidal suspensions. *J Rheol*. 1998;42(1):111-123.

183. Hoffman R. Discontinuous and dilatant viscosity behavior in concentrated suspensions. II. theory and experimental tests. *J Colloid Interface Sci*. 1974;46(3):491-506.

184. Foss DR, Brady JF. Structure, diffusion and rheology of brownian suspensions by stokesian dynamics simulation. *J Fluid Mech*. 2000;407:167-200.

185. Maranzano BJ, Wagner NJ. Flow-small angle neutron scattering measurements of colloidal dispersion microstructure evolution through the shear thickening transition. *J Chem Phys*. 2002;117(22):10291-10302.

186. Melrose JR, Ball RC. Continuous shear thickening transitions in model concentrated colloids—The role of interparticle forces. *J Rheol*. 2004;48(5):937-960.

187. Kalman DP, Wagner NJ. Microstructure of shear-thickening concentrated suspensions determined by flow-USANS. *Rheologica acta*. 2009;48(8):897-908.

188. Wagner NJ, Brady JF. Shear thickening in colloidal dispersions. *Phys Today*. 2009;62(10):27-32.

189. Brown E, Forman NA, Orellana CS, et al. Generality of shear thickening in dense suspensions. *Nature materials*. 2010;9(3):220-224.

190. Barnes H. Shear-thickening ("Dilatancy") in suspensions of nonaggregating solid particles dispersed in newtonian liquids. *J Rheol*. 1989;33(2):329-366.

191. Galindo-Rosales F, Rubio-Hernández F, Sevilla A. An apparent viscosity function for shear thickening fluids. *J Non Newtonian Fluid Mech*. 2011;166(5):321-325.

192. Brown E, Jaeger HM. The role of dilation and confining stresses in shear thickening of dense suspensions. *J Rheol*. 2012;56(4):875-923.

193. Ding J, Tracey PJ, Li W, Peng G, Whitten PG, Wallace GG. Review on shear thickening fluids and applications. . 2013.

194. Ding J, Tracey PJ, Li W, Peng G, Whitten PG, Wallace GG. Review on shear thickening fluids and applications. . 2013.

195. Azouni M, Kalita W, Yemmou M. On the particle behaviour in front of advancing liquid-ice interface. *J Cryst Growth*. 1990;99(1-4):201-205.

196. Wegst UG, Schecter M, Donius AE, Hunger PM. Biomaterials by freeze casting. *Philos Trans A Math Phys Eng Sci*. 2010;368(1917):2099-2121. doi: 10.1098/rsta.2010.0014 [doi].

197. Li W, Lu K, Walz J. Freeze casting of porous materials: Review of critical factors in microstructure evolution. *International materials reviews*. 2012;57(1):37-60.

198. Li W, Lu K, Walz J. Freeze casting of porous materials: Review of critical factors in microstructure evolution. *International materials reviews*. 2012;57(1):37-60.

199. Deville S, Saiz E, Tomsia AP. Ice-templated porous alumina structures. *Acta Materialia*. 2007;55(6):1965-1974.

200. Gibson L.J. and Ashby M. F. *Cellular solids: Structure and properties* Cambridge, UK: Cambridge University Press; 1997.

201. Harley BA, Leung JH, Silva EC, Gibson LJ. Mechanical characterization of collagen–glycosaminoglycan scaffolds. *Acta biomaterialia*. 2007;3(4):463-474.

202. Chen Q, Bruyneel A, Clarke K, Carr C, Czernuszka J. Collagen-based scaffolds for potential application of heart valve tissue engineering. *Tissue Sci.Eng.S*. 2012;11:1-6.

203. Ashby MF. The properties of foams and lattices. *Philos Trans A Math Phys Eng Sci*. 2006;364(1838):15-30. doi: 10.1098/rsta.2005.1678 [doi].

204. Kanungo BP, Gibson LJ. Density–property relationships in collagen–glycosaminoglycan scaffolds. *Acta biomaterialia*. 2010;6(2):344-353.

205. Tamaddon M. *Characterisation of collagen type I/ type II composite scaffolds for osteochondral tissue engineering.* University of Oxford; 2014.

206. Hutmacher DW. Scaffolds in tissue engineering bone and cartilage. In: *The biomaterials: Silver jubilee compendium.* Elsevier; 2006:175-189.

207. McCullen SD, Autefage H, Callanan A, Gentleman E, Stevens MM. Anisotropic fibrous scaffolds for articular cartilage regeneration. *Tissue engineering Part A*. 2012;18(19-20):2073-2083.

208. Makris EA, Gomoll AH, Malizos KN, Hu JC, Athanasiou KA. Repair and tissue engineering techniques for articular cartilage. *Nature Reviews Rheumatology*. 2015;11(1):21.

209. Martin I, Miot S, Barbero A, Jakob M, Wendt D. Osteochondral tissue engineering. *J Biomech*. 2007;40(4):750-765. doi: S0021-9290(06)00096-0 [pii].

210. Tamaddon M, Burrows M, Ferreira S, et al. Monomeric, porous type II collagen scaffolds promote chondrogenic differentiation of human bone marrow mesenchymal stem cells in vitro. *Scientific reports*. 2017;7:43519.

211. Tierney CM, Jaasma MJ, O'Brien FJ. Osteoblast activity on collagen-GAG scaffolds is affected by collagen and GAG concentrations. *Journal of biomedical materials research Part A*. 2009;91(1):92-101.

212. Farrell E, O'Brien FJ, Doyle P, et al. A collagen-glycosaminoglycan scaffold supports adult rat mesenchymal stem cell differentiation along osteogenic and chondrogenic routes. *Tissue Eng*. 2006;12(3):459-468.

213. Kanungo BP, Gibson LJ. Density–property relationships in collagen–glycosaminoglycan scaffolds. *Acta biomaterialia*. 2010;6(2):344-353.

214. Sachlos E, Gotora D, Czernuszka JT. Collagen scaffolds reinforced with biomimetic composite nano-sized carbonate-substituted hydroxyapatite crystals and shaped by rapid prototyping to contain internal microchannels. *Tissue Eng*. 2006;12(9):2479-2487.

215. Yang Y, Sun C, Wilhelm ME, Fox LJ, Zhu J, Kaufman LJ. Influence of chondroitin sulfate and hyaluronic acid on structure, mechanical properties, and glioma invasion of collagen I gels. *Biomaterials*. 2011;32(31):7932-7940.

216. Itoh H, Aso Y, Furuse M, Noishiki Y, Miyata T. A honeycomb collagen carrier for cell culture as a tissue engineering scaffold. *Artif Organs*. 2001;25(3):213-217.

217. Cao H, Xu S. EDC/NHS-crosslinked type II collagen-chondroitin sulfate scaffold: Characterization and in vitro evaluation. *J Mater Sci Mater Med*. 2008;19(2):567-575.

218. Daamen W, Van Moerkerk, H Th B, Hafmans T, et al. Preparation and evaluation of molecularly-defined collagen–elastin–glycosaminoglycan scaffolds for tissue engineering. *Biomaterials*. 2003;24(22):4001-4009.

219. Pieper J, Van Der Kraan P, Hafmans T, et al. Crosslinked type II collagen matrices: Preparation, characterization, and potential for cartilage engineering. *Biomaterials*. 2002;23(15):3183-3192.

220. Pieper J, Hafmans T, Veerkamp J, Van Kuppevelt T. Development of tailor-made collagen–glycosaminoglycan matrices: EDC/NHS crosslinking, and ultrastructural aspects. *Biomaterials*. 2000;21(6):581-593.

221. Shepherd JH, Ghose S, Kew S, Moavenian A, Best SM, Cameron RE. Effect of fiber crosslinking on collagen-fiber reinforced collagen–chondroitin-6-sulfate materials for regenerating load-bearing soft tissues. *Journal of Biomedical Materials Research Part A*. 2013;101(1):176-184.

222. Rosloniec EF, Cremer M, Kang AH, Myers LK, Brand DD. Collagen-Induced arthritis. *Current protocols in immunology*. 2010:15.5. 1-15.5. 25.

223. Walton R.S. *Preparation and analysis of type I/ type II collagens for tissue engineering scaffolds.* University of Oxford; 2010.

224. Tamaddon M, Walton R, Brand D, Czernuszka J. Characterisation of freeze-dried type II collagen and chondroitin sulfate scaffolds. *J Mater Sci Mater Med*. 2013;24(5):1153-1165.

225. Levental I, Georges PC, Janmey PA. Soft biological materials and their impact on cell function. *Soft Matter*. 2007;3(3):299-306.

226. MacKintosh F, Käs J, Janmey P. Elasticity of semiflexible biopolymer networks. *Phys Rev Lett*. 1995;75(24):4425.

227. Yang Y, Kaufman LJ. Rheology and confocal reflectance microscopy as probes of mechanical properties and structure during collagen and collagen/hyaluronan self-assembly. *Biophys J*. 2009;96(4):1566-1585.

228. Amis EJ, Carriere CJ, Ferry JD, Veis A. Effect of pH on collagen flexibility determined from dilute solution viscoelastic measurements. *Int J Biol Macromol*. 1985;7(3):130-134.

229. Chow AW, Fuller GG, Wallace DG, Madri JA. Rheooptical response of rodlike, shortened collagen protein to transient shear flow. *Macromolecules*. 1985;18(4):805-810.

230. Nicholson J. *The chemistry of polymers* Cambridge: The Royal Society of Chemistry; 1991.

231. Vasilev M. P. , Kotetskii V. V., Pukhova Z. I., Volf L. A. and Istranov L. P. Collagen precipitation from solutions. *fibre chemistry 4(5),* pp. 486-488. . 1973;4(5):486.

232. Kasapis S, Mitchell JR. Definition of the rheological glass transition temperature in association with the concept of iso-free-volume. *Int J Biol Macromol*. 2001;29(4-5):315-321.

233. Yoshimura K, Chonan Y, Shirai K. Preparation and dynamic viscoelastic characterization of pepsin-solubilized collagen from shark skin compared with pig skin. *Nihon Chikusan Gakkaiho*. 1999;70(4):227-234.

234. Piechocka IK, van Oosten AS, Breuls RG, Koenderink GH. Rheology of heterotypic collagen networks. *Biomacromolecules*. 2011;12(7):2797-2805.

235. Barth A. Infrared spectroscopy of proteins. *Biochimica et Biophysica Acta (BBA)-Bioenergetics*. 2007;1767(9):1073-1101.

236. Kong J, Yu S. Fourier transform infrared spectroscopic analysis of protein secondary structures. *Acta biochimica et biophysica Sinica*. 2007;39(8):549-559.

237. Bandekar J. Amide modes and protein conformation. *Biochimica et Biophysica Acta (BBA)-Protein Structure and Molecular Enzymology*. 1992;1120(2):123-143.

238. Chang MC, Tanaka J. FT-IR study for hydroxyapatite/collagen nanocomposite cross-linked by glutaraldehyde. *Biomaterials*. 2002;23(24):4811-4818.

239. Doyle BB, Bendit E, Blout ER. Infrared spectroscopy of collagen and collagen-like polypeptides. *Biopolymers: Original Research on Biomolecules*. 1975;14(5):937-957.

240. George A, Veis A. FTIRS in water demonstrates that collagen monomers undergo a conformational transition prior to thermal self-assembly in vitro. *Biochemistry (N Y)*. 1991;30(9):2372-2377.

241. Douglas T, Heinemann S, Bierbaum S, Scharnweber D, Worch H. Fibrillogenesis of collagen types I, II, and III with small leucine-rich proteoglycans decorin and biglycan. *Biomacromolecules*. 2006;7(8):2388-2393.

242. Öbrink B, Laurent TC, Carlsson B. The binding of chondroitin sulphate to collagen. *FEBS Lett*. 1975;56(1):166-169.

243. ÖBrink B. A study of the interactions between monomeric tropocollagen and glycosaminoglycans. *European journal of biochemistry*. 1973;33(2):387-400.

244. Snowden JM, Swann DA. Effects of glycosaminoglycans and proteoglycan on the in vitro assembly and thermal stability of collagen fibrils. *Biopolymers: Original Research on Biomolecules*. 1980;19(4):767-780.

245. Gelman RA, Blackwell J. Interaction between collagen and chondroitin-6-sulfate. *Connect Tissue Res*. 1973;2(1):31-35.

246. Tian H, Li C, Liu W, Li J, Li G. The influence of chondroitin 4-sulfate on the reconstitution of collagen fibrils in vitro. *Colloids and Surfaces B: Biointerfaces*. 2013;105:259-266.

247. Lindahl U, Hook M. Glycosaminoglycans and their binding to biological macromolecules. *Annu Rev Biochem*. 1978;47(1):385-417.

248. Lee J, Edwards H, Pereira C, Samii S. Crosslinking of tissue-derived biomaterials in 1-ethyl-3-(3-dimethylaminopropyl)-carbodiimide (EDC). *J Mater Sci Mater Med*. 1996;7(9):531-541.

249. Lewis JA. Colloidal processing of ceramics. *J Am Ceram Soc*. 2000;83(10):2341-2359.

250. Gardini D, Galassi C, Lapasin R. Rheology of hydroxyapatite dispersions. *J Am Ceram Soc*. 2005;88(2):271-276.

251. Knowles J, Callcut S, Georgiou G. Characterisation of the rheological properties and zeta potential of a range of hydroxyapatite powders. *Biomaterials*. 2000;21(13):1387-1392.

252. Zhang J, Maeda M, Kotobuki N, et al. Aqueous processing of hydroxyapatite. *Mater Chem Phys*. 2006;99(2-3):398-404.

253. Rodrıguez-Lorenzo L, Vallet-Regı M, Ferreira J. Colloidal processing of hydroxyapatite. *Biomaterials*. 2001;22(13):1847-1852.

254. Bouyer E, Gitzhofer F, Boulos M. Morphological study of hydroxyapatite nanocrystal suspension. *J Mater Sci Mater Med*. 2000;11(8):523-531.

255. Padilla S, Vallet-Regí M. Concentrated suspensions of hydroxyapatite for gelcasting shaping. . 2004;254:35-38.

256. Kikuchi M, Itoh S, Ichinose S, Shinomiya K, Tanaka J. Self-organization mechanism in a bone-like hydroxyapatite/collagen nanocomposite synthesized in vitro and its biological reaction in vivo. *Biomaterials*. 2001;22(13):1705-1711.

257. Wang Y, Yang C, Chen X, Zhao N. Biomimetic formation of hydroxyapatite/collagen matrix composite. *Advanced engineering materials*. 2006;8(1-2):97-100.

258. Ficai A, Andronescu E, Ghitulica C, et al. Colagen/hydroxyapatite interactions in composite biomaterials. *Materiale Plastice*. 2009;46(1):11-15.

259. Harley BA, Leung JH, Silva EC, Gibson LJ. Mechanical characterization of collagen–glycosaminoglycan scaffolds. *Acta biomaterialia*. 2007;3(4):463-474.

260. Monmaturapoj N, Soodsawang W, Thepsuwan W. Porous hydroxyapatite scaffolds produced by the combination of the gel-casting and freeze drying techniques. *Journal of Porous Materials*. 2012;19(4):441-447.

261. Hutmacher DW, Horch RE, Loessner D, et al. Translating tissue engineering technology platforms into cancer research. *J Cell Mol Med*. 2009;13(8a):1417-1427.

262. Mimeault M, Batra SK. Recent advances on skin-resident stem/progenitor cell functions in skin regeneration, aging and cancers and novel anti-aging and cancer therapies. *J Cell Mol Med*. 2010;14(1-2):116-134.

263. Ng KW, Leong DT, Hutmacher DW. The challenge to measure cell proliferation in two and three dimensions. *Tissue Eng*. 2005;11(1-2):182-191.

264. Quent VM, Loessner D, Friis T, Reichert JC, Hutmacher DW. Discrepancies between metabolic activity and DNA content as tool to assess cell proliferation in cancer research. *J Cell Mol Med*. 2010;14(4):1003-1013.

265. Ude CC, Sulaiman SB, Min-Hwei N, et al. Cartilage regeneration by chondrogenic induced adult stem cells in osteoarthritic sheep model. *PLoS One*. 2014;9(6):e98770.

266. Peletto S, Bertuzzi S, Campanella C, et al. Evaluation of internal reference genes for quantitative expression analysis by real-time PCR in ovine whole blood. *International journal of molecular sciences*. 2011;12(11):7732-7747.

267. Merten OW. Advances in cell culture: Anchorage dependence. *Philos Trans R Soc Lond B Biol Sci*. 2015;370(1661):20140040. doi: 10.1098/rstb.2014.0040 [doi].

268. Bacakova L, Filova E, Parizek M, Ruml T, Svorcik V. Modulation of cell adhesion, proliferation and differentiation on materials designed for body implants. *Biotechnol Adv*. 2011;29(6):739-767.

269. Fields GB. The collagen triple-helix: Correlation of conformation with biological activities. *Connect Tissue Res*. 1995;31(3):235-243.

270. Rodrigues C, Serricella P, Linhares A, et al. Characterization of a bovine collagen–hydroxyapatite composite scaffold for bone tissue engineering. *Biomaterials*. 2003;24(27):4987-4997.

271. Boyan BD, Hummert TW, Dean DD, Schwartz Z. Role of material surfaces in regulating bone and cartilage cell response. *Biomaterials*. 1996;17(2):137-146.

272. Kleinman HK, McGoodwin EB, Klebe RJ. Localization of the cell attachment region in types I and II collagens. *Biochem Biophys Res Commun*. 1976;72(2):426-432.

273. Filova E, Suchy T, Sucharda Z, et al. Support for the initial attachment, growth and differentiation of MG-63 cells: A comparison between nano-size hydroxyapatite and micro-size hydroxyapatite in composites. *Int J Nanomedicine*. 2014;9:3687-3706. doi: 10.2147/IJN.S56661 [doi].

274. Qing F, Wang Z, Hong Y, et al. Selective effects of hydroxyapatite nanoparticles on osteosarcoma cells and osteoblasts. *J Mater Sci Mater Med*. 2012;23(9):2245-2251.

275. Prosecká E, Rampichová M, Litvinec A, et al. Collagen/hydroxyapatite scaffold enriched with polycaprolactone nanofibers, thrombocyte-rich solution and mesenchymal stem cells promotes regeneration in large bone defect in vivo. *Journal of Biomedical Materials Research Part A*. 2015;103(2):671-682.

276. Tierney CM, Haugh MG, Liedl J, Mulcahy F, Hayes B, O'Brien FJ. The effects of collagen concentration and crosslink density on the biological, structural and mechanical properties of collagen-GAG scaffolds for bone tissue engineering. *Journal of the mechanical behavior of biomedical materials*. 2009;2(2):202-209.

277. Bačáková L, Filova E, Rypáček F, Švorčík V, Starý V. Cell adhesion on artificial materials for tissue engineering. *Physiol Res*. 2004;53(Suppl 1):S35-S45.

278. Bernhardt A, Lode A, Boxberger S, Pompe W, Gelinsky M. Mineralised collagen—an artificial, extracellular bone matrix—improves osteogenic differentiation of bone marrow stromal cells. *J Mater Sci Mater Med*. 2008;19(1):269-275.

279. Mueller SM, Shortkroff S, Schneider TO, Breinan HA, Yannas IV, Spector M. Meniscus cells seeded in type I and type II collagen–GAG matrices in vitro. *Biomaterials*. 1999;20(8):701-709.

280. Sun J, Liu H, Hong-Shong Chang W, Li J, Lin F, Tai H. Influence of hydroxyapatite particle size on bone cell activities: An in vitro study. *Journal of Biomedical Materials Research: An Official Journal of The Society for Biomaterials, The Japanese Society for Biomaterials, and the Australian Society for Biomaterials*. 1998;39(3):390-397.

281. O'Brien FJ, Harley B, Yannas IV, Gibson LJ. The effect of pore size on cell adhesion in collagen-GAG scaffolds. *Biomaterials*. 2005;26(4):433-441.

282. Golden M. Cell biology of extracellular matrix. *Journal of Vascular Surgery*. 1993;18(1):142.

283. Wight TN, Heinegård DK, Hascall VC. Proteoglycans. In: *Cell biology of extracellular matrix.* Springer; 1991:45-78.

284. Hardingham TE, Fosang AJ. Proteoglycans: Many forms and many functions. *FASEB J*. 1992;6(3):861-870.

285. Kjellen L, Lindahl U. Proteoglycans: Structures and interactions. *Annu Rev Biochem*. 1991;60(1):443-475.

286. Jalkanen M, Jalkanen S, Bernfield M. Binding of extracellular effector molecules by cell surface proteoglycans. *Receptors for extracellular matrix*. 1991;1:37.

287. Ruoslahti E, Yamaguchi Y. Proteoglycans as modulators of growth factor activities. *Cell*. 1991;64(5):867-869.

288. Wight TN, Kinsella MG, Qwarnström EE. The role of proteoglycans in cell adhesion, migration and proliferation. *Curr Opin Cell Biol*. 1992;4(5):793-801.

289. Sakaguchi K, Yanagishita M, Takeuchi Y, Aurbach GD. Identification of heparan sulfate proteoglycan as a high affinity receptor for acidic fibroblast growth factor (aFGF) in a parathyroid cell line. *J Biol Chem*. 1991;266(11):7270-7278.

290. Kim S, Turnbull J, Guimond S. Extracellular matrix and cell signalling: The dynamic cooperation of integrin, proteoglycan and growth factor receptor. *J Endocrinol*. 2011;209(2):139-151.

291. Marastoni S, Ligresti G, Lorenzon E, Colombatti A, Mongiat M. Extracellular matrix: A matter of life and death. *Connect Tissue Res*. 2008;49(3-4):203-206.

292. Pelham RJ,Jr, Wang Y. Cell locomotion and focal adhesions are regulated by substrate flexibility. *Proc Natl Acad Sci U S A*. 1997;94(25):13661-13665.

293. Smith L, Ma P. Nano-fibrous scaffolds for tissue engineering. *Colloids and surfaces B: biointerfaces*. 2004;39(3):125-131.

294. Palecek SP, Loftus JC, Ginsberg MH, Lauffenburger DA, Horwitz AF. Integrin-ligand binding properties govern cell migration speed through cell-substratum adhesiveness. *Nature*. 1997;385(6616):537.

295. O'Brien FJ, Harley B, Yannas IV, Gibson LJ. The effect of pore size on cell adhesion in collagen-GAG scaffolds. *Biomaterials*. 2005;26(4):433-441.

296. Fields GB. The collagen triple-helix: Correlation of conformation with biological activities. *Connect Tissue Res*. 1995;31(3):235-243.

297. Rowley JA, Mooney DJ. Alginate type and RGD density control myoblast phenotype. *Journal of Biomedical Materials Research: An Official Journal of The Society for Biomaterials, The Japanese Society for Biomaterials, and The Australian Society for Biomaterials and the Korean Society for Biomaterials*. 2002;60(2):217-223.

298. Murphy CM, Haugh MG, O'Brien FJ. The effect of mean pore size on cell attachment, proliferation and migration in collagen–glycosaminoglycan scaffolds for bone tissue engineering. *Biomaterials*. 2010;31(3):461-466.

299. Mandal BB, Kundu SC. Cell proliferation and migration in silk fibroin 3D scaffolds. *Biomaterials*. 2009;30(15):2956-2965.

300. Trappmann B, Gautrot JE, Connelly JT, et al. Extracellular-matrix tethering regulates stem-cell fate. *Nature materials*. 2012;11(7):642.

301. Nehrer S, Breinan HA, Ramappa A, et al. Matrix collagen type and pore size influence behaviour of seeded canine chondrocytes. *Biomaterials*. 1997;18(11):769-776.

302. Murphy CM, O'Brien FJ, Little DG, Schindeler A. Cell-scaffold interactions in the bone tissue engineering triad. . 2013.

303. McBride SH, Falls T, Knothe Tate ML. Modulation of stem cell shape and fate B: Mechanical modulation of cell shape and gene expression. *Tissue Engineering Part A*. 2008;14(9):1573-1580.

304. Guilak F, Cohen DM, Estes BT, Gimble JM, Liedtke W, Chen CS. Control of stem cell fate by physical interactions with the extracellular matrix. *Cell stem cell*. 2009;5(1):17-26.

305. Gleeson J, Plunkett N, O'Brien F. Addition of hydroxyapatite improves stiffness, interconnectivity and osteogenic potential of a highly porous collagen-based scaffold for bone tissue regeneration. *Eur Cell Mater*. 2010;20:218-230.

306. Levental I, Georges PC, Janmey PA. Soft biological materials and their impact on cell function. *Soft Matter*. 2007;3(3):299-306.

307. Murphy CM, Matsiko A, Haugh MG, Gleeson JP, O'Brien FJ. Mesenchymal stem cell fate is regulated by the composition and mechanical properties of collagen–glycosaminoglycan scaffolds. *Journal of the mechanical behavior of biomedical materials*. 2012;11:53-62.

308. Hadjipanayi E, Mudera V, Brown R. Close dependence of fibroblast proliferation on collagen scaffold matrix stiffness. *Journal of tissue engineering and regenerative medicine*. 2009;3(2):77-84.

309. Engler AJ, Sen S, Sweeney HL, Discher DE. Matrix elasticity directs stem cell lineage specification. *Cell*. 2006;126(4):677-689.

310. Discher DE, Janmey P, Wang YL. Tissue cells feel and respond to the stiffness of their substrate. *Science*. 2005;310(5751):1139-1143. doi: 310/5751/1139 [pii].

311. Even-Ram S, Artym V, Yamada KM. Matrix control of stem cell fate. *Cell*. 2006;126(4):645-647.

312. Discher DE, Janmey P, Wang YL. Tissue cells feel and respond to the stiffness of their substrate. *Science*. 2005;310(5751):1139-1143. doi: 310/5751/1139 [pii].

313. Reinhart-King CA, Dembo M, Hammer DA. Cell-cell mechanical communication through compliant substrates. *Biophys J*. 2008;95(12):6044-6051.

314. Harley BA, Lynn AK, Wissner-Gross Z, Bonfield W, Yannas IV, Gibson LJ. Design of a multiphase osteochondral scaffold. II. fabrication of a mineralized collagen–glycosaminoglycan scaffold. *Journal of Biomedical Materials Research Part A: An Official Journal of The Society for Biomaterials, The Japanese Society for Biomaterials, and The Australian Society for Biomaterials and the Korean Society for Biomaterials*. 2010;92(3):1066-1077.

315. Shu K, Thatte H, Spector M. Chondrogenic differentiation of adult mesenchymal stem cells and embryonic stem cells. . 2009:1-2.

316. Ohno T, Tanisaka K, Hiraoka Y, Ushida T, Tamaki T, Tateishi T. Effect of type I and type II collagen sponges as 3D scaffolds for hyaline cartilage-like tissue regeneration on phenotypic control of seeded chondrocytes in vitro. *Materials Science and Engineering: C*. 2004;24(3):407-411.

317. Dado D, Levenberg S. Cell–scaffold mechanical interplay within engineered tissue. . 2009;20(6):656-664.